Further understanding ground source heat pump system design using finite element methods and machine learning techniques

Nikolas Makasis

https://orcid.org/0000-0002-6678-1239

Submitted in total fulfilment of the requirements of the degree of

Doctor of Philosophy

November 2018

Department of Infrastructure Engineering

The University of Melbourne

Page intentionally left blank

Summary

Shallow geothermal, or ground-source heat pump (GSHP) systems, can be used to efficiently provide renewable low carbon emission energy for space heating and cooling purposes and contribute towards a greener and more sustainable future. These systems utilise the ground a few tens of metres below the surface, where the temperature is approximately constant throughout the year, as a heat source or sink. Geothermal pipes (usually high-density polyethylene, HDPE) are embedded in underground structures forming ground heat exchangers (GHEs). Traditionally, these GHEs consist of purpose-built structures, such as boreholes, which can result in relatively high capital costs. A more recent approach, that tackles this problem, is the utilisation of geo-structures as GHEs. These "*energy geo-structures*" consist of geothermal piping incorporated into underground structures primarily designed for geo-mechanical stability, such as piles or retaining walls. However, the additional constraints and different conditions related to energy geo-structures introduce new challenges for geothermal design.

This doctoral research contributes towards a better understanding and broader utilisation of GSHP systems. Even though the potential of these systems is widely acknowledged, there exist significant gaps and margins for improvement in our knowledge of how they can be better designed and utilised, particularly in the more recent field of energy geo-structures. A key challenge is how to best identify how much thermal energy can be provided by the energy geo-structures. Since their geo-mechanical design governs their geometry, provision of the entirety of the thermal demand of the building(s) cannot be guaranteed, as is usually the case for traditional systems. Instead, a hybrid heating and cooling system might be suitable where the remaining thermal energy is provided by a complementary auxiliary system. Moreover, the different potential geometries that energy geo-structures can have can make them hard to analyse/design without expensive computational simulations. Throughout this work, detailed numerical modelling techniques and statistical approaches have been employed to analyse the thermal performance of GSHP systems under various conditions. The results suggest ways to minimise uncertainties, provide new insights on the area of energy geo-structures and develop tools that complement geothermal design and make it more accessible to engineers.

Drawing from the experience of the research group, it is firstly acknowledged that one limitation in the thermal performance of GSHP systems stems from potential disparities

between the design assumptions and the actual installation and use. One such disparity relates to the separation of the geothermal pipes, once they have been placed within vertical GHE structures (such as boreholes). Usually, the pipes are designed assuming they will remain equally separated throughout the depth of the GHE. However, this assumption is not always justified and its potential implications can be significant to the thermal performance of the system. This research presents and quantifies these implications, showing that not accounting for variable pipe separation can result in an under-designed system and examines the design factors that are impactful to this effect, finding that a high thermal conductivity for the borehole grout (amongst others) can reduce the effects' impact. Moreover, a simple methodology is introduced that can be used to address this effect during the design stage.

The second area this research explores is the thermal design and performance of energy geo-structures, for which limited information is currently available, beginning with an exploratory research on the implementation of energy piles in loessial soil (i.e., low thermal conductivity). This work, undertaken with a team of collaborators from both Australia and Argentina, concentrates on answering how much energy can be provided by the system and how a hybrid system can be utilised to satisfy the thermal energy requirements. Furthermore, this research seized the unique opportunity to work on the large-scale Melbourne Metro project to undertake detailed analyses on how energy retaining walls can be utilised, given that currently the majority of available literature on energy geo-structures has focused on energy piles instead. As a result, detailed finite element models have been developed for both diaphragm and soldier pile retaining walls to examine their thermal performance under a variety of conditions. A key finding is the influence of the balance of the thermal demand, noting that provision of close to equal amounts of cooling and heating would be recommended, which in cases might need the cooperation of more than one entity or company.

Following the completion of the Melbourne Metro project (and therefore outside the associated time and monetary constraints), further analyses on the thermal performance of these structures were performed. One such analysis concentrating on the influence of the depth of embedment, shows that extending the retaining wall can significantly improve the performance of the system. A second analysis investigating the amount of pipe loops in a typical energy soldier pile shows minimal thermal gains when incorporating more than about 3 U-loops connected in series. These analyses provide further insights and show how the lack of available information on energy geo-structures can affect its design under realistic conditions (where limited time exists to explore various design alternatives). Lastly, the importance of correctly identifying

the new boundary conditions, introduced with energy retaining walls, is also discussed noting their potential implications on the design and thermal performance.

The final area investigated by this research relates to the fact that numerical modelling of GSHP systems, which in certain cases, such as complex or unusual geometries, is necessary for design, can be very computationally expensive. To address this problem, this research developed two statistical prediction models that can be used to complement numerical modelling and very significantly reduce computational resources and time. The models are based around answering the question *"how much energy can the system provide?"* and utilise statistical and machine learning techniques to learn the underlying relationships between the inputs and outputs of the numerical simulations. The introduction and evaluation of these models using a variety of parameters such as geometries, materials, thermal demands, which have been published during this work, are provided. The results of the evaluations show high accuracies in temperature predictions (within 1°C) and potential savings in time of days or weeks. A comparison of the two approaches is also provided, noting the circumstances where each one can be more beneficial.

Overall, this research provides insights and knowledge on different aspects of GSHP system design. The information included herein can be utilised by researchers, to build upon the foundations of these findings, as well as by engineers to directly implement in design. The main aim of this doctoral journey has been to make shallow geothermal system more accessible, contribute towards their more effective utilisation and thus towards a future with less greenhouse gas emissions and more sustainable energy sources.

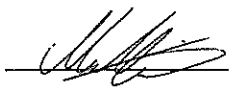
Declaration

This is to certify that:

i. The thesis includes only my original work towards the PhD,

ii. Due acknowledgement has been made in the text to all other material or work used,

iii. The thesis is fewer than 100,000 words in length, exclusive of tables, bibliographies and appendices



Nikolas Makasis

November 2018

Preface & Publications

This doctoral thesis presents the research undertaken during the course of my PhD candidature between November 2014 and November 2018. It contains 6 publications, 4 of which are included in the main body of the thesis and 2 as appendices. Chapters 3 and 5 each include 2 journal publications in sections 3.2 (Publication 1), 3.3 (Publication 2), 5.2 (Publication 3) and 5.3 (Publication 4). These four publications comprise the main parts of the respective chapters and result directly from the work of this doctoral research. Appendices A and B contain publications 5 and 6 respectively, the first being a journal publication and the second a publication in conference proceedings, both relating to Chapter 4 and included to complement the main body of the chapter.

1. Makasis N., Narsilio G.A., Bidarmaghz A. and Johnston I.W. (2018) Ground-source heat pump systems: the effect of variable pipe separation in ground heat exchangers, *Computers and Geotechnics*, 100 (August), 97-109.
2. Makasis N., Narsilio G.A., Bidarmaghz A. and Johnston I.W. (2018) Carrier fluid temperature data in vertical ground heat exchangers with a varying pipe separation. *Data in Brief*, 18 (June), 1466-1470.
3. Makasis N., Narsilio G.A. and Bidarmaghz A. (2018) A machine learning approach to energy pile design, *Computers and Geotechnics*. 97 (May) 189–203.
4. Makasis N., Narsilio G.A. and Bidarmaghz A. (2018) A prediction model for energy geo-structure design, *Computers and Geotechnics*, 104 (December), 140-151.
5. Bidarmaghz A., Makasis N., Narsilio G.A., Francisca F., and Carro Perez M. (2016) Geothermal Energy in Loess, *Environmental Geotechnics*, 4 (August), pp. 225-236.
6. Makasis N., Narsilio G.A., Bidarmaghz A. and Johnston I.W. (2018) The application of retaining walls and slabs as energy structures in underground train stations, In: Ferrari A., Laloui L. (eds) *Energy Geotechnics*, SEG 2018, Springer Series in Geomechanics and Geoengineering, Springer.

In terms of the authors' contributions towards these publications, I have contributed more than 50% towards publications 1, 2, 3, 4 and 6, being involved in all stages of the work including concept, methodology, analysis, discussion, writing and presentation. The co-authors, being the doctoral supervisors, contributed with their ideas and valuable insights to ensure that the research followed a fruitful path, as well as with reviewing the written material, editing and providing comments, feedback and advice towards the improvement and clarity of manuscripts, figures and contents. For publications 1-4, which are included as main bodies of thesis chapters,

the required co-author authorisation forms have been provided with this submission. Regarding publication 5, the leading author was Dr. Bidarmaghz and my contributions include my input in discussions regarding the direction of the research, parts of numerical modelling and analysis, data visualisation and revision of the manuscript.

In addition to the publications included within the thesis, listed above, findings from this research have also been presented in four international conferences and included in the proceedings, one being publication number 6 and the rest publications numbers 7-9. For publications 6-8, I was the leading contributor, as detailed above, while for publication 9, I was only a collaborator, contributing mainly with numerical modelling and the presentation of figures. Moreover, contributions from my work on the Melbourne Metro project (detailed in Chapter 4) have been presented in submitted reports 10 and 11. My contributions towards this work included leading the numerical modelling, presenting and discussing the results to/with the internal team at the university, attending meetings with industry to present our findings and collaborate with the different consulting parties to find realistic solutions to problems (since our work related to innovative technologies lacking standard practices), as well as with the writing and editing of the produced report.

7. Makasis N., Narsilio G.A., Bidarmaghz A. and Johnston I.W. (2016) Effects of ground heat exchanger variable pipe separation in ground-source heat pump systems, Proceedings of 1st International Conference in Energy Geotechnics, Kiel, Germany, Aug 29-31, pp. 155-161.
8. Makasis N. , Narsilio G.A. and Bidarmaghz A. (2017) Optimising the design of energy piles using machine learning Optimisation de la conception des pieux énergétiques par apprentissage automatique, in: 19th Int. Conf. Soil Mech. Geotech. Energy, Seoul, Sep 17-21, pp. 3455-3458
9. Narsilio G.A., Francisca F. M., Ferrero H., Bidarmaghz A., Serrano C., Carro Perez M., Makasis N., and Delacoste E. (2015) Geothermal Energy in Loess: A detailed numerical case study for Cordoba, Argentina. In D. Manzanal and A.O. Sfriso (Eds.) Proceedings of the XV Pan-american Conference on Soil Mechanics and Geotechnical Engineering, XV PCSMGE 2015, 15-18 November 2015, Buenos Aires, Argentina. pp. 704-711
10. Narsilio G.A., Bidarmaghz A., Disfani M., Johnston I. W. and Makasis N., Shallow geothermal ('Geoexchange') feasibility study - Stage 1, Parkville, University of Melbourne, Department of Infrastructure, 2016, 65 p.
11. Narsilio G.A., Makasis N., Lu Q., Jensen-Page L., Bidarmaghz A., Disfani M., "Shallow geothermal ('Geoexchange') feasibility study - Stage 2: Parkville", University of Melbourne, Department of Infrastructure, 2016, 65 p.

To conduct the presented doctoral research a number of powerful tools were utilised, including the finite element modelling software *COMSOL Multiphysics*, the high-level programming language *MATLAB* and high-performance computing facilities within the University of Melbourne, such as *Nectar*, *Spartan* and *Argali*. This work would not have been possible without the support and funding from the Australian Research Council (FT140100227, LP160100070), The University of Melbourne, The Department of State Development, Business and Innovation (The Sustainable Energy Research and Development Program) and the Victorian Government. Moreover, parts of the findings discussed in Chapter 4 comprise of the outcomes of a productive collaboration with the Melbourne Metro Railway Authority (MMRA). I am very grateful to MMRA for trusting in our research group and allowing us to gain further insights in the application of this technology, the University of Melbourne for facilitating this collaboration, as well as to A/Prof. Narsilio, without whom this collaboration would have never risen to the surface.

Acknowledgements

This doctoral research would not have been possible without the support of my primary supervisor A/Prof. Guillermo A. Narsilio. Thank you for trusting in me, supporting the pursuit of my research interests and welcoming the new challenges these brought, pushing me to excel and always treating me with honesty, kindness and respect. Your mentorship has made me stronger, more confident and more prepared for the challenges that await in my future.

I would also like to deeply thank my co-supervisors: Dr. Asal Bidarmaghz, thank you for allowing me to build on top of your hard work, offering valuable advice and direction along the way, as well as for accommodating the time difference between us with the either early morning or late evening conference calls that helped shape this research. Prof. Ian W. Johnston, thank you for offering your practical and valuable insights as well as for always being supportive, motivating and enthusiastic about my work.

My gratitude also goes to my colleagues and research family at the University of Melbourne who kept me company over the past years, enabled me to learn from them, provided willing ears and fresh ideas on my work and helped me further grow. This journey would not have been the same without you.

Very importantly, I would have never been able to start this journey, let alone finish it, without the limitless support and love of my parents, Andri and Christos, who make everything seem so easy, as well as of my sister, Katerina, who reminds me of the important things in life and keeps me grounded. I would also like to thank my aunt, Yianna, and uncle, Kostas, for teaching me the importance of good friends and for always being supportive, as well as my entire family back in Cyprus. Finally, my most heartfelt thanks to my loving partner, Alexia. Thank you for always believing in me, supporting me every step of the way and making me smile even on the rainiest of days.

Table of Contents

Summary i

Declaration iv

Preface & Publications v

Acknowledgements viii

Table of Contents ix

List of Figures xii

List of Tables xix

Chapter 1 Introduction 1

1.1 Research objectives 2

1.2 Thesis structure 2

Chapter 2 Literature review 5

2.1 Overview and structure 5

2.2 Geothermal energy 5

2.2.1 Need for change 5

2.2.2 Geothermal energy systems 6

2.2.3 GSHP system design 12

2.2.4 GSHP system design in this research - a validated numerical model 19

2.3 Machine learning 22

2.3.1 Overview 22

2.3.2 Types of learning 23

2.3.3 Supervised learning: training and testing 24

2.3.4 Feature importance 25

2.3.5 Machine learning applications in engineering 25

2.4 Summary 26

Chapter 3 Effects of realistic geothermal pipe installation in GSHP design: variable pipe separation 29

3.1 Overview and structure 29

3.2 Journal paper: Ground-source heat pump systems: The effect of variable pipe separation in ground heat exchangers 30

3.3 Journal paper: Carrier fluid temperature data in vertical ground heat exchangers with a varying pipe separation 55

3.4 Simplified method to account for variable pipe separation 61

3.5 Summary and conclusions 64

Chapter 4 Numerical modelling and design of energy geo-structures 66

4.1 Overview and structure 66

4.2 Energy piles modelling 67

4.3 Energy Retaining Walls 71

4.3.1 Overview, challenges and opportunities 71

4.3.2 Numerical modelling of energy retaining walls 72

4.3.3 Thermal load distributions 83

4.3.4 Thermal performance analyses of energy retaining walls 85

4.3.5 Importance of boundary conditions 113

4.4 Summary and conclusions 120

Chapter 5 Complementing numerical simulations with prediction models 122

5.1 Overview and structure 122

5.2 Journal paper: A machine learning approach to energy pile design 123

5.3 Journal paper: A robust prediction model approach to energy geo-structure design 151

5.4 Comparing the two developed prediction models 174

5.5 Summary and conclusions 175

Chapter 6 Conclusions and future work 178

6.1 Key findings and practical applications 179

6.2 Recommendations for future work 181

References 183

Appendix A – Geothermal energy in loess 192

Appendix B – The application of retaining walls and slabs as energy structures in underground train stations 213

List of Figures

Figure 2.1 Estimated Renewable Share of Total Final Energy Consumption, 2016 [1] 6
Figure 2.2 Ground temperature with depth in Melbourne, Australia using two different measurement methods [6] 7
Figure 2.3 GSHP system schematic illustrating the heat pump connecting to the primary and secondary circuits [9] 7
Figure 2.4 Schematic of a GSHP system in heating (winter) and cooling (summer) modes (Note: not to scale) [10] 8
Figure 2.5 Direct geothermal systems: open loop (a) and (reverse return) closed loop in horizontal (b) and vertical (c) GHE configurations [13] 9
Figure 2.6 Energy pile installations - collected within the University of Melbourne geotechnical research group 10
Figure 2.7 Schematic of (a) ILS, (b) ICS (c) FLS 13
Figure 2.8 Schematic top view of energy retaining wall (a) and energy pile (b) GSHP systems, highlighting the difference in the ground area around them 18
Figure 2.9 Finite element model validation: comparison between numerical and experimental results for single U-loop borehole: (a) a thermal response test (TRT19), (b) a 'normal' heat pump operation [112] 21
Figure 2.10 Finite element model validation: comparison between numerical and experimental results for pile: (a) a thermal response test (TRT19), (b) a 'normal' heat pump operation [112] 22
Figure 2.11 Machine learning types: (a) supervised and (b) unsupervised learning 23
Figure 2.12 Supervised learning: Training and testing/predicting 24
Figure 2.13 Example decision tree on slope stability classification [121] 25
Figure 3.1 Schematic showing the representative fixed pipe separation 61
Figure 3.2 Cross-section of double loop GHE (used in this analysis) with sinusoidal variable pipe separation as it varies along depth: (a) 'Inner' configuration, (b)'Mid' configuration, (c) 'Outer' configuration. (Figure 5 of paper in section 3.2) 62
Figure 3.3 Investigating the average absolute temperature difference between a fixed pipe separation GHE of varying χ value and a variable pipe separation GHE adopting (a) inner (b) mid and (c) outer configurations. The dashed vertical line represents χav the averaged separation of the pipes along the depth of the GHE 63

Figure 4.1 Case study in Cordoba, Argentina: (a) finite element model of the energy pile field (residential building footprint shown in yellow) (b) detail of one of the 600 mm piles (seen in orange colour in (a))....68
Figure 4.2 Energy pile case study in Cordoba, Argentina: (a) Thermal load distributions and (b) resulting average fluid temperatures....68
Figure 4.3 Investigating how additional GHEs affect the performance of the system: (a) the model and geometry (b) the resulting GHE fluid temperatures when providing the entirety of the building's heating and 60% of its cooling demand....70
Figure 4.4 Investigating the effect of the ground thermal conductivity on the thermal performance of the system....70
Figure 4.5 Validation modelling and material parameters....75
Figure 4.6 Validation results for the numerical (FE) model used showing the heat exchanged per unit of pipe length against time and compared against experimental results [138]....76
Figure 4.7 Energy diaphragm walls numerical modelling – model geometry and key boundary conditions....77
Figure 4.8 Energy diaphragm walls numerical modelling - geometry of single retaining wall panel model without thermally activating the slab....79
Figure 4.9 Energy diaphragm walls numerical modelling - geometry of the retaining wall with two thermally activated panels (see supply/return in the ‘Front View’), and the inclusion of a thermally activated slab (see supply/return in the ‘Top View’)....79
Figure 4.10 Energy soldier pile wall numerical modelling – model geometry and boundary conditions....80
Figure 4.11 Energy soldier pile wall numerical modelling - model geometry and dimensions. Side view and top view for (a) wall only thermal activation, with 1.8 m separation between soldier piles (b) both wall (soldier) piles and bottom slab thermally activated....81
Figure 4.12 Energy soldier pile wall numerical modelling - pipe configuration detail for each soldier pile. Total pipe length per pile approximately 220 m....82
Figure 4.13 Thermal load distribution to be provided by the geothermal system for energy diaphragm wall system....84
Figure 4.14 Thermal load distribution to be provided by the geothermal system for energy soldier pile wall system....85
Figure 4.15 Thermal performance results for energy diaphragm walls, indicating the fluid temperature results when providing different amounts of cooling (upper % value) and heating (lower % value) energy....88

Figure 4.16 Temperature distribution on 25th of May of 25th year, for diaphragm retaining walls when thermally activating (a) the walls only (b) both the wall and slab circuits – Unbalanced thermal load distribution adopted 89
Figure 4.17 Schematic representation of diaphragm wall geometry for different values of pipe spacing, s 91
Figure 4.18 Maximum and minimum fluid temperatures when varying the pipe loop spacing in a diaphragm energy wall 91
Figure 4.19 Temperature distribution on 25th of May of 25th year (end of cooling period) adopting unbalanced thermal load distribution: (a) Temperature distribution for s = 900 mm, (b) Temperature along line X-X' (placed centrally w.r.t wall width) for different loops spacings, s, (c) Section of plot (b) magnified for clarity, (d) Normalised version of plot (c) using depth/s 92
Figure 4.20 The effect of the pipe loop spacing in energy diaphragm walls - normalised results 94
Figure 4.21 Schematic showing a change in the depth of embedment by changing the total depth of the diaphragm wall (extending the wall) 96
Figure 4.22 Maximum and minimum average fluid temperature results when extending the embedment depth of the diaphragm retaining walls 96
Figure 4.23 The effect of extending the depth of embedment in diaphragm retaining walls - normalised results 97
Figure 4.24 Schematic cross section of basements showing a change in the depth of embedment without changing the total depth of the retaining wall 98
Figure 4.25 The effect of varying the embedment depth while keeping the overall retaining wall depth fixed – normalised results 98
Figure 4.26 Thermal performance results for energy solder pile walls, indicating the fluid temperature results when providing different amounts of cooling (upper % value) and heating (lower % value) energy 101
Figure 4.27 Schematic and details of varying the amount of pipe in each soldier pile of 750 mm in diameter 102
Figure 4.28 Maximum and minimum average fluid temperatures when varying the amount of pipe incorporated in soldier piles (pile depth 28 m, pile diameter 750 mm) 103
Figure 4.29 The effect of adding more pipe in the soldier pile retaining wall for different depths of pile - normalised results 103

Figure 4.30 Maximum and minimum average fluid temperatures when varying the horizontal spacing of the soldier piles incorporating 4 U- loops connected in series, while the total number of pile GHEs and thermal load per GHE are constant 105
Figure 4.31 Schematic of pipe configuration when thermally activating different number of soldier piles. (a) Every single soldier pile (b) every second soldier pile (c) every third soldier pile 106
Figure 4.32 Maximum and minimum average fluid temperature results when activating different number of soldier pile and therefore the number of pile GHEs and thermal load per GHE varies with spacing 107
Figure 4.33 Schematic showing a change in the depth of embedment by extending the wall 108
Figure 4.34 Maximum and minimum average fluid temperature when extending the depth of embedment in soldier pile retaining walls 108
Figure 4.35 The effect of extending the depth of embedment in soldier pile walls - normalised results 109
Figure 4.36 Schematic showing a change in the depth of embedment without changing the total depth of the soldier pile wall 110
Figure 4.37 The effect of varying the embedment depth while keeping the overall soldier pile retaining wall depth fixed – normalised results 110
Figure 4.38 Boundary condition modelling schematic showing the three approaches (a) insulation, (b) prescribing a temperature and (c) continuity of temperature between the wall and the basement space 114
Figure 4.39 Average fluid temperature when simulating the soldier pile retaining walls with the three different boundary conditions 115
Figure 4.40 Daily heat transferred through the wall and slab boundaries for the different boundary conditions per soldier pile GHE. Last year (25th) of operation, using the unbalanced thermal load distribution 116
Figure 4.41 Air temperature near the wall, at outflow (end of 10.8 m wide section), mid-depth of the wall 118
Figure 4.42 The influence of air velocity on the fluid temperature when using boundary condition (c) and the unbalanced thermal load distribution 118

Figures in the included journal papers:

Section 3.2 - Ground-source heat pump systems: The effect of variable pipe separation in ground heat exchangers

Figure 1 Schematic of a closed loop vertical GSHP system in heating mode with pipe separators (Not to scale)…….33

Figure 2 Modelling geometry – typically being used in Australia (ground domain to the left and detail of the embedded 114.5mm diameter GHE to the right, containing 25mm outer diameter HDPE pipes in a 50m long borehole)…….35

Figure 3 Overview of the structure and strategy followed for the multiple analyses undertaken……36

Figure 4 Illustration showing the modelling of variable pipe separation for a single loop GHE (Not to scale)…….37

Figure 5 Cross-section of double loop GHE (used in this analysis) with sinusoidal variable pipe separation as it varies along depth: (a) 'Inner' configuration, (b) 'Mid' configuration, (c) 'Outer' configuration.……...38

Figure 6 Random pipe separation geometry schematic……....40

Figure 7 Daily thermal load per GHE for a typical year for three different field sizes (note Melbourne is in the Southern Hemisphere)……..41

Figure 8 Comparison of average fluid temperature, $T_{ave\ fluid}$, for fixed and variable pipe separation simulations over one year of operation.……..43

Figure 9 Average absolute temperature difference, $\overline{T}_{diff}$, between fixed and variable pipe separation simulations over one year……....44

Figure 10 Temperature distribution and contour lines at a cross-section of the GHE, at: z=−25 m, t=7 Jul (heating mode) for the case shown in Figs. 7 and 8: (a) variable pipe separation (b) fixed pipe separation…….45

Figure 11 Average fluid temperature difference, $\overline{T}_{diff,random}$, between the random pipe separation simulations and equivalent variable pipe separation (VPS) and fixed pipe separation (FPS) simulations for the three configurations…….46

Figure 12 Sensitivity analysis results with indicative fitting lines between observations (circles), highlighting how λ_{grout} affects the other parameters……...47

Figure 13 Comparison of a variable pipe separation geometry with longer than 50m borehole length to a fixed pipe separation geometry with 50m length borehole (Parameters as Fig. 7 – configuration: (a) Inner, (b) Mid, (c) Outer)…….50

Figure 14 Excess in annual running cost of variable over fixed pipe separation simulations..51

Section 3.3 - Carrier fluid temperature data in vertical ground heat exchangers with a varying pipe separation

Figure 1 Average fluid temperature for each day of one year simulation, for the three different pipe separation geometries. (Note: Random id = 102)…….58

Figure 2 Annual maximum fluid temperature over the thermal conductivity of the grout, for the straight (fixed) and variable pipe separation geometries…….58

Figure 3 Annual maximum fluid temperature for 100 different randomised pipe geometries..……...59

Section 5.2 - A machine learning approach to energy pile design

Figure 1 Energy piles schematics in heating mode (Not to scale)..……..126

Figure 2 Generalised machine learning principles (blue=known, red=unknown). (For interpretation of the references to colour in this figure legend, the reader is referred to the web version of this article.)……128

Figure 3 Flow diagram of proposed design process for energy piles..…….129

Figure 4 Geometry and model parameters for the three case studies (ground domain to the left and detail of energy pile to the right, not to scale).……134

Figure 5 Creating variations of presented thermal load distributions..……136

Figure 6 Thermal load distributions for (a) Case study 1 and (b) Case studies 2 and 3 (Please note –ve load: cooling, +ve load: heating)..…….....137

Figure 7 Thermal load and fluid temperature distributions for Case Study 1 used in (a) training of the model – Distribution 22 (b) testing the model – Distribution 12.…….140

Figure 8 Validation results – evaluation metrics and errors……142

Figure 9 “Actual” temperature against predicted temperatures for all distributions of each case study. Separated into distribution types (rows) and case studies (columns)..…….143

Figure 10 “Actual” and Predicted values for Distribution 20, using (a) Case Study 2 (b) Case Study 3..……..144

Figure 11 Validation results of case study 1, when trained with different types of thermal load distributions..……..145

Section 5.3 - A robust prediction model approach to energy geo-structure design

Figure 1 Energy geo-structure design methodology with prediction model….……..155

Figure 2 Example prediction plane with three points……..157

Figure 3 Example of creating the prediction model plane(s)…….……..158

Figure 4 Finite element model.……...……159

Figure 5 Model geometry……....……160

Figure 6 Thermal Load distribution per energy wall section – one pipe circuit..……....161

Figure 7 Creation/training and testing points for the prediction plane at time-steps t=1514 days and t=1718 days..……...…….163

Figure 8 Predicted temperature values plotted against values obtained via full FEM simulations, for each thermal load distribution and each combination of design parameters…….165

Figure 9 Absolute error for each thermal load distribution and each combination of design parameters at two particular times……..….165

Figure 10 Average fluid temperature against the absolute error for distributions (a) 1C0.5H and (b) 0.8C0.4H at t=1514, for all parameter combinations (red areas – unrealistic situations included for completeness). (For interpretation of the references to colour in this figure legend, the reader is referred to the web version of this article.)……..166

Figure 11 Using different thermal load distribution to create the prediction plane (blue circles – training/creating points, red stars – testing points): (a) using 3 points reasonably far away (b) using 3 points closer together. (For interpretation of the references to colour in this figure legend, the reader is referred to the web version of this article.)..……167

Figure 12 The effect of each studied design parameter on the value of cooling coefficient A.168

Figure 13 Accuracy of Eqs. (4) and (5) on predicting the cooling coefficient A and B respectively…….169

List of Tables

Table 4.1 Domain modelling - material properties 78

Table 4.2 Parkville modelling - material properties 83

Tables in the included journal papers:

Section 3.2 - Ground-source heat pump systems: The effect of variable pipe separation in ground heat exchangers

Table 1 Material Properties..... 35

Table 2 Parametric analysis variables..... 40

Table 3 Sensitivity index of design parameters..... 49

Section 5.2 - A machine learning approach to energy pile design

Table 1 Material Properties..... 133

Table 2 Thermal load distributions..... 138

Table 3 Sample data for training a prediction model (Case study 1, thermal distribution 22)..139

Table 4 Sample of prediction model parameters after training (Case study 1, thermal distribution 22)..... 139

Table A1 Computational time comparison..... 150

Section 5.3 - A robust prediction model approach to energy geo-structure design

Table 1 Material properties..... 160

Table 2 Thermal load distribution combinations..... 161

Table 3 Design parameter values for different site and wall conditions analysis..... 162

Table 4 Total pipe circuit length per wall section modelled for different values of L_{wall} and s. 162

Table 5 Absolute error (°C) in predictions for the specific case study..... 164

Table 6 Prediction errors (°C) for each thermal load distribution at two particular times..... 164

Table 7 Prediction errors (°C) for each thermal load distribution, when training the prediction plane with 0.45C0.65H and 0.5C0.5H..... 167

Table 8 Using machine learning algorithms to predict the cooling coefficient A..... 170

Page intentionally left blank

Chapter 1 Introduction

Managing energy resources, reducing energy consumption and moving towards cleaner sources of energy are amongst the key challenges for the 21st century. A technology that can contribute towards these goals is shallow geothermal, which can be used to efficiently provide thermal energy for space heating and cooling. Shallow geothermal or ground-source heat pump (GSHP) systems are based on utilising the ground within a few tens of metres under the surface as a heat source or heat sink. They take advantage of the fact that at that depth the ground temperature is relatively constant throughout the year and close to the annual mean atmospheric temperate of the geographic location. As a result, the temperature differential between this source/sink of heat (the ground) and the ambient space to acclimatise is typically smaller than for the case of air source heat pumps, which leads to a much-reduced need for external work to satisfy the thermal demands of the building. GSHP systems have proven to operate with high efficiencies, providing a low energy demand and carbon emission option to substitute or complement traditional alternatives. Moreover, unlike other intermittent renewable energy options, shallow geothermal energy is always available.

A relatively recent application of this technology is utilising geo-structures as ground heat exchangers (GHEs) instead of the traditional use of purposely built GHEs in borehole or shallow trenches. In 'energy geo-structures', geothermal technology is incorporated in underground structures primarily designed for geo-mechanical stability, such as piles, retaining walls or tunnels, to also provide thermal energy. By utilising underground structures not explicitly built for geothermal purposes, this approach significantly reduces the capital costs associated with GSHP installations, of which the highest cost is usually drilling and/or excavation. However, energy geo-structures also pose new challenges to geothermal design, since the (structural) restrictions placed on the associated geometry mean that provision of the entirety of the thermal needs of the building cannot be guaranteed and instead a hybrid system might need to be used, combining geothermal with an auxiliary system.

Overall, even though the potential of GSHP systems is widely acknowledged, there exist significant gaps and margins for improvement in our knowledge of how they can be better designed and utilised. This is particularly the case for energy geo-structure design, given its relative recent adoption as well as the very different geometries and conditions that can exist between different structures. Therefore, energy geo-structure design is usually undertaken on a case-by-case basis using complex and computationally expensive numerical modelling. This

fact, together with the limited available information on energy geo-structure design can lead to sub-optimal, overly conservative and/or excessively costly designs, which can be hard to realise, especially in a less established and still-forming industry. Another knowledge gap, that can be found in both traditional and energy geo-structure systems consists of potential disparities between design and installation of the systems (e.g., actual placement location of pipes rather than the planned location), which can have a significant influence on their thermal performance.

This doctoral research utilises detailed numerical modelling, statistical and machine learning techniques in combination with high performance computing to address these issues and contribute towards an easier widespread utilisation of shallow geothermal energy.

1.1 Research objectives

Based on the preceding information as well as the current state of available research and literature (as presented in Chapter 2) the research objectives are defined as follows:

- To investigate potential disparities between design and as-built installations of GSHP systems, learning from the research group's (colleagues and supervisors) extensive installation experience, and identify ways to overcome these.
- To contribute towards the currently limited literature on energy geo-structures, focusing on the less researched energy retaining walls, by utilising numerical modelling to evaluate their thermal performance and study important design parameters that affect this performance, such as the thermal demand distribution, the pipe configuration and the geo-structure geometry.
- To develop and evaluate methodologies that can minimise the long computational time and large resources associated with numerical modelling of GSHP systems, utilising statistical, machine learning techniques and prediction models.

1.2 Thesis structure

This doctoral thesis is divided into six chapter and two appendices, including this introductory chapter which presents the research motivation, objectives and the structure of the thesis. Most chapters include published journal/conference papers, and where appropriate, additional analyses complementing the published work.

Chapter 2 presents a comprehensive literature review and background information on ground-source heat pump systems focusing on design methodologies and introducing the numerical

finite element approach utilised throughout this research. Moreover, a shorter section on machine learning is presented to provide a general understanding of the field.

Chapter 3 presents an investigation on the effect of variable pipe separation within GHEs, which poses a common and important disparity between design and as built installation of GSHP systems. The chapter introduces the effect, shows its potential significance and impact on thermal performance of the GHE field and concludes by introducing a methodology to address this in design.

Chapter 4 presents a detailed investigation on the thermal design of energy geo-structures. Firstly, a short section on energy piles is presented, summarising the published work on a case study in Argentina that can be found in Appendix A. Following, the numerical modelling of energy retaining walls and a number of detailed analyses on their thermal performance are presented, evaluating how various important design parameters affect it and providing suggestions on their utilisation. These analyses are performed for both soldier pile and diaphragm retaining walls and relate to a real technical feasibility study performed for the upcoming Melbourne Metro project. Some reflections on this project are also provided, noting the lack of available literature and research in this area and how the presented analyses can be useful in a real project. Lastly, a section on the importance of the boundary conditions that are newly introduced with energy retaining wall design is presented.

Chapter 5 presents two statistical approaches that can be used to complement the preceding numerical modelling and significantly reduce the associated computational time and resources. The two different approaches follow a similar methodology and can be used for any structure geometry and conditions but, as explained in a following section, they have important differences and are better suited for different situations.

Chapter 6 presents the concluding remarks and recommendations for future work.

The two appendices consist of published works. In the first, the author was a collaborator but not the main contributor and the second is a conference proceedings paper for which the author was the main contributor. These are:

- Appendix A: Geothermal Energy in Loess. Published in Environmental Geotechnics and awarded as Best of Research and Practice 2016. Co-authored with supervisors Associate Professor G.A. Narsilio and Dr. A. Bidarmaghz and collaborators from Argentina.

- Appendix B: The application of retaining walls and slabs as energy structures in underground train stations. A conference paper published in the proceedings of the International Symposium on Energy Geotechnics (SEG-2018) co-authored with supervisors Associate Professor G.A. Narsilio and Dr. A. Bidarmaghz

Chapter 2 Literature review

2.1 Overview and structure

This section presents the literature review and background relating to this research, which is divided into two main parts: Geothermal energy (section 2.2) and machine learning (section 2.3). These two sections comprise the main areas associated with this research, geothermal energy being the principal one.

Section 2.2 introduces geothermal energy, focusing on shallow geothermal or ground-source heat pump systems that are of most interest to this research. The motivation behind investing in this technology and the potential benefits are presented, as well as the key design methodologies with their respective limitations. Of particular note is the introduction of energy geo-structures and their respective design approaches, which is a relatively recent concept in shallow geothermal design. The majority of this doctoral research focuses on energy geo-structures.

Section 2.3 introduces the field of machine learning, focusing on the approaches and algorithms most relevant to the scope of this research. Examples of how this field has been utilised within the area of geothermal energy are also presented, indicating the applicability and potential of this approach. Lastly, section 2.4 presents a summary of this chapter. It should be noted that additional and more focused literature has also been included in the integrated publications.

2.2 Geothermal energy

2.2.1 Need for change

Energy provision is fundamental in modern life and the developed world. As technology advances, living standards improve and the world population increases, the demand and consumption of energy are ever growing and are bound to eventually surpass the available supply. Currently, the biggest source of energy provision globally is fossil fuels at about 80% [1], as seen in Figure 2.1, a number not expected to change much even by 2040 [2]. Other than the well-known facts about the environmental threats of fossil fuels, such as its significant impact on climate change and the urban heat island phenomenon, another big concern is their availability. Since there is a limited quantity in the world, which is constantly decreasing, humanity cannot rely on using these as its main source of energy. Therefore, the need for renewable energy is more urgent than ever and researchers worldwide are trying to discover

efficient ways to harvest renewable clean energy and move away from the diminishing and environment threatening fossil fuels.

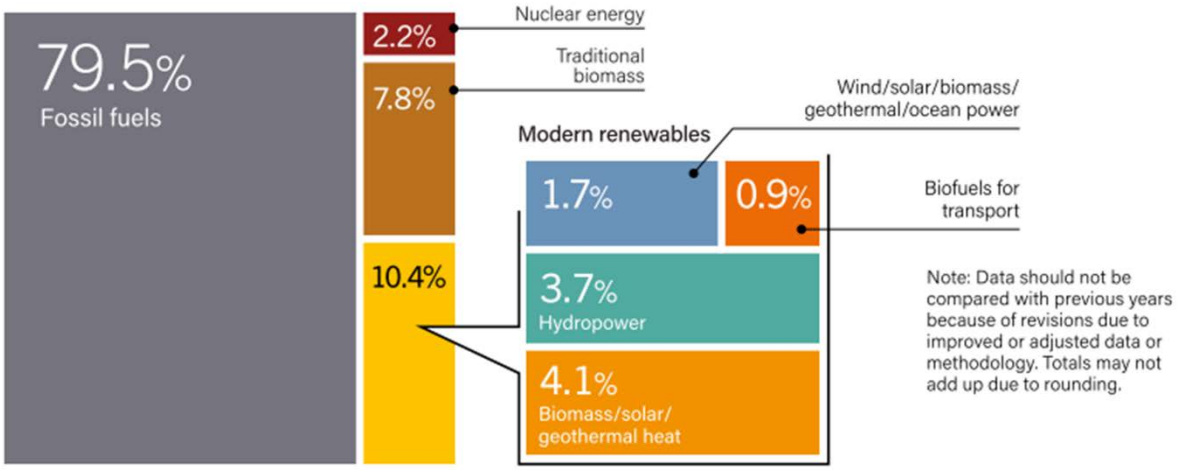


Figure 2.1 Estimated Renewable Share of Total Final Energy Consumption, 2016 [1]

2.2.2 Geothermal energy systems

2.2.2.1 Key principles

Geothermal energy is a clean and renewable energy source that comes from the interior layers of the ground. It can be accessed directly, used for the provision of heating and cooling to buildings, as well as indirectly, for power generation [3]. It is a very promising industry, with about 12.5 GW produced power within 2015 across 82 countries, with that number expected to reach 32 GW by the early 2030s [4]. Direct geothermal energy systems use the ground within a few tens of metres from the surface as a heat sink (cooling) or heat source (heating), utilising the fact that at that depth, after what is called the zone of seasonal fluctuation, the ground temperature is relatively constant throughout the year [5]. For Melbourne, this zone is approximately 5 to 10 metres and the temperature is close to 18 °C [6–8], as shown with experimentally measured ground temperature data in Figure 2.2.

Ground source heat pump (GSHP) systems use direct geothermal energy to efficiently cool and heat buildings. There are three main components to these systems: the primary circuit, the heat (and circulation) pump(s) and the secondary circuit, shown in Figure 2.3. The heat is transferred from and to the ground via a series of ground heat exchangers (GHEs), forming the primary circuit, while the heat pump upgrades and transfers the heat to and from the building through the secondary circuit, usually using air or water as the medium. A GHE contains loops (usually high-density polyethylene or HDPE pipes) with a circulating fluid (usually water) that acts as the heat conductor. Figure 2.4 shows a schematic of the GSHP system including the primary

circuit operating in the winter (cooling) and summer (heating) transferring the heat to/from the ground. This process of heat transfer between the circulating fluid within the GHEs (primary circuit) and the ground is the focus of this research.

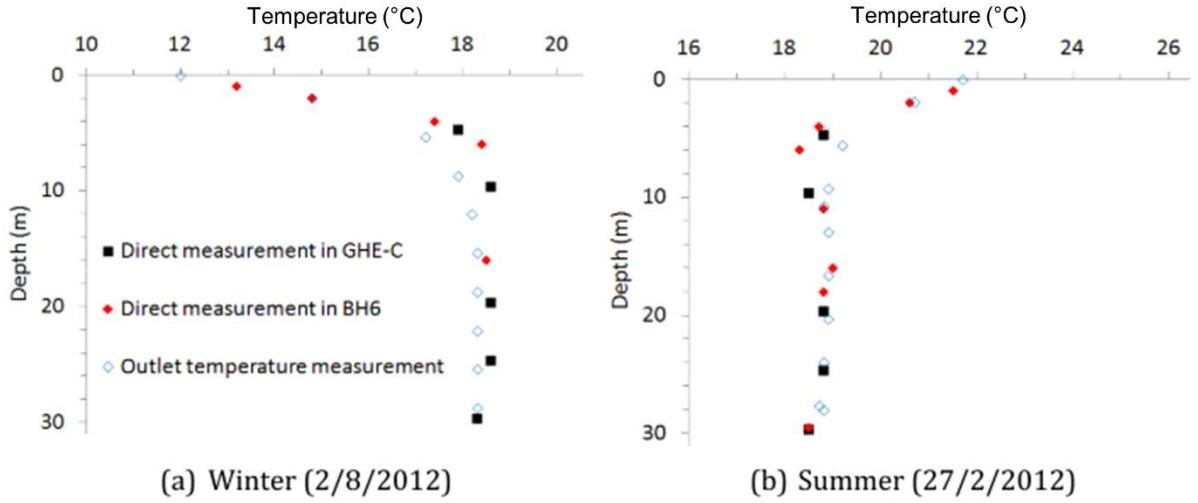


Figure 2.2 Ground temperature with depth in Melbourne, Australia using two different measurement methods [6]

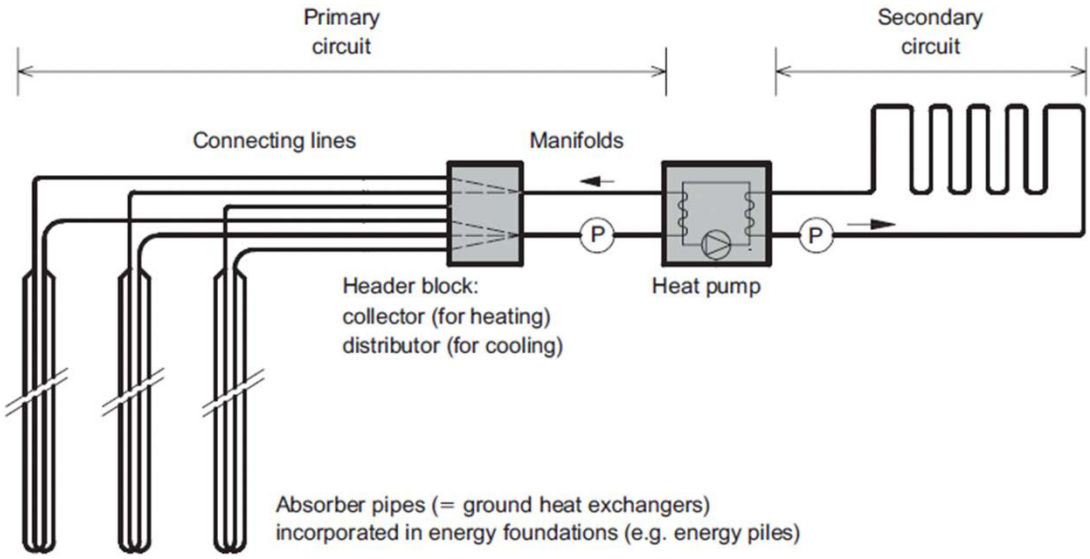


Figure 2.3 GSHP system schematic illustrating the heat pump connecting to the primary and secondary circuits [9]

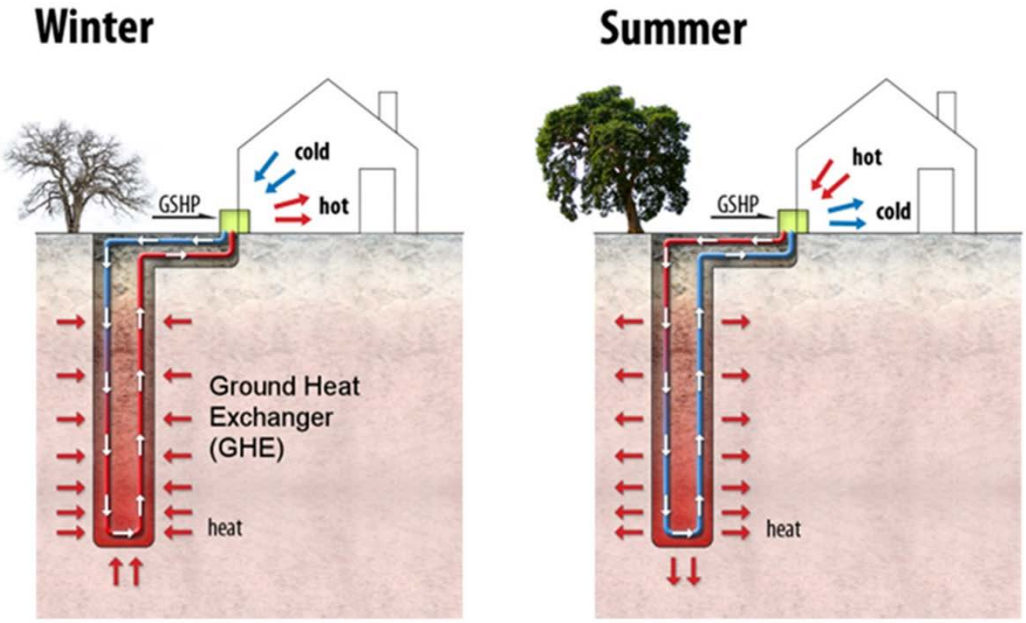


Figure 2.4 Schematic of a GSHP system in heating (winter) and cooling (summer) modes (Note: not to scale) [10]

2.2.2.2 Types of direct geothermal energy systems

GSHP systems can be 'open' or 'closed', as illustrated in Figure 2.5. The first type uses two separate wells, one for extraction and the other for re-injection of groundwater (Figure 2.5 (a)) and typically has hydrogeological requirements to be practical, such as a sufficiently high hydraulic conductivity, as well as can be regulated for water abstraction discharge [11]. The second type, which has less constraints and is of most interest to this research, uses HDPE pipes embedded in the ground or in boreholes (or piles/slabs/trenches) to circulate the fluid, thus creating a GHE. Compared to open loop systems, they are suitable in a larger variety of conditions, even though they are more dependent on the balance of the provided energy (same amount of heating and cooling being most optimal).

Closed systems can be arranged either horizontally (Figure 2.5(b)) or vertically (Figure 2.5(c)). Horizontal systems are generally cheaper and easier to install but require much more land. Due to the shallow depth of their placement (typically up to about 2 m), the temperature of their surroundings is not as stable as deeper in the ground, which affects their performance. However, it is easier to use a greater length of pipe, which can compensate for this effect. Vertical systems typically require a significant amount of drilling, which forms the largest part of their installation costs. However, they are more efficient and do not usually require as much piping and certainly not as much land as the horizontal systems [12]. It is also feasible to incorporate them into buildings under construction by using, for example, structural piles as GHEs (i.e., energy piles), thus creating *energy geo-structures*.

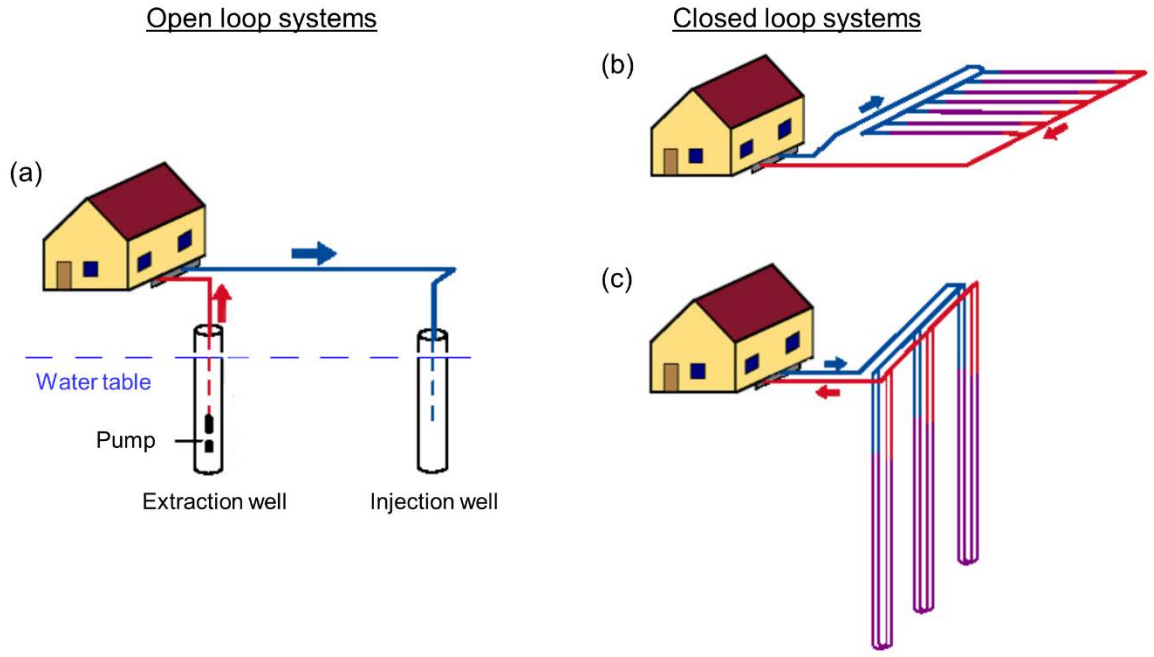


Figure 2.5 Direct geothermal systems: open loop (a) and (reverse return) closed loop in horizontal (b) and vertical (c) GHE configurations [13]

2.2.2.3 Energy geo-structures

In order to reduce the relatively high capital costs of traditional vertical GSHP systems, mainly due to drilling borehole GHEs, over recent years there has been a growing interest in the concept of energy geo-structures [14–17]. These structures are primarily underground structural elements, such as piles, retaining walls, tunnel linings and foundation slabs, which are required for structural stability. However, it is comparatively easy to incorporate HDPE pipes in these structures, also turning them to GHEs at relatively small extra cost, thus making energy provision their secondary function, after structural/geo-mechanical stability. A detailed presentation of some of these costs can be found in the literature [18]. Figure 2.6 shows examples of energy pile installations with the embedded HDPE pipes.

The main energy geo-structures that have been implemented and researched by the international communities are energy piles, energy retaining walls and energy tunnels. The majority of investigations on energy geo-structures have focused on energy piles (i.e. implementing the GHE pipe loops in structural piles) [15,17,19–22], possibly because of the geometrical and pipe configuration similarities between piles and boreholes. Energy walls can be created by adding geothermal pipe loops into retaining walls. There exist cases in which energy walls have been adopted, where most of them consist of small scale installations/sections mainly for monitoring, rather than full scale projects [23–25]. Typical retaining wall types that can be utilised include diaphragm and soldier pile retaining walls.

These two different wall types allow for different configuration/placement of the pipes and therefore a different geothermal design. Similar to energy walls, slabs can also be potentially incorporated with geothermal piping to be turned into energy geo-structures, given that they are placed directly above the ground, which can be used as a heat source/sink. Lastly, energy tunnels are formed by incorporating geothermal pipe loops in the tunnel linings. Some energy tunnel installations exist, mostly for experimental purposes, in Italy, Austria, United Kingdom, Germany and South Korea amongst others [26–29]. In Australia, the widely known Melbourne Metro, one of the country's largest scale infrastructure projects, funded a comprehensive study considering the implementation of geo-structures in the metro stations [30,31]. Parts of this study, investigating the integration of geothermal pipes in the underground station retaining walls and slabs are presented within this thesis.



Figure 2.6 Energy pile installations - collected within the University of Melbourne geotechnical research group

Overall, the research on energy geo-structures has centred around two categories: the first investigating the thermal performance of the structures and how their thermal capabilities can be maximised or enhanced [21,32,33] and the second investigating the geo-mechanical effects and the potential adverse structural stability effects due to the heat transfer [34–37]. The research relating to the second category has generally shown that no significant geo-mechanical issues arise from the operation of energy piles (unless when embedded in normally

consolidated clays) [9,36,38]. Limited information exists regarding these effects on other energy geo-structures, with some recent studies reporting a less negligible/more significant effect on energy walls [39–41]. The work presented herein is part of the first category and does not consider the geo-mechanical aspect of energy geo-structures, but rather focuses on the efficiency of the heat transfer process and how the design process can be enhanced.

2.2.2.4 Significance of shallow geothermal energy systems

Harvesting geothermal energy and investing in its development and further understanding can have significant economic and environmental benefits. Geothermal energy is not only renewable but also always available, something that is not true for other renewable sources like solar or wind. Moreover, it is highly efficient producing approximately 4 kW of clean thermal energy for every 1 kW of electricity required to run the system [11,42].

In Australia, more than 90% of the energy consumed is generated from fossil fuels [43] and therefore reducing the dependency on these fuels and increasing the amount of renewable energy being used is a critical issue. Looking at the residential sector, comprising about 11% or 458 PJ (10^{15}) of Australia's entire energy consumption [43], space heating and cooling accounts to about 40% of the consumed energy for a typical Australian household [44]. To satisfy this space heating and cooling demand, the main fuels used are natural gas, electricity, LPG and wood. Incorporating direct geothermal energy systems as an alternative to these would result in a reduction in energy consumption of about 100 PJ annually, which is approximately the equivalent savings in annual greenhouse gas emissions as removing 4.42 million cars from the road per annum [45]. Incorporating this technology in other industries, such as commercial, can even further aid in energy savings and reductions in greenhouse gas emissions.

Overall, there are numerous reasons to invest in shallow geothermal energy systems and aim to better understand their performance and behaviour. Brandl provides a comprehensive list of the benefits of shallow geothermal energy technologies (emphasising on energy), some of which are quoted below [46]:

- Environmentally friendly (non-polluting, sustainable energy).
- Reduction of fossil energy demand, hence of CO2-emissions.
- Economical, at least in the long-term.
- Low maintenance and long lifetime.
- Geothermal energy systems run fully automated.

- Geothermal energy may be easily combined with other energy systems.
- Geothermal energy is readily available and non-intermittent, as are other renewables.
- The cost of geothermal energy is not prone to unpredictable price fluctuations.
- Positive public image, and in several regions is supported by government grants.

2.2.3 GSHP system design

During the design process of a GSHP system, once the thermal load to be satisfied is estimated, some critical parameters need to be determined, for example the length of pipe in the GHEs, the configuration of the loops and the backfilling material to be used. All these parameters will define the thermal performance and efficiency of the system and therefore the viability and economic justification for its use. There exist various methods that can be used to design the GHE field in this design process, mainly based on `Analytical' and `Numerical' solutions.

2.2.3.1 Analytical solutions

The analytical solutions use a number of assumptions to model the geometry and conditions of a geothermal energy system typically in 1 or 2 dimensions. There are three main models that are currently used: the Infinite Line Source (ILS) model [47,48], the Infinite Cylindrical Source (ICS) model [47,49] and the Finite Line Source (FLS) model [47,50].

A schematic representation of the three models can be seen in Figure 2.7. All models calculate the conductive heat transfer between the ground and the GHE, for a constant unit power rate, using the temperature difference between them [51,52]. ILS makes the most approximations and considers the GHE as an infinite line, ICS similarly considers the GHE as an infinite hollow cylinder and FLS is the most sophisticated and makes the least approximations by considering the GHE as a finite line. FLS can also calculate the steady state temperature, unlike the others [52]. The key equations related to these approaches are provided in Equations (1), (2) and (3) for ILS, ICS and FLS respectively, noting that several adaptations of these have been introduced throughout the years.

$$T_{(r,t)} - T_0 = \frac{q}{2\pi\lambda_{ground}} I(x), \qquad x = \frac{r}{2\sqrt{at}} \tag{1}$$

$$T_{(r,t)} - T_0 = \frac{2Q}{\pi\lambda_{ground}} \int_0^{\infty} \left(1 - e^{-\alpha v^2 t}\right) \frac{\left[J_0(vr)Y_1(vr_b) - J_1(vr_b)Y_0\left((vr)\right]\right)}{v^2[J_1^2(vr_b) + Y_1^2(vr_b)]} dv\,, \quad Q = \frac{q}{2\pi r_b}, v = \frac{r^2}{4at} \tag{2}$$

$$T_{(r,z,t)} - T_0 = \frac{q}{4\pi\lambda_{ground}} \int_0^H \left[\frac{1}{r_1} erfc(x_1) - \frac{1}{r_2} erfc(x_2)\right] dh\,, \qquad x_i = \frac{r_i}{2\sqrt{at}} \qquad (3)$$

where $T_{(r,t)}$ is the temperature at a radial distance r and at a given time t [K], T_0 represents the farfield ground temperature $[K]$, q represents the constant power per unit length of GHE $[W/m]$, r is the distance from the line source $[m]$, λ_{ground} is the ground thermal conductivity $[W/(mK)]$, a is the ground thermal diffusivity $[m^2/s]$, t represents the time $[s]$, $I(x)$ is the exponential integral function, J_0, J_1 are Bessel functions of the first kind of order 0 and 1, respectively, Y_0, Y_1 are Bessel functions of the second kind of order 0 and 1 respectively, $T(r,z,t)$ represents the temperature near or at the GHE wall at the depth of z at a given time t [K], H is the GHE length [m] and $erfc$ represents the complimentary error function.

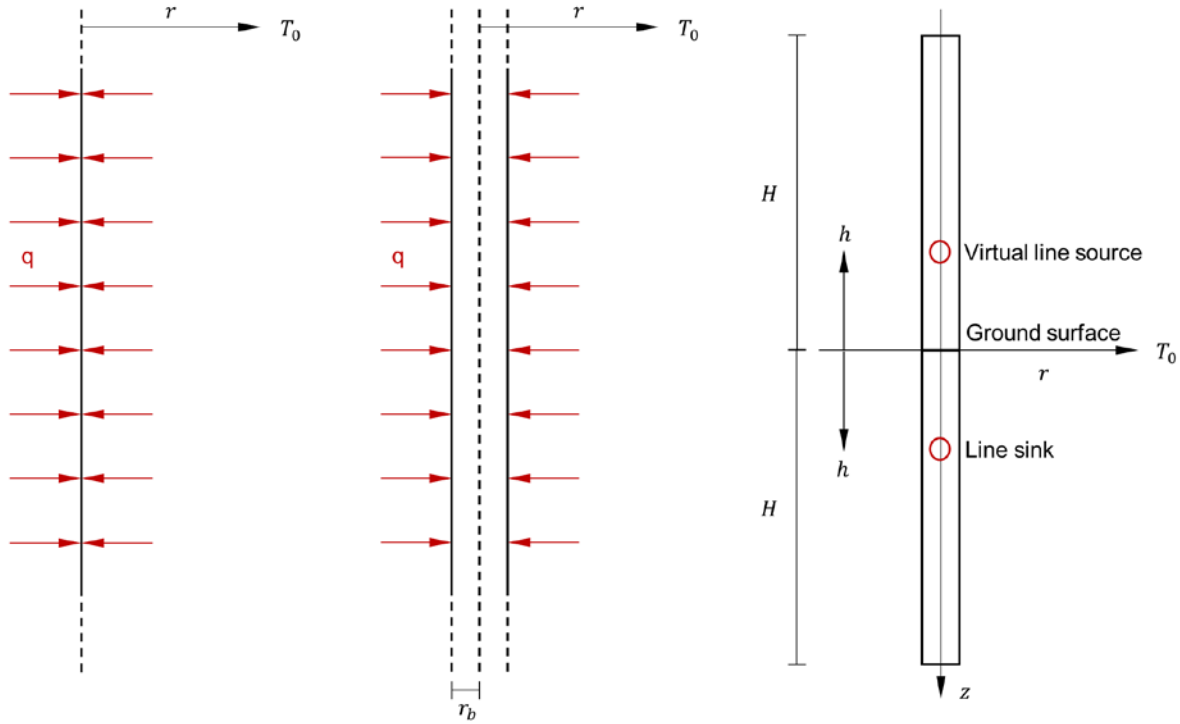


Figure 2.7 Schematic of (a) ILS, (b) ICS (c) FLS

Due to their assumptions, most analytical models are not able to capture the problem in its entirety. Some important elements are ignored, for example the axial heat transfer from the top and bottom of a GHE (ILS and ICS) or the non-traditional incorporation of the components within the GHE. Moreover, the performance of analytical solutions is especially poor for short term conditions [51] and the constant heat flux assumed limits the model's applicability for realistic conditions, even though methodologies have been developed to overcome this limitation, utilising the concept of load aggregation/superposition [53–55]. Arguably the most important limitation is the inability to properly model different geometries (GHE configurations and placement), and to properly take into account the effect of thermal

interference. However, due to their simplicity they are able to be easily implemented into design approaches or software [56], particularly for (vertical) borehole GHEs (and energy piles – with modifications [57–60]).

2.2.3.2 Numerical solutions

Several numerical models have been created to further understand the underlying processes involved in heat transfer, as well as for design purposes. Most models use finite element methods (FEM) in one, two or three dimensional space to compute the solutions [50,52,61–79]. The models were developed using various tools (for example TRNSYS) and the main differences between them are the scope of their modelling (i.e. short term/long term response), the equations they choose with which to model heat transfer and fluid flow, the detail with which they model different physical aspects, and how the boundary and initial conditions are set. Some were developed to investigate specific purposes or for specific geometries, making them of little use outside that scope.

It is worth discussing some key milestones in the chronological evolution of numerical simulations. It is also worth noting that technological advancements played an essential part, as the lack of computational power has been a major limitation of many models. Eskilson and Claesson first presented in 1988 [50] a 2D model combining analytical and numerical approaches, that calculated the temperature distribution of a GHE field. The model made several assumptions including neglecting the GHE thermal resistance and capacitance and provided results for a single GHE, proposing the use of superposition to account for multiple GHEs. They also developed `g-functions' using a numerical model, as described below, however, their model could not be used with short time steps, but only for long term. Overcoming this limitation, as well as other assumptions made, was the 2D finite volume model proposed by Yavuzturk et al in 1999 [71], expanding on the work of Eskilson, but still having limitations, like the inability to properly model the fluid. In 1997, Rottmayer et al [73] presented a transient numerical model, which considered the ground as a cylinder and was based on an explicit finite difference approach to the three dimensional transient conductive heat transfer in the ground. Also in 1997, Thornton et al [74] presented a detailed component-based simulation model, using TRNSYS as the software for detailed modelling and Hellstrom's duct storage model [80] to model GHEs. The model assumes conductive heat transfer in the ground and convective in the boreholes and uses superposition of three different solutions to obtain results. In 2008, Nam et al [78] developed a 3D simulation code modelling the heat transfer and the water transport in the ground, which included a GHE model with U-loop pipes.

The model used the finite element method code FEEFLOW and adapted it appropriately. The GHEs were modelled with a 1D advection-diffusion equation and convective heat transfer within the pipe. Also in 2008, Marcotte et al [79] developed a transient 3D finite element model, which even though accounted for some of the effects ignored in earlier models, did not incorporate others, such as axial effects. These effects were included in later work of the authors and were found significant. In 2010 Lazzari et al [64] developed a 2D finite element model to evaluate the long term thermal performance of double U-loop pipe fields within a year. The model ignores the temperature distribution along the depth and converts the 3D heat transfer problem to a 2D conduction model. In 2012, Al-Khoury et al [52] presented a 3D finite element modelling technique for double U-loop GHEs, by using 1D elements to simulate the 3D heat flow within the borehole and 3D elements to model the coupled heat and groundwater flow surrounding the borehole. In 2013, Rees et al [68] developed a 3D model for a single GHE that correctly represented the ground, pipes, fluid and grout. More recently, Ozudogru et al [69,70] developed a 3D numerical model for simulating vertical U-tube GHEs. 1D linear elements were used for the fluid flow in the pipes, coupled with 3D elements representing the heat transfer in the rest of the geometry. The model assumes a constant difference between the inlet and outlet fluid pipes.

The main advantage of numerical models and simulations in general is the lack of constraints regarding the site geometry and configuration. Moreover, the results obtained can contain much more data and also are usually more accurate, due to the higher detail and less assumptions in the model. However, because of their detail, much more computational time is needed, which is their main drawback and makes it harder to incorporate them to standardised design approaches or software [56].

It is also worth mentioning that using a finite difference numerical model, a set of approximation functions called `g-functions' were introduced [50]. The main concept of these semi-analytical functions is to capture the thermal behaviour of a GHE field and to relate the heat flow rate to/from the ground to the GHE wall temperatures, a seen in Equation (4). There are many different functions each representing a specific borehole configuration. They are used to easily (but approximately) calculate the temperature at the GHE wall, using dimensionless variables that define, for example, the geometry and/or simulation time. Since their initial introduction, several different forms of `g-functions' were created, each with its own approximations and assumptions [81–85]. These functions are used extensively with the

analytical solutions mentioned above as approximations to much more complex thermal transfer equations.

$$T_b - T_0 = \frac{q_0}{2\pi\lambda} g\left(\frac{t}{t_s}, \frac{r_b}{H}\right), \qquad t_s = \frac{H^2}{9\alpha} \tag{4}$$

where T_b is the borehole surface temperature (K), T_0 is the initial temperature of the ground [K], q_0 is the GHE heat flux [W/m], λ is the thermal conductivity of the ground [W/mK], t is time [s], t_s is the time when the steady-state condition has been reached [s], r_b is the borehole radius [m], L is the borehole length [m] and α is the thermal diffusivity [m^2/s].

2.2.3.3 Energy geo-structure design

The most important difference between energy geo-structures and traditional GSHP systems is the fact that the former are primarily designed for structural purposes, which results in these structures having geometrical or material parameters pre-determined and outside the scope of the geothermal design. Therefore, their use as GHEs usually introduces some limitations for thermal design. One of the most significant limitations is that when utilising energy geo-structures, the provision of the entirety of the thermal demand may not be possible. Instead, the systems need to be thermally designed to provide as much energy as the structural design allows with an auxiliary system providing the balance of the required thermal energy thereby forming a hybrid system [86–88]. Other than the geometry of the structures, the location is also pre-determined. Therefore, the spacing between, for example piles, cannot be specified for the geothermal design, making the GHEs prone to thermal interference if the energy piles are placed too close to each other and resulting in the need for careful consideration of these effects in the design. Moreover, the variability in types of structures (for example continuous flight auger or rotary bored piles [89], diaphragm or soldier pile retaining walls) as well as different construction methods, provide new challenges for the design of the geothermal components, as more processes need to be considered.

One approach to energy pile design is to use analytical solutions for borehole design, due to the similar geometry, however Fedejev et al. [90] advise against this approach and state that there is a notable absence of available reliable design tools for energy piles, and limited information on how the design can be undertaken and how efficient the technology can be. Nevertheless, some design approaches have been presented for energy geo-structures, such as software packages [91,92] as well as semi-analytical ones, such as developing g-functions for the design of energy piles based on their geometry [58,89,93]. The latter approach has been

validated for the short-term response, using thermal response tests, on small diameter piles; however, validation is still pending for longer term and for larger diameters, likely due to the absence of appropriate field datasets [59]. Still, the most significant disadvantage for analytical solutions (as is the case for traditional system design) is the fact that they adopt a large number of assumptions, which introduces substantial limitations. Therefore, significant amount of research has been devoted to numerically investigating the thermal performance of these structures usually adapting the models used in traditional borehole design, discussed in section 2.2.3.2, given the similarity in the associated geometries. Fedejev et al. [90] provide a comprehensive review of some of the developed analytical and numerical models for energy pile design, concluding that no model was found that was capable of simulating an energy pile field's thermal performance with a high level of detail.

Typical retaining wall types that can be utilised as energy geo-structures include diaphragm and soldier pile retaining walls. These two different wall types allow for different configuration/placement of the pipes and therefore a different geothermal design. Some work has been carried out, specifically regarding diaphragm walls, in further understanding how the design of energy walls can be undertaken, including drawing from energy pile design knowledge [94] as well as an electrical analogy that models resistance [95]. However, due to the large number of potential designs and configurations as well as the limited available literature on energy retaining walls, there is a lack of a standardised design approach and therefore design is undertaken on a case by case basis, typically adopting complex detailed numerical approaches (such as finite element methods) [39,40,96–99]. Moreover, the introduction of a less symmetrical geometry, including corners (such as between retaining wall and slab) makes heat transfer more challenging to predict/analyse compared to, for example, boreholes and piles. The design of energy tunnels, embedding geothermal loops in the tunnel lining, is similarly mostly undertaken using detailed numerical simulations, even though some analytical solutions have been proposed [100]. This is due to the complex and different geometries and conditions that can exist and the more comprehensive results that can be obtained (such as visual representations of the heat transfer through the different media). Moreover, with numerical approaches, effects such as the impact of groundwater flow on the system's performance can also be investigated [96,101].

Furthermore, there is a significant difference between energy retaining walls or energy tunnels and other GHE structures such as boreholes or energy piles. This is the fact that these two structures are only in contact with the ground on one of their sides, while the other side usually

consists of the inside of the tunnel or the underground level of the building/structure, the latter illustrated in Figure 2.8(a). Therefore, heat transfer on the building side of the retaining wall must be controlled, as it can affect the system operation negatively. For example, energy extracted from the ground and used to heat the basement on the inside of the retaining walls could be extracted by the retaining walls (leaked) to effectively short circuit the system. This is, therefore, a serious issue that must be considered during design and a constraint that energy piles or boreholes do not have since they are surrounded by the ground (Figure 2.8(b)). Currently, limited information exists on this issue; Bourne-Webb et al. explore this aspect of energy wall design, adopting steady state conditions, but emphasising that a greater understanding of this effect is required [102]. In the case of energy tunnels, generated heat inside the tunnel could be used in combination with the ground as a heat source, if applicable [103].

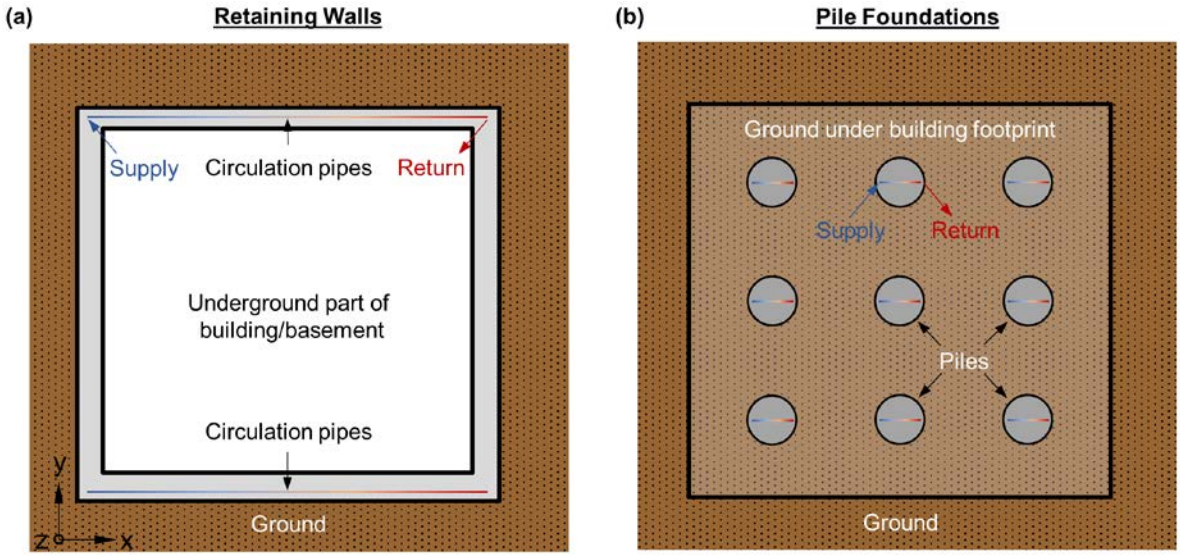


Figure 2.8 Schematic top view of energy retaining wall (a) and energy pile (b) GSHP systems, highlighting the difference in the ground area around them

2.2.3.4 System viability and the fluid temperatures

A main objective in the GHE design process is that the resulting (outlet) fluid temperatures, meaning those of the liquid within the GHE loops, are within an acceptable range. Firstly, they need to comply with commercial heat-pump specifications and secondly, to avoid an extreme response from the ground (for example freezing). If the resulting fluid temperatures for a specific system design are not acceptable, then the design is not viable. These fluid temperatures have proven to depend on various parameters such as the geometry of the site, the design thermal load distribution (the energy to be supplied) and the ground material properties such as thermal conductivity, amongst others. Throughout the presented research,

the fluid temperatures are used to assess and quantify the viability and thermal performance of designed systems as well as the potential for improvement in the design (such as providing more energy).

2.2.3.5 Lack of universal design approach

As explained above, there are different analytical and numerical design solutions, all with their advantages and disadvantages. In industry, several software can be used [92,104–108], using mostly analytical solutions and g-functions to find fast but approximate results. Usually, the main aim of the software is sizing the GHEs and identifying the total length of pipe required. However, different methods can produce different results [90,109–111], suggesting that there is still much room for improvement. Moreover, these improvements need to be easy to implement, so that they can be incorporated into existing methodologies.

In the case of energy geo-structures this issue is of even more significance, since there is less information on design approaches, compared to traditional systems, due to the comparatively less amount of research and installations being done and the greater variability in possible geometries, structures and conditions. Since no standardised design approaches exist, the thermal design of energy geo-structure is typically undertaken on a case by case. It commonly adopts numerical modelling, which allows flexibility and the ability to take into account the different structures, geometries and conditions between geo-structures.

2.2.4 GSHP system design in this research - a validated numerical model

To undertake thermal performance investigations of various GSHP systems, this research utilises and expands upon a state of the art computational model that has been created within the University of Melbourne Geotechnical Engineering Research Group [112]. It is based on coupling heat transfer in the GHE components to the fluid flow within the pipes and is implemented in the finite element software package COMSOL Multiphysics. The heat transfer is predominantly modelled by conduction (mainly in the soil, GHE backfill, GHE wall as well as in the fluid) and convection (in the fluid and if applicable groundwater). The flow in the pipes is considered as fully developed and therefore 1D elements are used for the pipes, coupled to the 3D heat transfer in the remaining geometry. To model the 1D fluid flow, the continuity and momentum equations for incompressible fluid are used, as seen in Equations (5) and (6) [113]. The energy equation for the convective-conductive heat transfer in the fluid flow can be seen in Equations (7) and (8) [114]. In the absence of groundwater flow, the heat transfer in the soil, GHEs and pipe wall is modelled by Equation (9), under purely conductive conditions.

$$\nabla.(A\rho_w \boldsymbol{v}) = \mathbf{0} \tag{5}$$

$$\rho_w \left(\frac{\partial \boldsymbol{v}}{\partial t}\right) = -\nabla p - f_D \frac{\rho_w}{2d_h} |\boldsymbol{v}| \boldsymbol{v} \tag{6}$$

$$\rho_w A C_{p,w} \frac{\partial T}{\partial t} + \rho_w A C_{p,w} \boldsymbol{v} \nabla T = \nabla(A\lambda_w \nabla T) + f_D \frac{\rho_w A}{2d_h} |\boldsymbol{v}| \boldsymbol{v^2} + Q_{wall} \tag{7}$$

$$Q_{wall} = f\left(T_{m,pipe\ wall}, T\right) \tag{8}$$

$$\rho_m C_{p,m} \frac{\partial T_m}{\partial t} = \nabla.(\lambda_m \nabla T_m) \tag{9}$$

where A is the inner cross-section of the HDPE pipe $[m^2]$, ρ_w the carrier fluid density $[kg/m^3]$, $\boldsymbol{v}$ the fluid velocity field within the pipes $[m/s]$, t is time $[s]$, p is pressure $[Pa]$, f_D represents the Darcy friction factor [-], d_h is the hydraulic diameter of the pipe $[m]$, $C_{p,w}$ is the specific heat capacity of the fluid $[J/kgK]$, λ_w the thermal conductivity of the fluid $[W/mK]$, Q_{wall} is the external heat exchange rate through the pipe wall $[W/m]$ and a function of the temperature of the pipe outer wall, $T_{m,pipe\ wall}$ $[K]$, and the temperature of the carrier fluid T $[K]$, ρ_m the solid material density $[kg/m^3]$, $C_{p,m}$ the specific heat capacity of a solid material $[J/kgK]$ and λ_m the thermal conductivity of a solid material $[W/mK]$.

The model has been validated against a well-known two-dimensional analytical solution (FLS model) as well as full-scale experimental data, under a variety of conditions. It is able to accurately model laminar and turbulent regimes, homogeneous and heterogeneous soil profiles, different GHE configurations in steady state and transient conditions. Results of the validation for a single U-loop borehole in both a thermal response test (TRT) scenario as well as in normal heat pump operation can be seen in Figure 2.9 and, similarly, results for a three U-loop pile can be seen in Figure 2.10. A detailed explanation of this validation can be found in [112]. An extension of this model has also been experimentally validated for energy tunnels, obtaining very good agreement between the numerical results and the experimental data [101,115].

Overall, the presented numerical model is used as a foundation and building block for the presented research. Throughout this research the model has been utilised to investigate the thermal performance of GSHP systems and provide further understanding on the conditions that affect this performance. Moreover, the model has been further expanded, incorporating other structures and conditions. As part of this work, validation for energy retaining walls, using experimental data, is also presented, in section 4.3.2.2.

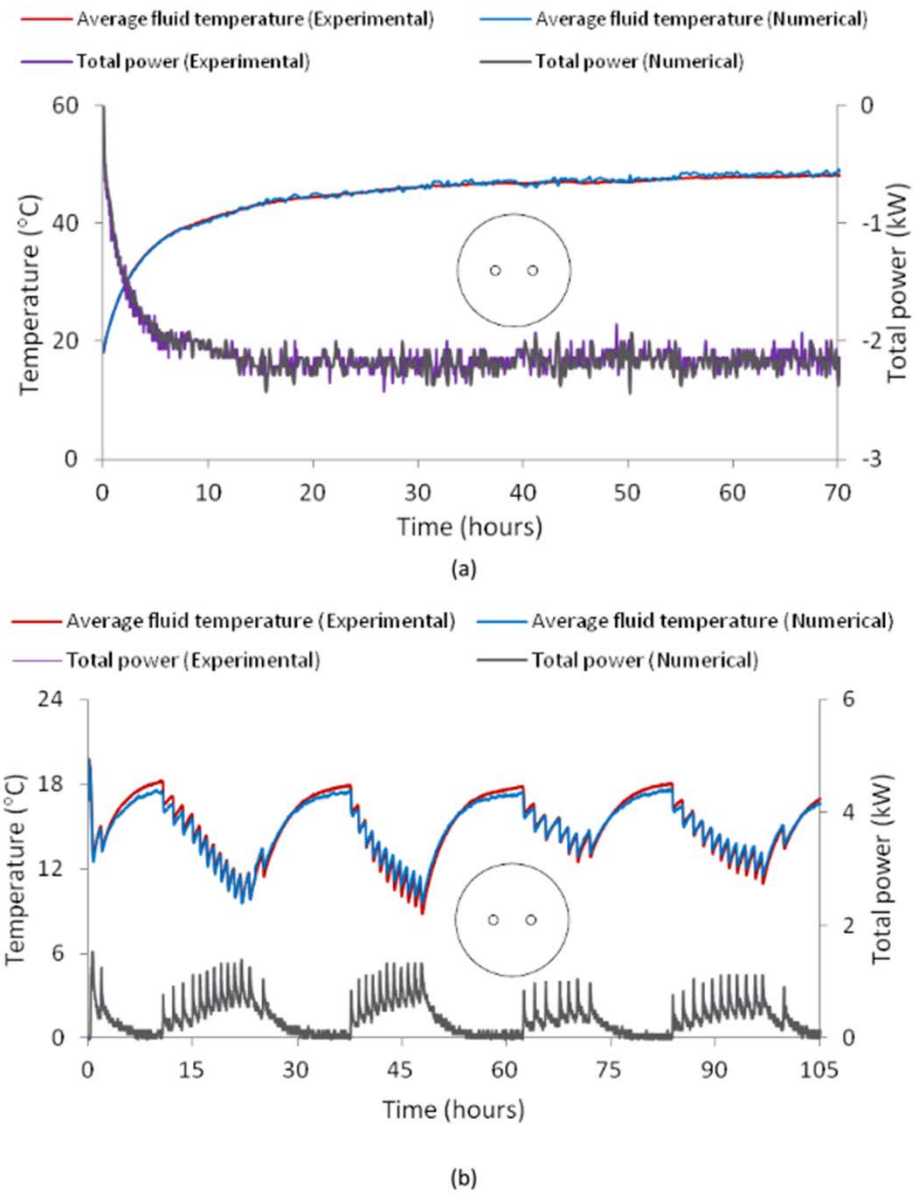


Figure 2.9 Finite element model validation: comparison between numerical and experimental results for single U-loop borehole: (a) a thermal response test (TRT19), (b) a 'normal' heat pump operation [112]

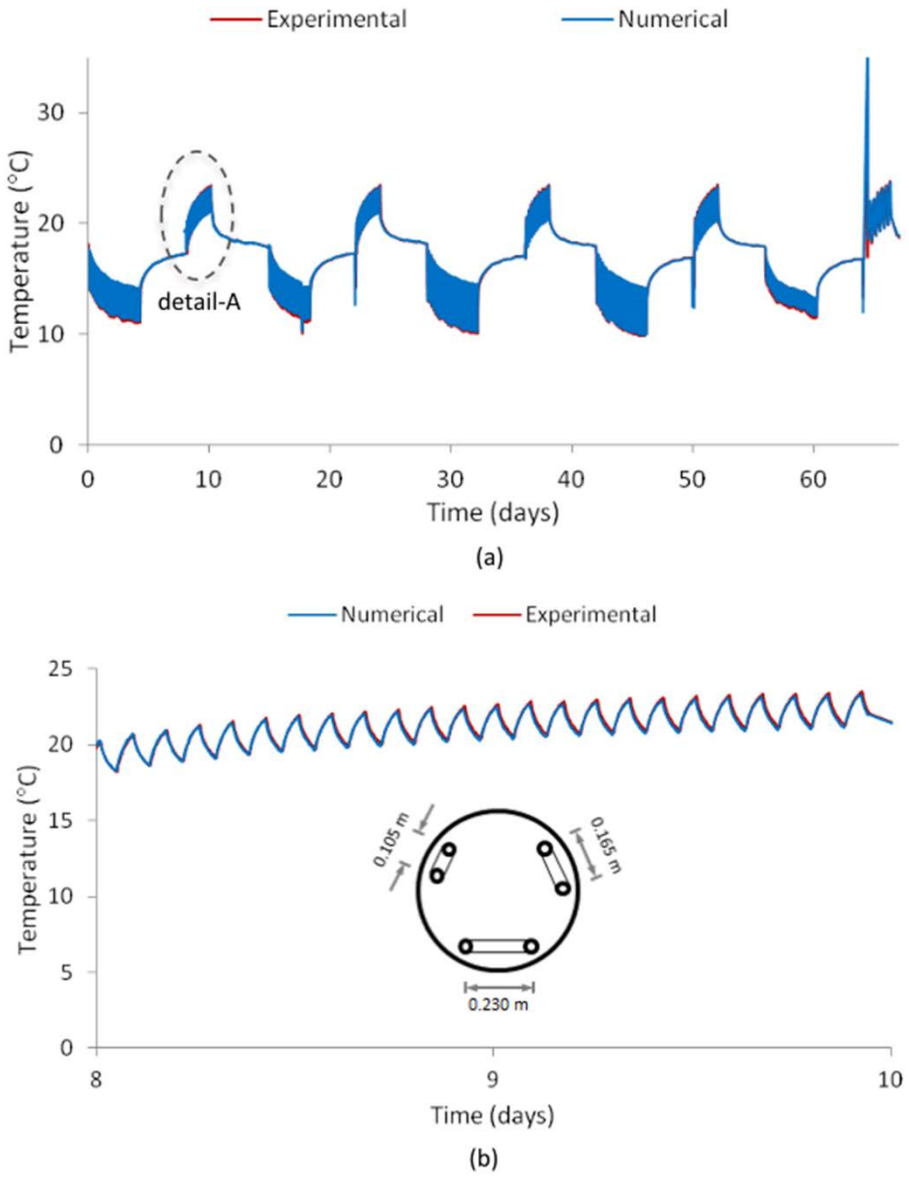


Figure 2.10 Finite element model validation: comparison between numerical and experimental results for pile: (a) a thermal response test (TRT19), (b) a 'normal' heat pump operation [112]

2.3 Machine learning

2.3.1 Overview

Machine learning (ML) is a computer science discipline that has gained a lot of popularity in the past few decades. It is closely linked with artificial intelligence and draws on many other disciplines such as statistics, philosophy, biology, information retrieval, psychology and others. Its main concept is trying to program a machine so that it can improve and "learn" over time, using a variety of techniques and algorithms. By learning, the machine can then aid in identifying patterns within (usually large) datasets, gaining knowledge, evaluating the importance of variables in a function, performing optimisation, fitting curves, estimating equations or functions and making predictions. The discipline is particularly known for

excelling at certain applications such as speech recognition and computer vision amongst others [116–118].

2.3.2 Types of learning

There are two main ways with which a machine learning model can learn, *Supervised* and *Unsupervised*, which also define two different problem natures [119]. Supervised learning is performed for problems that require the classification of data (either categorically or numerically). Therefore, the training data provided need to be "labelled", meaning that the outcome, which the model is trying to predict, is known. As an example, in order to train an image recognition model, required to identify dogs in images, a dataset of many images to learn from must be provided, each labelled as either showing or not showing a dog. Unsupervised learning is performed for problems where the machine does not know exactly what it is looking for, but instead needs to identify various patterns in the data. It usually involves clustering the data into groups that have common attributes [117]. An illustration of the difference between the two types of learning can also be seen in Figure 2.11. In the presented doctoral research, supervised learning has mostly been utilised, specifically the development of prediction models, to overcome the large computational times associated with GSHP numerical modelling, and the utilisation of feature selection techniques to gain insight on the importance of the various design parameters on different aspects of GSHP design and operation.

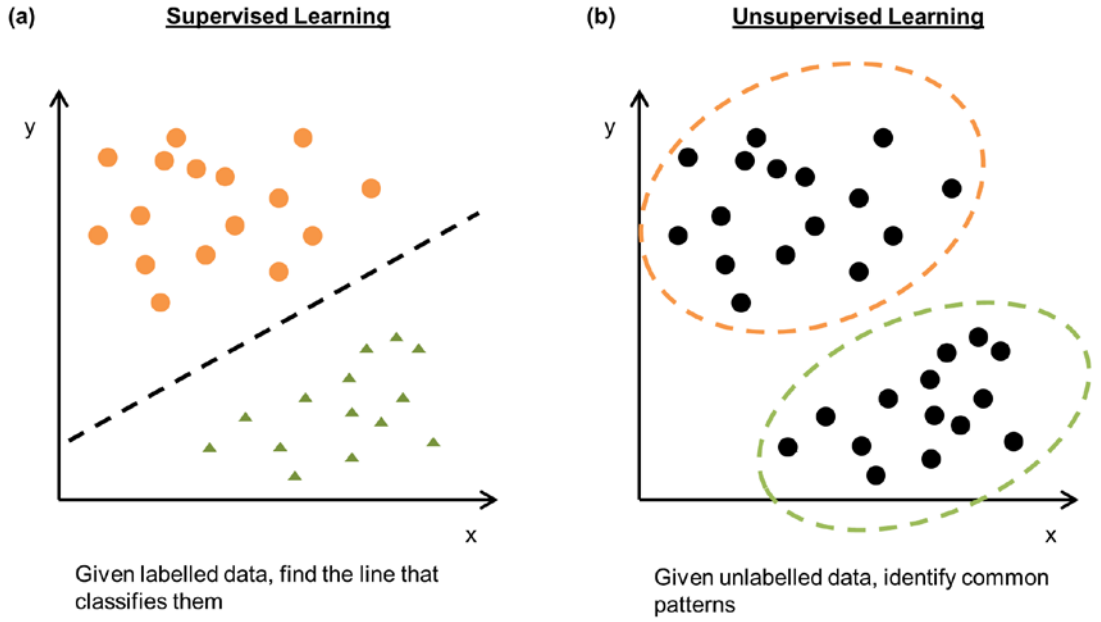


Figure 2.11 Machine learning types: (a) supervised and (b) unsupervised learning

2.3.3 Supervised learning: training and testing

As explained in section 2.3.2, supervised learning is the approach of making predictions based on known labels and therefore finding, understanding or simulating the relationships between data. In this case, the data are referred to as *input* and *output* where *input* represents the (generally known) data we provide to the prediction model and *output* the (generally unknown) data that the model predicts. The process involved in the creation of prediction models based on this approach has two main phases: *training* and *testing/predicting*, A simple representation of which is shown in Figure 2.12. During the training phase, both the input and output data are known and the algorithm attempts to find the parameters that best describe the relationships between them, in this case labelled β_ι. The type of the relationship is determined by the type of selected algorithm (the simplest example being linear regression) and its properties/parameters. Once the training phase has been completed, the created model needs to be tested to evaluate how well the model/calculated parameters β_ι represent the relationships between input and output. There are different ways for this evaluation, the most common being cross-validation, which is the process of training the algorithm with a subset of the available data and testing the created model with the remaining data (which the algorithm did not see prior) [120]. Therefore, by performing the prediction phase with data for which the output values are known, these known values can be compared with the output data the prediction model produces and evaluate how similar these are, by using metrics such as the root mean square error. Once the prediction model's accuracy is satisfactory, the model can be used for other/new values of input data and make predictions for the output data based on the relationships between them that it has established during the training phase and validated using cross-validation (amongst others).

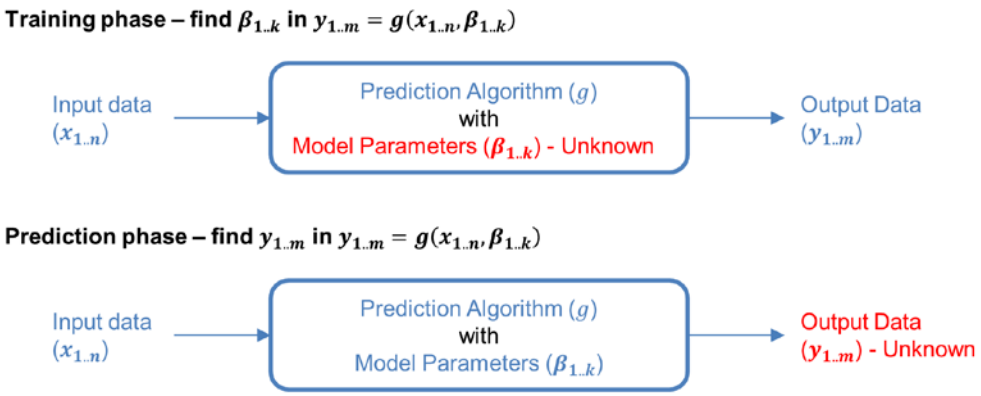


Figure 2.12 Supervised learning: Training and testing/predicting

2.3.4 Feature importance

A useful attribute of supervised learning algorithms is being able to classify the relative importance of the different input parameters with respect to the output parameters. This relative importance can therefore provide valuable insights about the strength of the relationships between the input and output data (or variables). For example, Figure 2.13 shows a sample decision tree (which is a supervised learning algorithm), that has been created to classify the stability of a slope based on different parameters such as soil type, vegetation and gradient. In this case the Classes 1 to 6 represent if a landslide is likely or not with Classes 1,3 and 6 predicting a high likelihood and the remaining low likelihood. It can be seen that the type of soil is found highly important to determining the stability of a slope, as in all possible cases it is the first parameter to be considered. Even though this is a simple example, this type of approach, determining the importance of parameters, can be used in investigations such as sensitivity analyses, to complement more traditional statistical approaches and provide additional valuable information on the relationships of different variables/parameters.

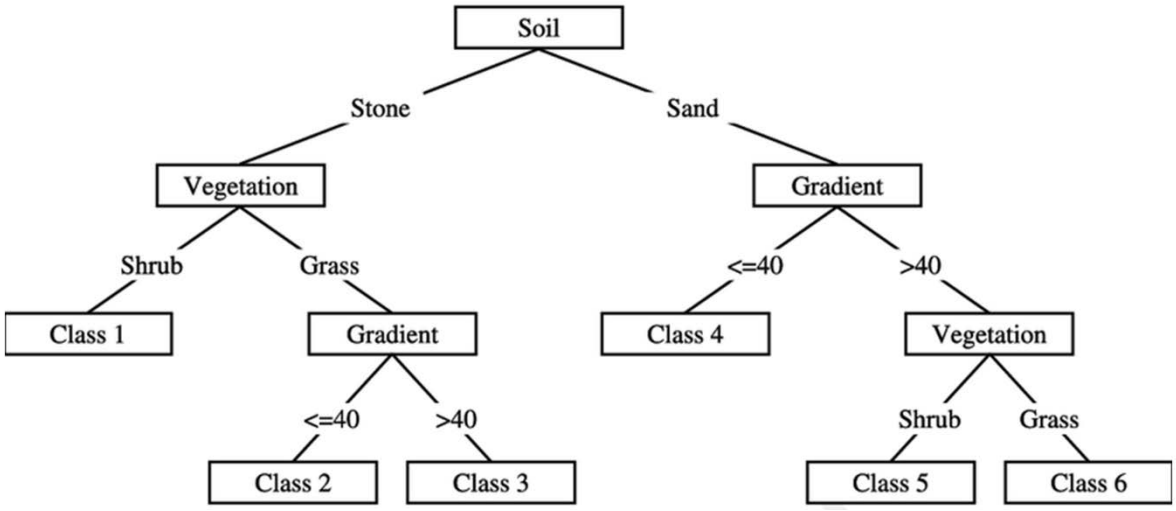


Figure 2.13 Example decision tree on slope stability classification [121]

2.3.5 Machine learning applications in engineering

Machine learning techniques have been applied to many problems in various fields. Their nature of using “big data” to perform prediction and optimisation with very low computational times have encouraged researchers to implement them in various problems in order to speed up, improve or complement their solutions. Many of these problems come from civil engineering and more specifically geotechnical engineering [121–136] , including some from the field of geothermal energy. A few of these examples are: Esen and Inali [125] present an artificial neural network model, a supervised learning algorithm, used to predict the coefficient

of performance of ground source heat pumps and provide insights on a better utilisation of the systems. Park et al. [127] similarly developed a methodology combining multiple linear regression and artificial neural networks to predict the hourly performance factor for a large-scale GSHP system. Casteleiro-Roca et al. [126] present another supervised learning approach, where the probability of failure for a GHE is predicted based on available information from the ground source heat pump. Finally, Zhang et al. [128] used artificial neural network models to predict the thermal conductivity of layered soil profiles, which can result in more accurately designed GSHP systems. The above case studies, as well as a number of others found both within the geothermal field as well as more broadly in engineering, show successful implementation of machine learning techniques to engineering problems, with very positive results and encourage the continuous investigation of their incorporation to further scenarios and problems. These findings specifically encourage geotechnical engineers to research and understand these techniques, as they would be the most suitable to decide where in the field they could be applied most efficiently and how they could best utilised.

2.4 Summary

This chapter presented the literature review related to this research, predominantly focusing on the area of geothermal energy and, where relevant, machine learning. Where published papers have been provided (Chapter 3 and Chapter 5 as well as in the appendices) an individual literature review section is also included within each paper.

The concept of direct geothermal energy was firstly introduced in this chapter, explaining how it can be used to efficiently provide clean and renewable energy for heating and cooling purposes and emphasising the worldwide need to shift towards renewables. Important design approaches, both analytical and numerical, have been discussed, noting their limitations, such as the large number of approximations and assumptions and narrow scope of suitability for analytical solutions and the large computational times and resources associated with numerical solutions. Emphasis was given on the more recent notion of energy geo-structures, which is an approach to shallow geothermal systems that attempts to reduce the associated high capital costs by utilising underground structures primarily designed for structural stability to also provide thermal energy. The new challenges energy geo-structures introduce, such as the wide variability of configurations and geometries and the restrictions due to the structural stability design of these structures, were discussed. Importantly, the current gaps in the knowledge regarding how to more effectively perform energy geo-structure design were noted, indicating the potential for further investigating the design of different cases (structures, geometries,

configurations, amongst others), using numerical modelling. Furthermore, a validated COMSOL numerical model was introduced, which has been further developed and utilised throughout the presented research for computational simulations.

The field of machine learning was also briefly presented, noting its ability to find patterns in data and make predictions as well as introducing important facets of the field that are related to this research, such as the different types of learning models, the main methodology of creating a prediction model (as utilised in the research) and the application of feature importance to assess the sensitivity of parameters. Importantly, the fact that machine learning has been used in many cases to aid with solving problems in engineering and other disciplines has been discussed, with a number of examples within the geothermal energy field, such as predicting the coefficient of performance of a GSHP system. Overall, the literature endorses the utilisation of machine learning techniques to aid towards solving problems encountered in GSHP system design and suggests that the merging of the two fields can be valuable.

Page intentionally left blank

Chapter 3 Effects of realistic geothermal pipe installation in GSHP design: variable pipe separation

3.1 Overview and structure

There exist different approaches to GSHP system design using borehole GHEs, as detailed in section 2.2.3, all of which incorporate assumptions to overcome constraints or uncertainties of the real world and be able to obtain sensible results timely. To be confident in the obtained results these assumptions need to be reasonable and realistic. One assumption that has been made throughout the available design approaches relates to the separation between the pipes when placed in a ground heat exchanger and generally assumes that this separation is fixed, suggesting (in the case of a vertical U-loop configuration) that the pipes will remain fixed along the depth of the borehole, equally separated from each other. When considering the realistic nature of a GHE installation, it can be argued that this assumption may be hard to justify and is therefore worth investigating how this could impact the resulting system design.

This chapter introduces the effect of variable pipe separation (the separation between the pipes varying along the depth of the borehole GHE) and considers its significance in GSHP system design. Section 3.2 presents a published journal paper titled *"Ground-source heat pump systems: The effect of variable pipe separation in ground heat exchangers"* investigating in detail the potential consequences of this effect on thermal performance as well as cost for a variety of ground, material and configuration conditions. Section 3.3 presents a secondary journal paper titled "*Carrier fluid temperature data in vertical ground heat exchangers with a varying pipe separation*" focusing on the produced data relating to the analysis, sharing this data with the scientific community and explaining how they can be used to extract further insights. Section 3.4 presents an additional study, undertaken following the analyses in the published paper from section 3.2, introducing an easily adopted methodology that can account for the effect of variable pipe separation in practice. Finally, section 3.5 provides a summary of the chapter's findings.

3.2 Journal paper: Ground-source heat pump systems: The effect of variable pipe separation in ground heat exchangers

This section consists of a journal paper titled: “Ground-source heat pump systems: The effect of variable pipe separation in ground heat exchangers”, published in the journal *Computers and Geotechnics.* The paper has been inserted in the following pages, in its Author’s Accepted Manuscript [AAM] version, with the only modification being the addition of the thesis page numbers at the bottom of the page (allowing consistent numbering throughout the thesis). This publication is the author’s original work, has been included with the co-authors’ authorisation (appropriate co-author authorisation forms have been included in this submission) and the co-authors’ contributions have been acknowledged in the *Preface & Publications* section.

Type of paper: full length article (Computers and Geotechnics - Elsevier Journal)
Date text written: August 2017
Number of words in main text and tables = 8262
Number of figures = 14
Number of tables = 3

Ground-source heat pump systems: the effect of variable pipe separation in ground heat exchangers

Author 1
Nikolas Makasis, MSc (Computer Science), MEng (CE)
Department of Infrastructure Engineering, The University of Melbourne, Parkville, Australia

Author 2
Guillermo A. Narsilio✉, PhD, MSc (Math), MSc (CE), CEng
Department of Infrastructure Engineering, The University of Melbourne, Parkville, Australia

Author 3
Asal Bidarmaghz, PhD, MSc (Eng), BSc (Eng)
Department of Engineering, University of Cambridge, Cambridge CB2 1PZ, United Kingdom
Department of Infrastructure Engineering, The University of Melbourne, Parkville, Australia

Author 4
Ian W. Johnston, PhD, BSc (Eng)
Department of Infrastructure Engineering, The University of Melbourne, Parkville, Australia

Full contact details of corresponding author
Guillermo A. Narsilio, ARC Future Fellow and Associate Professor
Engineering Block B 208, Department of Infrastructure Engineering, The University of Melbourne, Parkville, VIC 3010, Australia
Email: narsilio@unimelb.edu.au, Phone: +61 (3) 8344 4659, Fax: +61 (3) 8344 4616

Abstract:
Closed loop ground-source heat pump (GSHP) systems use ground heat exchangers (GHEs) to transfer heat to and from the ground and efficiently provide clean and renewable energy for heating and cooling purposes. Vertical GHEs contain pipes with circulating fluid (loops), which transfer thermal energy between the ground and the fluid. One very common assumption made in designing GSHP systems is that, when installed, these loops remain evenly separated along the length of the GHE, something that due to the nature of construction is rarely true. This can result in thermal interference not accounted for in the design, leading to a potential negative impact on the performance of the system. This paper investigates the effect of this interference, using detailed numerical simulations to compare different geometries, modelling fixed and variable pipe separations. A comprehensive parametric analysis is conducted to identify some of the most influential design parameters and the potential consequences on running and capital costs. Amongst the key findings of this study is the importance of the borehole filling material, as a highly thermally conductive material can minimise these negative effects from the thermal interference by up to 60%. Moreover, potential increases in drilling (capital) costs of up to 24% are shown, while the potential increases in running costs due to the reduced efficiency were found to be relatively minor.

Keywords
Numerical modelling; geothermal; ground heat exchangers (GHE); sensitivity analysis; pipe separation; shank spacing

List of Notations

COP	coefficient of performance, -
$C_{p\ material}$	specific heat capacity of material, J/(kg·K)
q	heat flux, W/m^2
q_{fluid}	flow rate of fluid, L/min
s	vertical spacing between separators, m
t	time, sec
$T_{ave\ fluid}$	average fluid temperature of a pipe loop, °C
$\bar{T}_{diff}$	average absolute fluid temperature difference between two numerical models, one using fixed pipe separation and the other variable pipe separation, for yearlong simulations, as defined in text, °C
$\bar{T}_{diff,random}$	average absolute fluid temperature difference between two numerical models, one of which uses random pipe separation, for yearlong simulations, as defined in text, °C
$T_{farfield}$	average annual ground temperature, °C
α	maximum movement of pipes from initial position, m
$\lambda_{material}$	thermal conductivity of material, W/(m·K)
$\rho_{material}$	density of material, kg/m^3
χ	distance of pipe from centreline of borehole, m

1 Introduction and Background information

Ground-source heat pump (GSHP) systems can be used to efficiently provide renewable geothermal energy for heating and cooling purposes, including domestic hot water. These shallow geothermal energy systems extract and reject heat from and to the ground within a few tens of metres below the surface. A heat pump is connected to an acclimatisation distribution circuit within the building, which transfers the heat to and from the building, as well as to a series of ground heat exchangers (GHEs), which transfer the heat from and to the ground [1,2]. Even though GHEs can take many forms (for example boreholes, piles, retaining walls, tunnels), typically in closed loop GSHP systems a vertical GHE consists of a borehole that contains loops (usually high-density polyethylene (HDPE) pipes) with a circulating fluid (usually water) that transports the heat between the system components. Vertical GHEs are commonly drilled to between 30 and 100 metres, though they can be deeper, and then backfilled (typically grouted). The pipes placed inside the GHE usually form either a single loop (one inlet and one outlet pipe) or a double loop (two inlet and two outlet pipes in pairs). These systems are known to typically run at a coefficient of performance of about four, meaning 4 kW of heating/cooling energy is produced for every 1 kW of electricity consumed [3–5]. Moreover, GSHP systems are the most used amongst the different applications of direct geothermal energy [6] and have attracted much attention over the past decade for the purpose of better understanding how they can be most suitably and efficiently utilised and designed [7–13].

There are many different design methods for GSHP systems, both analytical and numerical. In closed loop vertical systems, a common assumption for all these methodologies is that the pipes remain equally separated along the length of the GHE, after their placement and grouting. In order to be more confident in this assumption, pipe separators or spacers (e.g., geoclip^{TM}, sureclip^{TM}) are sometimes used during construction, to keep the pipe separation (also known as shank spacing) fixed at specified intervals (for example every couple of metres along the length of the GHE), as schematically shown in Figure 1. These separators have shown to generally improve the performance of GSHP systems [14]. However, even with the use of separators, an entirely fixed separation along the length of the borehole cannot be guaranteed, given the nature of construction and specifically the pouring of the grout on the placed pipes. Between the separators, the location of the pipes in the horizontal plane is highly likely to vary, possibly randomly. Clearly, without separators (a practise not uncommon), the location of the pipes is likely to be even more random within the confinement of the borehole.

< Figure 1 around here >

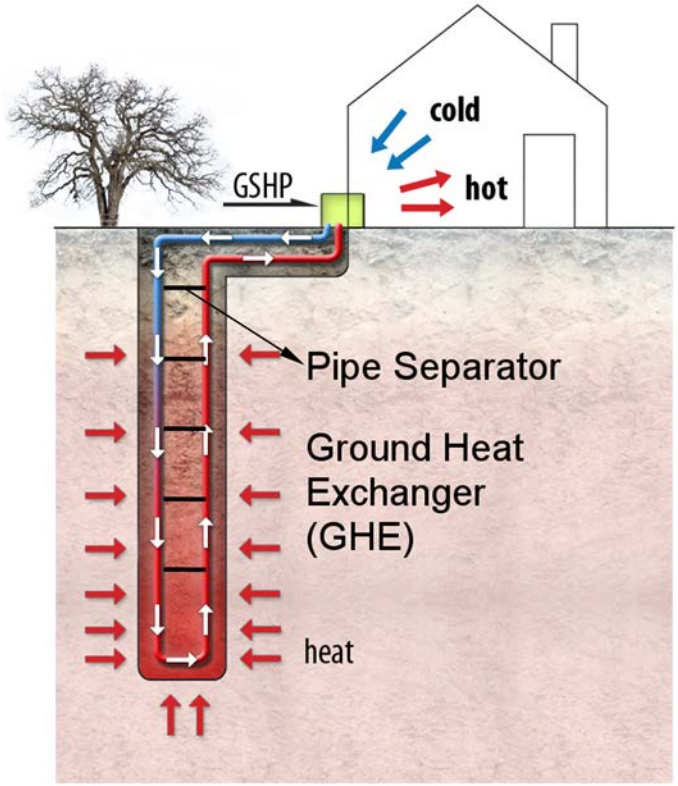


Figure 1. Schematic of a closed loop vertical GSHP system in heating mode with pipe separators (Not to scale)

A question then arises about what effect this *uneven* pipe separation may have in the thermal performance of the system. It has been repeatedly shown in the literature that the separation between GHE boreholes or piles in a GHE field can significantly affect its performance [15–20]. Following the same reasoning, studies have shown that different pipe separations (or shank spacing) within a GHE can also have an impact [9,21–24], as can generic installation anomalies [25]. However, no study exists that clearly investigates a pipe separation that *varies along the length of the borehole*, as expected in a realistic scenario (possibly due to the high computational power required to model such level of detail). This is important because if the inlet and outlet pipes come closer or even touch each other, then a thermal "short-circuiting" between these pipes is expected, which can hinder the operation of the system.

This behaviour and its impact on the effectiveness and performance of the geothermal energy systems has not been adequately investigated and therefore current design practises ignore its potential effects, thus hindering the accuracy and realism of the design and potentially increasing associated costs. This paper investigates the effect of this thermal interference using detailed numerical simulations, modelling fixed and variable pipe separations, adopting Australian temperate climate conditions to exemplify the analyses. Unlike previous related work, where only a limited number of design parameters and geometries were analysed and only in terms of thermal performance [26], herein a comprehensive parametric analysis is conducted to identify some of the most influential design parameters and, in combination with a cost analysis, the potential implications of ignoring variable pipe separation effects in the design of GSHP systems in terms of both efficiency and cost.

2 Finite Element Model

2.1 Brief Model Description

To conduct the research, a validated state of the art transient 3D numerical model, developed at the University of Melbourne, is used [9,27,28]. The model is built and solved using the finite element software COMSOL and is based on the coupling of the governing equations of heat transfer (energy balance) and fluid flow (momentum and continuity). The heat transfer is primarily modelled by *conduction*, occurring mainly in the ground, the grout filling the borehole GHE and the pipe walls and partially in the fluid, and *convection*, occurring mainly in the carrier fluid (note here that groundwater flow is not taken into account in this study). For the fluid flow in the pipes, 1D elements are used to solve the continuity and momentum equations for fluid flow and the energy equation for heat transfer, minimising the computational resources required (compared to 3D elements) while still accurately capture the pipe flow. The results are coupled to those of the 3D heat transfer elements representing the grout and ground surrounding the pipes.

This model has been thoroughly validated elsewhere against both established analytical solutions, such as the two-dimensional Finite Line Source Model, as well as full scale experimental data, including utilising a single U-loop borehole GHE as well as a three U-loop pile GHE [9]. The numerical results showed an excellent agreement with the experimental data, for a range of conditions, operating patterns and geometries. An extension of this model has also been experimentally validated for energy geo-structures (instead of the traditional borehole GHEs), such as tunnels, and obtaining very good agreement between the numerical results and the experimental data [29,30].

2.2 Model Parameters, Boundary and Initial Conditions

The modelling used in this research is based on typical weather and ground conditions for Melbourne, Australia, with the material properties used presented in Table 1 [31]. The geometry and dimensions used for the modelled GHE are of typical practice in the region as well and are depicted in Figure 2. It should be noted that while typical GSHP systems include a field with multiple GHEs, in this work each simulation focuses on one single GHE to isolate the effects of pipe separation within the GHE from the thermal interference that may arise from adjacent GHEs.

In this case, a radius of 10 metres of ground around the GHE is employed, as this is adequate to avoid any ground boundary effects in this study. In the outer boundary of the ground domain, a constant temperature is prescribed as a boundary condition equal to the average annual ground temperature $T_{farfield}$, as shown in Figure

2-left. Thermal insulation is applied at the top and bottom boundaries of the model to render zero thermal flux through these boundaries ($q_{z=0} = 0$). This condition at the surface of the model follows a conservative approach, in order to study the severity of the variable separation effect, as accounting for the surface air temperature effect enhances the performance of the system [32]. Moreover, this is the boundary condition (indirectly) assumed in most analytical models used in commercial design software (i.e. infinite line source models, infinite cylindrical models, finite line source models [33–36]). Lastly, an initial temperature based on the annual ground temperature for the geographical location is used, which for Melbourne is around 18 °C. The fluid flow rate prescribed in the pipes is typical of GHE operation and within the turbulent range and the resulting pressure difference between the pipe inlets and outlets is in the order of 25 kPa.

Table 1. Material Properties

Parameter	Value(s)	Unit	Description
λ_{ground}	0.7, 1.5, 2.1, 2.7	W/(mK)	Thermal conductivity of ground
ρ_{ground}	2353	kg/m^3	Density of ground
$C_{p\ ground}$	850	J/(kgK)	Specific heat capacity of ground
λ_{grout}	0.7, 1.5, 2.1	W/(mK)	Thermal conductivity of grout
ρ_{grout}	1600	kg/m^3	Density of grout
$C_{p\ grout}$	850	J/(kgK)	Specific heat capacity of grout
$T_{farfield}$	18	°C	Average annual ground temperature
λ_{fluid}	0.582	W/(mK)	Thermal conductivity of carrier fluid
ρ_{fluid}	1000	kg/m^3	Density of carrier fluid
$C_{p\ fluid}$	4180	J/(kgK)	Specific heat capacity of carrier fluid

< Figure 2 around here >

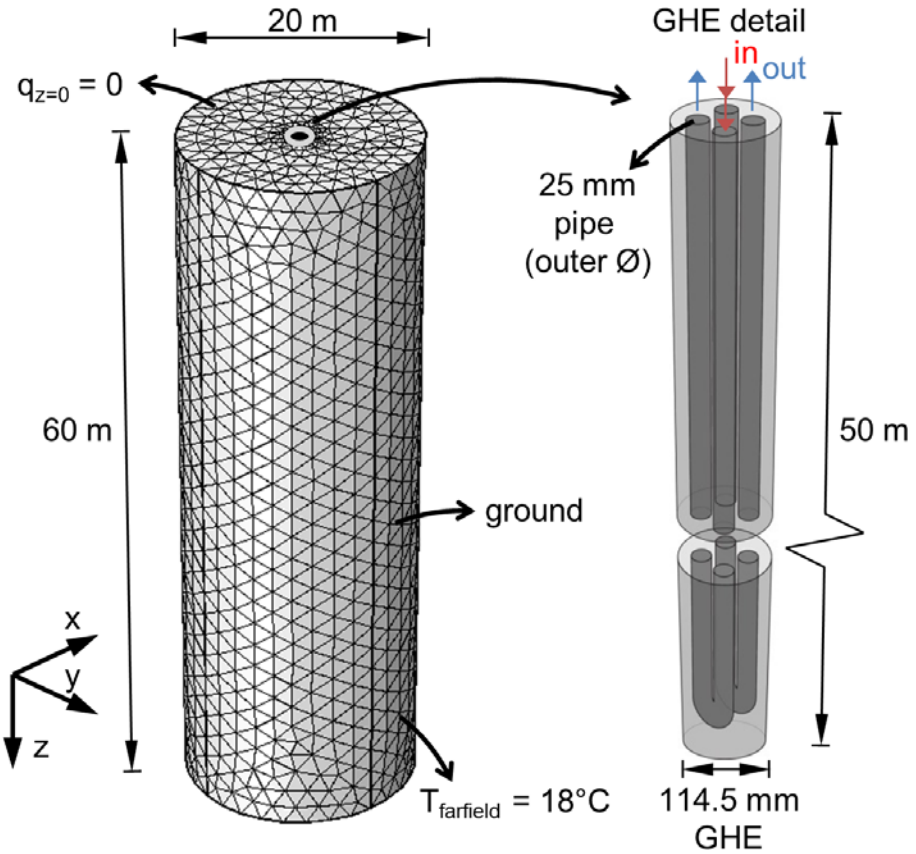


Figure 2. Modelling geometry – typically being used in Australia (ground domain to the left and detail of the embedded 114.5 mm diameter GHE to the right, containing 25 mm outer diameter HDPE pipes in a 50 m long borehole)

3 Methodology

In performing this study, the finite element model described in section 2 is used to run a number of numerical simulations, using different design parameters. Firstly, the two pipe separation geometries that are mainly used throughout this study are introduced, one with a fixed (constant) separation of pipes along the depth of the GHE and one with *varying* separation, where the pipes follow a sinusoidal pattern. Following, for a specific set of parameters, simulations using these two geometries are compared against a number of simulations that completely randomise the separation of pipes. This latter brief analysis mainly aims to show how well the two geometries represent the randomness of the movement of pipes within the borehole, as well as to investigate the variance of the performance of the system due to a changing separation of pipes. The parametric and cost analyses are then introduced, using the fixed and variable pipe separations, which comprise the main focus of this study. The first (parametric analysis) investigates the significance and sensitivity of important design parameters to this effect of variable pipe separation and the second (cost analysis) the potential monetary implications on the system both in terms of capital and running costs. A summary of these analyses and cross-references to the corresponding sub-sections and figures are included in Figure 3, noting that section 3.1 introduces the modelling of variable pipe separation and section 4.1 shows an example highlighting its effect. Lastly, an explanation is provided on the metrics used to make the comparisons between the simulations for all above analyses.

Sections 3.2 and 4.2: *Random Pipe Separation Analysis*	**Sections 3.3 and 4.3:** *Parametric Analysis*	**Sections 3.3 and 4.4:** *Cost Analysis*
Investigation: **Aim:** Investigate how closely the fixed and variable* separation geometries (Fig. 4) simulate a geometry where the separation is random (Fig. 5) **No. of Models:** 106 (3 fixed, 3 variable, 100 random)	Investigation: **Aim:** Investigate the sensitivity of the effect of variable* separation to important design parameters **No. of Models:** 248 (216 complete analysis + 32 selected analysis)	Investigation (a) – Capital cost: **Aim:** Investigate how much longer the borehole needs to be, to account for the effect of variable* pipe separation. **No. of Models:** 31 (28 variable (sinusoidal) separation with varying length, 3 fixed) Investigation (b) – Operational cost: **Aim:** Compare operational costs between fixed and variable* separation models for all configurations **No. of Models:** Same as Study 2
Design Parameters: $\lambda_{grout} = 0.7\ W/(mK)$ $\lambda_{ground} = 2.7\ W/(mK)$ $Thermal\ Load = High$ $q_{fluid} = 11\ L/min$ $GHE\ Length = 50\ m$ $Separation: fixed, variable, random$	Design Parameters (Table 2): $\lambda_{grout} = [0.7\ to\ 2.1]\ W/(mK)$ $\lambda_{ground} = [0.7\ to\ 2.7]\ W/(mK)$ $Thermal\ Load = [Low\ to\ High]$ $q_{fluid} = [5.5\ to\ 13]\ L/min$ $GHE\ Length = 50\ m$ $Separation: fixed, variable$	Design Parameters – (a): $\lambda_{grout} = 0.7\ W/(mK)$ $\lambda_{ground} = 2.7\ W/(mK)$ $Thermal\ Load = High$ $q_{fluid} = 11L/min$ $GHE\ Length = [50\ to\ 68]\ m$ $Separation: fixed, variable$

Note: for all fixed and variable separation geometries, three configurations were used throughout: Inner, Mid, Outer (Section 3.1)
*variable separation refers to the sinusoidal geometry that can be seen in Figure 5

Figure 3. Overview of the structure and strategy followed for the multiple analyses undertaken.

3.1 Modelling Variable Pipe Separation for Three Different Design Configurations

In order to simulate the effect of the varying separation between the pipes along the length of the GHE, for simplicity, the pipes are modelled as having a sinusoidal shape. This represents the case where the pipes come closer together and may even touch at the midpoints between the separators. In reality, this variable separation could have the pipes potentially touching for much greater lengths between some separators and less between others.

As shown in Figure 2, this study uses double U-loop GHEs, for which the adopted sinusoidal shape can be difficult to visualize. Therefore, for clarification, Figure 4 shows a simplified illustration of the two different separation models for a simple single U-loop GHE, where separators are placed at a spacing (*s*) from each other along the depth of the GHE. A representation of the sinusoidal variable pipe separation geometry for the double U-loop GHEs used in this study can be seen in Figure 5. The figure shows each of the three different configurations modelled in the parametric analysis, discussed in section 3.3 below; (a) shows the one where the pipes are initially placed relatively close to the centre of the borehole (separation of 40 mm), called 'Inner' and (b) and (c) show the other two configurations (herein called 'Mid' and 'Outer'), which have different initial/design separation (cross-sections A), the value being 50 mm and 60 mm respectively. For each configuration ('Inner' (a), 'Mid' (b), 'Outer' (c)), each cross-section (A, B, C, D) shows the location of the pipes at different depths of the borehole, as they approach each other between the separators. The schematics to the right of the cross-sections show the centreline of one of the pipes. Moreover, α denotes the maximum 'amplitude' of the sinusoidal wave, indicating the distance the pipes can move from their initial position and χ the distance of any pipe from the centre of the borehole. For this study, it is assumed that separators are placed every 1 metre along the length of the GHE (i.e., vertical spacing (*s*) = 1 m).

< Figure 4 around here >

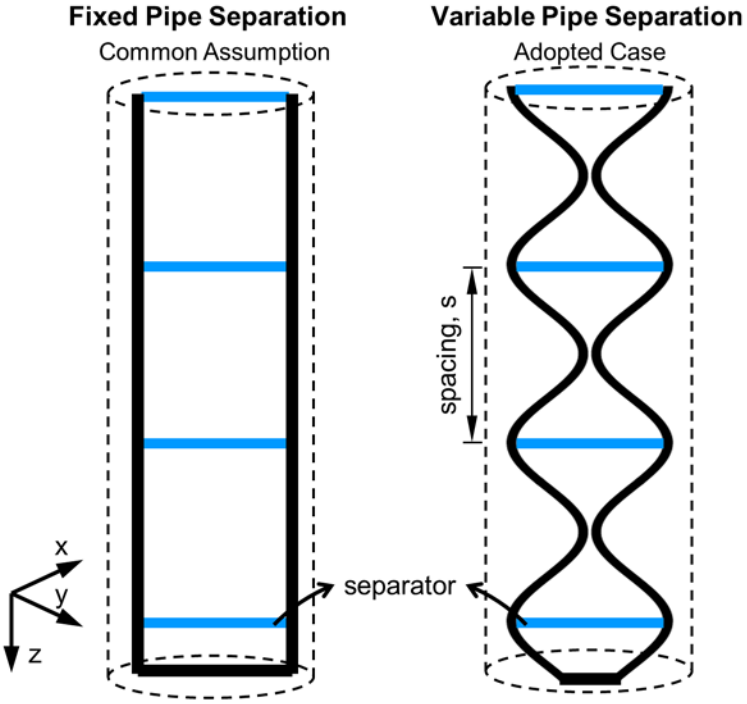


Figure 4. Illustration showing the modelling of variable pipe separation for a single loop GHE (Not to scale)

< Figure 5 around here >

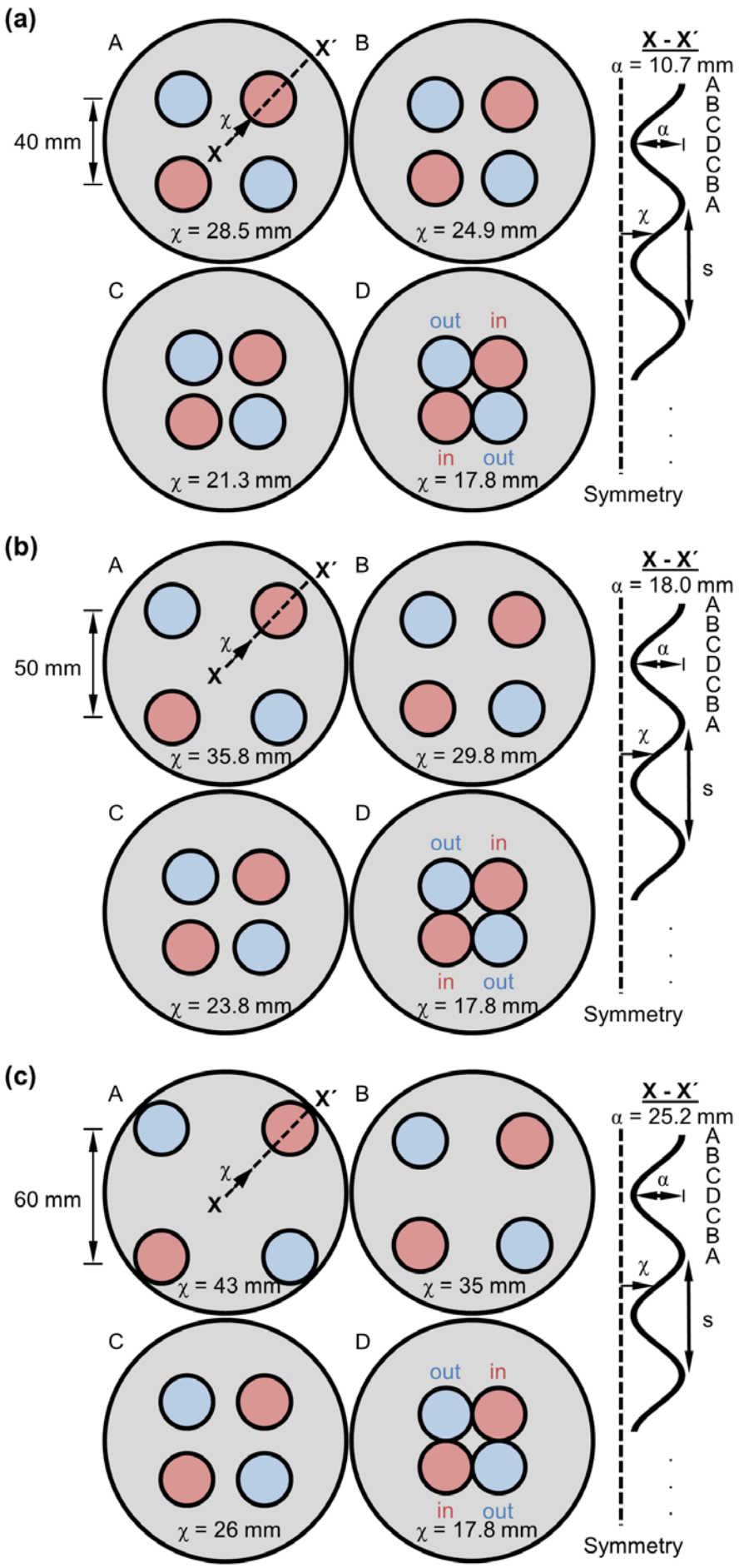


Figure 5. Cross-section of double loop GHE (used in this analysis) with sinusoidal variable pipe separation as it varies along depth: (a) 'Inner' configuration, (b) 'Mid' configuration, (c) 'Outer' configuration

The geometry depicted in Figure 5 is referred to as *'variable pipe separation'* throughout this study and for all three configurations, the pipes are assumed to bend and touch at the mid-length of the pipe between the separators (Figure 5 cross-sections D) and at the centre line of the GHE. On the other hand, in the geometry referred to as *'fixed pipe separation'*, the cross-section of the borehole is modelled as constant throughout the length. For example, for the 'Inner' configuration fixed pipe separation models, the cross-section of the borehole at any depth will be as in Figure 5(a) cross-section A.

Lastly, it should be noted that the models presented account only for the pipes deflecting towards the centre of the GHE and not towards its edge. For example, in Figure 5(a), throughout the depth of the borehole, the pipes will never be further away from each other than their design separation, as shown in cross-section A (where separators are placed). The reason for only investigating this behaviour and not movement towards the edge of the borehole is to focus the scope to the potential severity and impact that this movement can have on the design. Since it is expected that an increase in the separation of pipes enhances the heat extraction and the performance of the system, only a movement towards the centre is explored [9,21–24].

3.2 Random Pipe Separation Analysis

Given that there is no forensic literature on a varying pipe separation within GHEs and in order to be more confident in the model as well as examine how well it captures the potential effect of the movement of pipes within the borehole, another analysis is performed using a third type of geometry. In this, the pipe separation varies randomly along the length of the borehole, instead of adopting the assumed simplified sinusoidal variation. These random pipe separation models capture the nature of having no control over the separation of the pipes and may cover situations where pipe separators are not used or not implemented properly. To achieve this, the position of the pipes in the x-y plane is randomised at every metre along the borehole length, restraining the movement of each pipe in the equivalent borehole quadrant, and the pipes are then connected linearly between those points, as illustrated in Figure 6. Certain checks are set in place to make sure that the pipe position is realistic, such that ensuring that different pipes never occupy the same physical space, that the pipes remain within the borehole and that the pipe bending radius is not excessive. This geometry is referred to as *'random pipe separation'* throughout this study and a total of 100 simulations using random pipe separation are run and then compared to equivalent fixed and variable pipe separation results. For clarification, each of the 100 simulations has a unique randomised pipe separation geometry. The aim of this comparison is to verify the suitability of the variable pipe separation geometry as well as to investigate the extent of potential variance within the results. The simulations have the same input parameters, other than configuration, which form one case from Table 2 and the parametric analysis, as explained below. These input parameters are: a High thermal load (see section 3.3 below), 0.7 W/(mK) and 2.7 W/(mK) thermal conductivity of the grout and ground respectively and a fluid flow rate of 11 L/min.

< Figure 6 around here >

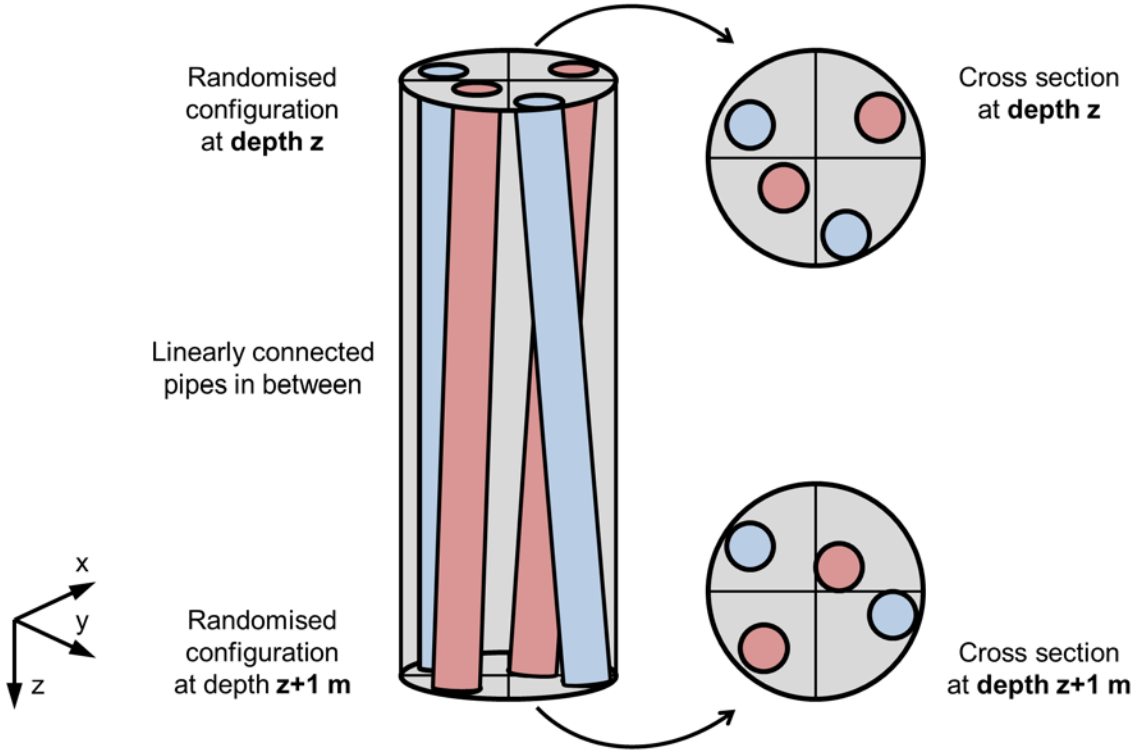


Figure 6. Random pipe separation geometry schematic

3.3 Parametric and Cost Analysis

Using the finite element model and configurations described in sections 2 and 3.1, various one year simulations are run to investigate the effects of variable pipe separation. For each set of parameters discussed below, two simulations are run, one modelling fixed pipe separation (U-loops remaining straight as in Figure 5 cross-sections A) and one modelling variable pipe separation (U-loop pipes adopting a sinusoidal shape along the GHE length as in Figure 5 cross-sections A-D).

Five of the model input parameters, believed amongst the most significant to the performance of the system, are varied in order to study their responses, as presented in Table 2. The values chosen are expected to be towards the upper and lower bounds of the range of values usually encountered.

Table 2. Parametric analysis variables

Parameter	Values Used	Unit	Analysis Type
Configuration (design separation)	Inner (40), Mid (50), Outer (60)	mm	Complete
λ_{grout}	0.7, 1.5, 2.1	W/(mK)	Complete
λ_{ground}	0.7, 1.5, 2.1, 2.7	W/(mK)	Complete
Thermal load	Low, Medium, High	kW	Complete
q_{fluid}	5.5, 11, 13	L/min	Selected

Firstly, three different initial configurations of the pipes are modelled (Figure 5) based on the distance of the pipes from the centre of the borehole and their design separation, as discussed in section 3.1. Secondly, three different values for the thermal conductivity of the grout (λ_{grout}) and four for the thermal conductivity of the ground (λ_{ground}) are used, varying from relatively low to relatively high. This is done to better understand the interplay between pipe to pipe thermal interference and the rate of heat transfer between the grout and the ground and how significant these are to the movement of the pipes and the varying separation. The choice of filling material of a borehole, and thus the thermal conductivity, are known to be significant on the performance of the system [37].

Thirdly, three different real thermal load distributions are used, as seen in Figure 7, to represent cases where the total thermal load for an average residential building in Melbourne (about 20 kW peak-cooling and 20 kW

peak-heating building load) is distributed over a different number of GHEs, i.e. the GHE field is smaller/bigger. The smaller the field, the more energy one single GHE must provide. For the 'High' case a total of 5 GHEs are used, 7 GHEs for the 'Medium' case and 9 GHEs for the 'Low' case, in each case the entire GHE field providing the same amount of energy using different number of GHEs for each case. It should be noted that the thermal load for each GHE, shown in Figure 7, is not directly proportional to the building load, as it is modified to also account for the heat generated by the operation of the heat pump. Moreover, the thermal load is provided as a daily average. Finally, the flow rate of the fluid within the pipes is varied within the turbulent range, as it is known to affect the heat extraction and thus the performance of the system [38].

< Figure 7 around here >

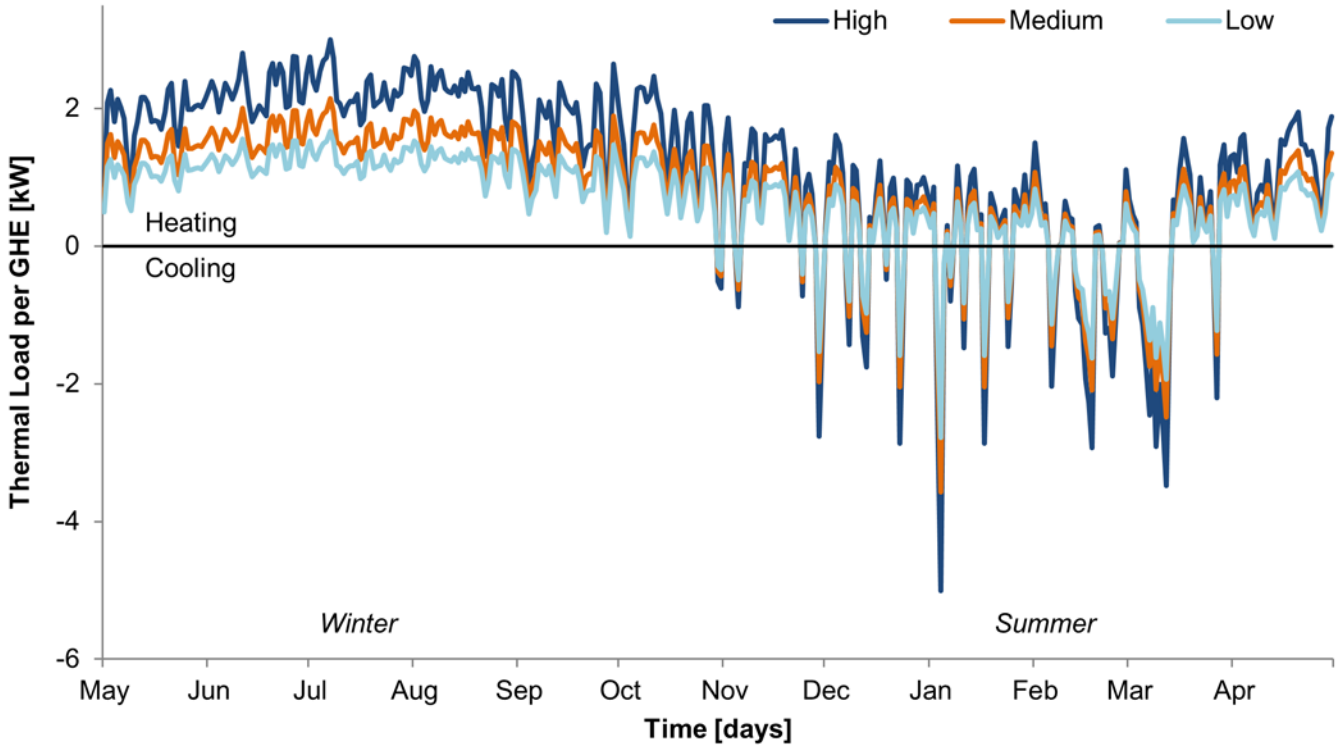


Figure 7. Daily thermal load per GHE for a typical year for three different field sizes (note Melbourne is in the Southern Hemisphere)

It should be noted that for the first four parameters of Table 2, all 108 different combinations of them are included in the analysis (having q_{fluid}=11 L/min) thus labelling it as a "*complete*" analysis. When varying the flow rate of the fluid in the pipes, a "*selected*" analysis is undertaken, meaning that only some of the combinations of the first four parameters are used, in order to limit the number of required computational simulations. More specifically, the values that are used are: Medium thermal load, 0.7 W/(mK) and 2.1 W/(mK) for the thermal conductivity of the grout, 1.5 W/(mK) and 2.7 W/(mK) for the thermal conductivity of the ground and the Inner and Outer configurations, such that a wide range of combinations is still represented.

Moreover, following from the parametric analysis, a cost analysis is undertaken to investigate the potential monetary consequences of the thermal interference effect due to variable GHE pipe separation, viewing cost from two different perspectives. Firstly, potential increases in *capital costs* are considered for the scenario when the effect of variable pipe separation is taken into account during the design phase and thus longer boreholes and pipes are needed to balance the reduced performance of the system due to the effect. Secondly, the *running costs* are calculated to investigate how the different efficiencies and coefficients of performance (COPs) of the two different geometries/models are affecting these costs.

3.4 Evaluating Performance and Comparison Metrics

As part of this study, various numerical simulations are run in order to evaluate the performance of a GSHP system under various conditions. For such numerical simulations using the finite element model presented in section 2, the performance of the modelled system can be evaluated by looking at the resulting fluid

temperatures within the circulating pipes. If the temperature of the fluid within the pipes stays within reasonable values and common GSHP operating temperature range limits (typically between -5 and 40 °C for efficient operation, e.g., Climate Master™ TC or TM Series, Water Furnace® 5 Series, though this range may vary between different heat pump brands and models) for the duration of the simulation (in this case 1 year) then the system is deemed as functional. On the other hand, if the temperature of the fluid exceeds the operating range of the heat pump, or reaches extreme values (either –ve or +ve), then the GSHP system will not be able to satisfy the energy demand and the system will need to be re-designed. In general, the less extreme these fluid temperatures are, the more efficient the system is. In this study, the average fluid temperature of a pipe loop, $T_{ave\ fluid}$, is used to quantify the temperature of the circulating fluid, calculated as an average of the temperature of the fluid at the inlet and outlet pipes ($T_{ave\ fluid} = (T_{in\ fluid} + T_{out\ fluid})/2$). Moreover, it should be noted that given the thermal imbalance used (Figure 7), ground temperature increases/decreases over longer periods of time are possible but only by a few degrees. For the purpose of this study, 1 year simulations are considered appropriate and conservative.

As mentioned in section 3.3, for the parametric analysis, for every different combination of input parameters presented in Table 2, two simulations are run, one having fixed pipe separation and one having variable pipe separation. The results of the two simulations are then compared, specifically looking at how different these results are and therefore how impactful can the effect of variable pipe separation be in design. In this comparison, the more similar the responses of the two models are, the less significant the effect of variable pipe separation and therefore the more suitable the use of the fixed pipe separation assumption. Since there are many different combinations of input parameters, in order to be able to perform a large scale analysis, a single value is needed. This single value should capture this difference between a fixed and variable pipe separation simulation for a specific set of input parameters. Since the computed fluid temperature for each model has a yearlong distribution (1 value for each day of simulation), the mean absolute error (MAE) metric is adopted for this study, in terms of temperature difference:

$$\bar{T}_{diff} = \frac{1}{365}\sum_{t=0}^{t=365}(|T^{VPS}_{ave\ fluid,t} - T^{FPS}_{ave\ fluid,t}|) \quad \textbf{(1)}$$

where $T^{VPS}_{ave\ fluid,t}$ represents the average fluid temperature in the circulating pipes on a day *t*, when using variable pipe separation, $T^{FPS}_{ave\ fluid,t}$ represents the average fluid temperature in the circulating pipes on a day *t* when using fixed pipe separation and $\bar{T}_{diff}$ (i.e. MAE) represents the average absolute fluid temperature difference between the two for the yearlong simulations. Other metrics, for example the root mean square error, have also been considered and have produced similar results.

To perform the random pipe separation analysis, the third type of geometry is introduced, where the pipe separation along the depth of the GHE varies randomly. For this study, the results from models with random pipe separation need to be compared to those of both variable (sinusoidal) and fixed pipe separation, separately. Therefore, similar to the parametric analysis, the MAE metric is again adopted:

$$\bar{T}_{diff,random} = \frac{1}{365}\sum_{t=0}^{t=365}(|T^{RPS}_{ave\ fluid,t} - T^{FPS\ OR\ VPS}_{ave\ fluid,t}|) \quad \textbf{(2)}$$

where $T^{RVPS}_{ave\ fluid,t}$ represents the average fluid temperature in the circulating pipes on a day *t* when using random pipe separation, $T^{FPS\ OR\ VPS}_{ave\ fluid,t}$ represents either $T^{FPS}_{ave\ fluid,t}$ or $T^{VPS}_{ave\ fluid,t}$, depending on the comparison being made, and $\bar{T}_{diff,random}$ represents the absolute average fluid temperature difference between the two models (one of which uses random pipe separation) for the yearlong simulations.

4 Results and Discussion

Adopting the methodologies and metrics discussed above, this section presents the key findings of the study. Firstly, a comparison between fixed and variable pipe separation simulations for a selected set of parameters is

presented, showing the yearlong results and the potential differences in $T_{ave\ fluid}$ ($\overline{T}_{diff}$) as well as the ground temperatures. Following, the random pipe separation analysis results are discussed, with the main aim to confirm the suitability of the variable pipe separation geometry to represent randomness in the movement of pipes (along the x-y plane) within the borehole. The parametric analysis is then presented, comparing fixed and variable pipe separations through a large number of numerical simulations and showing the sensitivity of design parameters to the effect of variable pipe separation. The numerical simulation data obtained and used for these analyses can be found in [39]. Lastly, the two-part cost analysis results are discussed, firstly investigating the additional borehole and pipe length (and thus capital costs) required in order to balance the negative effects of variable pipe separation and secondly the impact on the efficiency of the system and its running costs.

4.1 The effect of Variable Pipe Separation – A specific case

In order to gain an understanding of the potential influence of the variable pipe separation effect on the performance of a GSHP system, the yearlong simulation response for the two different separation geometry models for one specific set of parameters, as shown in Figure 8, is analysed first. This set of parameters is of particular note, as it very clearly highlights the extend of the difference between the fixed and variable pipe separation models/approaches. The response of the system is presented in terms of $T_{ave\ fluid}$, the average temperature of the GHE circulating fluid, as explained in section 3.4.

<Figure 8 around here>

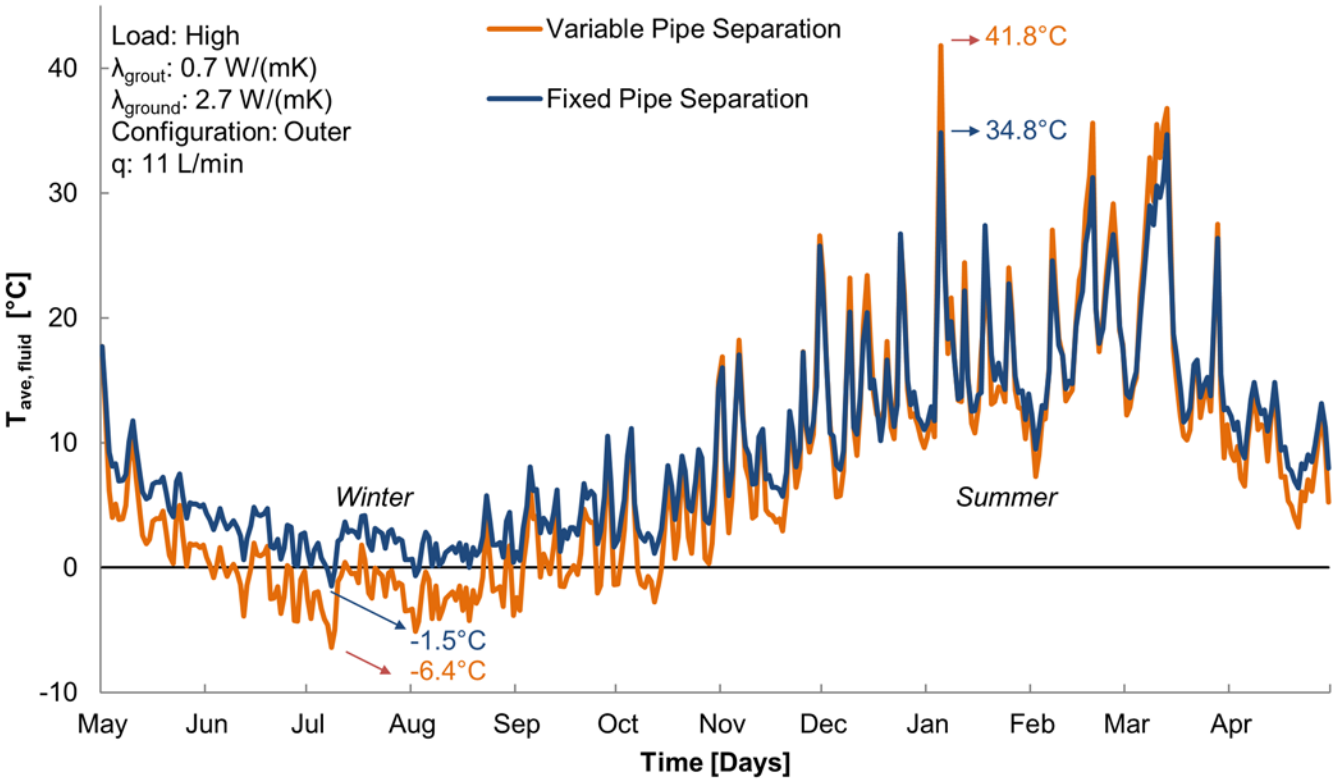


Figure 8. Comparison of average fluid temperature, $T_{ave\ fluid}$, for fixed and variable pipe separation simulations over one year of operation

As can be seen, the commonly used fixed pipe separation results in a minimum and maximum $T_{ave\ fluid}$ of -1.5 °C and 34.8 °C respectively, which are within the working range typically required by most heat pumps, suggesting an adequate initial design. However, when variable pipe separation is considered, these values change to -6.4 °C and 41.8 °C which could significantly reduce the performance of the system, and would in fact deem the initial design inadequate, thus requiring longer (or more) GHEs to reduce this max-min fluid temperature range. The $T_{ave\ fluid}$ values during winter for the variable pipe separation simulation in Figure 8 show how essential the use of an antifreeze solution as the carrier fluid is, something that is not obvious when considering the fixed pipe separation values. It should also be noted that for all cases, i.e. any combination of parameters shown in Table 2, the variable pipe separation model produced a more extreme response than the

fixed pipe separation model using the same parameters. A more extreme response is quantified by lower fluid temperatures being reached in heating mode and higher fluid temperatures in cooling mode with respect to those of the fixed pipe separation, as exemplified in Figure 8 for one specific set of parameters from Table 2.

Figure 9 shows the absolute values of the difference between the mean fluid temperature of the fixed and variable pipe separation simulations for the conditions of Figure 8. Looking closely, it can be observed that a relatively constant difference of about 3 to 5 °C exists during the heating period in winter, when the weather is less variable in Melbourne. During the summer, which has highly fluctuating climate conditions, the difference has short duration peaks, the highest being 7 °C on the 4th of January. These differences are significant and will not only influence the viability of a design but also result in inefficient or costly system designs. It is also worth noting that, as explained in section 3.4, by taking the average of the distribution presented in Figure 9 the value of $\overline{T}_{diff}$ can be calculated which in this case is 2.4 °C.

<Figure 9 around here>

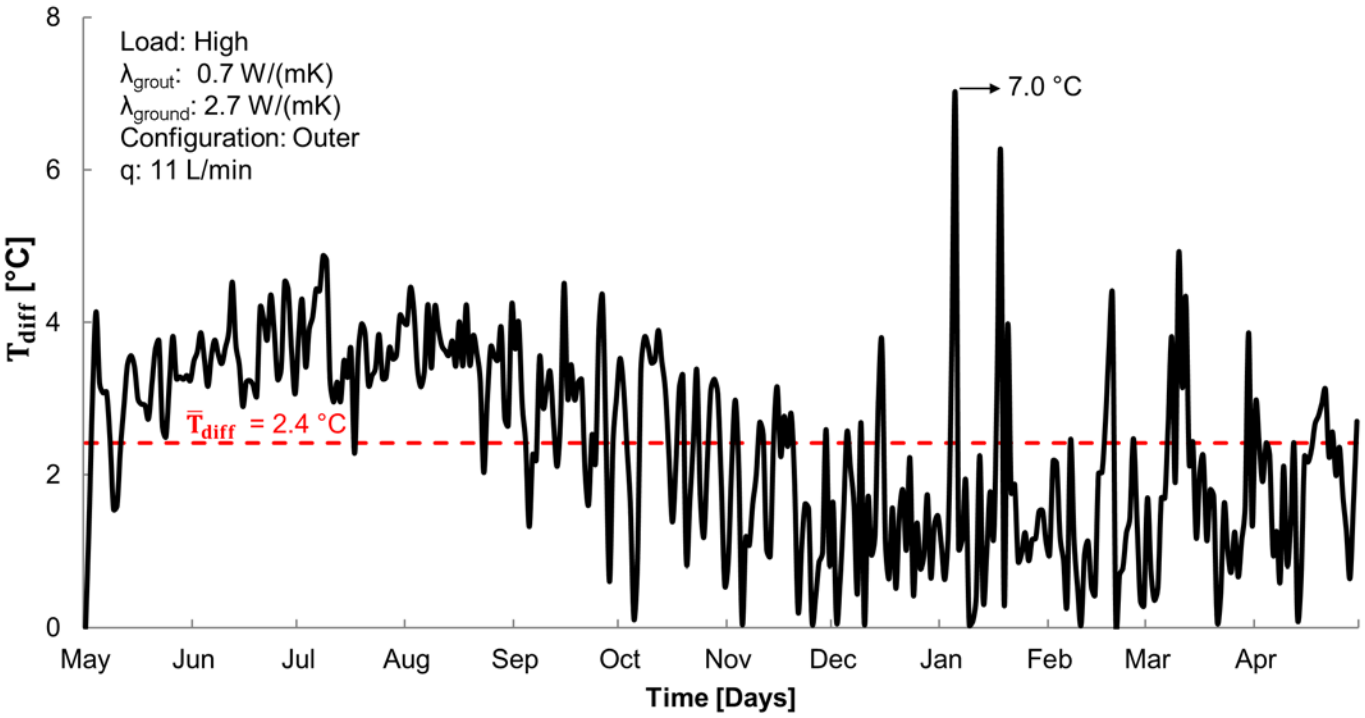


Figure 9. Average absolute temperature difference, $\overline{T}_{diff}$, between fixed and variable pipe separation simulations over one year

In order to better understand the effect of the variable pipe separation on the fluid temperatures and the performance of the system, Figure 10 shows the temperature distribution on the coldest day of the year, 7th of July, at the mid-depth of the borehole for the two separation models. The figure shows clearly that when the pipes move toward the centre of the borehole (Figure 10(a)) a higher variation of temperature exists within the borehole, with the contours showing the areas most influenced by this movement. On the fixed pipe separation model however (Figure 10(b)), the temperatures are much more uniform within the borehole, with only localised extremes around the pipes. This distribution of temperatures is due to the exchange of heat with the ground (which in this case is also of higher conductivity than the grout), in the direction away from the borehole. The movement of the pipes towards the centre of the borehole hinders the heat exchange as the heat is now required to travel through a larger portion of the grout to reach the ground. This effect accumulates over time and causes the more extreme response observed in the variable pipe separation simulations.

<Figure 10 around here>

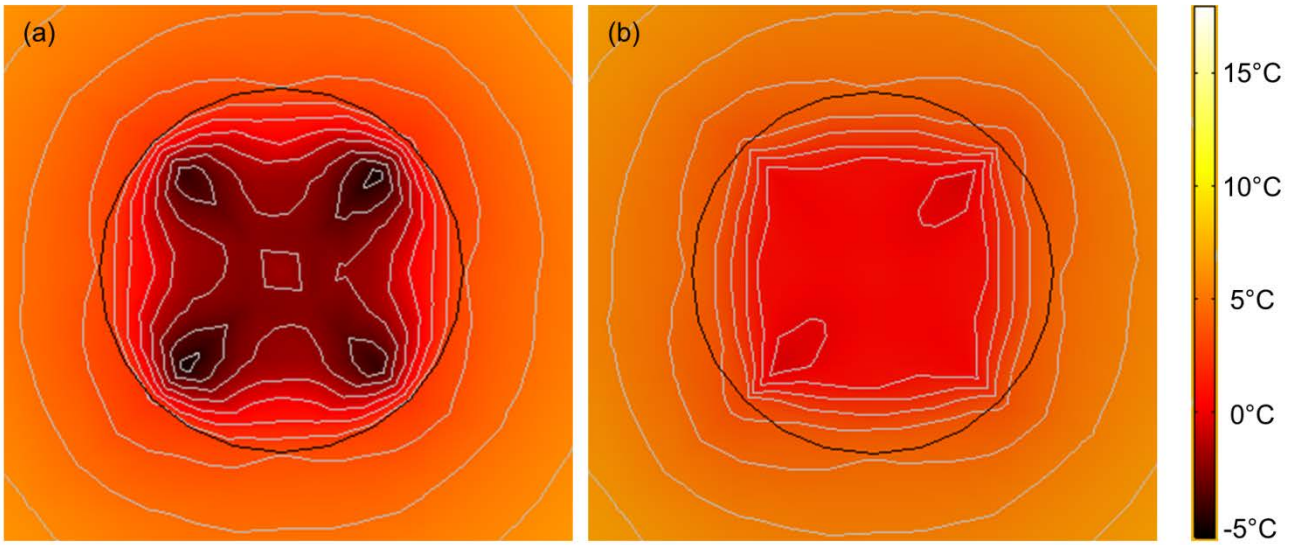


Figure 10. Temperature distribution and contour lines at a cross-section of the GHE, at: z = -25m, t = 7 Jul (heating mode) for the case shown in Figures 7 and 8: (a) variable pipe separation (b) fixed pipe separation

4.2 Random Pipe Separation Analysis

Before discussing the comprehensive parametric analysis, it is important to be confident in the variable pipe separation model presented and its ability to characterise randomness in the movement of the pipes, which is expected in real conditions. Moreover, it is worth investigating how this randomness can affect the expected results of the commonly adopted fixed pipe separation model. For that purpose, both fixed and variable pipe separation geometries (with each of the three pipe configurations presented in Table 2) are compared against 100 additional simulations, each employing a unique randomised pipe separation geometry, as explained in section 3.2. Other than the pipe configuration, all other parameters used for all simulations are the same as those shown in Figure 8. The comparison results are shown in Figure 11, where six different distributions are presented, each comparing 100 random pipe separation simulations to one simulation adopting either fixed or variable pipe separation and one of the three different configurations (inner, mid or outer). For example, each of the 100 points of the *'FPS_inner'* distribution shows the $\bar{T}_{diff,random}$ value comparing one random pipe separation simulation to the fixed pipe separation simulation adopting the inner configuration of pipes (all other input parameters are the same for the two simulations). It is worth noting here that the y axis has values both above and below zero, with the latter ones representing $\bar{T}_{diff,random}$ for an "under-designed" system. In this context, this means that the difference between the two simulations is such that adopting a random pipe separation results in more extreme fluid temperature values and therefore the system would experience more extreme temperatures than designed for, which could affect its performance and suitability.

<Figure 11 around here>

As it can be seen, the assumption that a GHE actually has a fixed pipe separation would result in an under-designed system in the case where random separation of pipes occurs within the borehole. Even with the inner configuration, which is the most conservative, only a handful of random pipe separation simulations resulted in a sufficiently designed system ($\bar{T}_{diff,random} > 0$). Moreover, the results indicate that the variable pipe separation model presented, with the sinusoidal movement of pipes, is in general an acceptable representation of the random movement of pipes within the borehole, specifically using the mid or inner configuration (the latter would be more conservative), which do not result in an under-designed system. This provides confidence to the validity of results in the parametric analysis and emphasises the potential severity of having a poorly designed or constructed GHE, which allows for movement of the pipes within the borehole in the horizontal plane. Finally, these results emphasise not only how essential the use of separators is for GHE boreholes, but also that the vertical spacing between them must be small enough to confidently ensure as little movement of the pipes as possible.

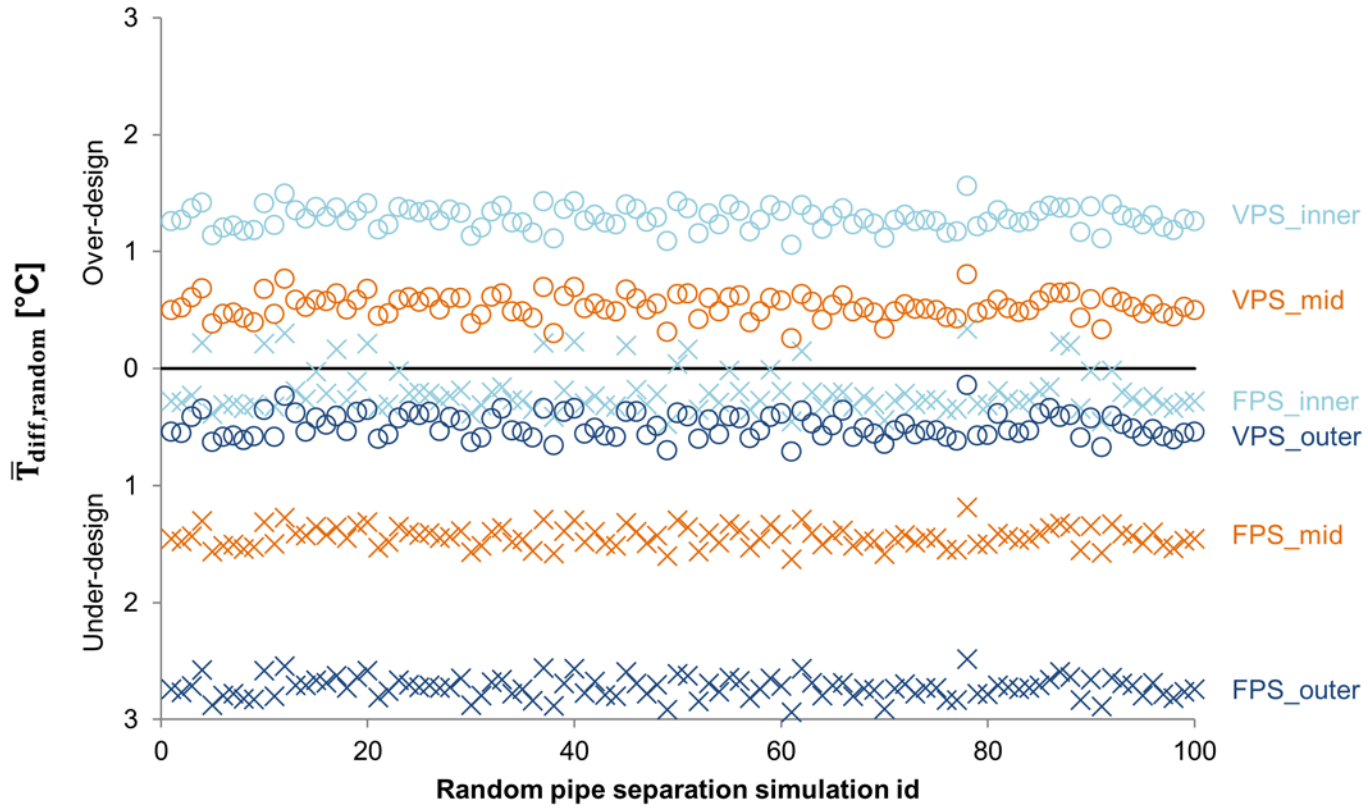


Figure 11. Average fluid temperature difference, $\overline{T}_{diff,random}$, between the random pipe separation simulations and equivalent variable pipe separation (VPS) and fixed pipe separation (FPS) simulations for the three configurations

4.3 Parametric Analysis

It has been demonstrated that variable pipe separation in a GHE can have negative effects on the performance of the system and result in more extreme fluid temperatures than expected. Therefore, it is important to gain an understanding of how sensitive this effect is to various GSHP design parameters. This information could aid in minimising the risks and potential consequences of variable pipe separation during the design phase and moreover provides an insight on the heat transfer interactions within the GHE.

Firstly, looking at the "*complete*" parametric analysis, all 108 different combinations of the first four parameters (configuration, thermal load, λ_{grout}, λ_{ground}) are taken into consideration, while q_{fluid} is fixed at 11 L/min. For each combination, the results from the fixed and variable separation simulations are compared and the average absolute fluid temperature difference, $\overline{T}_{diff}$, is computed, as explained in sections 3.3 and 3.4. Figure 12 shows a summary of the results for this analysis, each subplot showing the change in $\overline{T}_{diff}$ as one of the parameters varies, for each different combination of input parameters from Table 2, and highlighting the significance of λ_{grout}, which was found the most influential. It should be noted that since the analysis includes a large number of models, the plots in Figure 12 can seem clustered. However, the aim of these plots is to show the general trend regarding the sensitivity of the result to each design parameter and how consistent those trends are throughout a range of values for the other design parameters. Therefore, valuable insights can be extracted and identified as discussed below.

<Figure 12 around here>

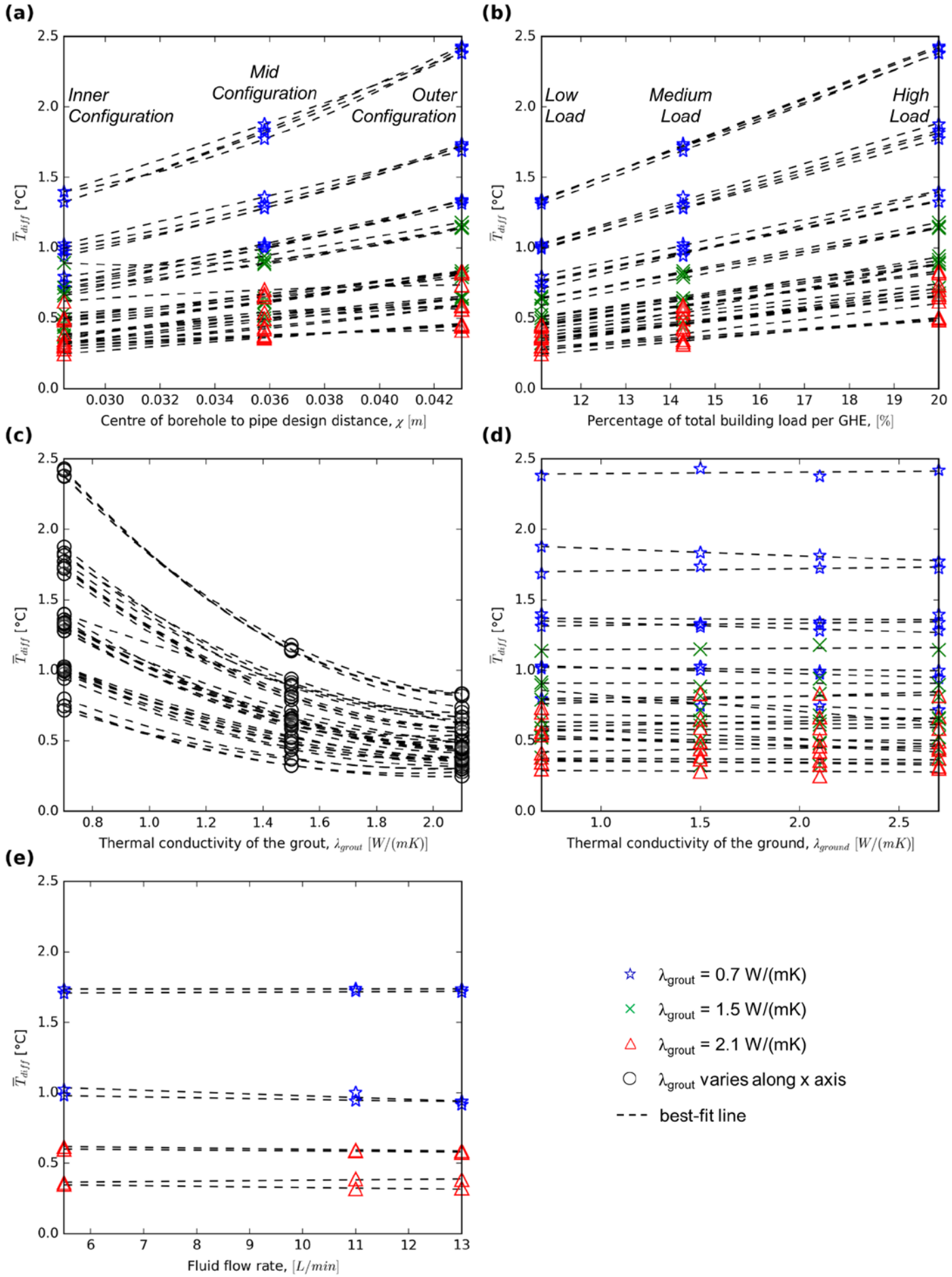


Figure 12. Sensitivity analysis results with indicative fitting lines between observations (circles), highlighting how λ_{grout} affects the other parameters

Based on Figure 12(a) it is clear that the further away the pipes are initially placed from the centre of the GHE, the higher the difference in the performance between the variable and fixed pipe separation simulations is. This is expected, as the further the pipes are placed from the borehole centre, the longer the distance they move in the x and y plane. From Figure 5(c), in the outer configuration the two separation models have the largest difference in the positioning of the pipes, as in fixed pipe separation the pipes remain close to the edge of the borehole throughout the depth (Figure 5(c) cross-section A) while in variable pipe separation the pipes are displaced towards the centre Figure 5(c)). As shown in Figure 10 and discussed above, the distribution of temperature within the borehole is very different for the two models and adopting the variable pipe separation shows more extreme temperatures within the borehole. It is therefore reasonable that the effect of the variable pipe separation is more significant the further the pipes are displaced. However, the magnitude of the distance should be noted here, as the pipes in the outer configuration only move 14.5 mm more than the ones in the inner configuration; a distance that seems insignificant when considering the usual nature of GHE construction, yet changes in fluid temperature can be significant (note that changes of just 1 or 2 °C in the fluid temperature represent significant changes in the amount of thermal energy exchanged with the ground).

Figure 12(b) shows how the effect of variable pipe separation changes when the GHE is required to provide different amounts of thermal energy. As can be seen, the more energy provided by each GHE in a GHE field, the more dominant the effect is and thus the higher $\bar{T}_{diff}$ is. This suggests that if the pipes adopt a variable pipe separation for a given GHE, which was designed using a fixed pipe separation, the higher the thermal load demand, the more extreme the resulting temperatures will be, compared to those expected in its design. Moreover, the figure suggests that this is close to a linear relationship, with the values of the other input parameters determining the gradient. The most important parameter determining the gradient has been discovered to be the thermal conductivity of the grout, indicating that it is critical to the significance of the thermal load on this effect. The lower the thermal conductivity of the grout, the steeper the gradient of a line of Figure 12(b) and thus $\bar{T}_{diff}$ increases more for the same increase in the thermal load, compared to results from cases with higher values of λ_{grout}. A similar observation can be made for the effect of the configuration, as seen in Figure 12(a), with the difference that the relationship shown for that parameter is not linear. Both of these figures suggest that the observed differences are due to accumulation of energy and that with more efficient energy transfer (i.e. higher λ_{grout}), the effect from the parameters can be minimised.

Figure 12(c) and Figure 12(d) show how the magnitude of the effect of variable pipe separation changes with the variation of the thermal conductivity of the grout and ground, respectively. As it can be seen, varying the thermal conductivity of the grout causes a very large change in $\bar{T}_{diff}$ (up to 60% reduction between using 0.7 and 2.1 W/(mK)), while varying the thermal conductivity of the ground shows no significant change in $\bar{T}_{diff}$. This can be understood more clearly by studying Figure 10 once again. Looking at the temperature distribution, it is evident that the highest difference between the two separation models occurs within the borehole, where the grout is located. The contour lines show not only the locations of the maxima/minima but also the high variation of temperatures within the borehole. Changing the thermal conductivity of the grout will affect the contour lines within the borehole, and since the thermal gradient is different between the two models, this will affect each one by a different magnitude and cause $\bar{T}_{diff}$ to vary. However, the contour lines outside the borehole, within the ground, are quite similar between the two models. Therefore, despite the fact that when changing the value of λ_{ground}, the response and average fluid temperature distribution of each of the two different pipe separation models changes significantly, the results suggest that this change is of equal magnitude and therefore, when comparing the two, $\bar{T}_{diff}$ does not change significantly.

In the "*selected*" parametric analysis, the fluid flow rate is varied, taking the values of 5.5 L/min and 13 L/min as well as the 11 L/min that is used throughout the *complete* parametric analysis. Fewer variations of the previous four parameters are used, as specified earlier, with the exception of the thermal load value which is constant for all simulations (Medium). The results, shown in Figure 12(e), show no significant change in $\bar{T}_{diff}$ with a change in the fluid flow rate. These observations agree with the literature that fluid flow rate within a GHE does not significantly affect the energy exchanged as long as a turbulent regime is maintained [38,40].

Lastly, it is worth objectively quantifying the importance of each of these parameters to the effect of variable pipe separation. To do this, three different statistical methods are used on the data from the analysis. These methods regard the sensitivity of models to input parameters and assign a relative score to each of these

parameters based on their significance on the outcome, which in this case is $\bar{T}_{diff}$. The first two of these techniques are machine learning algorithms: the Random Forests algorithm [41], labelled as RF, used primarily in prediction modelling and the "SelectKBest" feature selection algorithm, labelled as SKB, used primarily to evaluate 'features' for a machine learning model. The latter can be found implemented in the "scikit-learn" python library and uses mutual information scoring [42]. The last method is a much simpler sensitivity index [43], labelled as SSI. These three methods have different specific scopes (such as making predictions for RF or information scoring for SKB) and therefore use different algorithms and equations to calculate the exact value of their sensitivity index which is not expected to be numerically equal; however, what they share is the aim to rank parameters in terms of their significance on the outcome. The results can be seen in Table 3 and show that even though the three methodologies compute different score values, they all agree on the order of significance of the parameters, which is the critical outcome for this investigation. Moreover, they all agree that the thermal conductivity of the grout is by far the most important parameter, followed by the configuration of the pipes and the thermal load of the GHE, both being relatively important, while the thermal conductivity of the ground and the flow rate show no relative significance, for the one year simulations.

Table 3. Sensitivity index of design parameters

Parameter	Sensitivity Index		
	RF	**SKB**	**SSI**
Thermal Conductivity of the grout, λ_{grout}	0.6109	0.6127	0.9100
Configuration (α_{pipe})	0.1991	0.4198	0.5249
Thermal Load per GHE	0.1822	0.3556	0.4510
Thermal Conductivity of the grout, λ_{ground}	0.0075	0	0.0259
q_{fluid}	0.0002	0	0.0249

4.4 Cost Analysis

The changes in the GHE fluid temperature due to variable pipe separation can have important economic implications. Firstly, as it has been shown in section 4.1 (Figure 8) this effect could result in more extreme temperatures, which could be detrimental to heat pump operation and/or efficiency. Since a way to increase the performance of the system is increasing the length of the borehole and pipes (and/or number of GHEs which would be even more costly), it is worth investigating what the equivalent additional length required is, such that a variable pipe separation GHE with a longer than 50 metre borehole will perform equally to the 50 metre borehole straight pipe separation GHE. This additional length would result in increases in *capital costs* when building the system. Secondly, in less severe cases, variable pipe separation could compromise the operational efficiency of a GSHP system. If such a system is under-designed, it is expected that it will run at lower COPs than designed for, meaning that it will require more electricity to provide the required amount of thermal energy. This additional electricity, due to the lower running efficiency, will therefore increase the *running* costs of the system.

The important question to answer in order to identify the degree of additional capital costs is: "How much longer do the boreholes need to be for the variable pipe separation GHE to perform as sufficiently as the designed 50 metre borehole fixed pipe separation GHE?" Figure 13 shows a comparison of this for the set of parameters shown in Figure 8, but for all three different pipe configurations. As can be seen, $\bar{T}_{diff}$between the 2 cases (fixed pipe separation and longer variable pipe separation) decreases to a minimum point and then increases again. This is because $\bar{T}_{diff}$ measures the absolute difference between the two models. Therefore, for GHEs that are shorter than the length where $\bar{T}_{diff}$ is minimum, the difference is due to the variable pipe separation simulation producing more extreme temperature values (as in Figure 8, for example), meaning the system would be under-designed. However, when GHEs are longer than the length corresponding to the minimum $\bar{T}_{diff}$ in the figures, the difference is due to the fixed pipe separation simulation producing more extreme temperature values, meaning a length in this range would be over-designing the system. The minimum $\bar{T}_{diff}$lengths for the three configurations, inner, mid and outer, are 55, 58 and 62 metres respectively, for this

specific set of parameters. These are very significant, showing a required increase in drilling of 10%, 16% and 24% respectively, which suggests considerable increases in capital costs.

<Figure 13 around here>

Regarding the running cost implications of variable pipe separation in a 50 m GHE system, Figure 14 shows the percentage difference in running costs between the variable and fixed pipe separation simulations for a variety of different cases (i.e. input parameter sets from Table 2). The values of λ_{grout} have been added to the figure, indicating a trend of increasing costs with decreasing λ_{grout}. To compute these values, firstly the COP values have been calculated, based on the entering water temperatures (into the GSHP) and technical specifications of a typical heat pump (Climate Master™ TC Series 50 Hz TCH/V036 – HFC410A). Following, the calculation of the total running costs for a year was computed based on the different COP values between fixed and variable pipe separation simulations and the thermal load. The results are surprising and show that even though the differences in the temperatures of the fluid within the pipes for the two different separation models are relatively high and the resulting variation of the amount of geothermal energy is large, the monetary effect on the running cost is minimal, with the highest being around 5% for the case shown in Figure 8 (provided an antifreeze solution is used). It is believed that the reason for this relates to the efficiency of the heat pump used in this analysis, where a difference in entering water temperature of a few degrees does not significantly affect the COP, as well as the distribution of the thermal load, where in summer both heating and cooling are needed (Figure 7), with abrupt changes between one and the other over short periods of time, thus quickly relieving the negative effects of variable pipe separation.

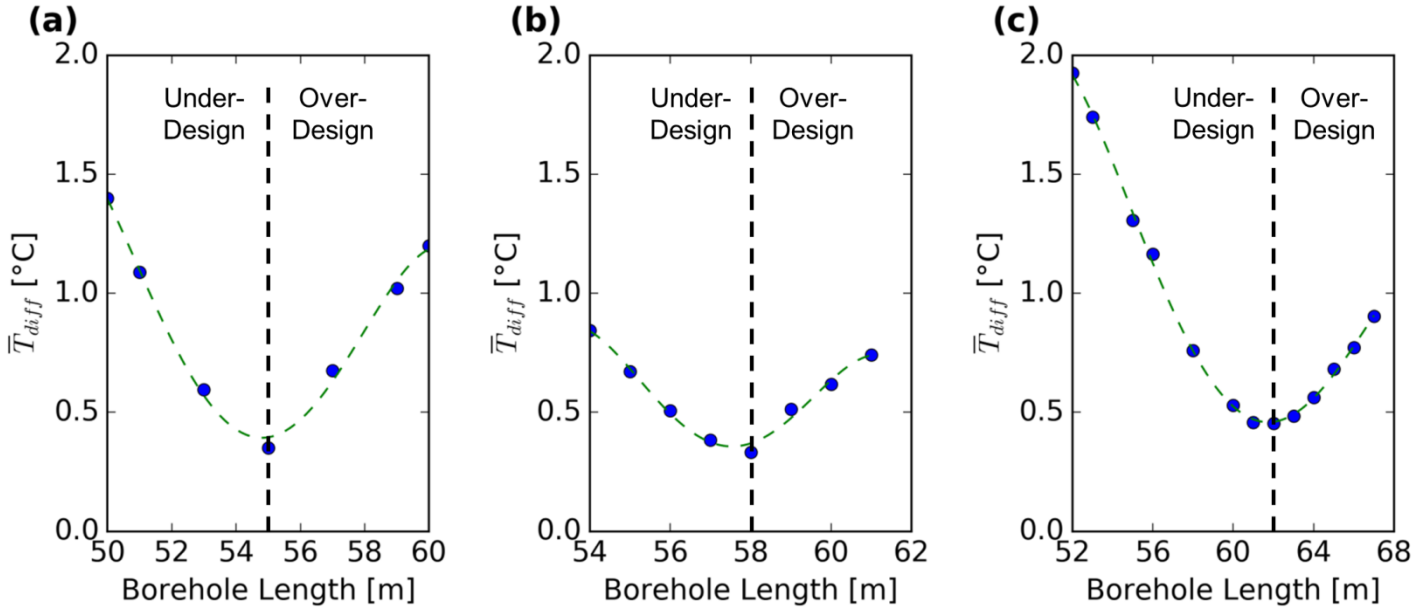


Figure 13. Comparison of a variable pipe separation geometry with longer than 50 m borehole length to a fixed pipe separation geometry with 50 m length borehole (Parameters as Figure 7 – configuration: (a) Inner, (b) Mid, (c) Outer)

<Figure 14 around here>

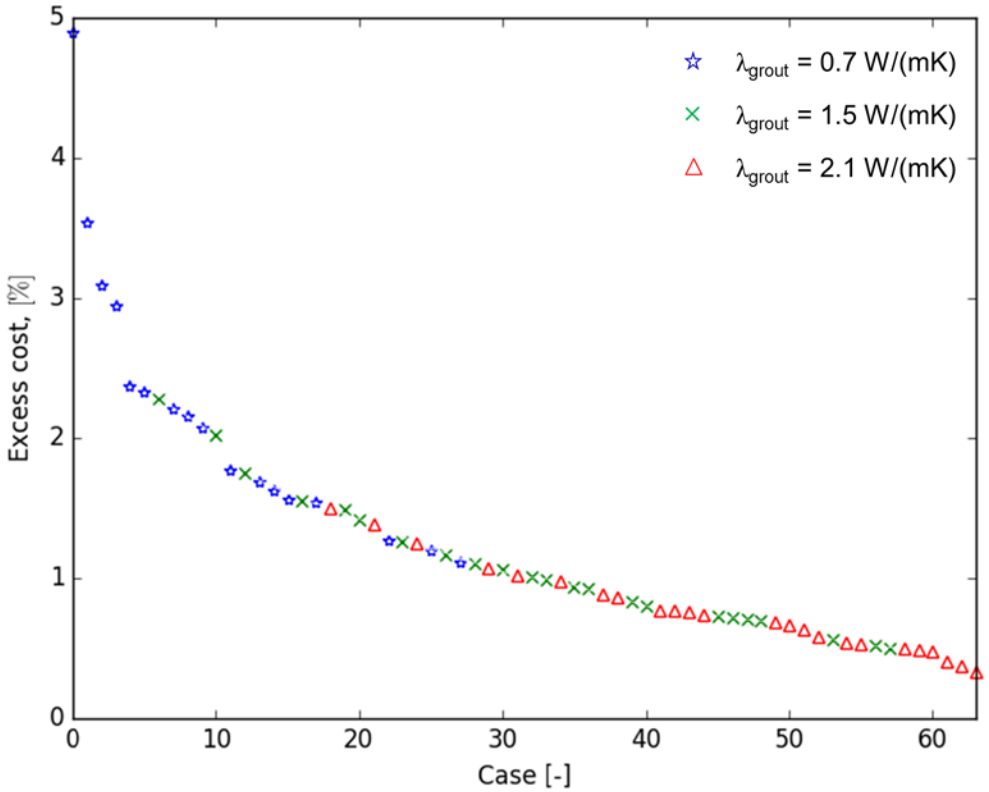


Figure 14. Excess in annual running cost of variable over fixed pipe separation simulations

This study shows that when accounting for the effect of variable pipe separation, if the more extreme temperatures that it produces are outside the working range for the heat pump, then there can be very high additional costs for drilling deeper GHEs (up to 24% deeper in the case presented) to compensate for the negative effect of variable pipe separation. On the other hand, if these temperatures are still within the working range for the heat pump and are not overly extreme, then the additional costs of running the system with a lower COP appear to be insignificant. However, it should be noted that this study focused on the weather profile of Melbourne, Australia, and that the presented values would be different for a different thermal demand. This would also be true for differences caused by the assumptions adopted in this study, for example not accounting for groundwater flow and assuming the pipes will only deflect towards the centre of the borehole. Therefore, further studies are required to fully quantify the extent of excess in running costs.

5 Summary and Conclusion

This study presented an investigation of the effect of variable pipe separation, which occurs when the separation between the pipes within a GHE varies along the length of the borehole. The study showed that ignoring this effect can leave the system under-designed, when the pipes move closer together compared to their design configuration. A model with a sinusoidal-based pipe geometry that simulates this effect was presented and a parametric analysis was undertaken to investigate the significance of important design parameters on this effect. The most influential of these parameters was found to be the thermal conductivity of the borehole filling material (grout), showing significant reductions in this effect when using a higher thermal conductivity material. The thermal load and the design configuration/separation of the pipes were also found significant, while the thermal conductivity of the ground and the fluid flow rate show no influence over this effect. Additionally, a random pipe separation analysis explored the response of GHEs where the pipe separation changed randomly along the length, confirming the degree of significance of the effect and the suitability of the model presented to represent the random nature of the movement of pipes within a GHE. It should be noted that it is expected that the effects of variable pipe separation can become positive if in ‘Inner’ or ‘Mid’ design configurations the pipes also move outwards (toward the borehole wall) as supposed to only inwards (this study). This behaviour and its impacts will be further explored in future works.

The potential economic impacts of variable pipe separation both on capital and running costs of the system were also investigated. A significant capital cost increase, of up to 24% in drilling costs for a particular case shown here, may be needed in order to compensate for the effect of variable pipe separation. This increase would be relevant when the more extreme temperatures caused by this effect would affect the viability of the design, thus requiring additional length in order to lower the magnitude of those temperatures. On the other hand, the running costs, calculated by comparing the different COPs and thus efficiencies of fixed and variable pipe separation models, showed only a relatively minor cost increase of up to 5% for Melbourne's weather profile (additional COP reductions arising from the use of antifreeze solution instead of plain water not included). Therefore, in these conditions, the cost impact of variable pipe separation is deemed mostly relevant when a GSHP system is designed (using fixed pipe separation) such that the fluid temperatures are near the operating heat pump limits.

Overall, even though different geometries, configurations and variables can give different results for the response of a specific GSHP system, the study presented shows that that the variability of the pipe location within the GHE, even with relatively short distances, can have a significant effect on the system performance and is therefore worthy of further investigation.

ACKNOWLEDGEMENTS

Funding from the Australian Research Council (ARC) FT140100227, The University of Melbourne and the Victorian Government is much appreciated.

REFERENCES

[1] Brandl H. Energy foundations and other thermo-active ground structures. Géotechnique 2006;56:81–122. doi:10.1680/geot.2006.56.2.81.

[2] Florides G, Kalogirou S. Ground heat exchangers-A review of systems, models and applications. Renew Energy 2007;32:2461–78. doi:10.1016/j.renene.2006.12.014.

[3] Preene M, Powrie W. Ground energy systems: from analysis to geotechnical design. Géotechnique 2009;59:261–71. doi:10.1680/geot.2009.59.3.261.

[4] Johnston IW, Narsilio GA, Colls S. Emerging geothermal energy technologies. KSCE J Civ Eng 2011;15:643–53. doi:10.1007/s12205-011-0005-7.

[5] Narsilio GA, Johnston IW, Bidarmaghz A, Colls S, Mikhaylova O, Kivi A, et al. Geothermal energy: Introducing an emerging technology. In: Horpibulsuk S, Chinkulkijniwat A, Suksiripattanapong C, editors. Proc. Int. Conf. Adv. Civ. Eng. Sustain. Dev. (ACESD 2014). Volume 1 o, Nakhon Ratchasima, Thailand: Suranaree University of Technology,; 2014, p. 141–54.

[6] Lund J, Boyd T. Direct Utilization of Geothermal Energy 2015 Worldwide Review. Proc World Geotherm Congr 2015:25–9. doi:10.1016/j.geothermics.2011.07.004.

[7] Bayer P, de Paly M, Beck M. Strategic optimization of borehole heat exchanger field for seasonal geothermal heating and cooling. Appl Energy 2014;136:445–53. doi:10.1016/j.apenergy.2014.09.029.

[8] Retkowski W, Thöming J. Thermoeconomic optimization of vertical ground-source heat pump systems through nonlinear integer programming. Appl Energy 2014;114:492–503. doi:10.1016/j.apenergy.2013.09.012.

[9] Bidarmaghz A. 3D Numerical Modelling of Vertical Ground Heat Exchangers. The University of Melbourne, 2014.

[10] Huang S, Ma Z, Wang F. A multi-objective design optimization strategy for vertical ground heat exchangers. Energy Build 2015;87:233–42. doi:10.1016/j.enbuild.2014.11.024.

[11] Atam E, Helsen L. Ground-coupled heat pumps: Part 1 - Literature review and research challenges in modeling and optimal control. Renew Sustain Energy Rev 2016;54:1653–67. doi:10.1016/j.rser.2015.10.007.

[12] Atam E, Helsen L. Ground-coupled heat pumps: Part 2—Literature review and research challenges in optimal design. Renew Sustain Energy Rev 2016;54:1668–84. doi:10.1016/j.rser.2015.07.009.

[13] Pandey N, Murugesan K, Thomas HR. Optimization of operating parameters of ground source heat pump system for space heating and cooling by Taguchi method and utility concept. Appl Energy

2017;190:421–38. doi:10.1016/j.apenergy.2013.10.065.
[14] Blázquez CS, Martín AF, Nieto IM, García PC, Santiago L, Pérez S, et al. Efficiency Analysis of the Main Components of a Vertical Closed-Loop System in a Borehole Heat Exchanger. Energies 2017;10:1–15. doi:10.3390/en10020201.
[15] Rivera JA, Blum P, Bayer P. Increased ground temperatures in urban areas: Estimation of the technical geothermal potential. Renew Energy 2016;103:388–400. doi:10.1016/j.renene.2016.11.005.
[16] Law YLE, Dworkin SB. Characterization of the effects of borehole configuration and interference with long term ground temperature modelling of ground source heat pumps. Appl Energy 2016;179:1032–47. doi:10.1016/j.apenergy.2016.07.048.
[17] Yuan Y, Cao X, Wang J, Sun L. Thermal interaction of multiple ground heat exchangers under different intermittent ratio and separation distance. Appl Therm Eng 2016;108:277–86. doi:10.1016/j.applthermaleng.2016.07.120.
[18] Gultekin A, Aydin M, Sisman A. Thermal performance analysis of multiple borehole heat exchangers. Energy Convers Manag 2016;122:544–51. doi:10.1016/j.enconman.2016.05.086.
[19] Dehghan B, Sisman A, Aydin M. Parametric investigation of helical ground heat exchangers for heat pump applications. Energy Build 2016;127:999–1007. doi:10.1016/j.enbuild.2016.06.064.
[20] Dehghan B. B. Experimental and computational investigation of the spiral ground heat exchangers for ground source heat pump applications. Appl Therm Eng 2017;121:908–21. doi:10.1016/j.applthermaleng.2017.05.002.
[21] Bidarmaghz A, Narsilio G, Johnston I. Numerical modelling of ground loop configurations for Direct geothermal applications. Aust Geomech J 2012;47:21–6.
[22] Hu P, Yu Z, Zhu N, Lei F, Yuan X. Performance study of a ground heat exchanger based on the multipole theory heat transfer model. Energy Build 2013;65:231–41. doi:10.1016/j.enbuild.2013.06.002.
[23] Cho H, Choi JM. The quantitative evaluation of design parameter's effects on a ground source heat pump system. Renew Energy 2014;65:2–6. doi:10.1016/j.renene.2013.06.034.
[24] Selamat S, Miyara A, Kariya K. Numerical study of horizontal ground heat exchangers for design optimization. Renew Energy 2016;95:561–73. doi:10.1016/j.renene.2016.04.042.
[25] Cosentino S, Sciacovelli A, Verda V, Noce G. Optimal operation of ground heat exchangers in presence of design anomalies: An approach based on second law analysis. Appl Therm Eng 2016;99:1018–26. doi:10.1016/j.applthermaleng.2015.11.130.
[26] Makasis N, Narsilio GA, Bidarmaghz A, Johnston IW. Effects of ground heat exchanger variable pipe separation in ground-source heat pump systems. In: Wuttke F, Bauer S, Sanchez M, editors. Energy Geotech. - Proc. 1st Int. Conf. Energy Geotech. ICEGT 2016, Kiel: CRC Press; 2016, p. 155–61.
[27] Narsilio GA, Bidarmaghz A, Johnston IW, Colls S. Geothermal Energy: detailed modelling of ground heat exchangers. Comput Geotech 2016.
[28] Bidarmaghz A, Makasis N, Narsilio GA, Franco F, Perez MEC. Geothermal Energy in Loess. Environ Geotech 2016;4:225–36.
[29] Bidarmaghz A, Narsilio GA, Buhmann P, Moormann C, Westrich B. Thermal interaction between tunnel ground heat exchangers and borehole heat exchangers. Geomech Energy Environ 2017;10:29–41. doi:10.1016/j.gete.2017.05.001.
[30] Bidarmaghz A, Narsilio GA. Heat exchange mechanisms in energy tunnel systems. Geomech Energy Environ 2018:conditionally accepted.
[31] Colls S. Ground Heat Exchanger Design For Direct Goethermal Energy Systems. The University of Melbourne, 2013.
[32] Bidarmaghz A, Narsilio GA, Johnston IW, Colls S. The importance of surface air temperature fluctuations on long-term performance of vertical ground heat exchangers. Geomech Energy Environ 2016;6:35–44. doi:10.1016/j.gete.2016.02.003.
[33] Carlslaw KS, Jaeger JC. Conduction of Heat in Solids. Oxford: Clarendon Press; 1959.
[34] Ingersoll LR, Zobel OJ, Ingersoll AC. Heat Conduction with Engineering, Geological and Other Applications. University of Wisconsin Press; 1954.
[35] Kakac S, Yener Y. Heat Conduction. Washington DC: Hemisphere Publishing Corp; 1985.
[36] Eskillson P. Thermal Analysis of Heat Extraction Boreholes. University of Lund, Sweden, 1987.

[37] Florides GA, Christodoulides P, Pouloupatis P. An analysis of heat flow through a borehole heat exchanger validated model. Appl Energy 2012;92:523–33. doi:10.1016/j.apenergy.2011.11.064.
[38] Bidarmaghz A, Narsilio G, Johnston I. Numerical Modelling of Ground Heat Exchangers with Different Ground Loop Configurations for Direct Geothermal Applications, Paris: International Conference on Soil Mechanics and Geotechnical Engineering (18th ICSMGE); 2013, p. 3343–6.
[39] Makasis N, Narsilio GA, Bidarmaghz A, Johnston IW. Carrier fluid temperature data in vertical ground heat exchangers with a varying pipe separation. Data Br 2017;"submitted.
[40] Cecinato F, Loveridge F. Influences on the thermal efficiency of energy piles. Energy 2015;82:1021–33. doi:10.1016/j.energy.2015.02.001.
[41] Breiman L. Random forests. Mach Learn 2001;45:5–32. doi:10.1023/A:1010933404324.
[42] Kraskov A, Stögbauer H, Grassberger P. Estimating mutual information. Phys Rev E - Stat Nonlinear, Soft Matter Phys 2004;69:1–16. doi:10.1103/PhysRevE.69.066138.
[43] Hoffman FO, Gardner RH. Evaluation of uncertainties in environmental radiological assessment models. In: Till JE, Meyer HR, editors. Radiol. Assessments A Textb. Environ. Dose Assess., Washington D.C.: US Nuclear Regulatory Commission, Report no. NUREG/CR-3332; 1983, p. 11.1-11.55.

3.3 Journal paper: Carrier fluid temperature data in vertical ground heat exchangers with a varying pipe separation

This section consists of a journal paper titled: “Carrier fluid temperature data in vertical ground heat exchangers with a varying pipe separation”, published in the journal *Data in Brief*. The paper has been inserted in the following pages, as published by the journal, with the only modification being the addition of the thesis page numbers at the bottom of the page (allowing consistent numbering throughout the thesis) and the repositioning of the journal page numbering to the top of the page. This publication is the author’s original work, has been included with the co-authors’ authorisation (appropriate co-author authorisation forms have been included in this submission) and the co-authors’ contributions have been acknowledged in the *Preface & Publications* section.

Data in Brief 18 (2018) 1466–1470

Contents lists available at ScienceDirect

Data in Brief

journal homepage: www.elsevier.com/locate/dib

Data article

Carrier fluid temperature data in vertical ground heat exchangers with a varying pipe separation

Nikolas Makasis [a], Guillermo A. Narsilio [a], Asal Bidarmaghz [a,b], Ian W. Johnston [a]

[a] Department of Infrastructure Engineering, The University of Melbourne, Parkville, Australia
[b] Department of Engineering, University of Cambridge, Cambridge CB2 1PZ, United Kingdom

ARTICLE INFO

Article history:
Received 14 February 2018
Accepted 3 April 2018
Available online 6 April 2018

ABSTRACT

The dataset in this article is related to shallow geothermal energy systems, which efficiently provide renewable heating and cooling to buildings, and specifically to the performance of the vertical ground heat exchangers (GHE) embedded in the ground. GHEs incorporate pipes with a circulating (carrier) fluid, exchanging heat between the ground and the building. The data show the average and inlet temperatures of the carrier fluid circulating in the pipes embedded in the GHEs (which directly relate to the performance of these systems). These temperatures were generated using detailed finite element modelling and comprise part of the daily output of various one-year simulations, accounting for numerous design parameters (including different pipe geometries) and ground conditions. An expanded explanation of the data as well as comprehensive analyses on how they were used can be found in the article titled *"Ground-source heat pump systems: the effect of variable pipe separation in ground heat exchangers" (Makasis N, Narsilio GA, Bidarmaghz A, Johnston IW, 2018)* [1].

© 2018 The Authors. Published by Elsevier Inc. This is an open access article under the CC BY license (http://creativecommons.org/licenses/by/4.0/).

DOI of original article: https://doi.org/10.1016/j.compgeo.2018.02.010
E-mail address: narsilio@unimelb.edu.au (G.A. Narsilio).

https://doi.org/10.1016/j.dib.2018.04.005
2352-3409/© 2018 The Authors. Published by Elsevier Inc. This is an open access article under the CC BY license (http://creativecommons.org/licenses/by/4.0/).

Specifications Table

Subject area	*Geothermal Energy, Geotechnics, Engineering*
More specific subject area	*Effect of variable (non-fixed with depth) pipe separation in borehole ground heat exchangers*
Type of data	*Figures, MS Excel file*
How data was acquired	*Generated using experimentally validated finite element modelling*
Data format	*Raw, Analysed*
Experimental factors	*Data processed using statistical methods*
Experimental features	*The effect of a variable pipe separation is determined, as well as its sensitivity to important design parameters*
Data source location	*Data maintained in University of Melbourne servers/databases*
Data accessibility	*Data supplied in article as excel file – supplementary data*
Related research article	*N. Makasis, G.A. Narsilio, A. Bidarmaghz, I.W. Johnston, Ground-source heat pump systems: the effect of variable pipe separation in ground heat exchangers, Comput. Geotech.* ***100*** *(2018), 97–109.*

Value of the data

- The data were generated using complex and computationally expensive numerical methods (requiring several months to be completed) and can be of use to researchers that are interested in modelling the heat transfer process in shallow geothermal systems.
- The data allow researchers to further expand on the analyses presented in [1] and/or use other statistical tools in investigating this effect.
- The range of input parameters used to generate the data allow researchers to investigate different aspects of this technology and the importance of these parameters.
- The dataset that incorporates randomness can lead to a more extensive statistical analysis of the impact of randomness on these systems.

1. Data

The data describe the operation of vertical ground heat exchangers (GHE), used in shallow geothermal technologies to provide efficient and renewable heating and cooling to buildings. A modelled GHE consists of a borehole that has pipe loops embedded within it and transfers heat to and from the ground. The data of this article describe the daily average temperature of the circulating (carrier) fluid in the pipes (average of inlet and outlet) as well as the inlet temperature from which the outlet and the thermal load over time can be derived. These temperatures result from the simulated annual operation of various geothermal systems, each having different design parameters and/or ground conditions, ensuring a large number of annual datasets that satisfy a wide range of possible designs and/or locations. The data provide insights regarding the performance and efficiency of shallow geothermal systems.

2. Experimental design, materials, and methods

The data were generated using a validated finite element numerical methodology, and applied through the software COMSOL Multiphysics, which was developed at the University of Melbourne [2–4]. This methodology models the conduction and convection heat transfer processes taking place during the operation of a shallow geothermal system (see for example [5,6] for a detailed description

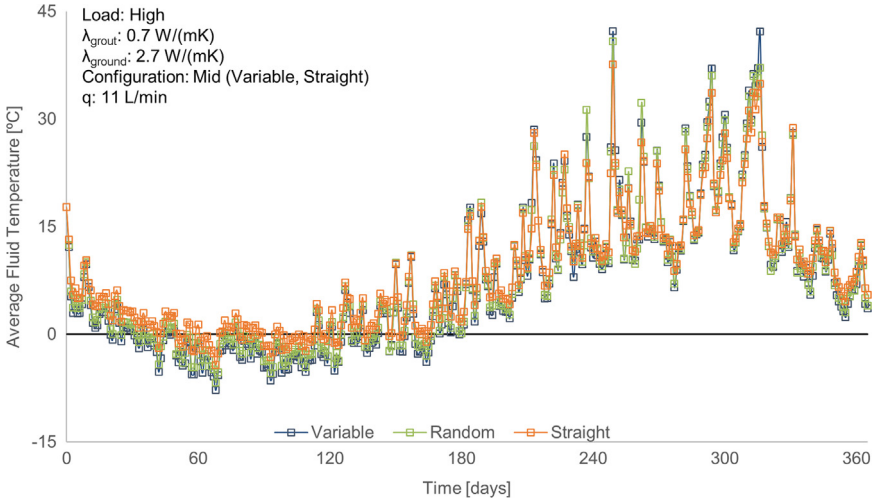


Fig. 1. Average fluid temperature for each day of one year simulation, for the three different pipe separation geometries. (Note: Random id = 102).

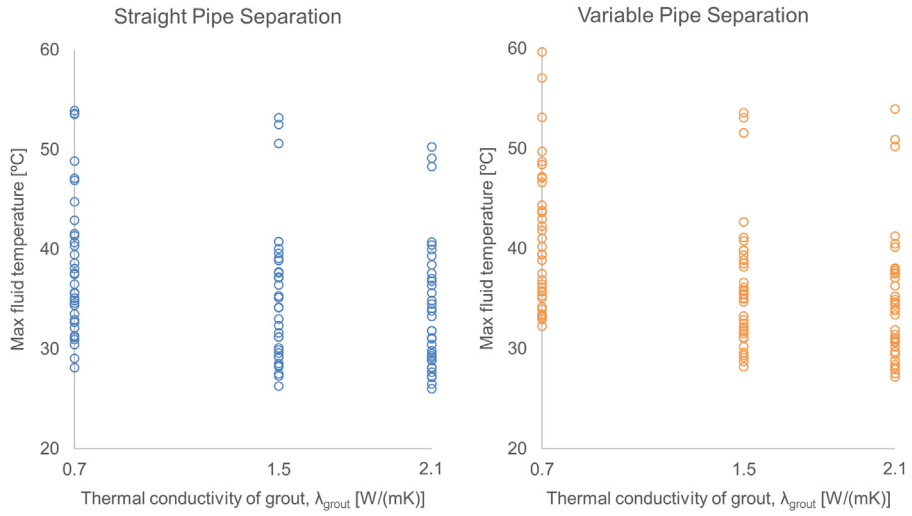


Fig. 2. Annual maximum fluid temperature over the thermal conductivity of the grout, for the straight (fixed) and variable pipe separation geometries.

of these systems). The simulation process is very computationally expensive and to generate this rich dataset of over 300 simulations, high performance computing was utilised over the course of several months.

For each simulation, different design parameters and conditions were used. Overall, the data are separated into three main categories, based on the geometry of the pipes within the GHE, describing the potential effect on the system performance when the placement of the pipes along the depth of the GHE is not as expected or varies. The first category describes the pipes being fixed in place along

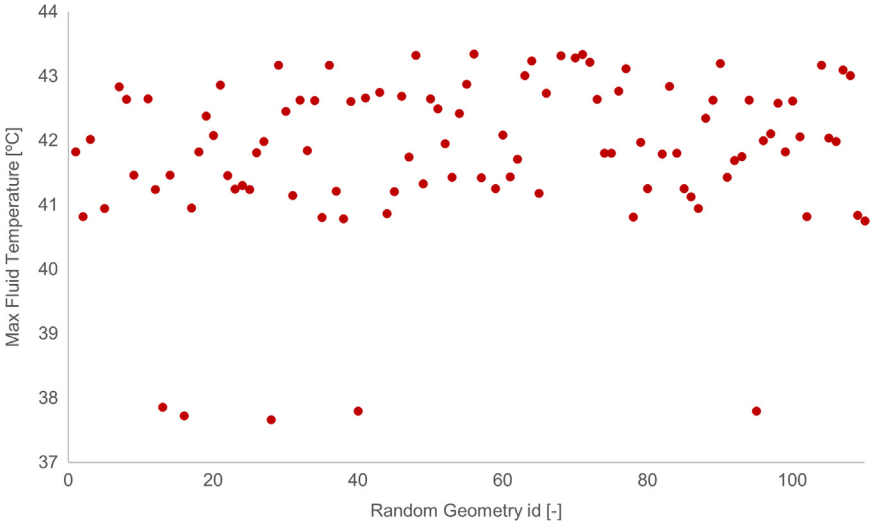


Fig. 3. Annual maximum fluid temperature for 100 different randomised pipe geometries.

the depth of the GHE (labelled "Straight"), the second category describes the pipes moving in a sinusoidal pattern along the depth of the GHE (labelled "Variable") and the third category describes the pipes moving randomly along the depth of the GHE (labelled "Random"). Fig. 1 shows a comparison between these three geometries for one sample set of input parameters, while Figs. 2 and 3 show sample plots that can be created from the supplied data to extract insights. Fig. 2 compares the straight and sinusoidal varying geometries (category 1 and 2) in comparison to one of the design parameters (thermal conductivity of the grout in the GHE, λ_{grout}) and Fig. 3 demonstrates the design inaccuracy due to randomness in the pipe geometry (category 3). It should be noted that for the case where the pipes move randomly, around 100 different variations of this random geometry were used (seen in x axis of Fig. 3), all using the same set of input parameters. The exact geometries and parameters used to generate the dataset as well as expanded analyses on this topic can be found in [1].

Acknowledgements

Funding from the Australian Research Council (ARC) FT140100227, The University of Melbourne and the Victorian Government is much appreciated.

Appendix A. Supporting information

Supplementary data associated with this article can be found in the online version at https://doi.org/10.1016/j.dib.2018.04.005.

References

[1] N. Makasis, G.A. Narsilio, A. Bidarmaghz, I.W. Johnston, Ground-source heat pump systems: the effect of variable pipe separation in ground heat exchangers, Comput. Geotech. 100 (2018) 97–109. http://dx.doi.org/10.1016/j.compgeo.2018.02.010.
[2] A. Bidarmaghz, 3D Numerical Modelling of Vertical Ground Heat Exchangers, The University of Melbourne, Australia, 2014.
[3] A. Bidarmaghz, N. Makasis, G.A. Narsilio, F. Franco, M.E.C. Perez, Geothermal energy in loess, Environ. Geotech. 4 (2016) 225–236. http://dx.doi.org/10.1680/jenge.15.00025.

[4] A. Bidarmaghz, G.A. Narsilio, P. Buhmann, C. Moormann, B. Westrich, Thermal interaction between tunnel ground heat exchangers and borehole heat exchangers, Geomech. Energy Environ. 10 (2017) 29–41. http://dx.doi.org/10.1016/j.gete.2017.05.001.
[5] H. Brandl, Energy foundations and other thermo-active ground structures, Géotechnique 56 (2006) 81–122. http://dx.doi.org/10.1680/geot.2006.56.2.81.
[6] G. Florides, S. Kalogirou, Ground heat exchangers-a review of systems, models and applications, Renew. Energy 32 (2007) 2461–2478. http://dx.doi.org/10.1016/j.renene.2006.12.014.

3.4 Simplified method to account for variable pipe separation

Section 3.2 shows the importance of accounting for the effect of variable pipe separation and the degree at which it can influence the GSHP design. Building on the presented information and acknowledging that modelling a varying instead of fixed separation is computationally expensive, it is important to identify an easily adoptable approach that can be used to account for this effect in design practice. This section presents one such methodology which involves utilising a representative fixed pipe separation model, in which the pipes are accounted as if placed closer together than designed (and placed in reality), shown schematically in Figure 3.1.

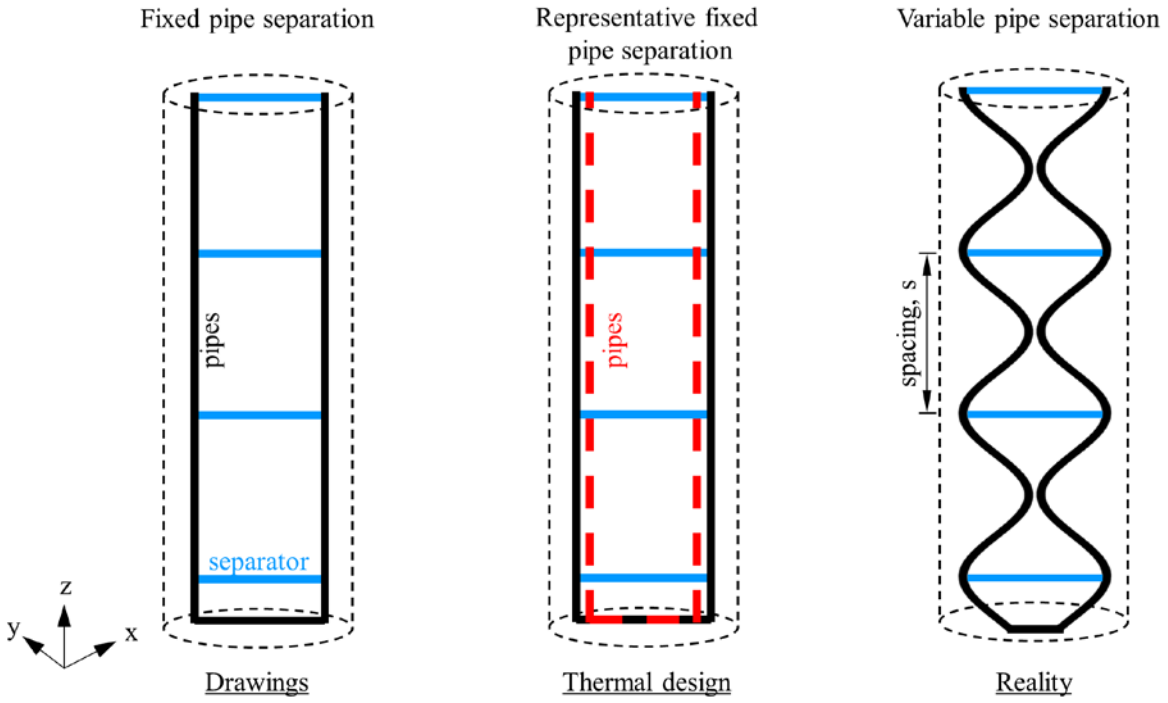


Figure 3.1 Schematic showing the representative fixed pipe separation

In determining a representative fixed pipe separation, results from a range of separation values for the variable pipe separation case were examined. Looking at Figure 3.2 (Figure 5 of the journal paper in section 3.2), χ is the distance from the centre of the borehole to the centre of each pipe (assuming they are moving uniformly away/towards the centre along the depth. When the pipes are closest together, this distance is $17.8\,mm$, for all potential design separations – configurations (inner, mid, outer). The position where the pipes are the furthest away from each other for each configuration is at depth 'A' (when a separator is placed and the pipes are at the positions they are designed to be) where $\chi = 28.5\,mm$, $\chi = 35.8\,mm$ and $\chi = 43\,mm$ respectively. Therefore, since the separation between the pipes varies between $\chi = 17.8\,mm$ and the above values, it can be expected that a fixed separation value within

these ranges could provide a good approximation to the varying separation pipe thermal behaviour.

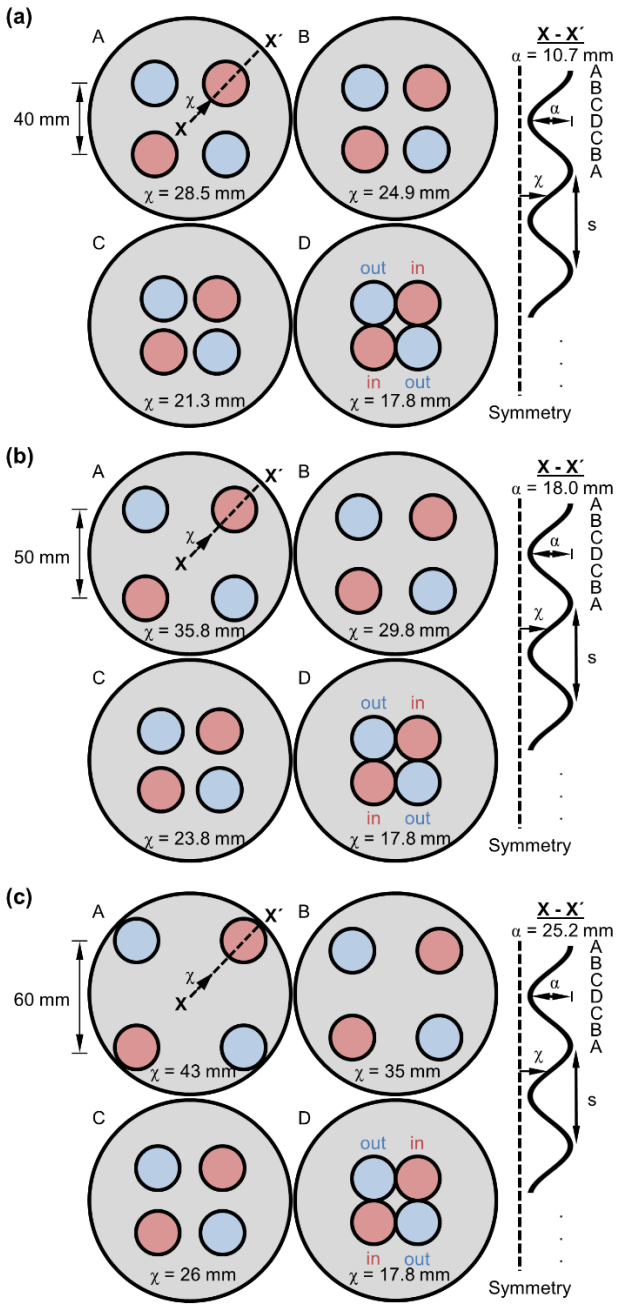


Figure 3.2 Cross-section of double loop GHE (used in this analysis) with sinusoidal variable pipe separation as it varies along depth: (a) 'Inner' configuration, (b)'Mid' configuration, (c) 'Outer' configuration. (Figure 5 of paper in section 3.2)

To investigate the above hypothesis, several fixed pipe separation numerical models were run, each with a different value of χ, from about 21 mm to about 33 mm. The averaged absolute fluid temperature difference was calculated between each of these fixed pipe separation models and the respective variable pipe separation model for each of the three configurations (similarly to explanation in section 4.1 of the paper in section 3.2). Moreover, multiple values for the

thermal conductivity of the grout and concrete as well as the thermal load were used to consider their effect and produce a complete analysis.

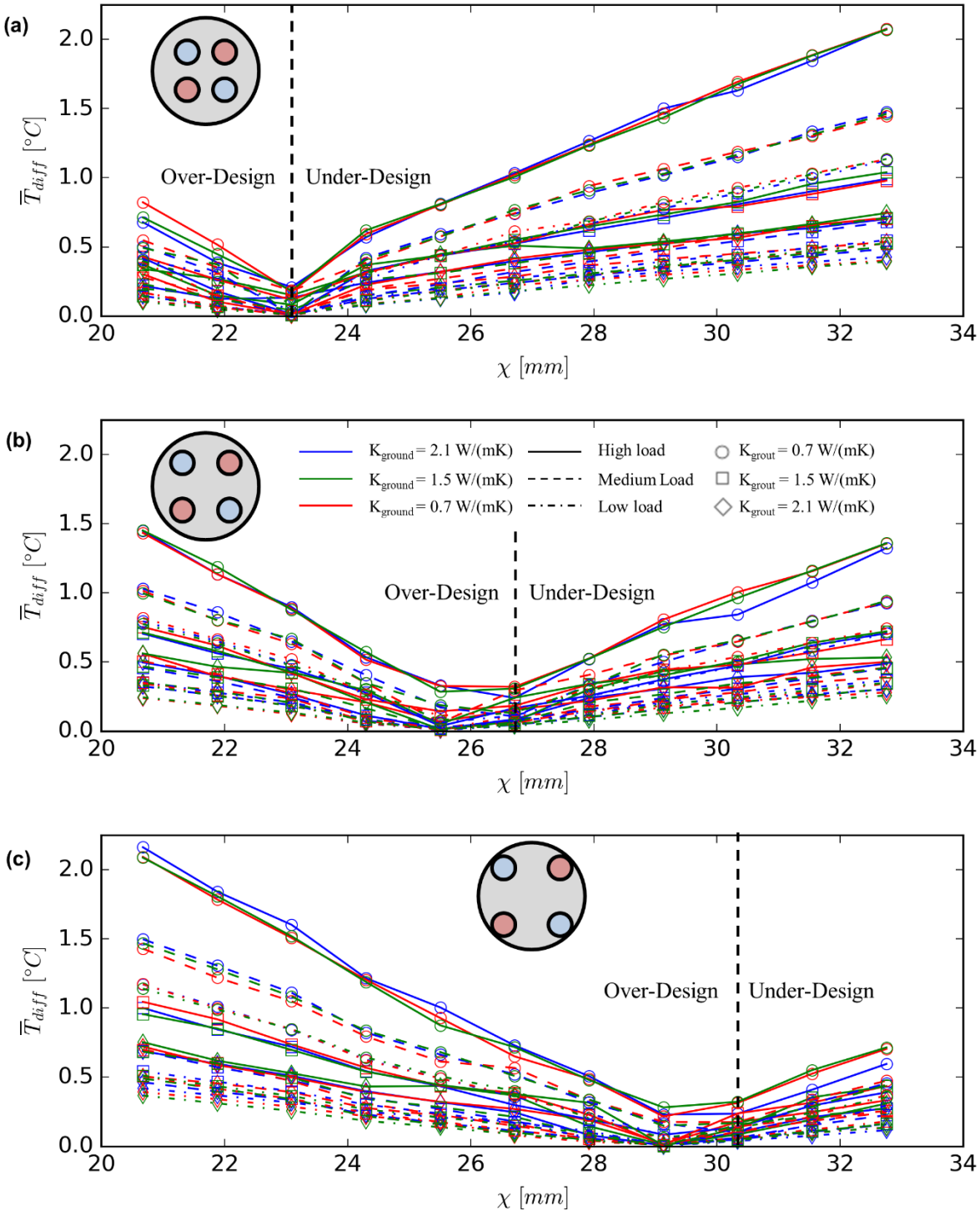


Figure 3.3 Investigating the average absolute temperature difference between a fixed pipe separation GHE of varying χ value and a variable pipe separation GHE adopting (a) inner (b) mid and (c) outer configurations. The dashed vertical line represents χ_{av} the averaged separation of the pipes along the depth of the GHE

The results can be seen in Figure 3.3 for each of the three configurations, (a) inner, (b) mid and (c) outer. Similar to the extended borehole length analysis of the paper (section 4.4 – Figure 13), the results are presented in two regions, under-designed and over-designed. In the under-

designed region, the values of the average temperature difference are such that the expected resulting temperatures (from the variable pipe separation model) are more extreme than those predicted by the fixed separation model. In the over-designed region, the opposite is true, resulting in less risk in the design but potentially under-utilisation of the system. As seen in Figure 3.3, the values of $\bar{T}_{diff}$ come to a minimum point – close to a value of 0 °C – when the value of χ is about $\chi_{av} = 23.2\ mm, \chi_{av} = 26.8\ mm, \chi_{av} = 30.4\ mm$ (indicated by the dotted lines) respectively, for the three configurations inner, mid and outer tested. When considering the varying separation of the pipes, it turns out that these χ_{av} values, representing the averaged separation of the pipes along the depth of the borehole, can be calculated simply using Equation (10). The results show that near identical fluid temperature values between a fixed pipe separation with the averaged (smaller) value of χ and the variable pipe separation as described in the paper can be achieved, the former being much simpler and faster to compute than the latter. This pattern is in general consistent for all three configurations, for all values of the thermal conductivity of the grout/grout and the thermal loads.

$$\chi_{av} = (\chi_{max} - \chi_{min})/2 \tag{10}$$

This suggests that, as a general approach, to minimise discrepancies between unaccounted movement of the pipes and variations in the separation, one could use the averaged position of the pipes (given that the separation varies throughout the depth towards the centre of the borehole) for thermal performance evaluation/design purposes and still adopt a fixed separation model, which is much easier to model and solve compared to a varying separation model. Based on the presented results, it would be suggested to use a value slightly less than the averaged χ, to ensure the results will be in the over-designed region. Therefore, the value of χ_{av} can be used when evaluating the thermal performance of the system, while the design drawings for construction include χ_{max} as the loop shank/spacing (instead of χ_{av}).

3.5 Summary and conclusions

This chapter introduced the effect of *variable pipe separation*, which can result due to the installation conditions of pipes in GSHP systems (specifically in vertical boreholes) and is currently not typically accounted for during GSHP system design. The importance of this effect and potential consequences of not accounting it in the design have been presented in the attached publications along with the data stemming from this work (obtained over a number of weeks of numerical modelling using high performance computing), for the scientific community to utilise. Section 3.5 introduces a simple methodology that can be incorporated in

GSHP system design to overcome this potentially unjustified assumption and incorporate the effect of variable pipe separation in real applications.

The key findings of this chapter can be summarised as below:

- Ignoring the effect of variable pipe separation can result in an under-designed GSHP system, with a lacking performance or in certain cases the system not functioning.
- The thermal conductivity of the grout material in the borehole was found to be the most influential for the magnitude of this effect, over the one-year simulations, with high values of conductivity minimising the effect of variable pipe separation.
- The thermal load distribution and the designed separation of the pipes were also found significant, to a lesser extent, with lower magnitude thermal loads and smaller designed pipe separations resulting in a reduced effect of variable pipe separation.
- The fluid flow rate and the thermal conductivity of the ground were found to be relatively insignificant to the effect of variable pipe separation, the latter possibly being due the relatively short simulation duration.
- Having the pipes change their position randomly along the depth of the borehole showed similar results to when adopting a sinusoidal pattern of movement, indicating the suitability of the selected geometry to model this effect.
- Accounting for the effect of variable pipe separation by increasing the depth of the borehole, showed a significant increase in capital costs of up to 24%.
- Investigating the effect of variable pipe separation on the running costs, due to the change in the COP values, showed a relatively insignificant cost increase of up to 5%.
- A simple methodology to account for the effect of variable pipe separation has been introduced, where a shorter separation of pipes that the one used during installation is adopted, assuming the pipes are placed closer together than in reality and thus accounting for them potentially moving closer together. This assumed shorter separation can be taken as the average position of the pipes, based on the expected movement and maximum/minimum values of separation.
- The data generated from this chapter, using complex and computationally expensive numerical modelling, have been shared with the scientific community. allowing researchers to expand on the presented analyses, investigate different aspects, as well as use the data more broadly in the field of heat transfer and/or shallow geothermal systems.

Chapter 4 Numerical modelling and design of energy geo-structures

4.1 Overview and structure

Energy geo-structures, being a relatively recent concept in the shallow geothermal energy field, lack standardised design approaches. There exists limited research undertaken on the impact of design parameters on energy geo-structures' thermal performance. This is particularly the case for energy retaining walls, for which available literature is much more limited than that for energy piles, leading to energy retaining walls being the focus of this research. This chapter presents a numerical modelling investigation focused on energy geo-structure design approaches and it aims to further understand how they can be better designed and utilised.

Section 4.2 presents a summary of an energy pile investigation, undertaken during the early stages of the doctoral research. This investigation served as a stepping stone in the field of energy geo-structures and was impactful for the course of the doctoral research because it introduced a number of research questions and highlighted the room for improvement and further understanding of energy geo-structures. Findings of this work were published in the UK Institution of Civil Engineers' *Environmental Geotechnics* technical journal[1].

Section 4.3 constitutes the main body of this chapter, presenting detailed investigations on the design of energy retaining walls. The investigation was initially undertaken as part of a technical feasibility study for incorporating geothermal technologies in the new Melbourne Metro project, working closely with representatives of the Melbourne Metro Railway Authority (MMRA) and their technical advisors. Following the outcomes of the feasibility study, further and more detailed investigations were undertaken towards a more complete analysis that is not subject to project constraints, both monetary and time-based. The section presents the geometry, materials and finite element approach adopted to model the thermal performance of retaining wall structures as well as the thermal load distributions, representing the amount of energy they needed to provide. The results for the different investigations are then presented, for two types of energy walls, diaphragm walls and soldier pile walls. The impact of various parameters on the design, such as the balance of the thermal load distribution and the amount of geothermal pipe embedded in the structures was investigated. Lastly, the importance of the

[1] The paper (found in Appendix A) was recognised as "Best of Research and Practice 2016" by the editorial board.

boundary conditions used in numerical modelling of energy retaining walls is examined in section 4.3.5. Different approaches found in the literature are utilised and compared to emphasise the consequences of this choice regarding the results of the numerical modelling.

Section 4.4 provides a summary of the chapter's findings.

4.2 Energy piles modelling

Energy piles are currently the most utilised and well researched energy geo-structure, likely due to their similarities in geometry with traditional GHE boreholes, as explained in detail in section 2.2.3.3. Therefore, naturally, the entry point in energy geo-structures for this doctoral research was an energy pile case study that investigated the potential of energy piles in loessial soils, undertaken with a team of academics from Australia and Argentina. The outcome was a publication in the ICE's *Environmental Geotechnics* journal, titled: "Geothermal energy in loess" (2nd author), found in Appendix A.

This work concentrated on a realistic energy pile case study, located in Cordoba, Argentina, and developed a 3D finite element model to evaluate the thermal performance of the energy pile field. Research collaborators from Argentina provided insights about the site (including measured data for parameters such as the soil thermal conductivity and thermal load estimations), while the team at the University of Melbourne concentrated on the numerical modelling and analyses. Figure 4.1 illustrates the developed finite element model, including the geometrical arrangements as well as the boundary conditions used, further explained in the published paper. It is worth noting that, since this case study consists of a realistic scenario, it also resulted in challenges usually absent from theoretical work. As it can be seen, two different diameters of piles were utilised, resulting in different length of pipe for each, which required careful consideration of the flow rate and the connections between the pipe loops embedded in each pile. Moreover, the pile field placement is non-symmetrical, meaning that the numerical representation could not exploit symmetry but instead the entirety of the field had to be modelled, which was computationally expensive.

Unlike traditional borehole GSHP system design, in energy geo-structure design a significant challenge is the fact that the geometry and configuration of the structures (in this case piles) is determined by the structural design, while energy provision is a secondary function. Therefore, providing the entire thermal demand for the building cannot be guaranteed. Instead, in energy geo-structure design, the important question to answer is: "*How much energy can the system provide?*". This work focused around answering this question. Figure 4.2 shows the thermal

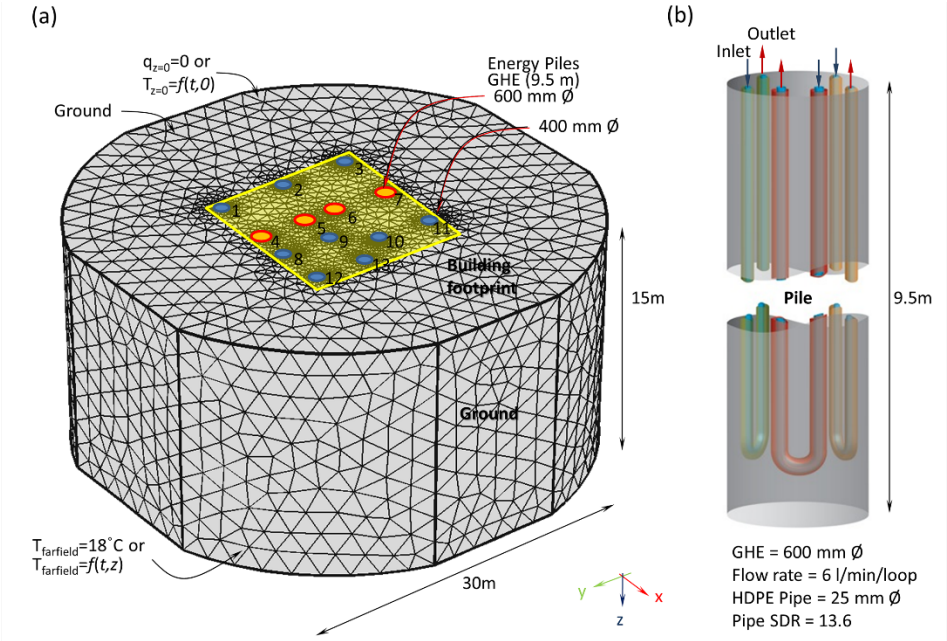
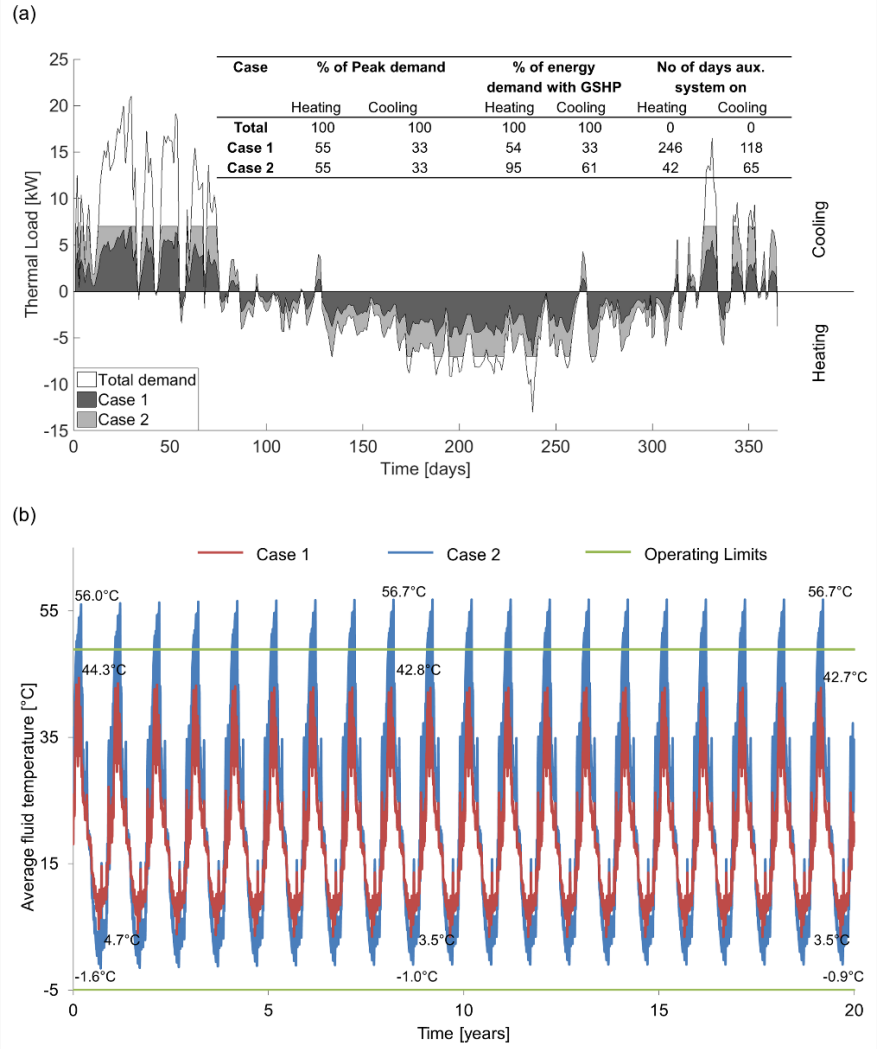


Figure 4.1 Case study in Cordoba, Argentina: (a) finite element model of the energy pile field (residential building footprint shown in yellow) (b) detail of one of the 600 mm piles (seen in orange colour in (a))



Case	% of Peak demand		% of energy demand with GSHP		No of days aux. system on	
	Heating	Cooling	Heating	Cooling	Heating	Cooling
Total	100	100	100	100	0	0
Case 1	55	33	54	33	246	118
Case 2	55	33	95	61	42	65

Figure 4.2 Energy pile case study in Cordoba, Argentina: (a) Thermal load distributions and (b) resulting average fluid temperatures

load distributions utilised, based on the typical climate conditions for the area and building envelopes, as well as the resulting GHE fluid temperatures, showing that the majority of the heating and a good portion of the cooling demands can be satisfied with this design. Moreover, two different types of thermal load distributions were adopted, accounting for different usage behaviours for the system, either always using a combination of the GSHP and auxiliary systems (Case 1), or only using the auxiliary system when the GSHP system cannot provide the required demand (Case 2).

Moreover, further investigations were undertaken to better understand and evaluate the thermal performance of the energy pile field. Firstly, the thermal performance enhancement from the addition of (non-structural) piles to the field was considered, finding that with these twelve additional 9.5 m GHEs the entire building's heating demand and a large portion of its cooling demand could be comfortably satisfied, as shown in Figure 4.3. However, this could be a very costly addition if done purely for the geothermal system and therefore a hybrid system could be better suited in this case. In a hybrid system, part of the thermal load is satisfied by the geothermal system, while the remaining balance, by an (small) auxiliary system (e.g., traditional gas furnace or split aircon system). Furthermore, the effect of the thermal conductivity of the loess material was considered, since loessial soils in Cordoba have relatively low thermal conductivities which is known to hinder the performance of the system. The results, seen in Figure 4.4, show the average GHE fluid temperature when the "Case 1" thermal load distribution is adopted (Figure 4.2(a)), showing a significant decrease in the temperatures with increasing thermal conductivity of the ground and confirming that the energy pile field would be performing considerably better in locations with higher thermal conductivity soils.

Overall, this work showed how energy piles can be used in providing heating and cooling for a realistic case study. It also included a variety of further investigations, such as identifying that providing the entirety of the thermal load using the energy piles might not be the most beneficial solution, but instead a hybrid system could work well for this case. Very importantly, this work served as an important introduction to the challenges associated with energy geo-structure design. Standardised approaches were not available and adopting numerical modelling was extremely time and resource consuming, especially for large models with geometries where symmetries could not be exploited (to reduce the computational domain). Moreover, the change of focus of the design to estimate the amount of energy to be provided by the geothermal system with energy geo-structures, instead of sizing the system (such as boreholes in traditional GSHP) to ensure provision of the required load, is a key question that

this doctoral research has aimed to answer using different approaches, such as further detailed in Chapter 5.

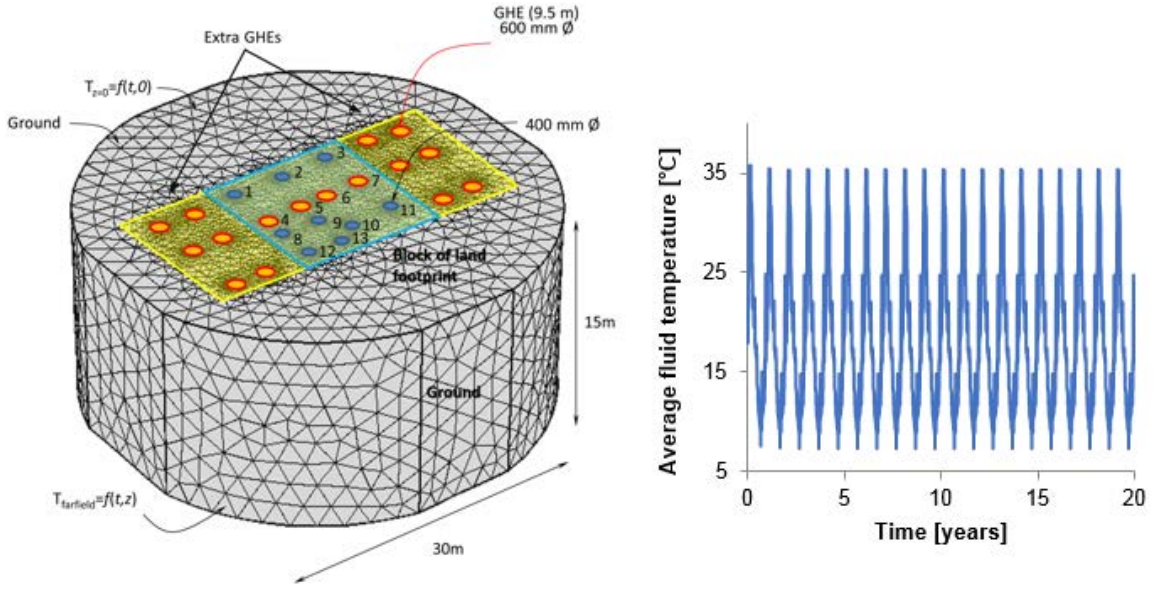


Figure 4.3 Investigating how additional GHEs affect the performance of the system: (a) the model and geometry (b) the resulting GHE fluid temperatures when providing the entirety of the building's heating and 60% of its cooling demand

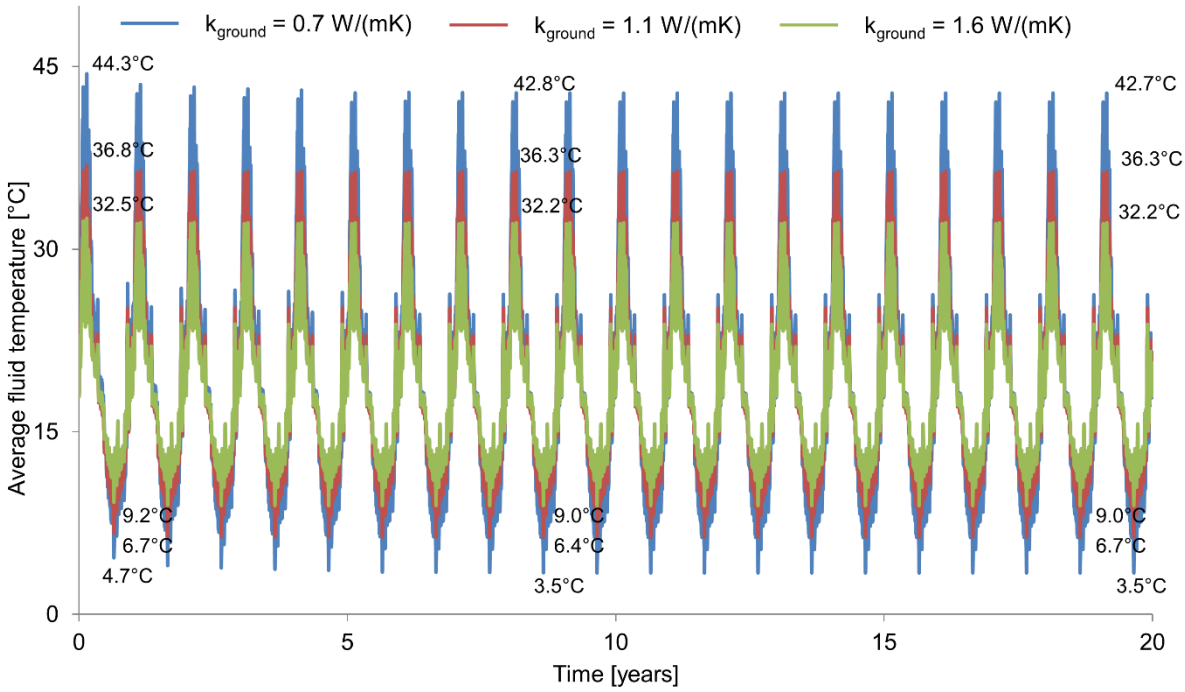


Figure 4.4 Investigating the effect of the ground thermal conductivity on the thermal performance of the system

4.3 Energy Retaining Walls

4.3.1 Overview, challenges and opportunities

A significant focus of this doctoral research has been the thermal design and performance of energy retaining walls. This considerably less researched and understood energy geo-structure has substantially different geometry and conditions compared to traditional borehole GSHP systems and therefore the modelling and analyses are arguably different. Retaining walls introduce further challenges and constraints to the design, specifically with regards to the fact that they are not in contact with the ground on all their sides, but instead one of their faces consists of the underground building (such as a basement floor or an underground station), as explained in section 2.2.3.3. This means that heat transfer towards the building side needs to be carefully considered and controlled to make sure it does not impact the operation of the system or the comfort within the building.

This research utilised the unique opportunity to work with a real large-scale project and perform energy retaining wall design for different wall types and conditions. This opportunity came through the Melbourne Metro Railway Authority (MMRA) and the well-known Melbourne Metro project, which is expected to be finished by 2026 and is building five new underground metro stations and adding 9 km of metro tunnelling to ease the congestion of public transport in the city centre. A team of researchers from the geotechnical/geothermal research group at the University of Melbourne were appointed to investigate the potential of applying shallow geothermal technology using two representative stations, known as *Domain* and *Parkville*, the first adopting diaphragm and the second soldier pile retaining walls, due to the different dominant geologies. This unique opportunity allowed for realistic investigations, as part of this doctoral research, working closely together with structural engineers, mechanical engineers and project managers from MMRA and its technical consultants and associates. Through this collaboration a number of significant conclusions were drawn, further understanding these systems and adding to the worldwide knowledge pool of energy retaining walls. Outcomes of this work can be found in the completed design reports [30,31], as well as a conference paper (focusing on the diaphragm walls thermal performance) published in the proceedings of the International Symposium on Energy Geotechnics 2018. This paper can be found in Appendix B.

Following the completion of the work with MMRA, additional numerical investigations were undertaken, unaffected by the budgetary and time constraints on delivery for this real project,

to provide further understanding on how certain geometrical parameters, such as the extend of the depth of embedment or the spacing of the pipe loops, can affect the structure's thermal performance. These allow for a reflection on the work undertaken under industry conditions (with strict deadlines and limited resources), to evaluate how the design could be improved if this information was available during that time, suggesting its potential value for future projects. Moreover, an analysis on the importance of the boundary conditions adopted on the building faces was considered important to undertake to stress the potential implications on the design.

4.3.2 Numerical modelling of energy retaining walls

To model the energy retaining walls, the numerical methodology presented in section 2.2.4 were utilised and implemented in the COMSOL Multiphysics finite element software, and the necessary modifications and additions were incorporated to enable the modelling of retaining walls (such as different boundary conditions and less symmetrical/more angular geometries compared to other structures such as boreholes and piles). This section presents the details of the numerical methodology adopted, a validation for retaining walls utilising experimental data, as well as the details of the finite element models including the geometry and material parameters adopted for the two different cases/types of retaining walls.

4.3.2.1 Governing equations

The adopted numerical model is based on the coupling of the heat transfer and fluid flow equations, as explained in section 2.2.3.5 [112]. Heat conduction and convection both take place in the simulation of the GHEs' operation. Heat conduction is present in the ground, the concrete or backfilling material of the GHE and the geothermal pipe wall, as well as partially in the carrier fluid (usually water). Heat convection is dominant in the carrier fluid, as it flows through the pipes, as well as in the ground if groundwater movement is taken into consideration. To model the conductive heat transfer Equation (11) is adopted, assuming no presence of groundwater flow. In the presented work groundwater flow is not incorporated, however [115] presents how this can be included (by modifying Equation (11) and incorporating Darcy's law), which in general can improve the GSHP system performance. The flow in the pipes is considered as fully developed and for its modelling the continuity and momentum equations for incompressible fluid are used, as seen in Equations (12) and (13) respectively [113]. The energy equation that describes the convective-conductive heat transfer in the fluid flow can be seen in Equations (14) and (15) [114].

$$\rho_m C_{p,m} \frac{\partial T_m}{\partial t} = \nabla.(\lambda_m \nabla T_m) \tag{11}$$

$$\nabla.(A\rho_w \boldsymbol{v}) = \mathbf{0} \tag{12}$$

$$\rho_w \left(\frac{\partial \boldsymbol{v}}{\partial t}\right) = -\nabla p - f_D \frac{\rho_w}{2d_h} |\boldsymbol{v}| \boldsymbol{v} \tag{13}$$

$$\rho_w A C_{p,w} \frac{\partial T}{\partial t} + \rho_w A C_{p,w} \boldsymbol{v} \nabla T = \nabla (A \lambda_w \nabla T) + f_D \frac{\rho_w A}{2d_h} |\boldsymbol{v}| \boldsymbol{v^2} + Q_{wall} \tag{14}$$

$$Q_{wall} = f(T_{m,pipe\ wall}, T) \tag{15}$$

where ρ_m is the solid material density $[kg/m^3]$, $C_{p,m}$ the specific heat capacity of a solid material $[J/kgK]$, t is time $[s]$, λ_m the thermal conductivity of a solid material $[W/mK]$, A is the inner cross-section of the HDPE pipe $[m^2]$, ρ_w the carrier fluid density $[kg/m^3]$, $\boldsymbol{v}$ the fluid velocity field $[m/s]$ in the pipes, p is pressure $[Pa]$, f_D represents the Darcy friction factor [-], d_h is the hydraulic diameter of the pipe $[m]$, $C_{p,w}$ is the specific heat capacity of the fluid $[J/kgK]$, λ_w the thermal conductivity of the fluid $[W/mK]$ and Q_{wall} is the external heat exchange rate through the pipe wall $[W/m]$, and a function of the temperature of the pipe outer wall, $T_{m,pipe\ wall}$ $[K]$, and the temperature of the carrier fluid T $[K]$

The equations are numerically solved for the pressure, velocity field and the temperature field. Utilising these equations, the heat transfer occurring throughout the 3D elements and 1D pipe elements and the fluid flow in the 1D pipe elements are coupled using the temperature of the pipe wall, $T_{m,pipe\ wall}$. Appropriate boundary and initial conditions are also required to undergo the modelling, for this work presented in sections 4.3.2.3 and 4.3.2.4. Overall, the presented model can accurately simulate the heat transfer processes in both laminar and turbulent regimes, homogeneous and heterogeneous soil profiles and for steady state or transient conditions.

Moreover, in the case where the air flow inside an underground building (such as a metro station) is incorporated (section 4.3.5), the air domain is modelled as a single phase compressible flow [137]. The Reynolds-averaged Navier-Stokes (RANS) equations are implemented for conservation of momentum as well as the continuity equation for conservation of mass, as seen in Equations (16) and (17) respectively. Equations (18) and (19) present the transport equations for the turbulent kinetic energy, k, and the turbulent dissipation rate, ϵ, respectively. Lastly, Equations (20) and (21) further define factors of the previous equations.

$$\rho_a \left(\frac{\partial \boldsymbol{u_a}}{\partial t}\right) + \rho_a (\boldsymbol{u_a} \cdot \nabla) \boldsymbol{u_a} = \tag{16}$$

$$\nabla \cdot \left[-\mathrm{p}_\alpha I + (\mu + \mu_T)(\nabla \boldsymbol{u_a} + (\nabla \boldsymbol{u_a})^T) - \frac{2}{3}(\mu + \mu_T)(\nabla \cdot \boldsymbol{u_a})I - \frac{2}{3}\rho_a k I \right] + F$$

$$\frac{\partial \rho_a}{\partial t} + \nabla \cdot (\rho_a \boldsymbol{u_a}) = 0 \tag{17}$$

$$\rho \frac{\partial k}{\partial t} + \rho(\boldsymbol{u_a} \cdot \nabla)\mathrm{k} = \nabla \cdot \left[\left(\mu + \frac{\mu_T}{\sigma_k} \right) \nabla_\mathrm{k} \right] + P_k - \rho_a \epsilon \tag{18}$$

$$\rho_a \frac{\partial \epsilon}{\partial t} + \rho_a(\boldsymbol{u_a} \cdot \nabla)\epsilon = \nabla \cdot \left[\left(\mu + \frac{\mu_T}{\sigma_\epsilon} \right) \nabla_\epsilon \right] + \frac{C_{\epsilon 1}\epsilon}{k} P_k - \frac{C_{\epsilon 2}\rho_a \epsilon^2}{k} \tag{19}$$

$$\mu_T = \frac{\rho_a C_\mu k^2}{\epsilon} \tag{20}$$

$$P_k = \mu_T \left[\nabla \boldsymbol{u_a} : (\nabla \boldsymbol{u_a} + (\nabla \boldsymbol{u_a})^T) - \frac{2}{3}(\nabla \cdot \boldsymbol{u_a})^2 \right] - \frac{2}{3}\rho_a k \nabla \cdot \boldsymbol{u_a} \tag{21}$$

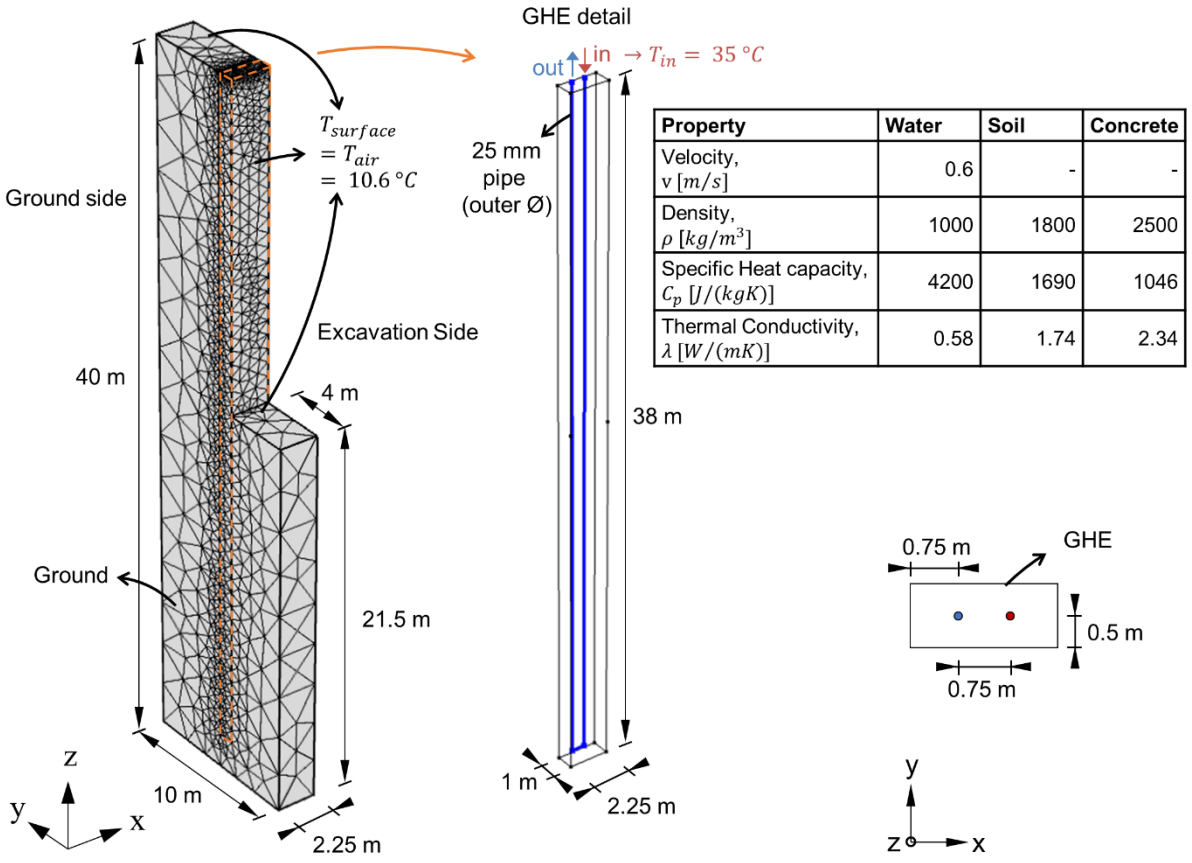
where ρ_a is the density of air ($kg/m\text{^}3$), $\boldsymbol{u_a}$ is the velocity vector for the air (m/s), p_α is the pressure of air (Pa), I the identity matrix (-), μ the dynamic viscosity of air ($Pa \cdot s$), μ_T the eddy or turbulent viscosity(m^2/s), k is the turbulent kinetic energy (m^2/s^2), F is the volume force vector (N/m^3), ϵ is the turbulent dissipation rate (m^2/s^3) and the empirically calculated coefficients $\sigma_k, \sigma_\epsilon, C_{\epsilon 1}, C_{\epsilon 2}, C_\mu$ have values of: $1, 1.3, 1.44, 1.92, 0.09$ respectively (as per [137]).

4.3.2.2 Numerical modelling validation

The numerical model methodology utilised builds upon one that has been previously thoroughly validated against both established analytical solutions, such as the two-dimensional Finite Line Source Model, as well as full scale experimental data, including utilising a single U-loop borehole GHE as well as a three U-loop pile GHE [112]. The numerical results showed an excellent agreement with the experimental data, for a range of conditions, operating patterns and geometries. An extension of this model has also been experimentally validated for energy tunnels, obtaining very good agreement between the numerical results and the experimental data [101,115]. However, energy retaining walls are a relatively recent concept and therefore very limited installations or sources of data exist. One available dataset consists of experimental data for an energy retaining wall case study from the Shanghai Museum of Natural History [94,138]. Therefore, this section presents a validation of the numerical model for energy retaining walls, following a similar approach as that adopted by Di Donna et al. [139].

The experiment used for validation run over a period of two days [138] and Figure 4.5 shows the geometry adopted for the validation model, having single pipe loops embedded in the retaining wall structure at mid-thickness and with a separation between the pipes of 750 mm.

Before the experiment began, the temperature of the ground, wall and air are reported as measured at 16.3 °C, 23 °C and 10.6 °C respectively. However, the reported wall temperature seems inconsistent, as it is stated that the experiment was undertaken 14 months after the pouring of the concrete, meaning the cement heating hydration would have already ceased long before testing; therefore, for this validation both the ground and wall are modelled as having an initial temperature of 16.3 °C. For the duration of the experiment, the inlet temperature was kept at 35 °C and the outlet temperature was recorded. The experiment was conducted as the project was still being constructed and consists of a retaining wall panel embedded in the soil and having part of one face exposed to the surface air. Therefore, a boundary condition of a constant temperature of 10.6 °C, as measured on site, was set on the appropriate model faces (e.g., on the excavation side and the top surface). On the other surfaces of the model, the boundary condition was set as a fixed temperature of 16.3 °C, representing thermally undisturbed conditions of the ground.



Property	Water	Soil	Concrete
Velocity, v $[m/s]$	0.6	-	-
Density, ρ $[kg/m^3]$	1000	1800	2500
Specific Heat capacity, C_p $[J/(kgK)]$	4200	1690	1046
Thermal Conductivity, λ $[W/(mK)]$	0.58	1.74	2.34

Figure 4.5 Validation modelling and material parameters

The validation results can be seen in Figure 4.6 and show that the computational results match well the experimental results. The results are presented in the form of heat extracted per unit length of pipe ($q = Q/PipeLength$) and is computed using the temperature of the supply (T_{in}) and return pipes (T_{out}) and Equation (*22*):

$$Q = \dot{m} C_p (T_{out} - T_{in}) \quad (22)$$

where Q is the heat transferred by convection $[W]$, $\dot{m}$ is the mass flow rate $[kg/s]$ (equal to $\dot{m} = 0.2kg/s$ equivalent to a water velocity of 0.6 m/s in a pipe of 25 mm outer diameter and SDR 11), and C_p represents the fluid heat capacity $[J/(kgK)]$.

Over the course of two days, the heat transfer reached a steady rate of approximately 50 W/m (Watts per meter length of pipe), in both experimental and numerical cases, while in the very initial stages of the experiment some inconsistencies exist, which is believed to be mainly due to experimental errors, given the very high values of q. Therefore, the experimental and numerical data are considered in agreement. It should be noted that this simple and short experiment and its adopted boundary conditions do not exactly match the energy retaining walls investigated in this section (which are thermally insulated towards the basement). For example, the fact that the excavation side was bare meant that as the system was operating the heat was dissipating in the air instead of being stored in the ground. However, it is still considered a valuable addition to the validation of the numerical model. These results, along with those of other validation studies for the model mentioned above, provide confidence on the validity of the numerical model and suggest its suitability for undertaking a numerical investigation on the thermal performance of energy retaining walls.

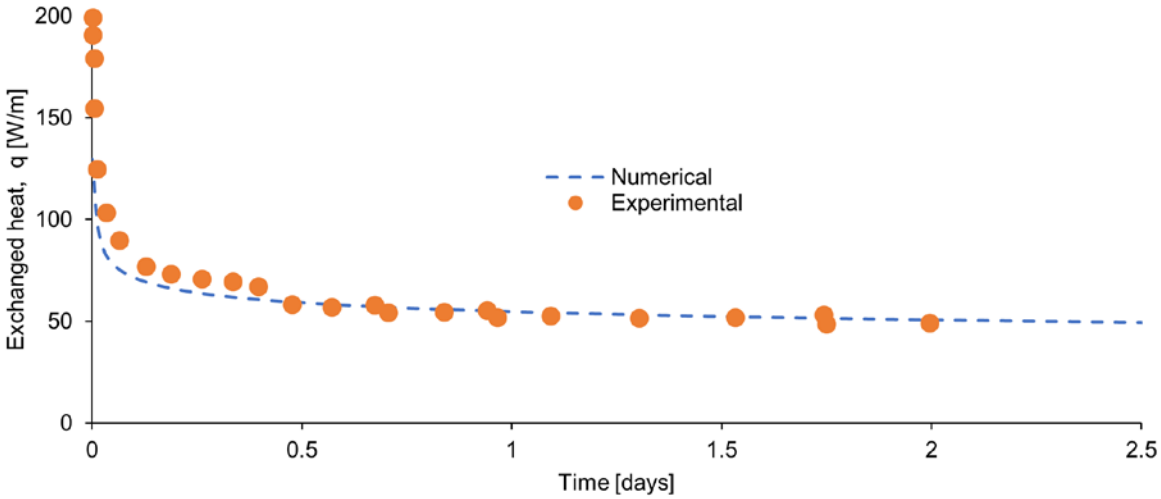


Figure 4.6 Validation results for the numerical (FE) model used showing the heat exchanged per unit of pipe length against time and compared against experimental results [138]

4.3.2.3 Energy diaphragm retaining wall numerical modelling

The finite element model for the diaphragm walls is presented in Figure 4.7, indicating the geometry as well as the boundary conditions utilised. As it can be seen, only a section (along the *x*-axis) of the wall is modelled (either a 6.5-metre or a 13-metre section depending on

whether loops are inserted in the slab in addition to the walls). However, the *symmetry* boundary condition is adopted on the *zy* plane to simulate the thermal effects from the neighbouring pipe loop circuits (along the *x*-axis), since the retaining wall is activated throughout, along its length. The *symmetry* boundary condition was also adopted on the *zx* plane, representing the effects of the retaining wall opposite the modelled one (-ve values along the *y*-axis), which is also thermally activated (note here that columns between the two walls along the y-axis are not modelled as their impact on the system is negligible). The utilisation of symmetry is important, since it substantially reduced the size of the computational model and therefore the running times and computational resources required. Another boundary condition is the constant temperature at the far end surface of the model (farfield boundary, *xz* plane, y = 120 m), which is set to the average undisturbed ground temperature of 18.5 °C. Thermal insulation is also used to render zero thermal flux through both the top (in city centre under buildings as well as being a conservative approach [33]) and bottom surfaces. Regarding the latter, adopting a farfield temperature would also yield similar results, since the surface is located far away from the GHEs to not influence the thermal transfer, however, thermal insulation is less restrictive as it allows the temperature at the boundary to vary. Thermal insulation is also applied at the wall and slab surfaces, inside the underground building, to prevent heat leakage. A detailed investigation of the importance of the boundary conditions, specifically for these inner surfaces, is presented in section 4.3.5.

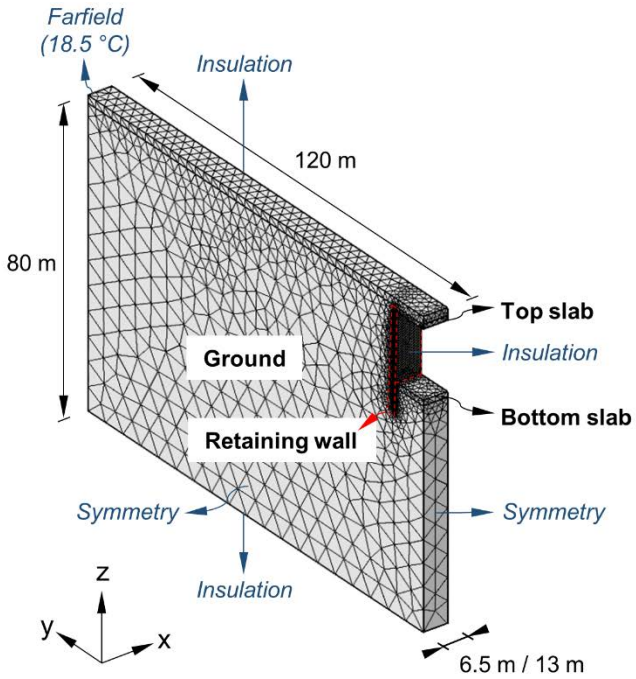


Figure 4.7 Energy diaphragm walls numerical modelling – model geometry and key boundary conditions

Two different geometries/models are used to simulate the diaphragm retaining walls, the first thermally activating only the retaining walls and the second also thermally activating the

bottom slab in addition to the retaining walls. This allows for an investigation of the impact of thermally activating the bottom slab, which is a relatively less established concept. In the case of only activating the diaphragm walls and not the slab, a 6.5-metre-wide section was adopted, modelling a single pipe loop circuit within one diaphragm wall cage, as can be seen in Figure 4.8. Each circuit consists of about 280 metres of HDPE pipe. The pipes are placed such that the carrier fluid follows a meandering path into/down the wall, and after the meandering pipe has reached the bottom end of the wall, it returns through a straight vertical path upwards, via the return pipe, connected to the most bottom horizontal pipe leg. The pipes can be attached (e.g. with cable ties) to the reinforcement cage (ground side) off-site, before being placed in the ground. The 450 mm pipe leg separation allows for the bending of pipe, removing the need for fittings. Moreover, it is acknowledged that the wall to slab structural connection can increase the density of reinforcement, however, with careful planning sufficient room to install the pipes can be found. When the slab is also thermally activated a 13-metre wide section was adopted for the numerical model, as seen in Figure 4.9. This model width allows for two of the wall pipe circuits (each about 280 metres of HDPE pipe) to be fully modelled, as well as one pipe circuit located in the bottom slab (about 275 m of HDPE pipe). The pipes in the wall have 275 mm cover on the ground side while the ones in the slab have 156 mm cover on the bottom and 100 mm cover on each end along the y-axis. The modelling parameters utilised can be seen in Table 4.1. These represent the soil conditions for the Domain area in Melbourne, Australia. Where applicable, these were obtained through site investigations; for example, the thermal conductivity of the ground was obtained via in situ TRT test results, performed by other members of the author's research group [60,140]. It should also be noted that the flow rate of the carrier fluid used throughout the analysis is 5.5 L/min, to allow time for the thermal transfer to take effect and to minimise pressure losses impacting on the size of the circulations pumps.

Table 4.1 Domain modelling - material properties

Parameter	Value(s)	Unit	Description
λ_{ground}	3.4	W/(mK)	Thermal conductivity of ground
ρ_{ground}	2400	kg/m^3	Density of ground
$C_{p\ ground}$	830	J/(kgK)	Specific heat capacity of ground
$\lambda_{concrete}$	2.1	W/(mK)	Thermal conductivity of concrete
$\rho_{concrete}$	2250	kg/m^3	Density of concrete
$C_{p\ concrete}$	890	J/(kgK)	Specific heat capacity of concrete
$T_{farfield}$	18.33	°C	Average annual ground temperature
λ_{fluid}	0.58	W/(mK)	Thermal conductivity of carrier fluid
ρ_{fluid}	998	kg/m^3	Density of carrier fluid
$C_{p\ fluid}$	4185	J/(kgK)	Specific heat capacity of carrier fluid

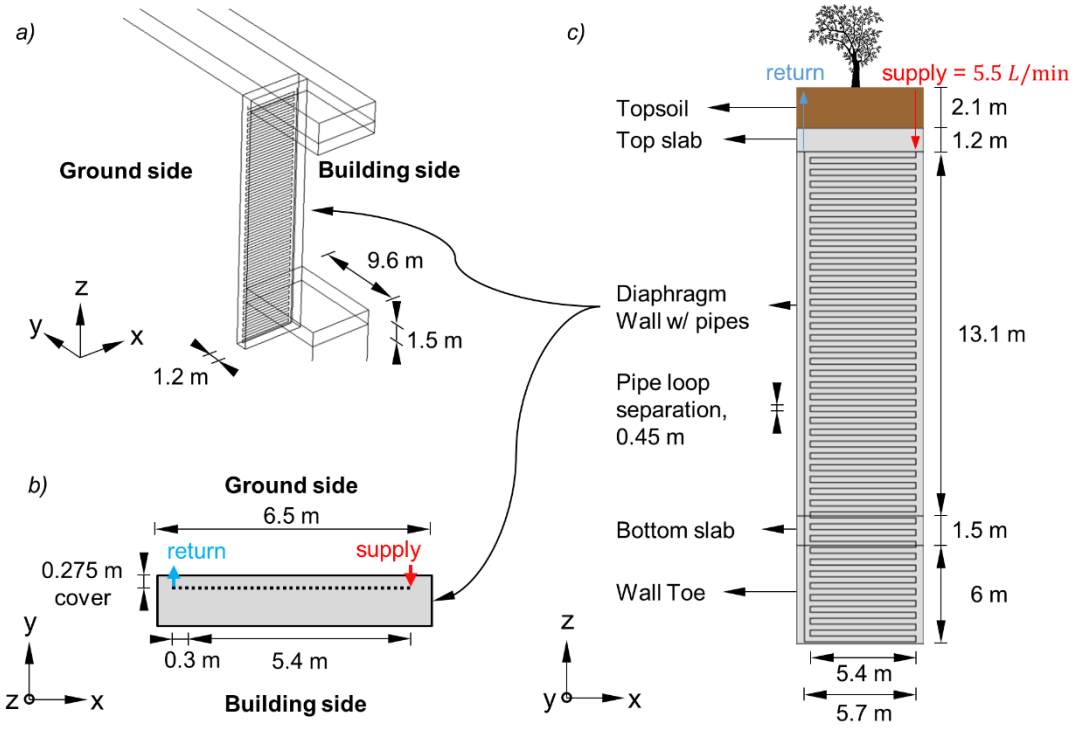


Figure 4.8 Energy diaphragm walls numerical modelling - geometry of single retaining wall panel model without thermally activating the slab

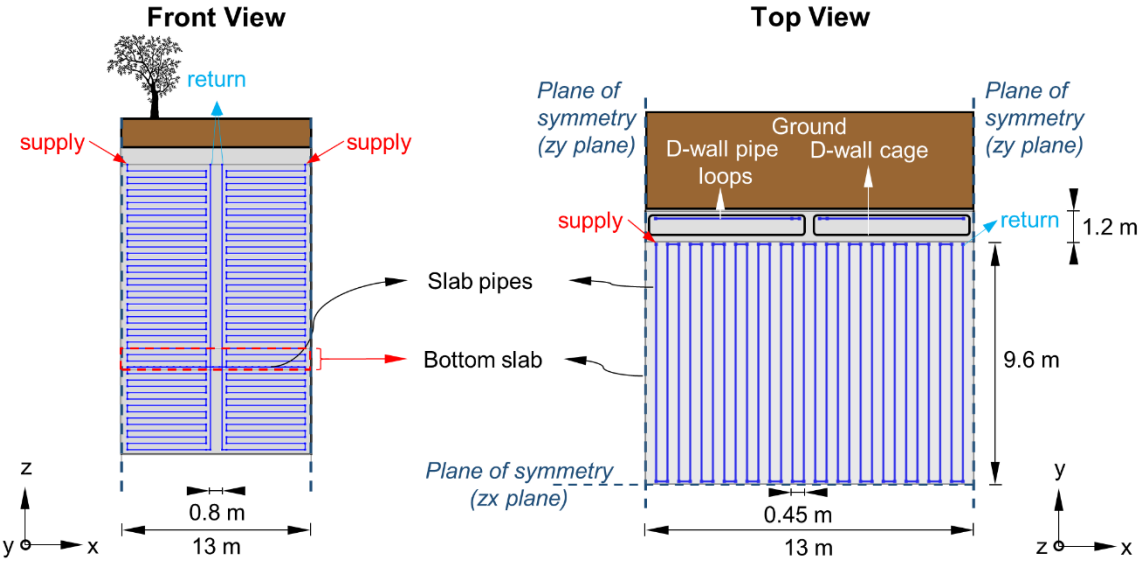


Figure 4.9 Energy diaphragm walls numerical modelling - geometry of the retaining wall with two thermally activated panels (see supply/return in the 'Front View'), and the inclusion of a thermally activated slab (see supply/return in the 'Top View')

4.3.2.4 Energy soldier pile retaining wall numerical modelling

In modelling the energy soldier pile retaining wall a similar approach was adopted as the modelling of the diaphragm walls, outlined in section 4.3.2.3. The model overall boundary conditions, shown in Figure 4.10, are similar to those of the diaphragm walls with the only difference being the value of the farfield temperature, which is 19.5 °C, representing the Parkville area in Melbourne which is closer to the city centre and is likely subjected to the urban heat island effect. The geometry of the retaining wall structures and the placement and configuration of the HDPE pipe loops, however, are significantly different between the two cases, due to the different structural components (and construction sequencing), such as the diaphragm wall cages and the soldier pile reinforcement. Moreover, it is worth noting again that supporting columns between the two walls along the y-axis are not modelled as their impact on the geothermal system is negligible.

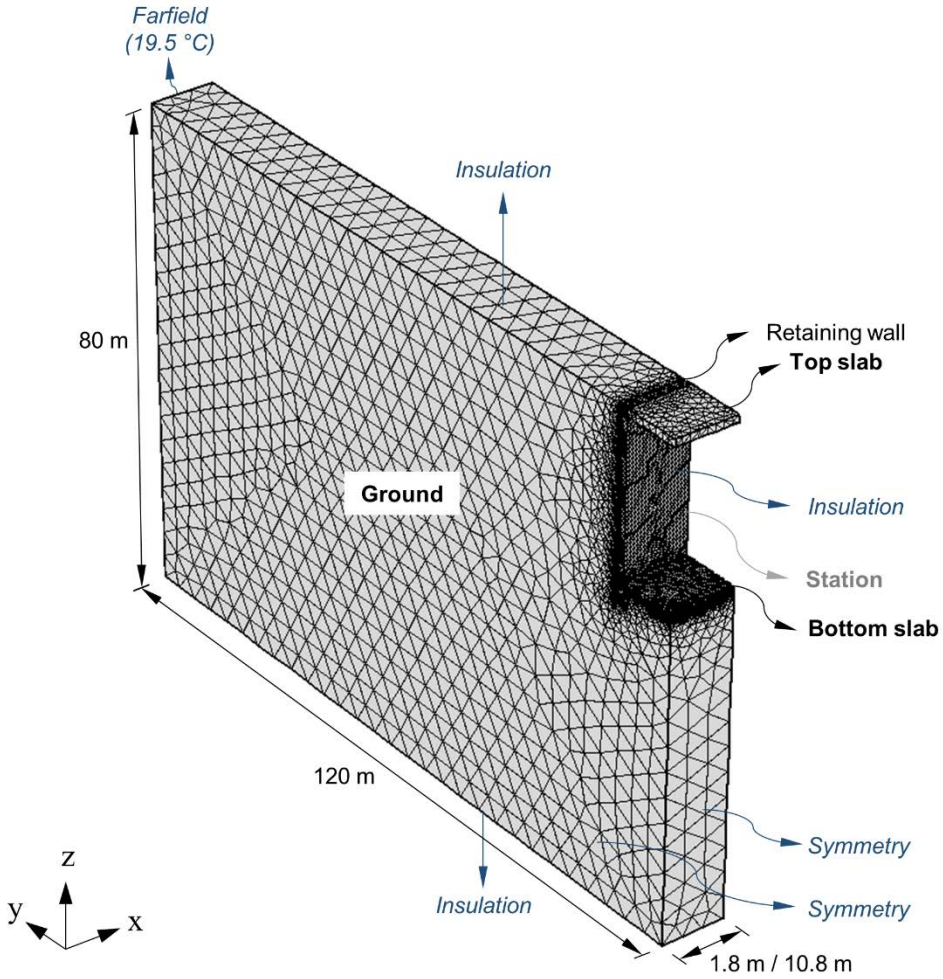


Figure 4.10 Energy soldier pile wall numerical modelling – model geometry and boundary conditions

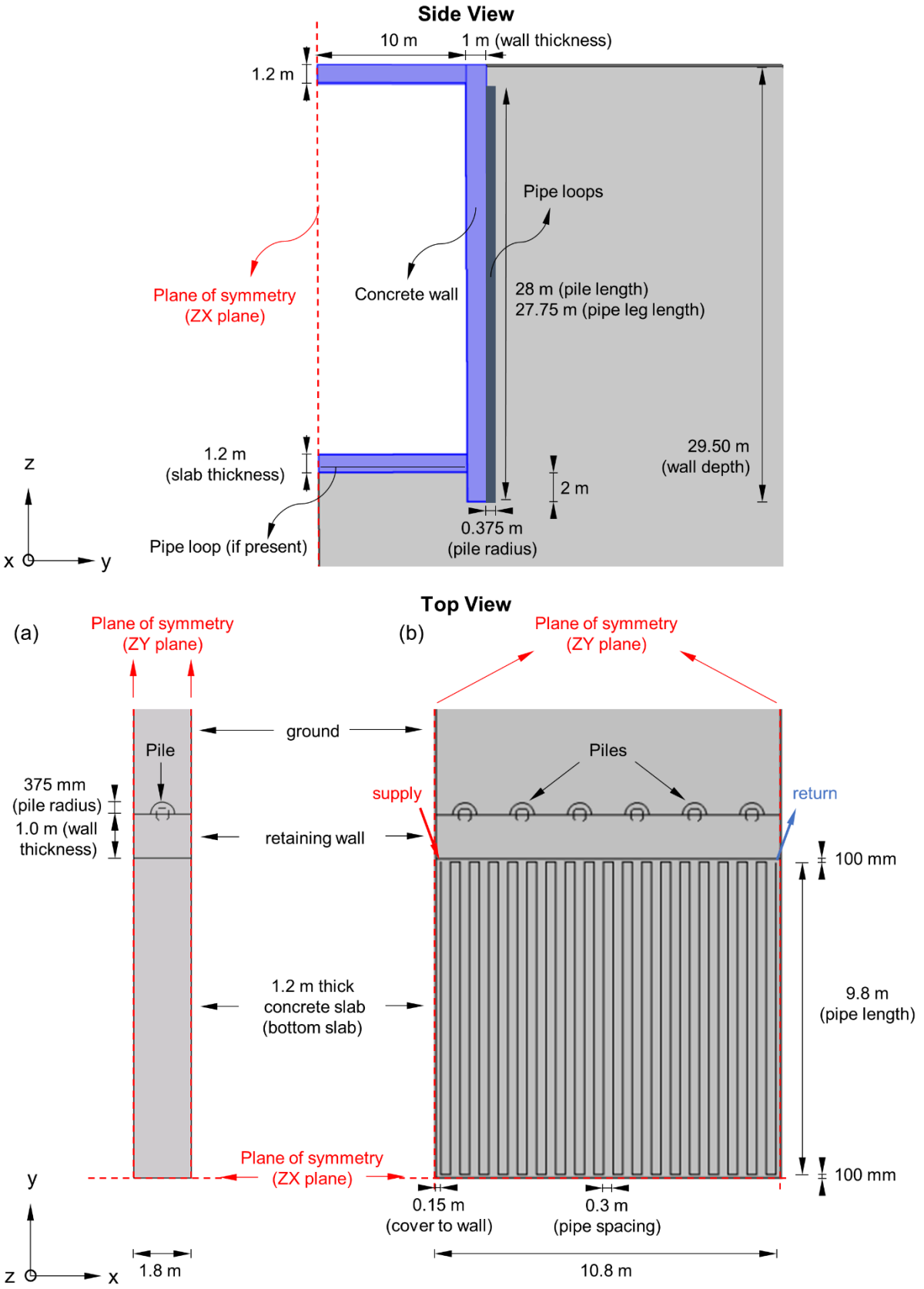


Figure 4.11 Energy soldier pile wall numerical modelling - model geometry and dimensions. Side view and top view for (a) wall only thermal activation, with 1.8 m separation between soldier piles (b) both wall (soldier) piles and bottom slab thermally activated

Similar to section 4.3.2.3, this modelling also adopts two main geometries: the first one models the case where only the wall is geothermally activated while the second one models the case

where geothermal pipes are included in both the soldier piles and the bottom concrete slab of the station. In both cases symmetry is used to reduce the size of the computational model. Due to the width of an activated slab section, the geometry for the second set of models is larger, incorporating 6 soldier piles with 1.8m centres as well as the bottom slab with geothermal pipes included in both (model width of 10.8 m), while the first set only models 1 of the soldier piles with geothermal pipes (model width of 1.8 m), representing an infinitely long geothermal wall with energy soldier piles every 1.8 m centres. Detailed dimensions of the modelling for both geometries, as well as the pipe configuration of the bottom slab, can be seen in Figure 4.11. It is worth noting here that the only difference between the two geometries in the *Side View* is the existence of the pipe loop in the bottom slab which is only present in the second/wider geometry (Figure 4.11 – Top View (b)). The slab pipe loop, totalling approximately 360 m per section, is placed 275 mm above the bottom surface of the slab. The pipe configuration for each soldier pile, using four pipe U-loops connected in series at the top of the pile and totalling approximately 220 m per pile, results in a single inlet and outlet per pile, shown in Figure 4.12. An *upper bend* corresponds to a connection at the top of the pile and a *lower bend* corresponds to a U-loop connection at the bottom of the pile. The pipes are connected in series to facilitate constructability and to allow longer residence time for the fluid and thus ensure sufficient transfer of heat between the fluid and the concrete/ground. Their installation can be done off-site, attaching the loops on the pile/slab reinforcement (e.g. with cable-ties) with only minimal connections between sections as the cages are lowered into the ground.

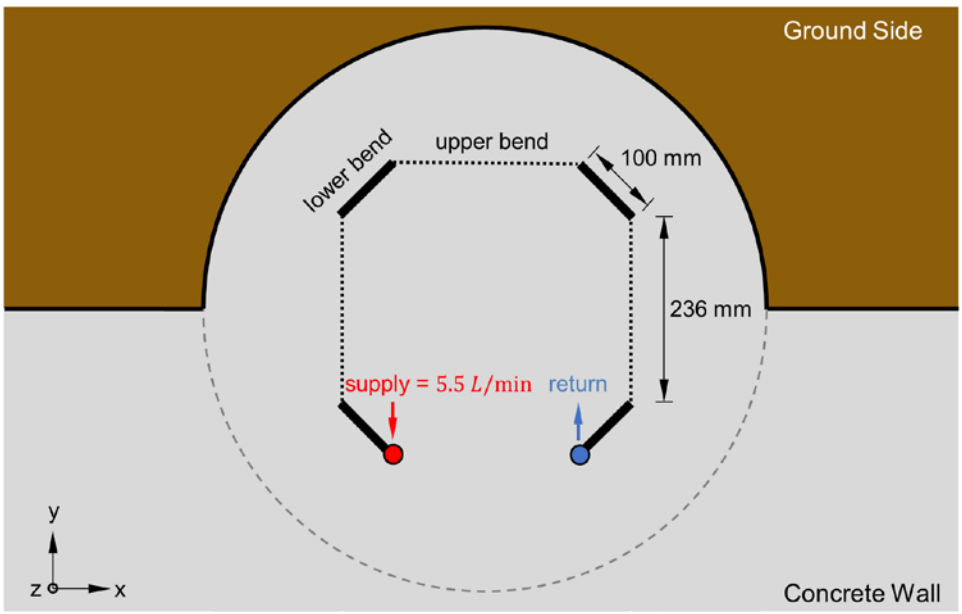


Figure 4.12 Energy soldier pile wall numerical modelling - pipe configuration detail for each soldier pile. Total pipe length per pile approximately 220 m

Lastly, the material properties utilised in the modelling can be seen in Table 4.2. These represent the soil conditions for the Parkville area in Melbourne, Australia. As mentioned in section 4.3.2.3, where applicable, these were obtained through in situ and laboratory testing (such as TRT). Moreover, as with diaphragm walls, the flow rate of the carrier fluid used throughout the soldier pile wall analyses is also 5.5 L/min.

Table 4.2 Parkville modelling - material properties

Parameter	Value	Unit	Description
λ_{ground}	2.8	W/(mK)	Thermal conductivity of ground
ρ_{ground}	2400	kg/m^3	Density of ground
$C_{p\ ground}$	830	J/(kgK)	Specific heat capacity of ground
$T_{farfield}$	19.5	°C	Average annual ground temperature
$\lambda_{concrete}$	2.1	W/(mK)	Thermal conductivity of concrete
$\rho_{concrete}$	2250	kg/m^3	Density of concrete
$C_{p\ concrete}$	890	J/(kgK)	Specific heat capacity of concrete
λ_{fluid}	0.58	W/(mK)	Thermal conductivity of carrier fluid
ρ_{fluid}	998	kg/m^3	Density of carrier fluid
$C_{p\ fluid}$	4185.5	J/(kgK)	Specific heat capacity of carrier fluid

4.3.3 Thermal load distributions

The thermal load distribution is an important parameter in shallow geothermal system design, as it represents the amount of thermal energy the system is tasked with providing. In energy retaining wall design it can be even more significant, compared to traditional systems, due to the fact that less ground volume is available to use as a heat source or sink, making the design more sensitive to the thermal load distribution. The effect that the thermal distribution has on energy retaining wall design, as well as how much thermal energy the structures can provide in each case, is studied throughout this chapter.

For each of the two structures/case studies (Domain – diaphragm walls and Parkville – soldier pile walls) different thermal load distributions are adopted (as provided by the project consultants). These provided distributions are significantly cooling dominant and are labelled as *"unbalanced"*. Understanding that these are not favourable conditions for the geothermal system operation, a second "*balanced*" thermal load distribution was also included in the analyses (for each case). The thermal load distributions utilised in the analyses can be seen in Figure 4.13 and Figure 4.14. The "*unbalanced*" distribution represents the thermal energy target for the geothermal system to provide when the requirement is mostly in cooling. The "*balanced*" distribution represents a modified version of the "*unbalanced*", one where heating is also provided such that equal thermal energy is provided in heating and cooling and represents a more ideal case where demand is equal in the two modes. This distribution

provides more energy in total in addition to being expected to be more beneficial for the system, due to being less prone to heat accumulation in the ground. To balance the heavily cooling dominant thermal load required for a typical metro station, heat is to be provided to nearby buildings on the surface, such as hospitals, universities, or schools, that can have heating demands throughout the year. This additional heating load is introduced mostly during the winter months (June-August for Australia) but also throughout the year at a lesser degree. This is the reason that there is a difference between the cooling energy peaks between the "*unbalanced*" and "*balanced*" distributions, as for the latter heating is also provided and the net effect is the cooling being lowered.

It is worth noting that the presented distributions represent the thermal energy required by the (entire) geothermal system (i.e. not a single GHE). This load is then distributed to the loop circuits in the diaphragm walls or soldier piles and where applicable the slab loop circuits. In the case where the slab is not activated the load shown in the figures is equally distributed over 67 diaphragm wall pipe loop circuits (for the diaphragm wall model) or 157 soldier pile pipe loop circuits (for the soldier pile wall model). When the slabs are activated, the load is distributed based on the length of the pipe in each circuit.

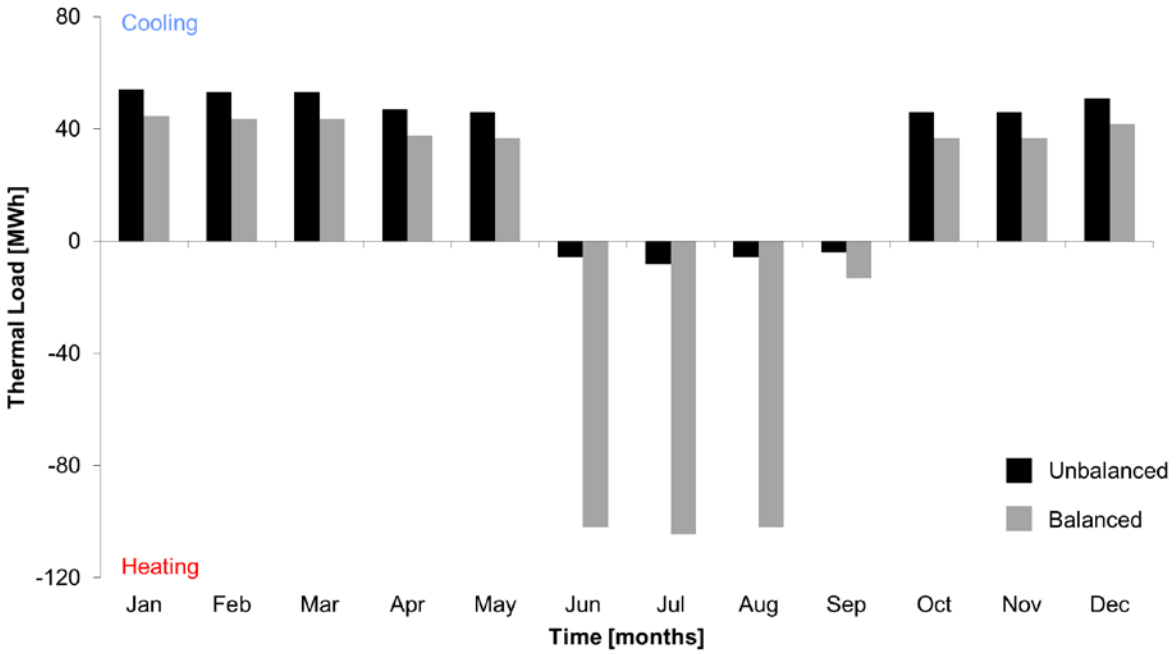


Figure 4.13 Thermal load distribution to be provided by the geothermal system for energy diaphragm wall system

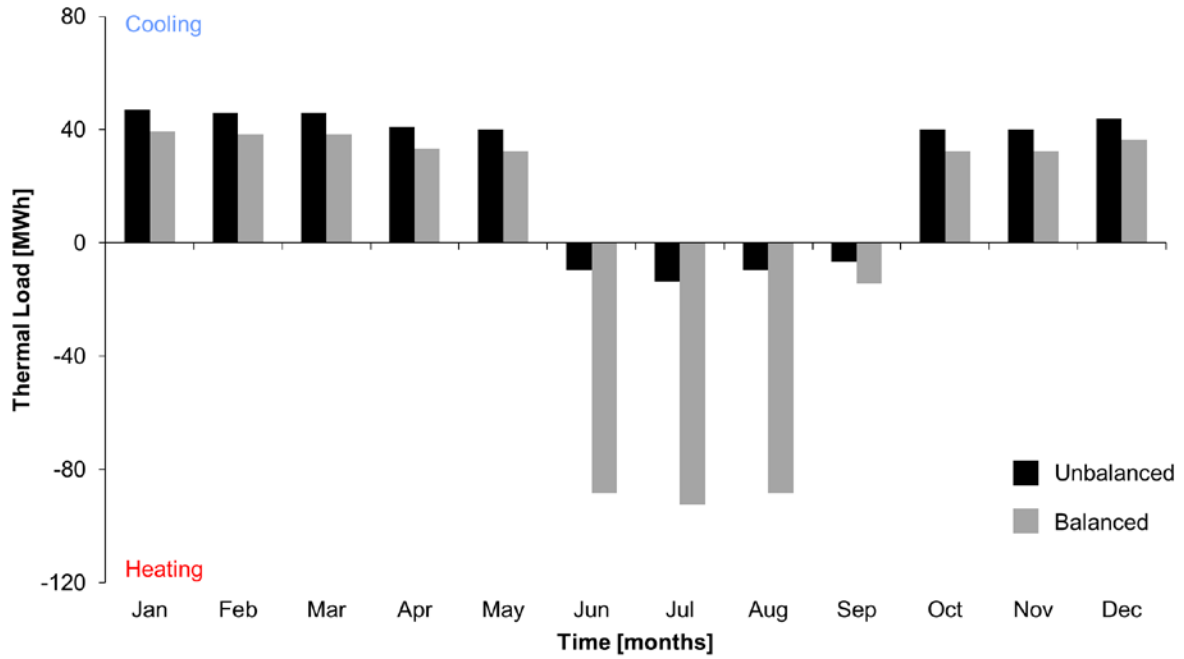


Figure 4.14 Thermal load distribution to be provided by the geothermal system for energy soldier pile wall system

4.3.4 Thermal performance analyses of energy retaining walls

This section presents the results of the numerical modelling for both the energy diaphragm and the soldier pile retaining wall models. Following an explanation of the thermal performance evaluation, the two results sections are presented, for each of the two different types of energy retaining walls, following a similar structure. Firstly, the analyses focusing on how much energy can be provided by each designed system are presented, as well as the effect of balancing the thermal load and the incorporation of the (thermal) slab circuits. These are key outcomes of the feasibility study work with MMRA. Following, additional analyses are presented, which were undertaken after the completion of the feasibility study project, allowing for longer and more detailed investigations without the real-world project time constraints. These relate to the effect of pipe density[2] on thermal performance, which allows, for example, to identify the most beneficial spacing/amount of pipe loops in the pile or diaphragm wall circuits as well as the importance of geometrical parameters such as the depth of embedment of the retaining walls. For all cases the numerical simulations are run for a duration of 25 years, which is considered sufficient to provide a complete evaluation and identify the thermal trends and viability of the system. Finally, a reflection on these analyses is presented, focusing on how information availability on energy retaining wall design can aid the industry and improve the quality of design in real-project applications.

[2] Metres of geothermal pipe per unit length or unit area of the retaining wall incorporated into the geo-structure.

4.3.4.1 Assessing the thermal performance

The thermal performance of GSHP systems is considered throughout section 4.3.4. As discussed in section 2.2.3.4 an important parameter that can determine the viability of the system and its thermal performance is the temperatures of the fluid inside the pipes, which need to be maintained within the operating limits of the heat pump (for example, 0 and 40 °C) . The average fluid temperature in the pipes (average of inlet and outlet temperatures, $T_{average} = \frac{T_{in}+T_{out}}{2} = \frac{LWT+EWT}{2}$) is reported herein. Where applicable, temperature limits for energy wall design have been indicated on the results, noting that these limits are more conservative than for typical GSHP systems to further prevent thermal leakage inside the building. Moreover, in various parts of the following analyses the maximum or minimum of the average fluid temperatures reached over the simulations are used as a measure of the system's effectiveness and suitability. These are labelled as T_{max} and T_{min} respectively. When the unbalanced thermal load is adopted, since it is cooling dominant and the viability of the GSHP system is determined by the maximum fluid temperatures, only T_{max} is shown and T_{min}.is not reported. When the balanced thermal load is adopted both T_{max} and T_{min} are considered important and are presented. It should also be mentioned that, given the nature of the following analyses, there are cases where the presented maximum/minimum temperatures fall outside the operating limits of typical GSHPs. However, the identified patterns within these results can be used to better understand the thermal behaviour of the systems across a range of temperatures and scenarios and therefore are still considered worth including in the investigations.

Another important parameter in GSHP design is the difference between the fluid temperatures at the inlet/supply and outlet/return pipes (expressed as $\Delta T = |T_{out} - T_{in}| = |EWT - LWT|$). This value depends mainly on the magnitude of the thermal energy being provided (with more energy resulting in higher ΔT), the flow rate of the carrier fluid (with higher rate resulting in lower ΔT) as well as the material properties, such as the heat capacity and thermal conductivity of the ground and concrete. The value is specified by the heat pump manufacturer with typical values in the range of a few degrees Celsius. In this research, the values of ΔT are not reported and the focus is put on the maximum and minimum of the fluid temperatures to indicate viability, and even performance, of the GSHP system. For example, the coefficient of performance of the heat pump when operating in cooling mode increases with decreasing $T_{average}$, of which T_{max} represents its worse condition. Conversely, COP increases with increasing $T_{min}$when the heat pumps operate in heating mode. To increase the value of ΔT for the presented configurations, based on the specifications of a particular heat pump, a simple

approach would be to link in series the separate soldier pile or diaphragm wall pipe circuits, thus increasing the thermal energy each (linked) circuit is providing and therefore the value of the ΔT.

4.3.4.2 Energy diaphragm retaining walls

This section presents a number of thermal performance analyses for energy diaphragm retaining walls. The effect of the thermal load distribution balance and the potential benefits of thermally activating the slab as well as the retaining walls are discussed first, where the geometry and conditions are as described in section 4.3.2.3. Following, two more analyses are presented, both altering the geometry and/or configuration to investigate the influence of design parameters on the thermal performance. The first analysis investigates the pipe density (how closely the pipes are placed within the diaphragm wall) and the second one the depth of embedment of the retaining wall and the potential thermal gains obtained by extending/deepening it.

The effect of the thermal load distribution balance and thermally activating the slab

Figure 4.15 shows the average fluid temperature for both thermal load distributions (*unbalanced* or *balanced*) as well as geometries (thermally activating only the diaphragm walls or the slabs as well). As it can be seen, adopting the unbalanced thermal load distribution (Figure 4.15-a) results in the GSHP system being unable to provide the required amount of cooling energy beyond year 12 and instead only about 80% of the cooling can be comfortably provided, without exceeding the indicative 40 °C upper limit over 25 years. Still, the trend is clearly increasing and therefore for longer periods of continuous operation even lower amounts of energy would need to be considered. In contrast, when the balanced distribution is adopted (Figure 4.15-c) the geothermal system can provide the required load comfortably and more reliably. Since the steady state condition (where the increase in the fluid temperatures over time is minimal) is achieved relatively early, the performance of the system can be expected to be consistent throughout its entire operating life. Moreover, when the balanced thermal load distribution is adopted, the system can provide up to double the amount of thermal energy (assuming an anti-freeze solution is utilised for sub-zero temperatures). These findings showcase the degree of significance that the balance of the thermal load distribution can have on the performance of the system, especially when considering the long-term effects of heat accumulation in the ground. It is worth noting that these accumulation effects also reduce the operational efficiency of the heat pumps, since they increase the fluid temperature range, and,

for example, more energy input into the heat pump is required to extract cooling from a liquid the warmer it is.

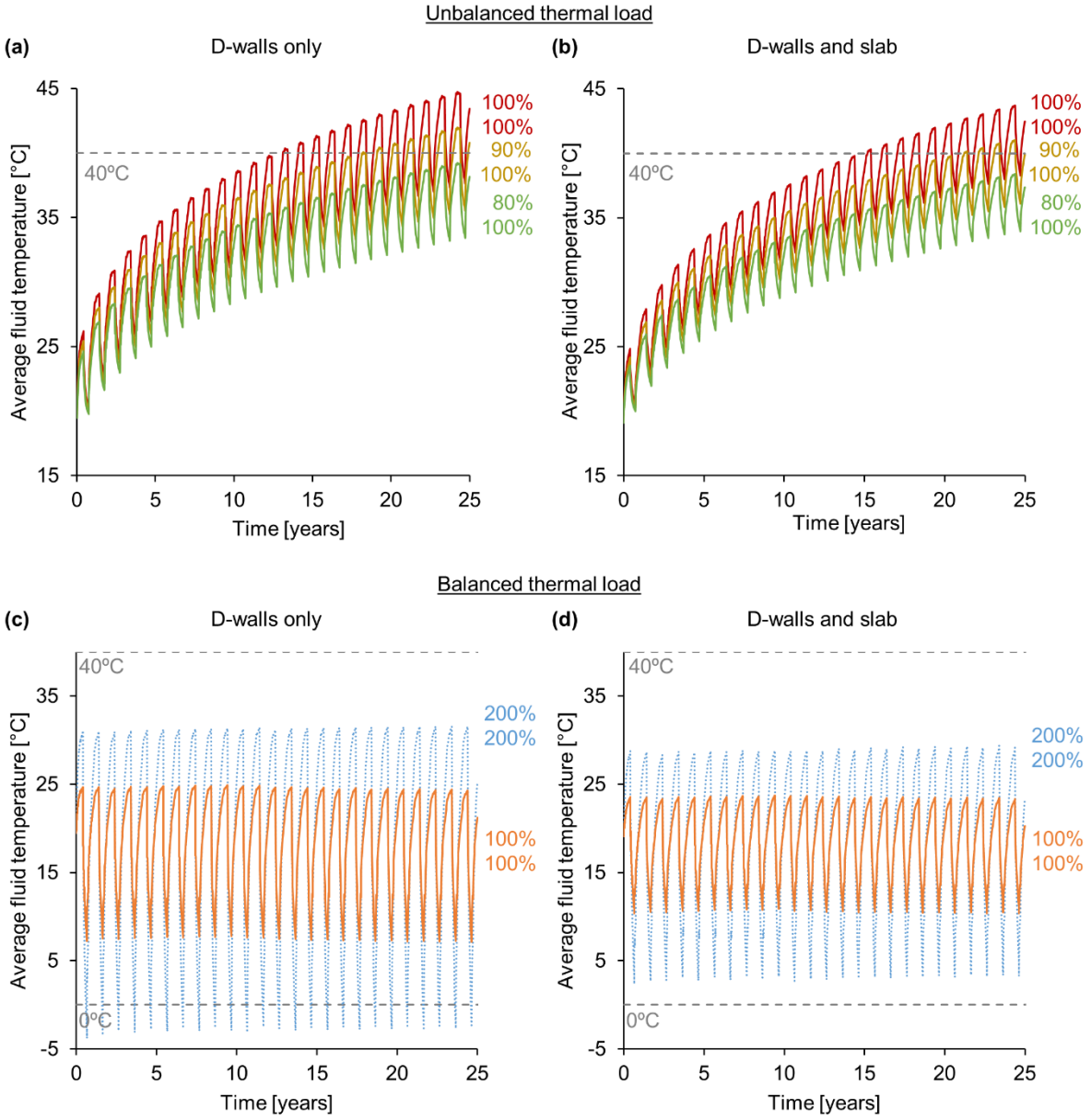


Figure 4.15 Thermal performance results for energy diaphragm walls, indicating the fluid temperature results when providing different amounts of cooling (upper % value) and heating (lower % value) energy

Regarding the effect of thermally activating the slab, there is undoubtedly an improvement in the performance of the geothermal system, since the fluid temperatures become less extreme and therefore the system is able to provide more energy. However, it is questionable if the gain in energy justifies the costs associated with thermally activating the slab and the magnitude of the effect would differ from case to case. In the case of the *unbalanced* distribution, the system can provide approximately 85% of the cooling (instead of 80% for the D-wall only case), which is a relatively minor increase (Figure 4.15-b). In the case of the *balanced* distribution, activating the slab allows for over double the amount of energy originally requested and also eliminates

the need for incorporating an anti-freeze solution (Figure 4.15-d). In general, even though a detailed cost-benefit analysis would be needed to evaluate the addition of the slab circuits, it seems unlikely for most cases that this could be a justified approach. One scenario that could be considered would be when activating the slabs would allow the geothermal system to provide 100% of a required thermal load (that it could not provide otherwise) and therefore eliminate the need for an auxiliary system. Moreover, it should be mentioned that the novelty of these concepts makes it harder to properly evaluate their associated costs, since non-standard practice approaches in the construction industry often occur more costs and training could be necessary.

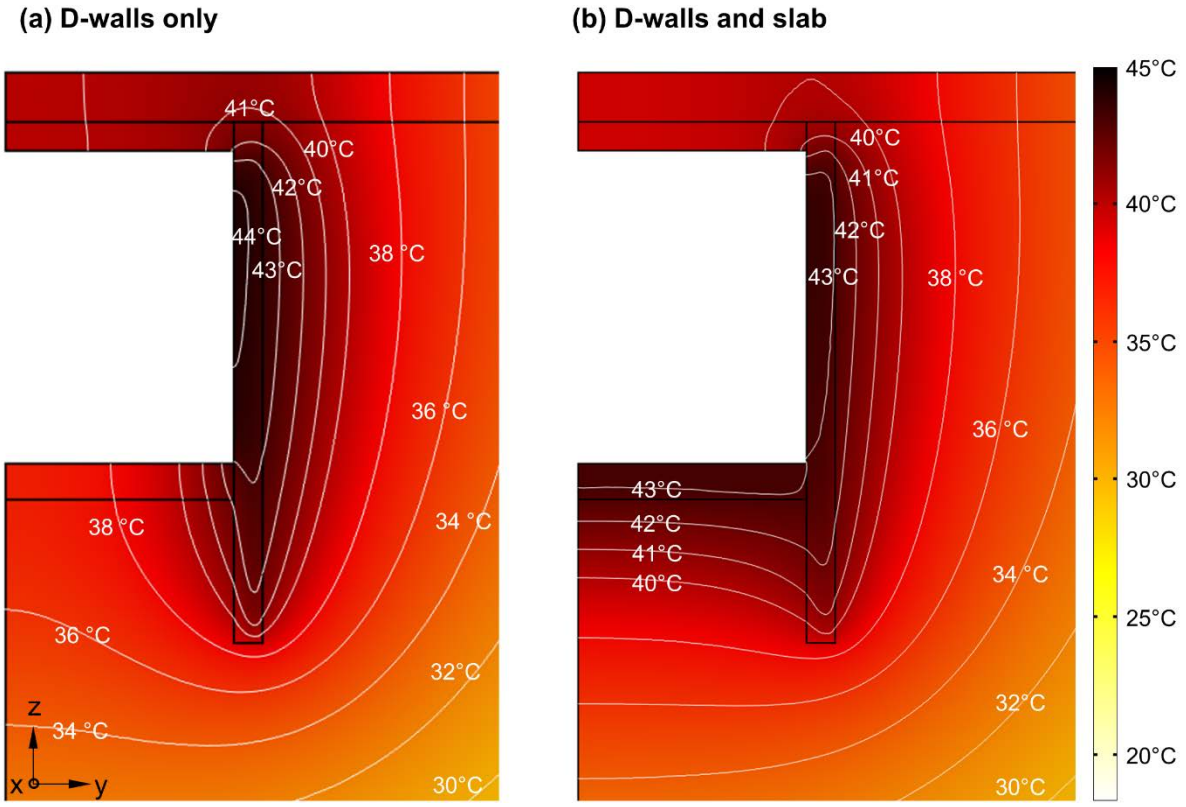


Figure 4.16 Temperature distribution on 25th of May of 25th year, for diaphragm retaining walls when thermally activating (a) the walls only (b) both the wall and slab circuits – Unbalanced thermal load distribution adopted

To better understand how thermally activating the slab affects the system operation, Figure 4.16 shows the temperature distribution for both geometry models when adopting the *unbalanced* thermal load distribution. The temperature distribution is for the 25th of May of the 25th year of simulation, which produces the most extreme results since it is the end of the cooling period when the heat has accumulated (note here that the thermal demand does not peak on this date, but the fluid temperatures are most extreme due to heat accumulation over the cooling period). The figure shows contour lines of the temperature, incrementing by 2 °C from 30 °C to 40 °C and by 1 °C from 40 °C to 44 °C. As it can be seen, when only the

diaphragm wall circuits are incorporated (Figure 4.16(a)) the temperatures are higher within the wall, reaching over 44 °C, due to the higher thermal load the wall circuit needs to provide compared to when the slab circuits are also activated (and take some of that thermal load). The temperatures near the slab are not as high, since there are no geothermal loops, but the material still reaches temperatures over 36 °C from the operation of the wall geothermal circuits. When both the wall and slabs are thermally activated (Figure 4.16(b)) the temperatures towards the top of the wall are slightly lower, however the temperatures near the slab are as high as near the wall, at over 43 °C. What can be seen by comparing the two plots is that the addition of the geothermal loops in the slab is not as significant because the soil underneath them (that they are aiming to use as a heat sink/source) is already significantly utilised by the geothermal loops in the wall circuits due to the very close proximity of the two. Therefore, there is much less available thermal storage from the soil underneath the slab and the thermal interference between the two pipe loops influences their joint performance. What the slab circuits manage to do is distribute the thermal load more uniformly around the combined structure, but in this case having less impact due to the geometries and the small area the slab circuits influence. Moreover, Figure 4.16 also showcases how the non-symmetrical geometry and introduction of angles/corners (such as the slab/wall connection) in energy retaining walls result in a less symmetrical (along the y-axis) heat transfer compared to the more traditional boreholes/piles.

The effect of pipe density: pipe loop separation

An interesting question that is often unanswered in energy retaining wall design is how much geothermal piping should be placed within the walls. It is commonly believed that the more the amount of pipe the better the system will perform. However, it also needs to be accounted that the closer the pipes are placed to each other the more thermal interference is expected to occur. In this analysis, the spacing s between the pipe loops (and therefore the total pipe length incorporated) is varied from 300 mm (based on reasonable bending radius values) to a maximum of 900 mm to examine the effects on the thermal performance, as schematically shown in Figure 4.17. In order to visualise the results, the maximum and minimum temperatures are reported, which represent the overall increase/decrease of the fluid temperatures and therefore the impact on the effectiveness of the design.

The results are summarised in Figure 4.18 for both the unbalanced and balanced thermal load distributions and show an interesting effect on the thermal performance with two relatively distinct phases/patterns. For relatively short (< about 550-600 mm) and for relatively large loop spacings (s > about 750-800 mm), the performance of the system increases with decreasing

loop spacing, and therefore with increasing total pipe length, since the results show lower maximum fluid temperatures and higher minimum fluid temperatures. This behaviour is unsurprising and is labelled as phase (i). However, for intermediate loop spacings of approximately between 600 mm and 750 mm, the max/min fluid temperatures do not change significantly as the loop spacing (and pipe length) varies. The results within this range, labelled as phase (ii), are more unexpected and require further consideration.

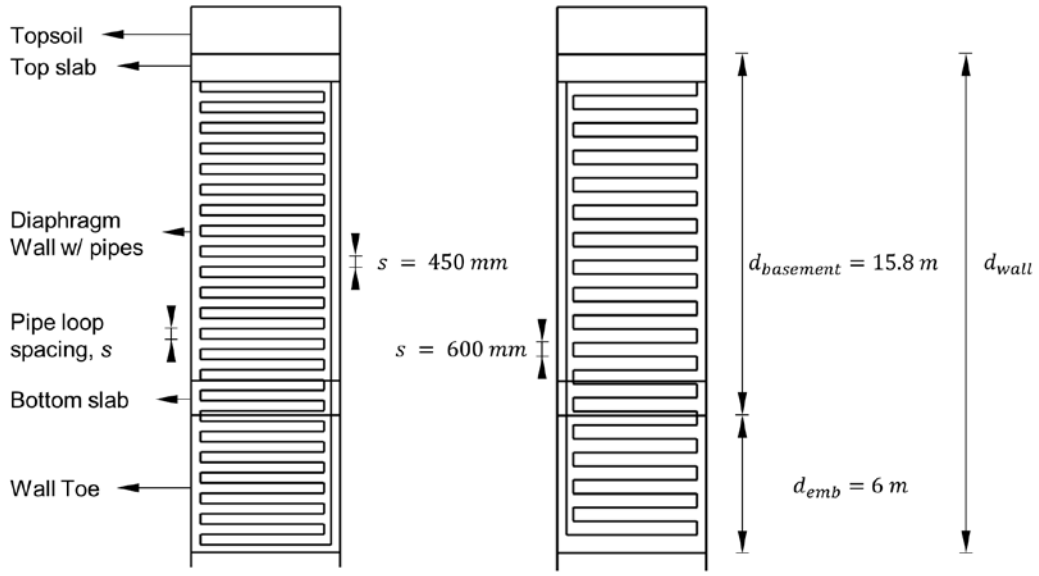


Figure 4.17 Schematic representation of diaphragm wall geometry for different values of pipe spacing, s

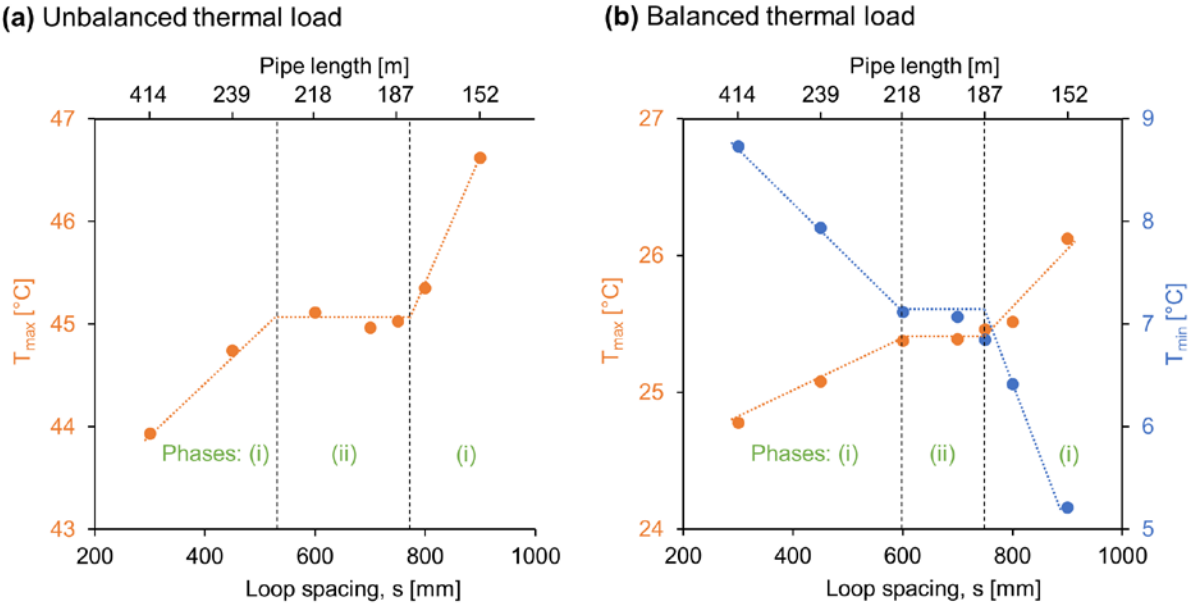


Figure 4.18 Maximum and minimum fluid temperatures when varying the pipe loop spacing in a diaphragm energy wall

The results can be further understood by observing Figure 4.19, which shows how the temperature varies with the depth of the wall for different pipe spacing values investigated, using the unbalanced thermal load distribution. Figure 4.19(a) shows the temperature

distribution along the depth and width of the wall when s = 900 mm, as an example. Figure 4.19(b) shows the temperature along line X-X' (indicated in Figure 4.19(a)) for four different pipe spacing values. Figure 4.19(c) presents a closer view over a small depth segment for clarity, while Figure 4.19(d) shows the temperatures along a relative depth (normalised over the spacing and starting from the indicative purple lines on Figure 4.19(c)). Overall, it can be seen that the temperatures rise and fall along the depth, with the high temperatures (crests) being at locations where the pipes are placed and the lower temperatures (troughs) being in between the pipe legs. Looking at the two extremes first, for $s = 300\ mm$ the temperatures are generally lower and there is very little variation between crests and troughs, while for $s = 900\ mm$ the values as well as the variation are much greater. When looking at the two intermediate values, $s = 600\ mm$ and $s = 750\ mm$ the results are less straight forward. For $s = 600\ mm$ the overall temperature values seem slightly higher, however for $s = 750\ mm$ the difference between crests and troughs is larger.

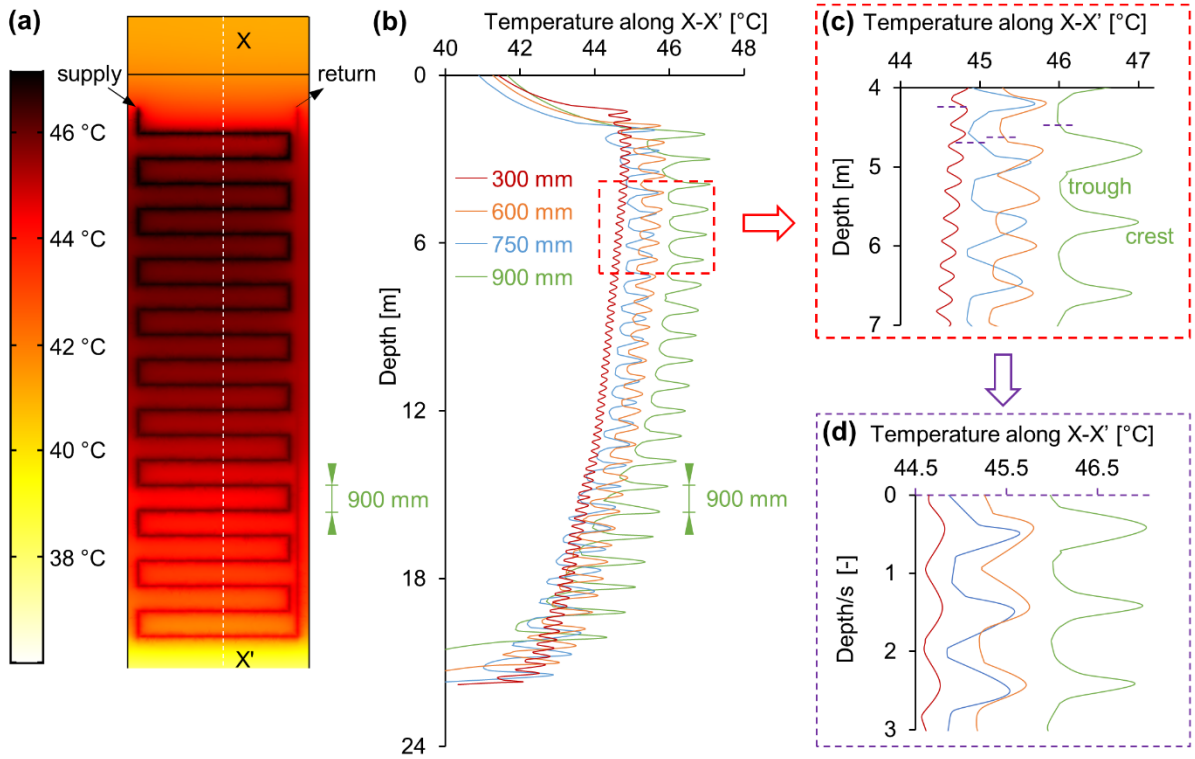


Figure 4.19 Temperature distribution on 25th of May of 25th year (end of cooling period) adopting unbalanced thermal load distribution: (a) Temperature distribution for s = 900 mm, (b) Temperature along line X-X' (placed centrally w.r.t wall width) for different loops spacings, s, (c) Section of plot (b) magnified for clarity, (d) Normalised version of plot (c) using depth/s

The degree of variation (how far the crests are from the troughs) is important to consider, as it relates to the thermal interference between the pipe legs. Based on the results, a small variation is seen when the pipes are placed close to each other, thermally interfere with each other and tend to act as a thermal plate. A large variation represents pipe legs that are placed significantly

apart from each other, limiting the thermal interference and exchanging heat with the ground more individually. As mentioned, both the amount of pipe incorporated (which is widely known and expected to affect the performance) and the thermal interference between the pipe legs are significant factors. Generally, it is expected that with increasing values for s the performance decreases because of the less amount of geothermal pipe placed, but also increases because of the reduction on the effects of thermal interference between the pipe legs. For the two extreme spacing values ($s = 300mm$ and $s = 900\ mm$), the amount of geothermal pipe governs the performance, even though there exists a notable thermal interference difference between the two (identified by the temperature variation between troughs and crests). On the other hand, for the intermediate spacing values this is not the case, as thermal interference is more impactful. As the spacing increases from $600\ mm$ to $750\ mm$, the thermal interference between the pipe legs reduces (which benefits the thermal performance), however, so does the total length of geothermal pipe incorporated in the GHE (which hinders the thermal performance). Therefore, the spacing range seen in Figure 4.18 (phase (ii)), where the temperatures remain relatively constant with increasing s can be interpreted as a result of these two factors cancelling each other out, as the thermal interference between the pipe legs transitions between the GHE acting as a plate and as separated pipes.

It is worth acknowledging that the results presented are for the specific geometry utilised, which gives rise to the question whether the observed results would differ for a different diaphragm wall geometry. To investigate this, a longer diaphragm wall was also adopted, using $d_{wall} = 27.8\ m$, producing similar results. Combining the results for the two different cases together, Figure 4.20 shows an indication of the discussed behaviour in a dimensionless form, in order to emphasise the common patterns, by using the loop spacing, s, divided by the total length of pipe used (proportional to the depth of the wall, $s_{normalised} = s/L_{pipe}$) and a normalised temperature as indicated on the figure. It should be noted here that the value used to normalise the temperatures ($s_{normalised} = 2.75$) is chosen based on the available results since it is a common value between the two different cases (for different wall depths), however other values could also be considered. Importantly, the observed behaviour of the separation not having a considerable thermal effect for intermediate separation values is present in the normalised version of the temperatures.

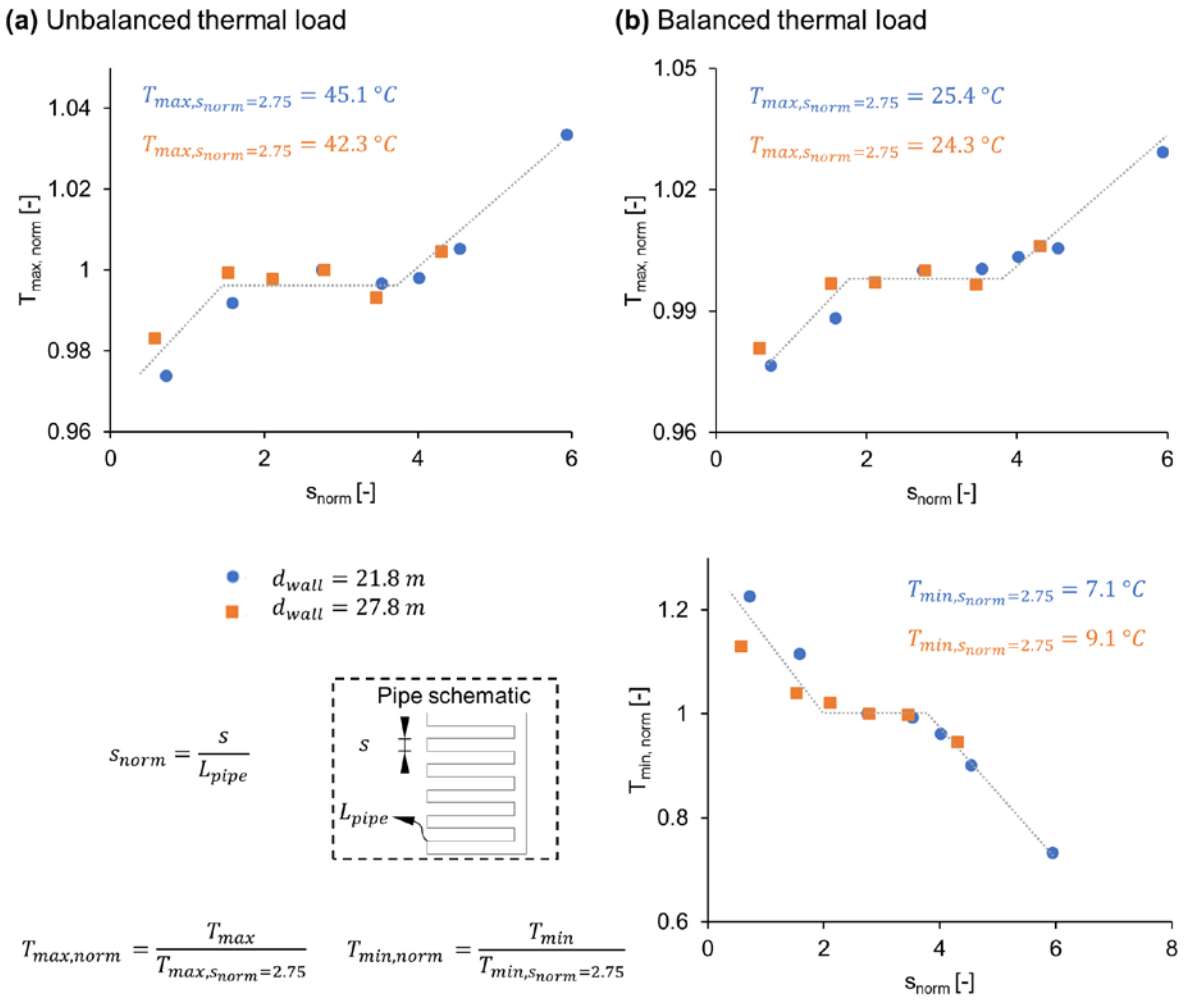


Figure 4.20 The effect of the pipe loop spacing in energy diaphragm walls - normalised results

Overall, the results suggest that the total pipe length and the thermal interference, which are affected by the choice of pipe spacing, are influencing factors on the thermal performance of the system. In general, the former tends to govern, resulting in the best thermal performance being achieved when the spacing of the pipe loops is small and therefore more length of pipe is used. However, a short pipe spacing also results in a potentially substantial cost increase as the more loops are placed, the more pipe connections and labour are needed and the more time it takes for the piping to be installed. Therefore, if a more intermediate spacing is deemed suitable, then a wide spacing that is still within the transition phase (ii) indicated on the figures would be most beneficial, since it would yield lower costs without a significant difference in the thermal performance of the energy wall. Because of the expensive and time-consuming nature of running computational simulations and the complexity of such an analysis, typical energy retaining wall design can fail to account for these effects, likely resulting in placing the pipe loops close together, overdesigning the system and therefore higher than required capital costs.

The effect of the depth of embedment

As mentioned throughout this chapter, a notable difference between energy retaining walls and other structures, such as piles, is the fact that the former is not completely surrounded by the ground. Therefore, it is worth investigating how impactful this difference is and the sensitivity of thermal performance to the depth of embedment. This investigation is performed in two stages. In the first, the option to extend the wall is considered, by increasing the depth of embedment, not for structural purposes, but in an attempt to engage more soil volume to exchange heat with the energy wall. This represents a realistic scenario where the designer has a target (fixed) basement height, but the depth of embedment can be extended and therefore the amount of geothermal pipe incorporated in the retaining wall is also increased. In the second stage of the investigation, to isolate the influence of the portion of the structure in contact with the soil, the wall depth is kept fixed (i.e., the total loop length is kept constant), while the basement height and depth of embedment are varied.

In the first stage of this analysis (extending the depth of embedment) the potential thermal performance benefits resulting from the additional contact with the ground as well as the longer pipe length incorporated are examined. A schematic representation of the analysis can be seen in Figure 4.21 and the results are summarised in Figure 4.22, showing the maximum and minimum average fluid temperatures for both the unbalanced and balanced thermal load distributions (shown in Figure 4.13) at the end of 25 years of operation. Four different values of $d_{basement}$ are used and for each the depth of the embedment d_{emb} is varied/extended accordingly. As it can be seen, extending d_{emb} can be significant to the performance of the system, with fluid temperature improvements in the range of 5-10°C. The impact is more significant for initially small values of d_{emb}, suggesting that in certain cases it might be worth extending a shallow embedment to improve the system performance. The impact is also more significant for smaller values of $d_{basement}$, meaning that extending a relatively short (overall) retaining wall will be more beneficial compared to extending a deeper wall. Moreover, it is interesting to notice that the longer d_{emb} becomes the closer the maximum and minimum average fluid temperatures become between the four cases, converging together. This is likely because the deeper the embedment is, the less relative disparity exists between the total pipe length of the different cases and they therefore perform more similarly. Figure 4.23 shows the results in a normalised form, highlighting the common behaviour between the different depths, which is well approximated by a single equation. Based on the obtained results it could be suggested that extending the embedment up to a value of $d_{ratio} \approx 0.75$ could be potentially justified, after which there is a decline in the performance gains.

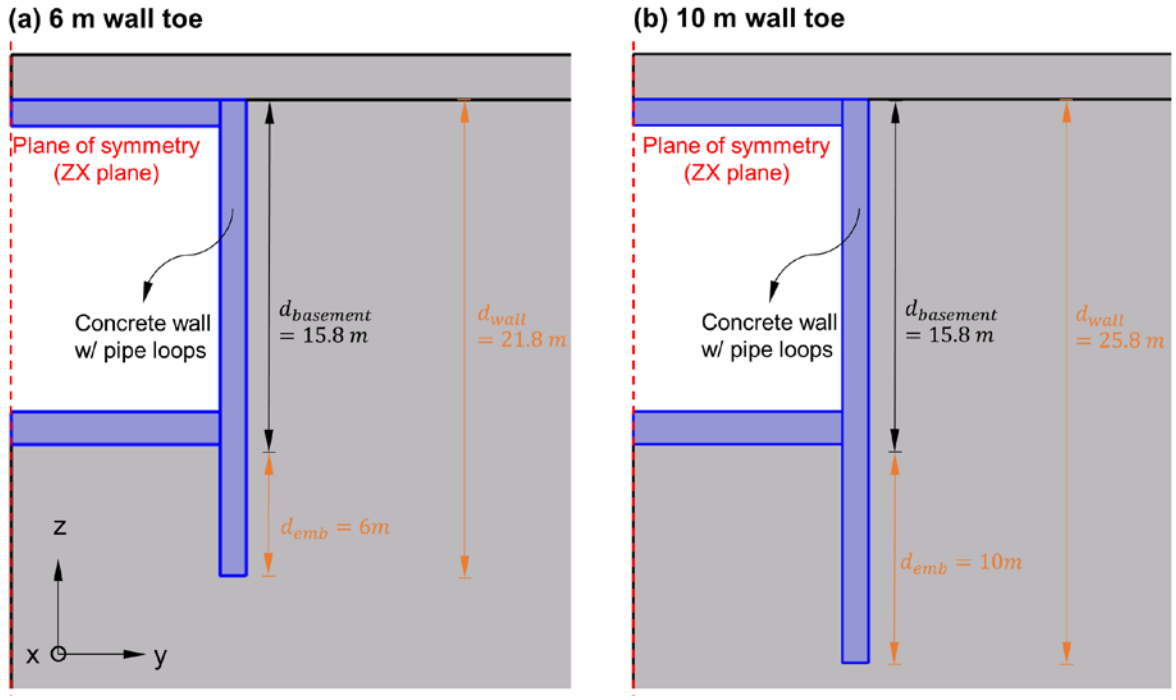


Figure 4.21 Schematic showing a change in the depth of embedment by changing the total depth of the diaphragm wall (extending the wall)

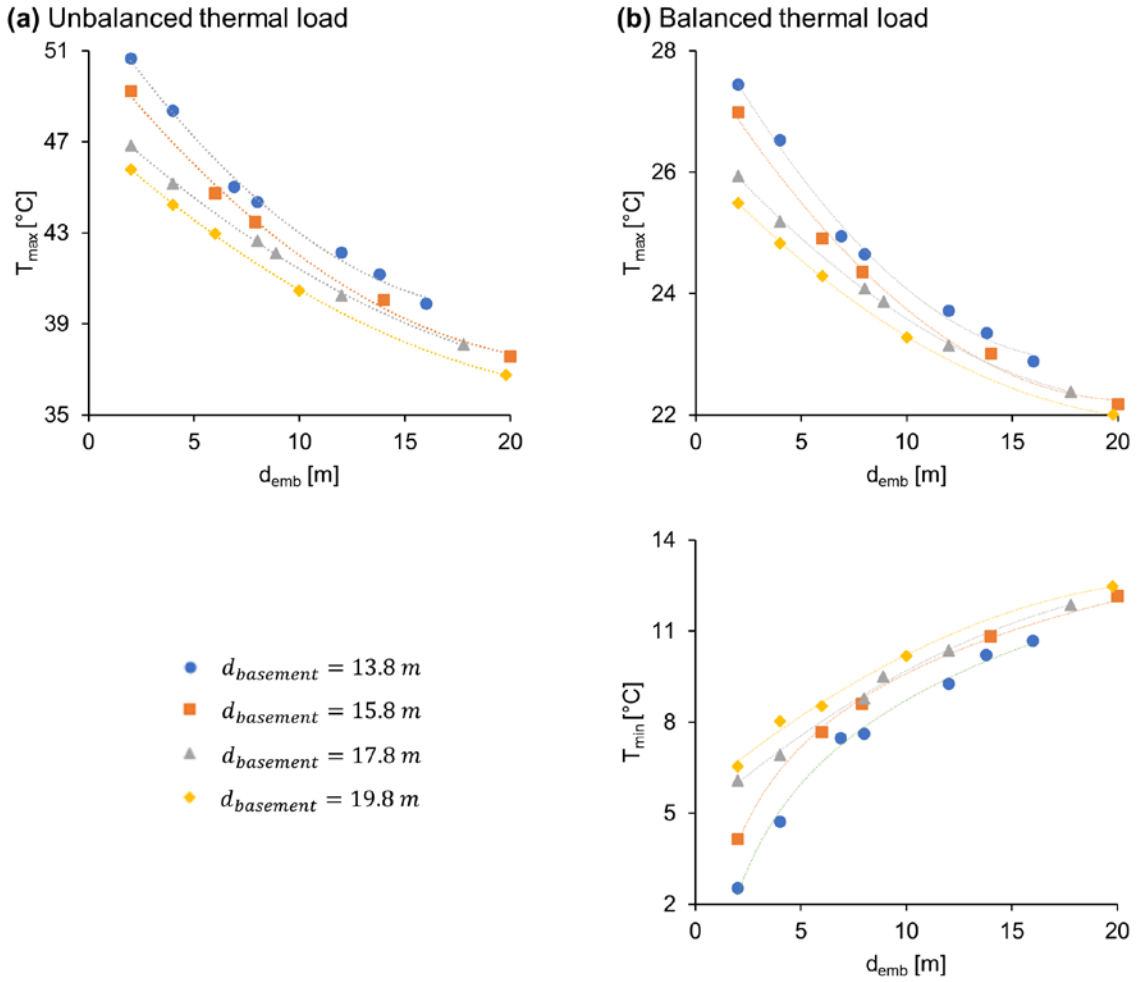


Figure 4.22 Maximum and minimum average fluid temperature results when extending the embedment depth of the diaphragm retaining walls

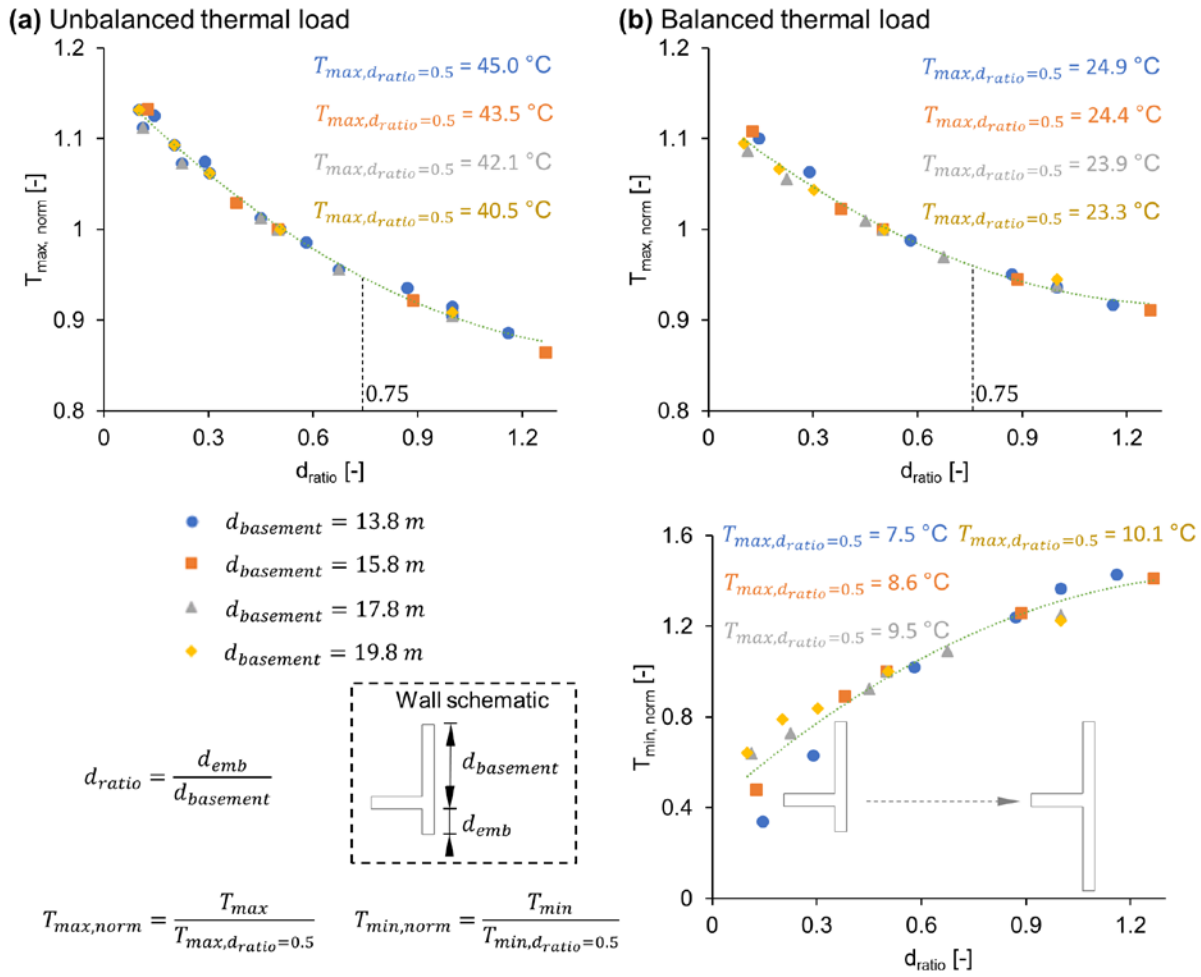


Figure 4.23 The effect of extending the depth of embedment in diaphragm retaining walls - normalised results

A visual representation of the second stage of the analysis, which aims to isolate the effect of the portion of ground engaged by the GHE, can be seen in Figure 4.24. The depth of the embedment d_{emb} is altered, to increase/decrease the amount of soil surrounding the retaining wall, by varying the portion of the wall that determines the height of the basement ($d_{basement}$). While d_{emb} and $d_{basement}$ vary, the entire depth of the retaining wall, d_{wall}, remains constant, and so does the amount of geothermal piping in the wall, therefore, between these variations the only variable is the amount of soil around the wall. Moreover, three different values of d_{wall} are used in detailed numerical simulations ($d_{wall} = 21.8\,m$ – shown in Figure 4.24, $d_{wall} = 25.8\,m$ and $d_{wall} = 29.8\,m$) while also varying d_{emb} and $d_{basement}$ for each case. This analysis represents a theoretical situation, to examine the importance of the ratio between d_{emb} and $d_{basement}$, as in reality the geothermal design would not likely be able to affect the geometry and the value of $d_{basement}$. However, it also provides insights on the applicability of different geometries of retaining walls as energy geo-structures.

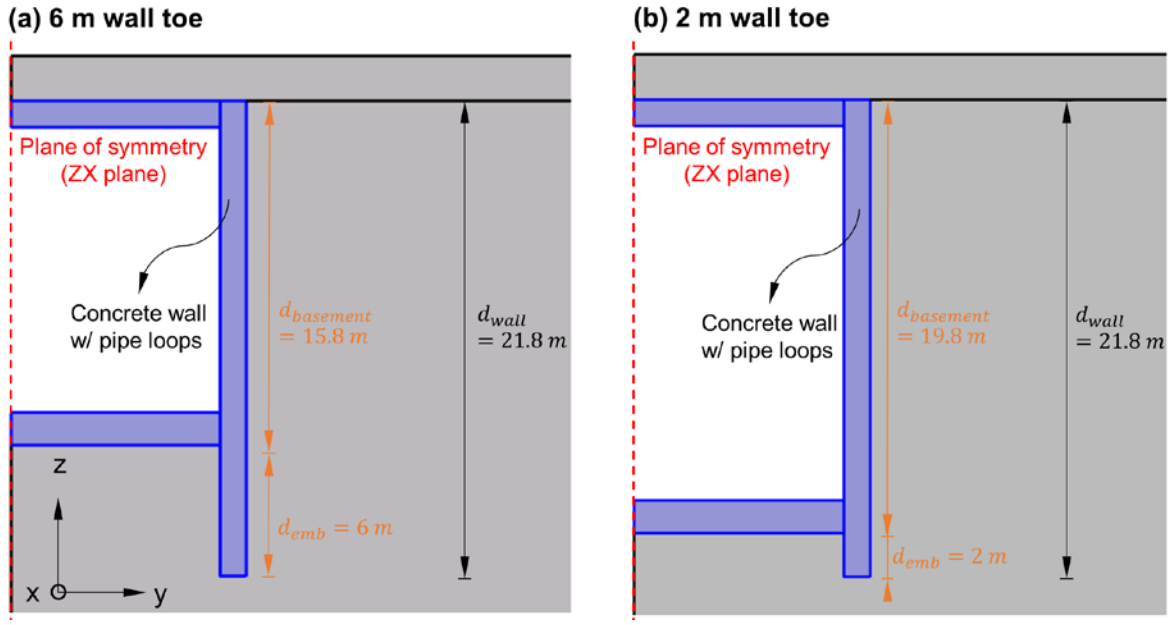


Figure 4.24 Schematic cross section of basements showing a change in the depth of embedment without changing the total depth of the retaining wall

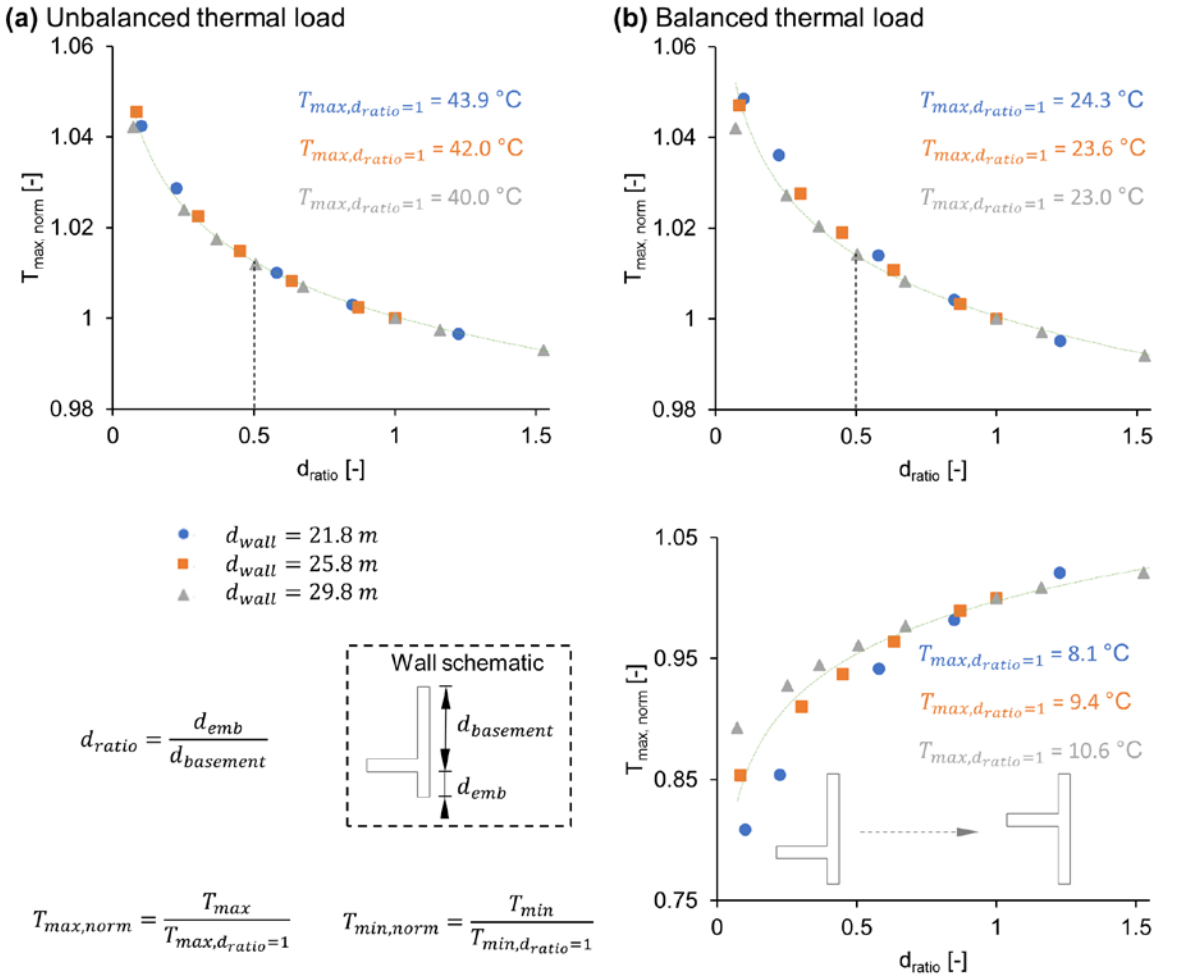


Figure 4.25 The effect of varying the embedment depth while keeping the overall retaining wall depth fixed – normalised results

The results are summarised in Figure 4.25 in a normalised, dimensionless form, that highlights the common patterns between the different values of d_{wall}. As expected, there is an improvement in the performance of the system when more ground is in contact with the wall surface(s) (d_{ratio} increases). However, surprisingly, the magnitude of the change in the temperatures is relatively small for all cases with changes in the magnitude of 1-2 °C (or up to 5% for the maximum temperatures and 15% for the minimum temperatures). The normalised form highlights the decreasing relationship between the relative change in temperature resulting from a change in d_{ratio} and shows that beyond a d_{ratio} close to 0.5 there are little extra performance gains. In other words, increasing the exposure of the wall to soil on both sides beyond about 1/3 of the total depth of the D-wall does not carry much additional benefits to the thermal performance of the energy wall. Overall, this second analysis shows that the depth of embedment to depth of basement ratio of a retaining wall is relatively insignificant to the performance of the system. Even though a d_{ratio} of over about 0.5 is beneficial, the results suggest that no retaining walls should be discarded from potentially being used as energy geo-structures for having a short depth of embedment.

For both analyses, when adopting a normalised representation, the maximum temperatures can very well be approximated by a single equation/line, however the minimum temperatures for the balanced thermal load have less good fit. This is likely due to the smaller values of temperature being more sensitive to the normalisation (dividing over a smaller number compared to maximum). However, for the same reasons the minimum values have a higher margin for errors, as being within 5% of a value of 10°C results can still be acceptable. It is also worth noting that even though when the unbalanced thermal load is adopted the values of the temperatures are beyond the acceptable limits, similar patterns are found between the maximum temperatures of the unbalanced and balanced thermal load cases, suggesting that the insights gained are applicable to a range of fluid temperatures and scenarios.

Comparing the two stages of analyses of this section, it is very clear that the impact is much greater when extending the embedment (Figure 4.23), compared to when only changing the ratio of the wall in contact with the ground (Figure 4.25), suggesting that the main impact comes from the additional wall depth and pipe length. For a fixed depth retaining wall, varying how much ground was in contact with the wall face on the building side, made relatively insignificant difference. Therefore, having a short depth of embedment should not discourage the utilisation of the retaining wall as an energy geo-structure, but a short overall depth could be such a factor. On the other hand, when extending the wall can be built relatively cost

efficiently, the results also show that the thermal performance gains could be significant for initially small values of d_{ratio}, short depths of embedment or short retaining walls, but perhaps not as fruitful and justified otherwise.

4.3.4.3 Energy soldier pile retaining walls

This section presents a number of thermal performance analyses for energy soldier pile retaining walls, following a similar structure as section 4.3.4.2 discussing energy diaphragm walls. The effect of the thermal load distribution balance and the potential benefits of thermally activating the slab in addition to the retaining walls are discussed first, where the geometry and conditions are as described in section 4.3.2.4. Following, three more analyses are presented, all altering the geometry and/or configuration to investigate the influence of design parameters on the thermal performance. The first analysis investigates the pipe density in terms of the length of pipe (number of pipe U-loops) embedded in the pile. Following, the spacing of the piles is studied, for both the case when only the spacing is varied as well as when this affects the total number of piles activated (and therefore how much thermal energy each pile is expected to provide), which is more realistic. The final analysis investigates the depth of embedment of the soldier pile retaining wall and the potential thermal gains obtained by extending/deepening it, similarly to the respective analysis for energy diaphragm walls.

The effect of the thermal load distribution balance and thermally activating the slab

The thermal performance results for the soldier pile models (recall Figure 4.10 – Figure 4.12), in terms of the average fluid temperature, are presented in Figure 4.26. In this case, when the *unbalanced* thermal load distribution is adopted close to 60% of the cooling load can be provided when only the piles are thermally activated (Figure 4.26(a)) and close to 70% when both the piles and slabs are activated (Figure 4.26(b)). On the other hand, when the *balanced* distribution is adopted, up to double the cooling and heating demand can be provided when only the piles are thermally activated (Figure 4.26(c) – assuming anti-freeze solution used) and over double when both the piles and slabs are activated (Figure 4.26(d)), since the fluid temperatures are well within the GSHP operating range limits. These results again show how significant the distribution of the thermal load is for energy retaining walls, as the geothermal system works most efficiently when it both rejects and takes heat to/from the ground, therefore returning it (close) to its original state at the end of each cycle and preventing heat accumulating effects.

As it can be seen, overall the patterns and learnings are similar to those for the diaphragm walls discussed in section 4.3.4.2. When adopting energy soldier pile walls once again the *balanced*

thermal load distribution results in an extremely more beneficial outcome regarding the system thermal performance and the thermal activation of the slab increases the thermal performance of the entire GSHP system. However, in this case activating the slab in addition to the soldier pile retaining wall is more impactful compared to diaphragm retaining walls (for example the maximum temperatures in the unbalanced case are reduced by about 3-4 °C when activating the slab in the soldier pile wall case, compared to about 1°C in the diaphragm wall case). This is likely due to the fact that in soldier pile walls only the piles are activated (and not the spacing in between) and therefore the ground underneath the slab is only thermally affected around each pile, thus, to a lesser degree compared to energy diaphragm walls. Nevertheless, the impact is still relatively minor and unlikely to justify the associated additional costs.

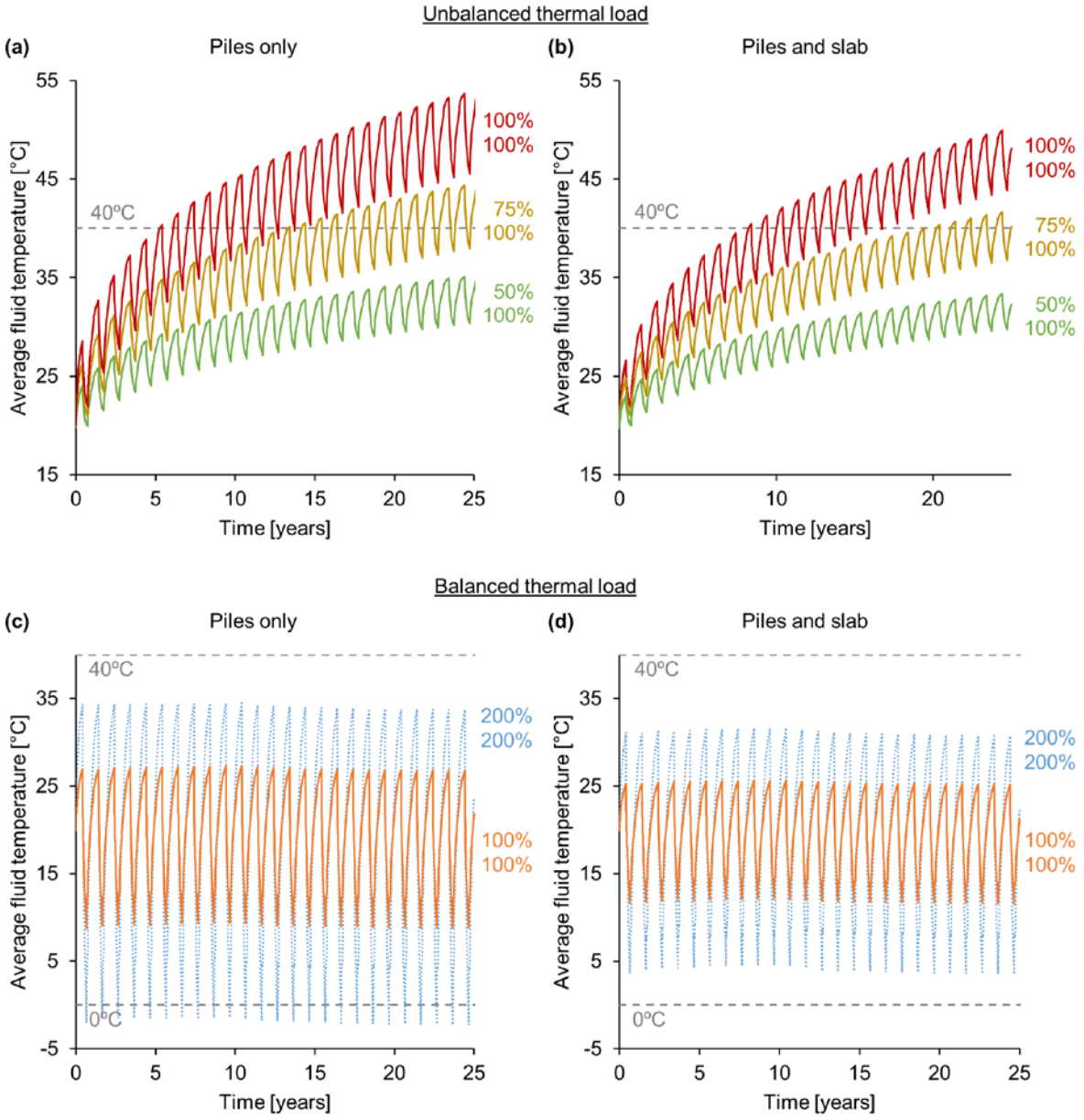
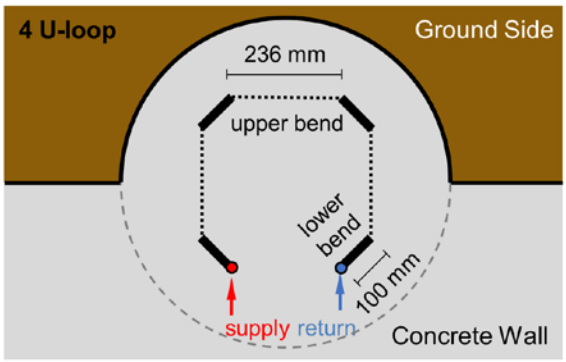
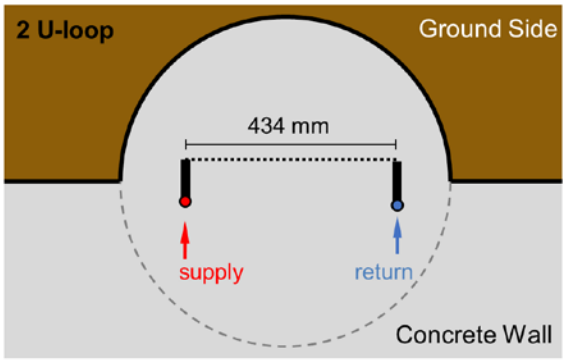


Figure 4.26 Thermal performance results for energy solder pile walls, indicating the fluid temperature results when providing different amounts of cooling (upper % value) and heating (lower % value) energy

The effect of pipe density: pipe loop separation

An important design decision when working with soldier pile retaining walls is the configuration of the geothermal pipes inside the soldier piles. In traditional vertical borehole design single and double U-loops are commonly adopted, given the small borehole radius. In soldier piles however, which can have much larger diameters, this is no longer a constraint as more loops can be incorporated. However, there exists no clear and easy way of determining an optimal length of pipe that can be placed in each pile. This analysis varies the pipe length per soldier pile (depth = 28 m; diameter = 750 mm), from a single U-loop, to up to 6 U-loops connected in series as shown in Figure 4.27, aiming to identify the benefits of increasing the pipe length. It should be noted that *upper bend* refers to a connection made at the top of the pile (adopting the appropriate right-angle or U-loop (180°) fittings or bending the pipe) and *lower bend* to a connection made at the bottom of the pile (with a standard U-loop fitting – in this case 100 mm).





Loop Number [-]:	1	2	3	4	6
Upper bend [mm]:	-	434	236	236	130
Lower bend [mm]:	100	100	100	100	100

Figure 4.27 Schematic and details of varying the amount of pipe in each soldier pile of 750 mm in diameter

Figure 4.28 shows the results in terms of the maximum and minimum average fluid temperatures, for both cases of the thermal load distribution. It is clear that the more pipe is incorporated in the soldier pile the better the thermal performance, with less extreme maximum and minimum temperatures observed. However, after a certain pipe length, in this case between 3 and 4 loops, the difference is minimal and therefore the additional costs of incorporating additional loops and connections would likely not be justified.

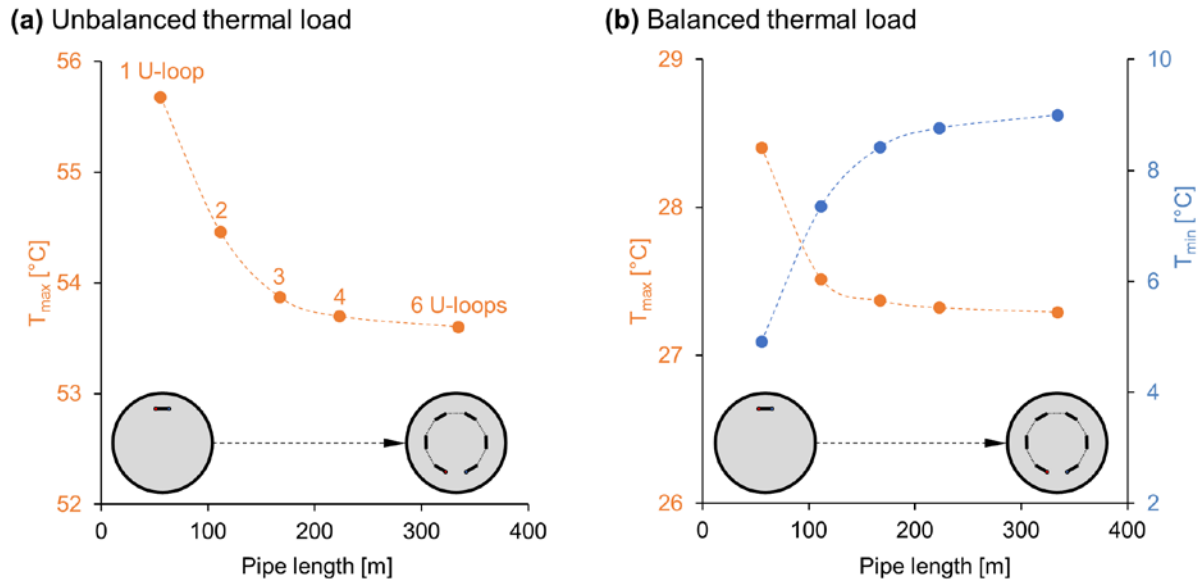


Figure 4.28 Maximum and minimum average fluid temperatures when varying the amount of pipe incorporated in soldier piles (pile depth 28 m, pile diameter 750 mm)

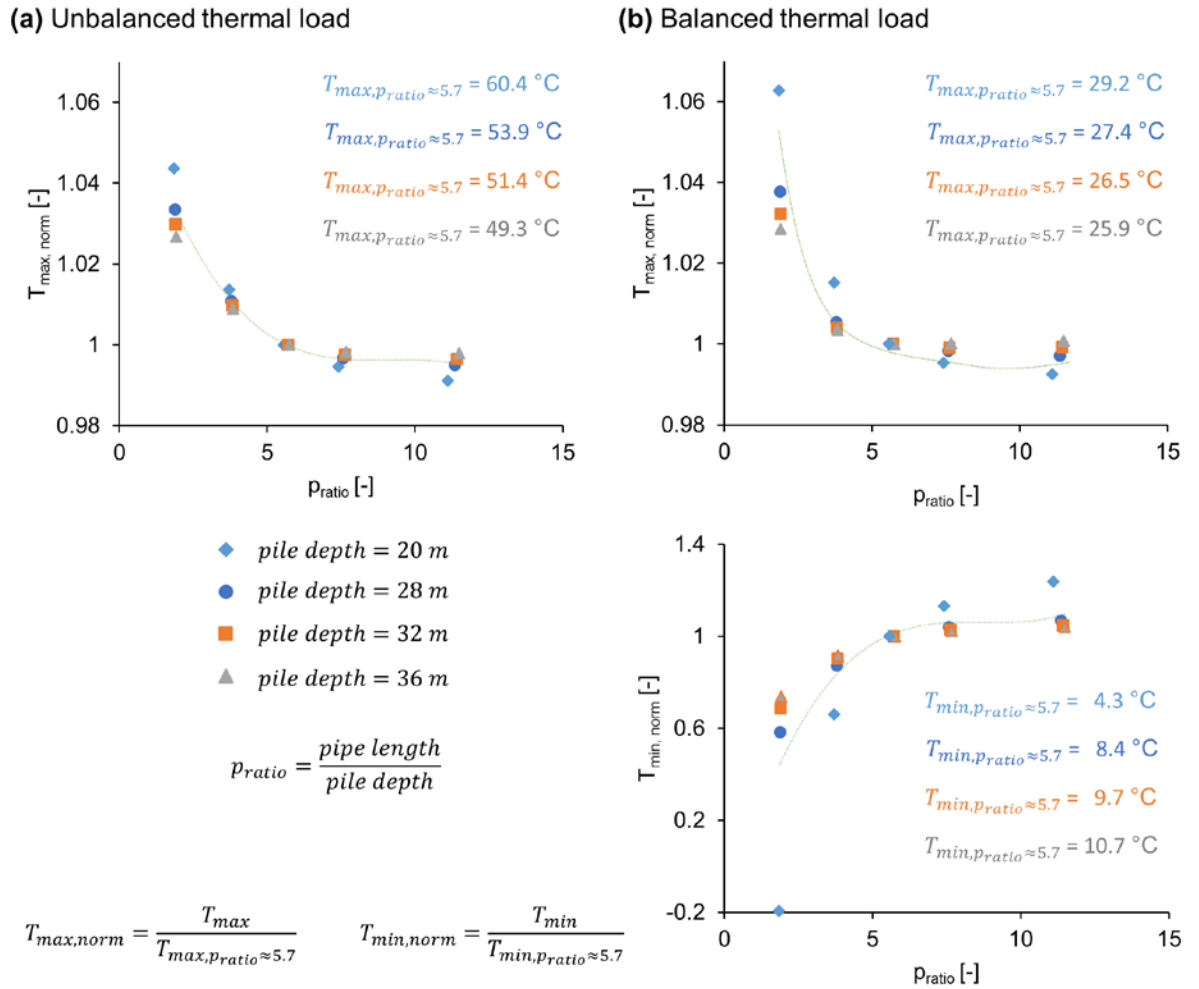


Figure 4.29 The effect of adding more pipe in the soldier pile retaining wall for different depths of pile - normalised results

To investigate whether this pattern is affected by the soldier pile depth, additional simulations were undertaken with shorter/deeper piles. The results can be seen in a normalised form in

Figure 4.29 exemplifying the observation that the performance returns of incorporating more pipe diminish the more pipe is incorporated, a pattern that is seen for all pile depths. For the three deeper pile depths ($28\,m$, $32\,m$ and $34\,m$) the normalised temperatures, showing the relative change, are very close suggesting that after a certain wall depth the ideal amount of pipe placed does not change. However, for the shortest pile depth ($20\,m$) the results start to diverge, suggesting that for shorter piles the ideal number of pipe loops is likely different than for longer piles. For completeness, it should also be mentioned here that there exist other factors that could affect these results, such as the diameter of the pipe, not investigated by this research. However, this investigation does show the potential for the number of pipe loops (and pipe length) implemented in a soldier pile wall to be optimised, to balance the expected thermal gains with the associated costs.

The effect of pile spacing

Another important parameter that affects the performance of energy soldier pile walls, implementing geothermal piping in the piles, is the pile spacing. When the energy piles are placed closer together, each pile GHE is potentially engaging less volume of soil and therefore less thermal storage. Furthermore, the operation of the system in each pile GHE thermally interferes with its surrounding pile GHEs. In order to identify the extend of the impact of this effect, the pile spacing in the soldier pile retaining walls is varied from the initial 1.8 metres to up to 4 times as much, 7.2 metres spacing. In this first analysis, other parameters such as total number of pile GHEs, pipe length and thermal load per GHE remain constant and as introduced in sections 4.3.2.4 and 4.3.3. Therefore, the only varying parameter is the spacing of the soldier piles, to isolate its effect on the thermal performance, and represents the spacing at which the soldier piles are being constructed, which is determined by their structural design. The results are shown in Figure 4.30. Placing the GHEs close together can severely affect the fluid temperatures, increasing them in cooling mode and decreasing them in heating mode. The impact is more dominant in the unbalanced case where the temperatures are decreased by over 15 °C when doubling the original spacing of 1.8 metres to 3.6 metres. The magnitude of the improvement of the temperatures decreases with increased spacing as the thermal influence of neighbouring GHEs becomes less influential for the fluid temperatures. The threshold pile spacing is similar to that recommended for smaller diameter boreholes GHEs (~4 to 5 m) [141].

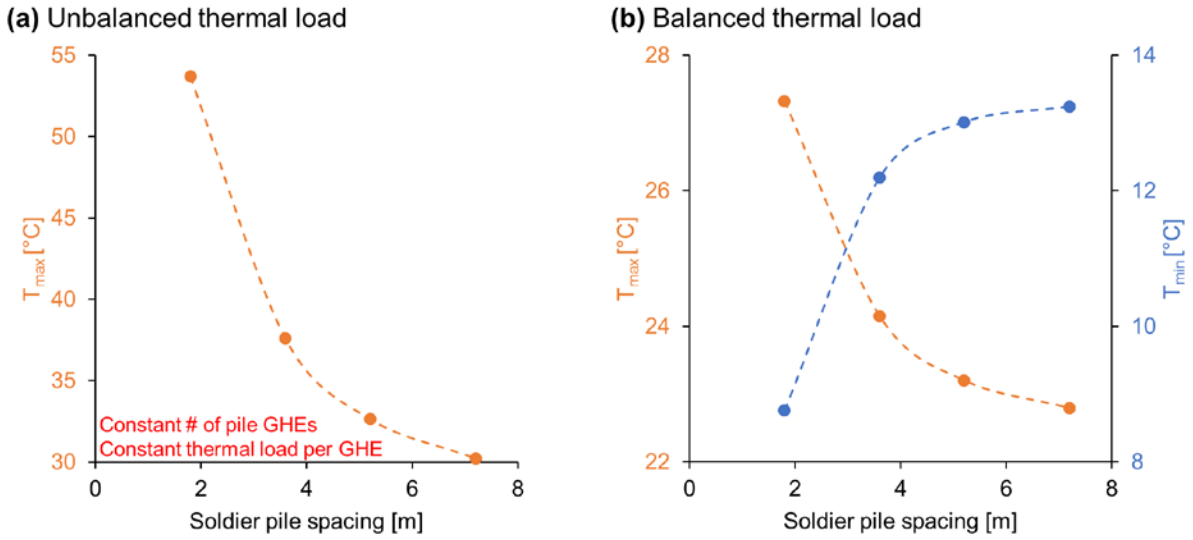


Figure 4.30 Maximum and minimum average fluid temperatures when varying the horizontal spacing of the soldier piles incorporating 4 U- loops connected in series, while the total number of pile GHEs and thermal load per GHE are constant

It is crucial, however, to recognise that pile spacing is not a parameter that the geothermal design of the system can commonly influence and therefore it is very unlikely that the structural design can be modified to improve the performance of the geothermal system. On the other hand, a decision that does fall on the geothermal design is how many of the soldier piles to activate. By choosing to activate, for example, every second soldier pile along the retaining wall, the spacing between them is doubled. Moreover, the less soldier piles are activated the lesser the associated costs for materials and installation. However, the increase in soldier pile spacing (and decrease in the number of total GHEs) increases the amount of thermal energy *each* soldier pile GHE needs to provide. To better illustrate this concept, Figure 4.31 shows a schematic of the pipe connections within a series of soldier piles for three different cases: (a) thermally activating every single soldier pile, (b) thermally activating every second pile and (c) thermally activating every third pile. To provide the thermal load required by the entire system, each soldier pile GHE in case (b) and case (c) needs to provide twice and three times as much thermal energy as those in case (a) respectively.

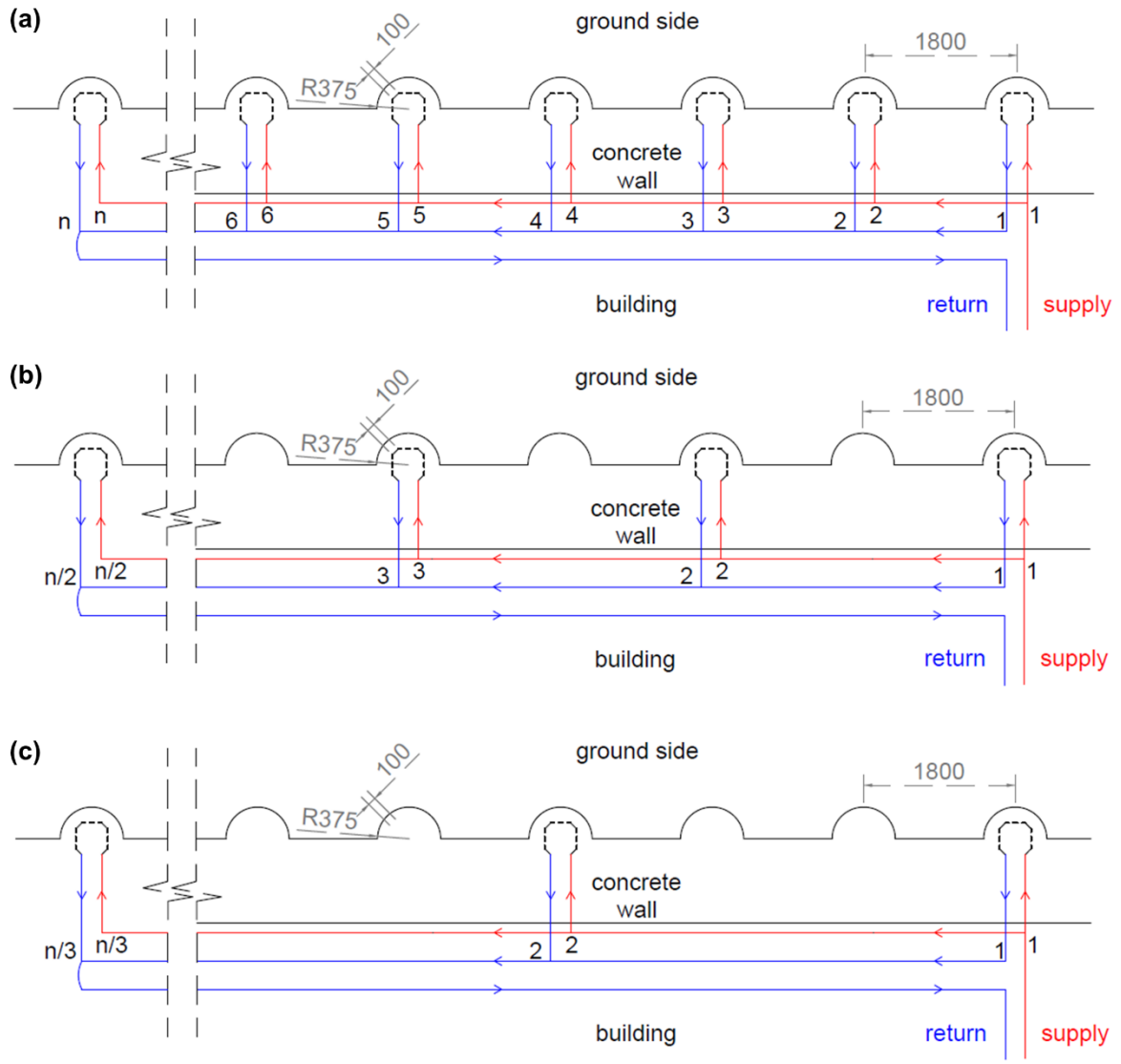


Figure 4.31 Schematic of pipe configuration when thermally activating different number of soldier piles. (a) Every single soldier pile (b) every second soldier pile (c) every third soldier pile

The results, summarised in Figure 4.32, show that in this case the thermal performance impact by the higher thermal energy that needs to be provided overshadows the increased performance due to the wider spacing of the piles, resulting in a negative net effect, where the maximum and minimum fluid temperatures increase/decrease accordingly. However, even though the performance is decreased, it is important to carefully assess the cost benefits associated with activating less piles, such as shorter installation time and lower likelihood to affect the project's otherwise structural-based timeline. In the case of a balanced thermal load, for example, where 100% of the load can easily be satisfied, reducing the number of soldier piles thermally activated can be a significant benefit with the fluid temperatures still being within acceptable limits. Moreover, increasing the thermal load per GHE will also increase the supply and return temperature difference, ΔT (in this case, for example, from 1 °C to 3.2 °C for the balanced load), which can be beneficial for the operation of the heat pump.

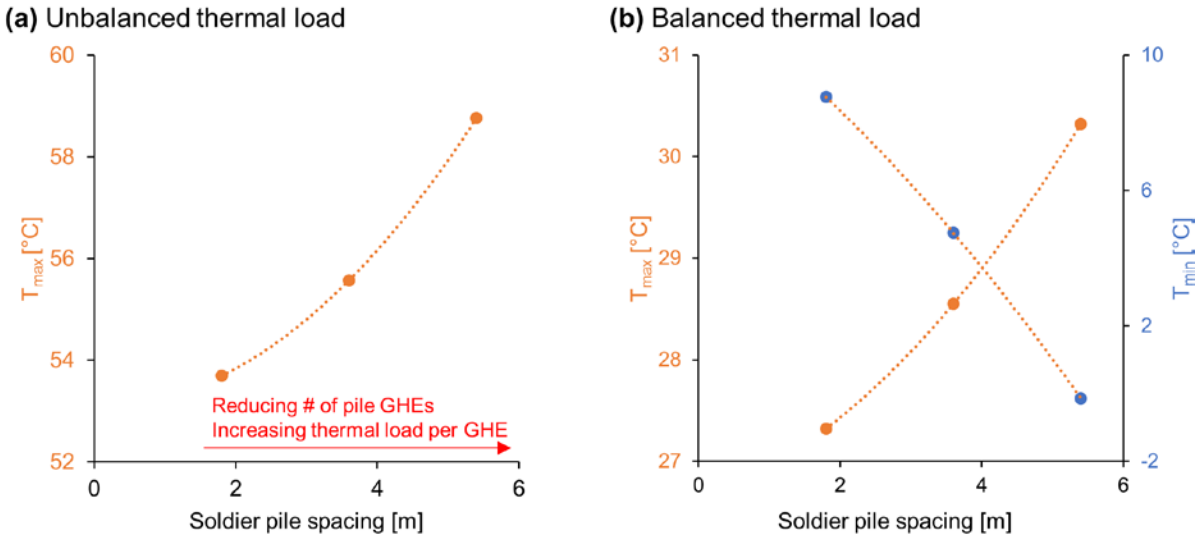


Figure 4.32 Maximum and minimum average fluid temperature results when activating different number of soldier pile and therefore the number of pile GHEs and thermal load per GHE varies with spacing

The effect of the depth of embedment

An important difference between retaining walls and other structures, as it has been mentioned, is the amount of surrounding soil in contact with the structure, which in the case of energy retaining walls can be limited. This analysis aims to further understand and quantify the importance of this difference by following a two-leg analysis, similarly to the one performed for energy diaphragm walls in section 4.3.4.2. Where applicable, normalisation has been used to generalise the results and show that similar patterns exist between retaining walls of different depths (which is considered an important parameter for the thermal performance), as further explained in the respective diaphragm wall analysis.

Firstly, the scenario of extending the depth of embedment of the soldier pile, d_{emb}, is investigated, where the total wall depth d_{wall}, (and therefore the geothermal pipe length) is increased, as illustrated in Figure 4.33. The value of $d_{basement}$ remains constant and the analysis adopts four values to investigate how the initial depth of the wall affects the potential benefits of increasing d_{emb}. The results are summarised in Figure 4.34, showing the maximum and minimum average fluid temperatures, concluding the 25-year operating period. Similar to diaphragm walls, extending the soldier piles has a noticeable effect on the performance of the GSHP system, with the maximum fluid temperatures lowered, by up to about 10 °C for the unbalanced case and about 5 °C for the balanced case, and the minimum values increased by up to about 5 °C. The improvement is higher for shallower basements (small $d_{basement}$ and therefore initially shorter walls) as well as for smaller values of d_{emb}. Therefore, the most significant benefits of increasing the retaining wall depth are found in geometries with either short walls or short depths of embedment. If the retaining wall is relatively deep, then further

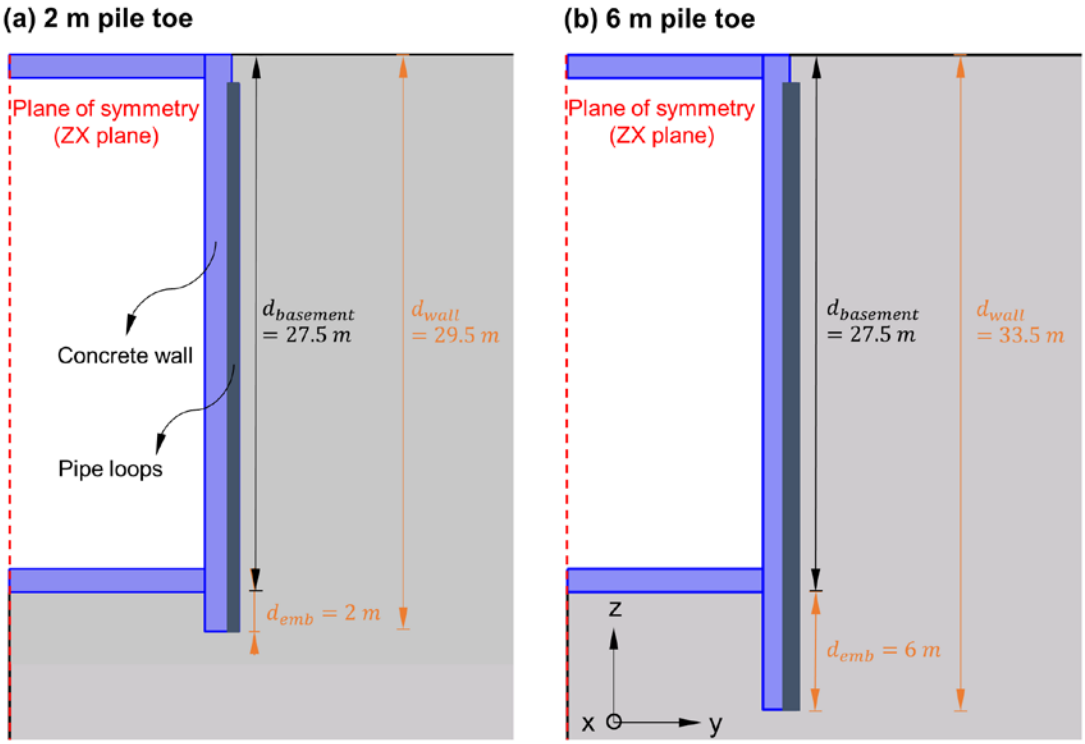


Figure 4.33 Schematic showing a change in the depth of embedment by extending the wall

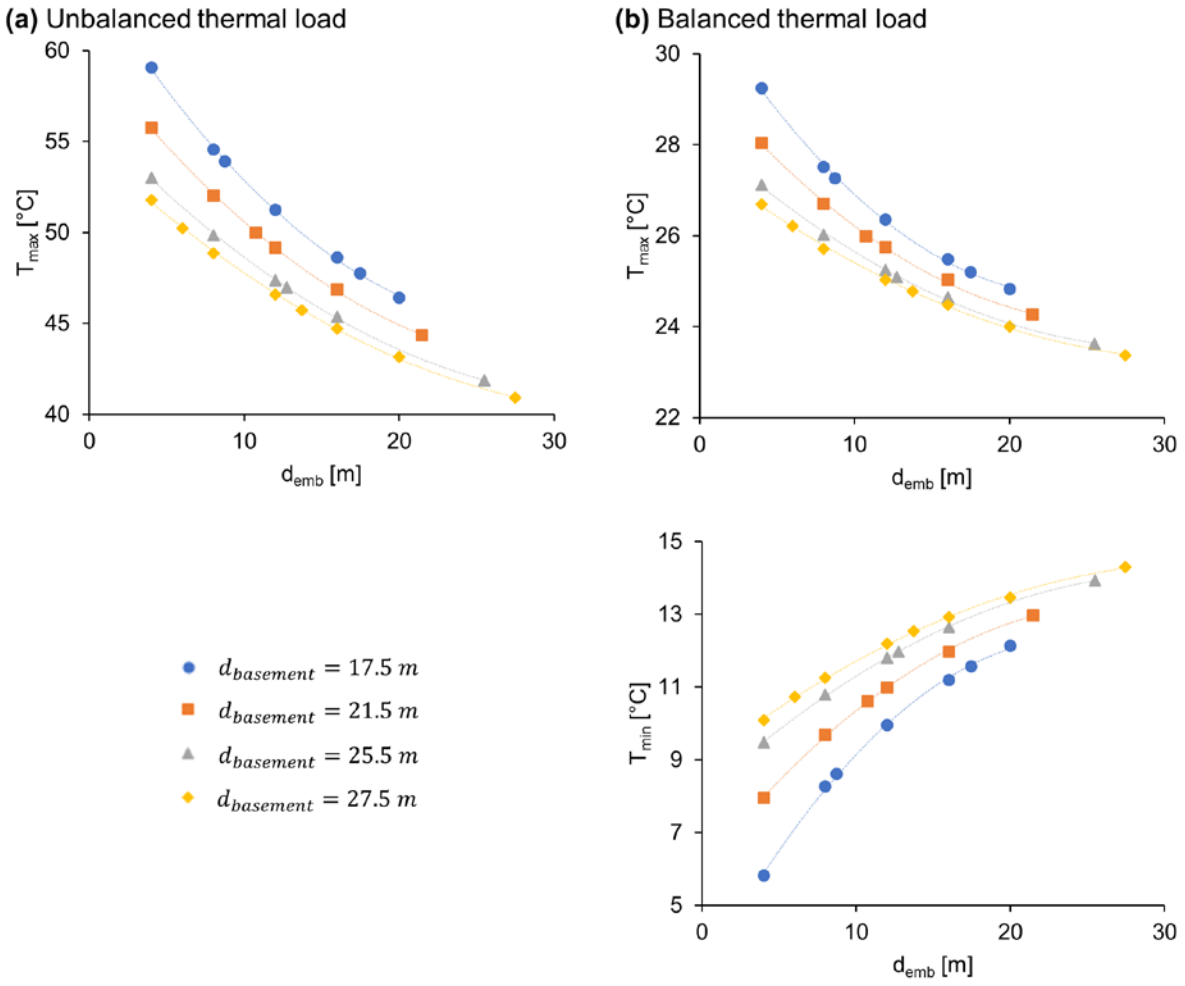


Figure 4.34 Maximum and minimum average fluid temperature when extending the depth of embedment in soldier pile retaining walls

increasing it is still beneficial but at a lesser degree. Moreover, when d_{emb} becomes high, the results tend to converge to a similar value, likely because the depth of embedment surpasses the depth of the rest of the wall ($d_{basement}$) and governs the performance. The normalised results of Figure 4.35, once again highlight the common behaviour for different depths and show that the results can be well approximated by a single normalised equation.

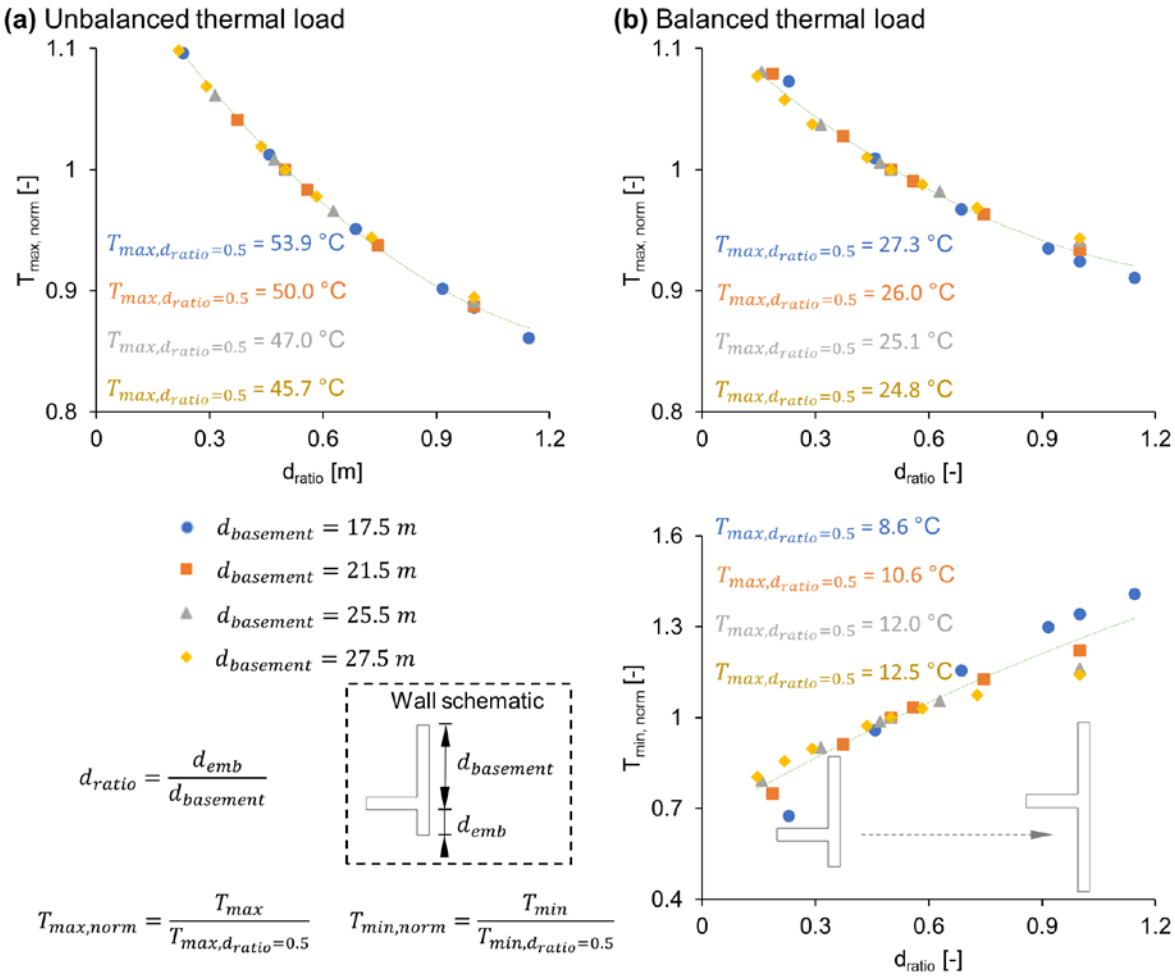


Figure 4.35 The effect of extending the depth of embedment in soldier pile walls - normalised results

The second leg of the analysis follows the same reasoning as the respective one for diaphragm retaining walls with the depth of embedment, d_{emb}, (which is in contact with the ground on both sides) being varied while keeping the entire depth of the wall, d_{wall}, (and therefore the amount of pipe implemented in the wall) constant. A schematic showing the variation of d_{emb} in this way can be seen in Figure 4.36. Even though this does not represent a realistic scenario, this analysis can provide insights on the applicability of retaining walls with different geometries as energy geo-structures. The results of this analysis can be seen in Figure 4.37, noting the maximum/minimum average fluid temperature values for three different values of d_{wall}, in a normalised dimensionless form. The results are similar to the respective ones for diaphragm walls, with a variation in temperatures in the range of 1-2 °C.

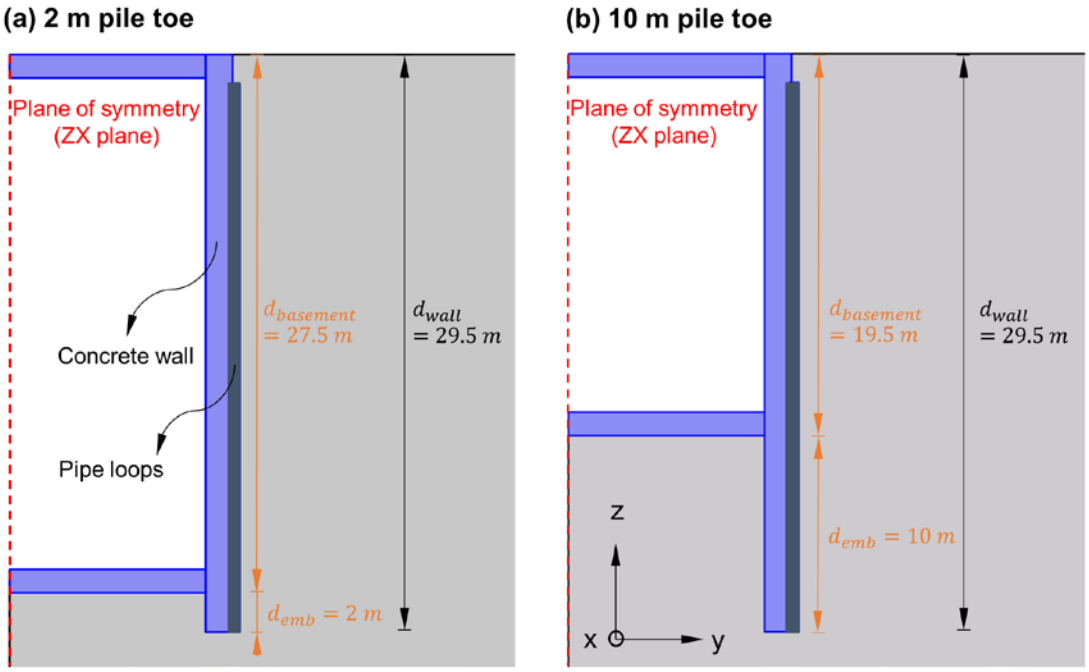


Figure 4.36 Schematic showing a change in the depth of embedment without changing the total depth of the soldier pile wall

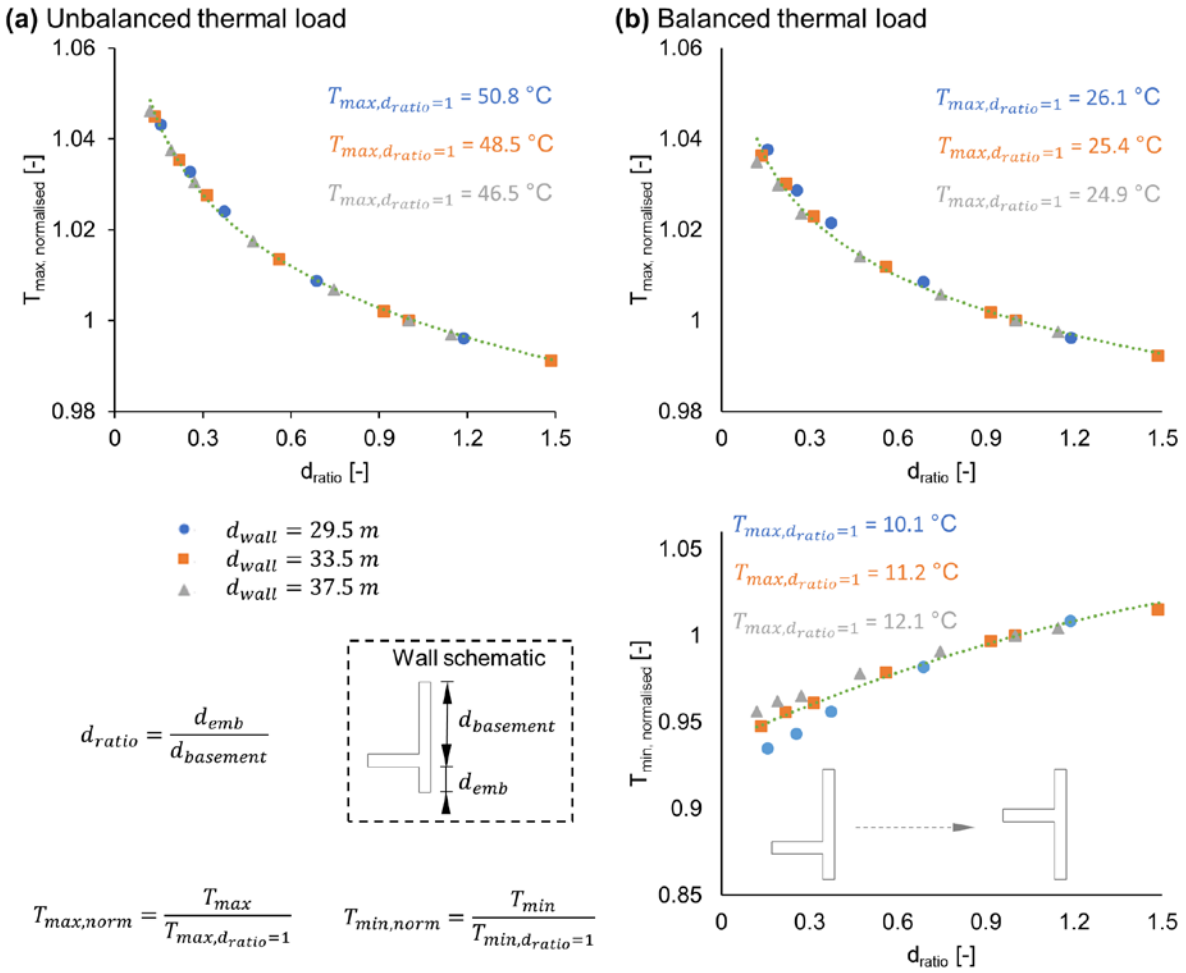


Figure 4.37 The effect of varying the embedment depth while keeping the overall soldier pile retaining wall depth fixed – normalised results

As expected, higher values of d_{ratio} (and therefore more soil in contact with the structure), generally improve the system's performance, even though for values of d_{ratio} greater than about 50% (the depth of embedment being about 1/3 of the entire wall depth) the increase in thermal performance is relatively marginal. Moreover, the change is relatively insignificant and the range of values is in general similar for the different values of d_{ratio}, showing that the relative value of the depth of embedment compared to the basement is not very significant and therefore not limiting different geometries of retaining walls from potentially being utilised as energy geo-structures.

Overall, the investigation on the importance of the depth of embedment on the thermal performance of soldier pile retaining walls resulted in similar outcomes as the respective one on diaphragm retaining walls. For either type of retaining wall, extending the depth of embedment can be significantly beneficial to the thermal performance, especially for cases where the depth of embedment or of the entire wall is initially relatively short and especially when it can be done without excessive additional costs or when the thermal benefits remove other costs, for example from a no longer needed auxiliary system. Investigating the impact of the ratio between the depth of the basement and the embedment without changing the wall total depth showed a relatively insignificant effect, suggesting that the additional degree of piping involved with extending the wall is crucial to increasing the thermal performance. Importantly, the latter also suggests that retaining walls (of either type) with a short depth of embedment should not be disregarded from being utilised as energy geo-structures, since the total depth of the retaining wall governs the thermal performance and not the depth of embedment. Lastly, it has been shown that both analyses are generally well represented in a dimensionless form, suggesting the potential creation of generalised energy retaining wall charts in the future that could aid geothermal designers to more effectively design these systems.

4.3.4.4 Reflections and real-world projects

As it has been stated, the work undertaken on energy retaining walls and the analyses presented in section 4.3.4 began with a feasibility study on a large scale real-world project, the Melbourne Metro, and an investigation on the potential of turning the retaining walls of city metro stations to energy structures. This work followed the industry approach, working with the industry partners, revising designs, and very importantly adhering to strict deadlines. The thermal design was undertaken using numerical modelling and utilising engineering knowledge, experience and the limited information on the literature to carefully select the number of models/cases to investigate within the allowed time frame. The final proposed design of the feasibility study

for each case study has been presented in section 4.3.2 and some of the main findings have been presented in the first analysis of sections 4.3.4.2 and 4.3.4.3, focusing mainly on how much energy can viably be provided, how balancing the thermal load distribution can affect the thermal performance and whether thermally activating the slab in addition to the walls can be of significant thermal benefits. It is therefore worth looking back and reflecting on this work and utilising the information presented in the other analyses of section 4.3.4, which were undertaken outside of the industry project and with more flexibility to investigate many scenarios and cases, to acknowledge how having this information beforehand would have potentially been able to improve the design.

Firstly, looking at diaphragm retaining walls and section 4.3.4.2, the analysis on the effect of pipe density investigated how varying the vertical pipe loop spacing can affect the performance. Based on its findings, utilising a spacing larger than the proposed 450 mm, between 700 mm and 800 mm would yield very similar results while at the same time significantly reducing the installation and material costs. If a balanced thermal load was adopted, even larger spacing could be adopted and comfortably provide the required energy. Regarding the soldier pile retaining walls and section 4.3.4.3, the analysis on the pipe loop spacing within each soldier pile found that using three U-loops in series would yield very similar results to the proposed four U-loops in series, which would also reduce the installation costs. Finally, the analyses for both wall types on the effect of the depth of embedment showed significant gains in thermal performance when extending this depth. It is important to note here that during the undertaking of the feasibility study the depth of embedment was not finalised by the structural design team of the project and hence the geothermal design adopted very conservative values for the depth of embedment. Therefore, it could have been beneficial to also present results for less conservative (and more realistic) values in the final feasibility report, which would result in the system being able to satisfy more thermal demand and would be a more accurate representation of the potential of energy retaining walls.

Overall, the presented work shows that because limited information currently exists on the design of energy retaining walls, it can be difficult to produce an optimal thermal design, especially under the conditions of a real-world project. Therefore, thorough analyses on the optimality of different configurations and geometries, similar to and extending the ones presented in this chapter, could be very useful to geothermal designers, providing insights and information to aid towards a more economical or more efficient energy retaining wall design.

4.3.5 Importance of boundary conditions

The boundary and initial conditions define important information necessary to complete the system of governing partial differential equations that underlie the complex numerical problem. Their selection should ensure a high degree of realism for a given scenario and therefore the usefulness and applicability of the results. It is therefore crucial to be confident that the set conditions consist of realistic representations of the real-world problem being simulated. In energy retaining wall design, there have been different approaches to model the interaction between the thermally activated structure and the inside space of the underground building. In this section, the boundary conditions used on the inner wall and slab surfaces of the underground energy structure are investigated and further analysed to identify their validity and applicability for design.

4.3.5.1 Modelling the wall and slab surfaces

Three different boundary conditions have been adopted, as indicated in Figure 4.38, utilising the soldier pile retaining wall geometry as a case study. The first boundary condition (a) is simply thermal insulation, as has been utilised throughout this chapter, which thermally isolates the underground part of the inner space of the building (e.g., a building basement, an underground metro station, etc.) from its structural elements and surrounding ground; however, building the wall with thermal insulation may result in additional costs. The second condition (b) is using a constant temperature of 21 °C on these surfaces, which is a commonly adopted condition as found in the literature [40,95,99]. However, it can be argued that the assumption that the temperature at these surfaces will be unchanged is less suitable since the temperatures inside the thermally activated structures will be changing due to the operation of the geothermal system. Lastly, condition (c) – labelled "continuity" – models the air space as a fluid volume that moves through predominantly in the x-axis direction (the air can move in other directions as well, but this x-axis is the predominant induced air flow direction due to ventilation). This air modelling is achieved by incorporating the Reynolds-Averaged Navier-Stokes equations for a compressible flow and coupling them to the governing equations for heat transfer, as explained in detail in section 4.3.2.1. Modelling the inner wall and slab surfaces using continuity allows heat transfer between the concrete elements and the modelled air flow.

It should also be noted that the continuity boundary condition introduces additional parameters such as the air velocity ($V_{air} = 0.5\, m/s$ used here as typical value [142]) and temperature (21°C) of the air initially entering the section (from forced ventilation). As expected, this method increases the computational complexity and time requirements of the simulations.

Therefore, the mesh of the air volume was selected to keep the requirements reasonable while still providing acceptable accuracy (different mesh types were utilised with quicker time-independent simulations in making this selection). It should also be mentioned that in order to properly simulate an adequate portion of the structure (along the x-axis), several simulations are computed in sequence, using the outflow boundary results of each as the entering boundary conditions for the next. This allows the investigation of air flowing through a *10.8-metre-long* section of the station, simulating the average length of the tunnel between two ventilation systems/shafts.

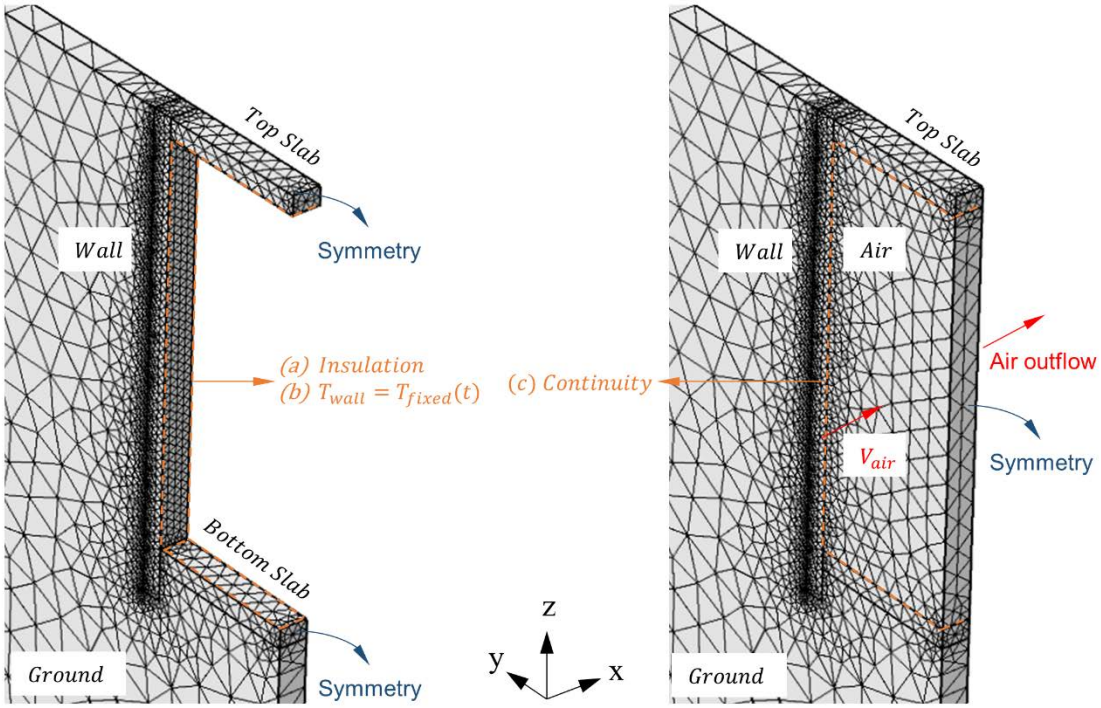


Figure 4.38 Boundary condition modelling schematic showing the three approaches (a) insulation, (b) prescribing a temperature and (c) continuity of temperature between the wall and the basement space

4.3.5.2 Temperature results for the different boundary conditions

The simulation results can be seen in Figure 4.39 and show a very significant difference between the three approaches. When the unbalanced thermal load distribution is used, thermal insulation on the surfaces results in the fluid (and surrounding soil) temperatures increasing over time (blue line), due to the cooling dominant load, reaching excessive temperatures of over 50 °C, as seen in section 4.3.4.3. However, a boundary condition adopting either a constant temperature or continuity (green and orange lines) results in the average fluid temperatures only fluctuating between about 20 °C and 26 °C and showing no signs of heat accumulation despite the cooling dominant load. The difference between the sets of results is extreme, as the first shows a system unable to provide the required thermal load, that needs further consideration; while the second, an optimal system that can operate very efficiently for

a long period of time. When a balanced thermal load distribution is used, the temperature difference is less extreme between adopting the different boundary conditions, however it is still present. Utilising thermal insulation results in the average fluid temperatures fluctuating between about 9°C and 27°C while for the constant temperature or continuity conditions between about 13 °C and 25 °C. These results once again show a better performing system when boundary conditions (b) and (c) are adopted, which is peculiar.

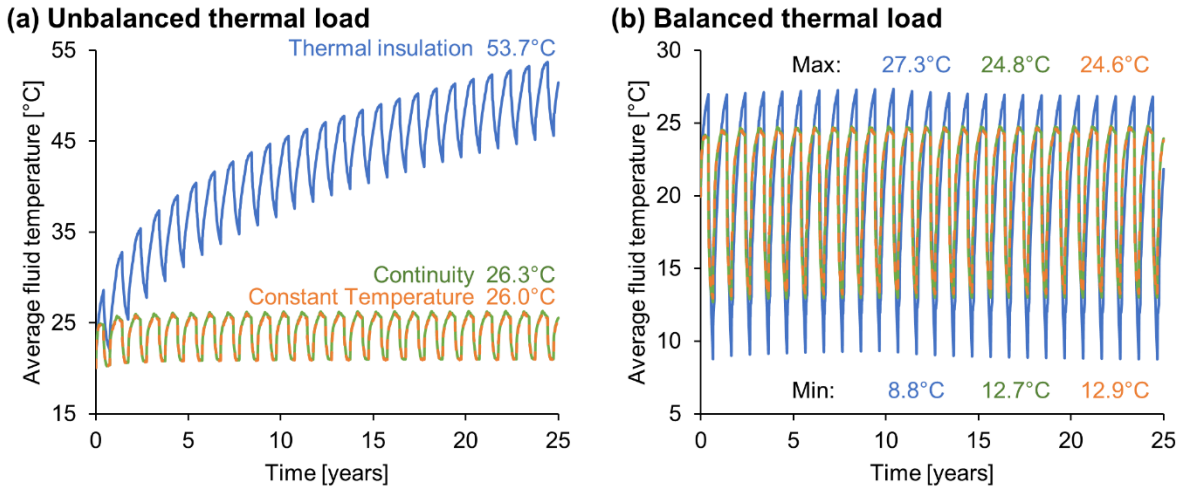


Figure 4.39 Average fluid temperature when simulating the soldier pile retaining walls with the three different boundary conditions

It is also worth comparing the results for the two different thermal load distributions, for each adopted boundary condition. When considering the thermal insulation scenario, as it has been discussed in section 4.3.4.3, a balanced thermal load results in a much more well performing GSHP system compared to the unbalanced case. However, the results for boundary conditions (b) and (c) show a wider temperature range when the balanced thermal load is adopted compared to the unbalanced case. Therefore, even though the temperature ranges for both thermal load cases are acceptable, the results suggest that adopting an unbalanced thermal load distribution would be more beneficial for the GSHP system, which is illogical and goes against our understanding of these systems. Consequently, the validity of these results should be questioned.

4.3.5.3 The heat transfer through the surfaces

In order to have a deeper understanding of the reasoning behind the results discussed in section 4.3.5.2, one can analyse the heat transfer through the boundaries highlighted in Figure 4.36. The heat transferred daily for the last year of operation and the unbalanced thermal load distribution can be seen in Figure 4.40. The left y-axis shows the heat provided by the GHE (the thermal load – shown for reference) and relates to the respective (grey) line. The right y-

axis shows the amount of heat transferred through the wall and slab boundaries every day, which is referred to as heat "leaked" inside the underground building (the reverse – heat flowing from the building to the ground through the wall/slab surfaces is not relevant in this case), for the three boundary conditions considered.

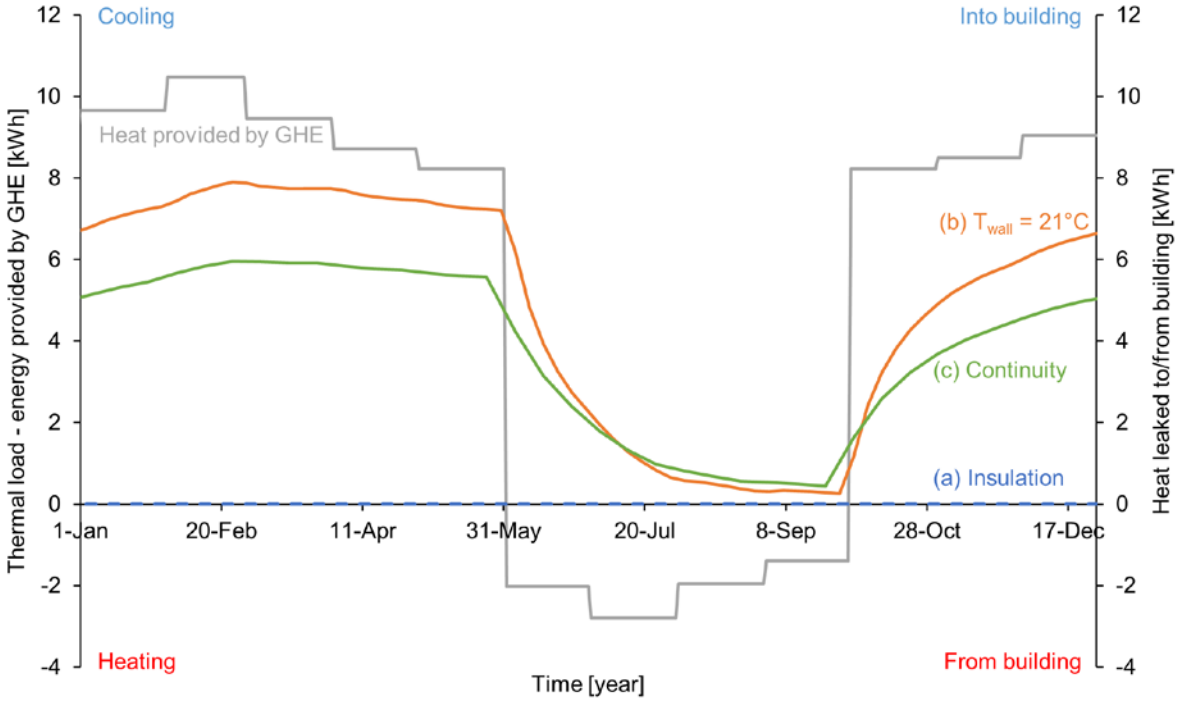


Figure 4.40 Daily heat transferred through the wall and slab boundaries for the different boundary conditions per soldier pile GHE. Last year (25th) of operation, using the unbalanced thermal load distribution

As it can be seen, the thermal energy solicited to each GHE to satisfy the target thermal loading (grey line) is mostly in cooling, with some minimal heating requirements between June and September (winter in Australia). Looking at the heat transfer under the three different boundary conditions tested, when thermal insulation (boundary (a) – blue line) is used, as per its definition, no heat transfer occurs through those boundaries (in reality, no insulation is perfect and some minor heat leaks may occur). However, when the constant temperature of 21 °C is prescribed on the boundaries, a significant amount of heat flows through the boundaries, into the building area (orange line). During the first cooling period from January to May, the daily heat being "leaked" reaches about 8 kWh, while the heat provided by the GHE is around 10 kWh. This means that while in cooling mode, instead of the heat being transferred from the building side to the ground via the GSHP-GHEs, a large portion is being transferred back into the building. This is because, the fixed temperature at the wall and slab surfaces always render a large temperature difference between the temperature around the HDPE pipes (being increased by the circulating fluid) and these surfaces, which directs the heat towards them and back into the station. During the heating period, the heat still flows into the building, due to the

fact that the wall elements have risen in temperature and that temperature never falls below 21 °C due to the very small amounts of heating required. Overall, since the boundary condition assumes a temperature at the wall and slab surfaces, it implies that an infinite amount of thermal storage is available which is not a valid assumption.

When the continuity boundary condition (c) is adopted and the air is modelled, similar results can be seen as when adopting a constant temperature (b), although at a lesser degree, meaning less amount of heat is leaked back into the building (green line). The reason for the similar outcome is that the continuity boundary condition adopts a similar reasoning to the constant temperature boundary condition, where the inflow of air (entering at 21 °C) constantly transfers the heat towards the outflow (over a section of 10.8 m). Therefore, the heat passes through the wall and slab surfaces and is carried through the air. Since the temperature value of the air near the wall is not forced at a value of 21 °C, however, but instead is allowed to rise as heat is transferred, the degree of heat transfer decreases and therefore the magnitude of this effect is less than boundary condition (b).

One important difference between boundary conditions (b) and (c) is that the latter models the air passing through the section, which means that the results can be used to gain a better understanding of the overall heat transfer process. Figure 4.41 shows the temperature of the air at the outflow point (after it has travelled over the 10.8 m section) at about the mid-depth point adjacent to the retaining wall. Acknowledging that the speed at which the air flows into the section is also influential to the results, two different speeds are presented: $V_{air} = 0.5\ m/s$, as has been adopted so far, as well as the slower $V_{air} = 0.01\ m/s$ illustrating the degree this parameter can have on the results. The figure shows how the air temperature fluctuates annually, based on the heating and cooling cycle. When $V_{air} = 0.5\ m/s$, this temperature rises from 21 °C to about 21.8 °C, when heat from the cooling operation leaks into the building heating the air up. Since the air is moving relatively quickly the increase is relatively small, however, when considering the volume of air flowing through this section (due to the high speed), the heat being transferred from this difference is significant. When a lower air ventilation speed is adopted and the air moves slower through the section, the temperatures rise much higher, peaking at about 35.3 °C. Moreover, annual accumulation is visible in this case, because the temperature of the air has more time to increase and therefore the outcome has more similarities to adopting thermal insulation (a), though at a lesser magnitude.

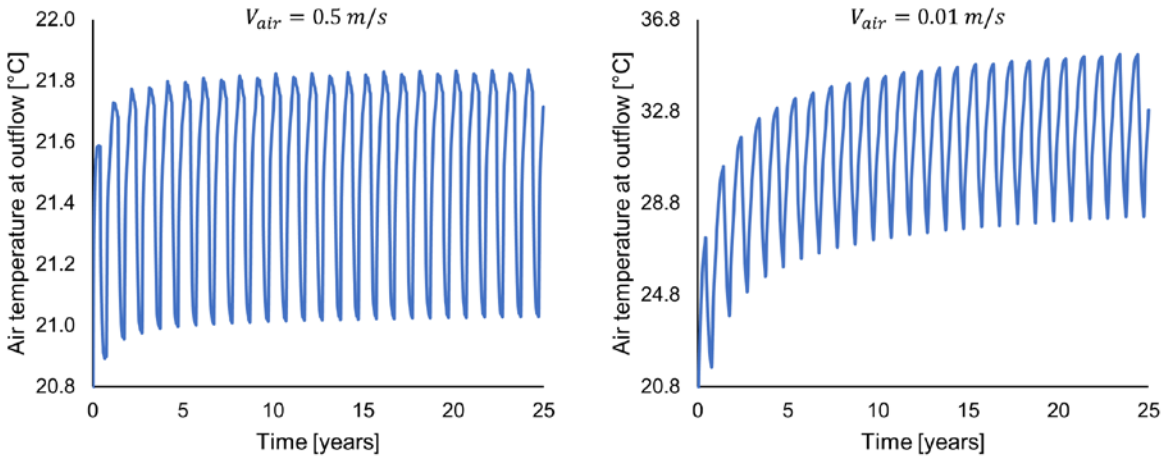


Figure 4.41 Air temperature near the wall, at outflow (end of 10.8 m wide section), mid-depth of the wall

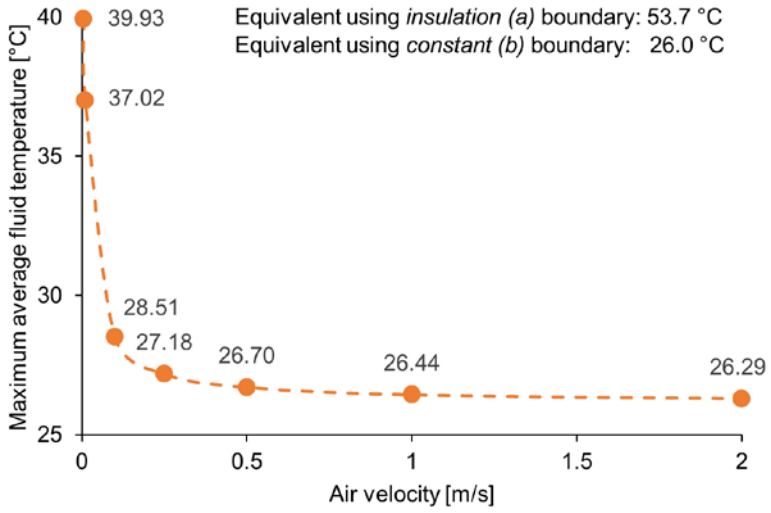


Figure 4.42 The influence of air velocity on the fluid temperature when using boundary condition (c) and the unbalanced thermal load distribution

Considering the above and how the air velocity can affect the thermal transfer results, an additional analysis was undertaken, where various values for the air velocity were adopted. Figure 4.42 summarises the outcomes of that analyses, showing the maximum value of the average fluid temperature reached over the 25-year simulations, which is an indication of the system's performance. The results show that when the velocity is higher than about 0.25 m/s, the results of the continuity boundary condition and the modelling of the air flow become similar to those of boundary condition (b). On the other hand, when slower air velocities are considered and heat accumulation occurs within the air, the temperatures rise and the thermal performance tends towards the performance when adopting thermal insulation.

4.3.5.4 Remarks on appropriate boundary conditions

Overall, it is very important to consider very well what applying these boundary conditions means physically when prescribed into the numerical model. Applying a constant temperature at the inner building surfaces suggests that the transfer of heat inside and outside those surfaces does not affect the value of the temperature. More importantly, both boundary conditions (b) and (c) allow the heat to be transferred through the boundaries without accounting for where the heat is going to and therefore having no constraint on how much heat can be transferred through the walls and slab. Boundary condition (b) simply ignores the inner building, while boundary condition (c) assumes the air flowing will "wash away" the heat towards the "heat outflow", which is adding an additional unaccounted load to the ventilation system.

The question of "*where is the heat going to*" is a crucial aspect that needs to be fully understood when applying these conditions and allowing heat transfer between the wall/slab surfaces. Starting at the case of a non-ventilated underground area, such as a car park, the validity of the boundary conditions could depend on the magnitude of the thermal load and temperatures used at the boundaries. If excessive heat is transferred inside the structure, without accounting for the temperatures at the wall rising, the assumptions would likely be unrealistic; however, if the heat transferred is moderated, it could be an acceptable approximation. Another example where these boundary conditions could be potentially suitable is the case of an underground train tunnel, where the trains keep generating heat and a high fixed surface temperature value could be set to simulate the effect, assuming that it can be guaranteed that heat will only be flowing from the tunnel to the GHEs (i.e., when the surrounding ground is not thermally saturated); however, a more thorough investigation would be necessary, considering the associated costs and other alternatives to extracting the heat.

In the case where the underground structure is ventilated, allowing heat to be flowing through the boundaries is likely unacceptable/unwanted, as it will affect the temperature of the inner structure that the ventilation is trying to control and monitor, and therefore thermal insulation would be a more suitable (but potentially costly) approach. Even more importantly, if the underground structure is ventilated and climatised via the GSHP system, applying these boundary conditions to the surfaces suggests that much of the heat extracted from this area through the ventilation system will simply be flowing back through these boundaries (as was the case demonstrated throughout this section); therefore, the heat will be flowing in circles, entirely defeating the purpose of the GSHP system. Hence, careful consideration is

recommended regarding the adoption of these new boundary conditions that energy retaining walls introduce, and which ones are most appropriate in each scenario and application.

4.4 Summary and conclusions

This chapter presents work undertaken towards further understanding the design of energy geo-structures, including contributing to the worldwide pool of available knowledge. This work utilised numerical modelling, adopting finite element methods and building upon a methodology developed within the geothermal research group at the University of Melbourne.

Section 4.2 presented a summary of a case study on energy piles that served as a stepping stone in the field of energy geo-structure design and introduced important concepts such as the different approach to geothermal design, with a hybrid system focus, and the need to answer the question "*how much energy can the system provide?"*

Section 4.3 consists of the main body of this chapter, focusing on the design of energy retaining walls, both diaphragm and soldier pile walls, and utilising the opportunity to work on a real large-scale project, Melbourne Metro, to undertake a technical feasibility study for energy retaining walls. The modelling of the two case studies (one for each type of retaining wall) is presented and followed by the required energy to be provided, the thermal load distributions. Section 4.3.4 presents the thermal performance analyses for each case study, focusing on how much energy can be provided and investigating how different important parameters can affect this performance. Section 4.3.5 investigates the importance of the boundary conditions for the building side surfaces of the structure for numerical modelling. Some of the main findings of the section are summarised as below:

- The thermal load balance is extremely important in both cases. The thermal load should be aimed to be as balanced as possible, resulting in optimally performing GSHP systems.
- Activating the slab did not result in sufficient thermal benefits to justify the expected associated costs in either case. This is likely because of the geometry and configuration, with the available ground underneath the slab already being affected by the operation of the energy walls.
- For energy diaphragm retaining walls, increasing the spacing of the pipe loops can result in negligible effects (for an intermediate value range) where the increased spacing results in a lesser thermal interference between the pipe loops (thermally beneficial) but also less total geothermal pipe length (thermally detrimental) and the two effects tend

to cancel each other. Therefore, longer loop spacings might results in similar thermal performance for lower installation costs. Overall, if costs are not considered then small spacings will benefit the thermal performance the most. However, the most cost-effective spacings seem to be the larger values of the intermediate range, for this research around 700 to 800 mm.

- For soldier pile retaining walls, increasing the number of pipe loops is significant for small loop number but has minimal gains after a certain number, in this case around 3 U-loops connected in series.
- For soldier pile retaining walls, the soldier pile spacing can have an extreme impact on the thermal performance of the system, indicating that soldier pile walls with relatively large spacing (over about 3 m in this case) would make more ideal energy structures.
- For soldier pile retaining walls, when the geothermal system can comfortably satisfy the thermal needs, activating every second or every third pile instead of each one can be a more cost-effective and beneficial solution.
- For either type of retaining walls, the portion of the inner wall in contact with the ground seems to have a relatively insignificant effect on the thermal performance. However, extending the depth of embedment can be very beneficial, especially for initially short retaining walls (about < 20 m) or short depths of embedment (about < 10 m).
- Currently, undertaking energy retaining wall design under time and budgetary industry conditions is challenging given the limited or inexistent design guidelines and can be benefitted by further investigations on the best way to thermally utilise these structures.
- Careful consideration is recommended in the boundary conditions used for the inner surfaces of an energy retaining wall/slab. Using incorrect boundary conditions, such as assuming a constant surface temperature when trying to acclimatise the underground space, can result in unrealistic results and significantly under-designed systems. Typically, using thermal insulation and separating the interior of the building from the ground that is used as thermal storage is the most conservative approach, even though this can accrue additional costs.

Chapter 5 Complementing numerical simulations with prediction models

5.1 Overview and structure

When analysing the thermal performance of GSHP systems, numerical approaches incorporate significantly less assumptions and are bounded by less constraints compared to analytical solutions, allowing much greater flexibility on the analysis of a GHE structure. However, numerical approaches have a noteworthy drawback which is the long computational times associated as well as the computational resources required, making these approaches less accessible. A significant focus of this doctorate research has been to establish ways to overcome this important drawback and contribute towards making numerical approaches easier to adopt while at the same time further understanding GSHP systems. To achieve this goal, statistical and computational methods were adopted, including machine learning techniques, in combination with the understanding of the underlying relationships between relevant GSHP parameters (for example geometrical values or material properties), to develop prediction models that can be used alongside numerical modelling and very significantly hasten the design process while minimising the need of expensive high-performance computing.

This chapter presents two prediction models developed to complement numerical modelling for the above purposes and make GSHP system design using numerical modelling more feasible and accessible to engineers. Section 5.2 presents a *time-series* multi-linear regression model, that iteratively predicts the results of GHE operation, as published in the journal paper: *"A machine learning approach to energy pile design"*. Section 5.3 presents a second, simpler but powerful prediction model, that focuses on single *time points* (such as the days that the GSHP system performance is expected to be critical), as published in the journal paper: *"A robust prediction model approach to energy geo-structure design"*. Both above sections/papers provide thorough validations of the prediction models and explain the physical theory on which they are built and how they can be efficiently used. Following, section 5.4 discusses and compares the two models/approaches suggesting scenarios at which utilising one approach would be beneficial over the other and lastly section 5.5 presents a summary of the key findings of the chapter.

5.2 Journal paper: A machine learning approach to energy pile design

This section consists of a journal paper titled: “A machine learning approach to energy pile design”, published in the journal *Computers and Geotechnics.* The paper has been inserted in the following pages, in its Author’s Accepted Manuscript [AAM] version, with the only modification being the addition of the thesis page numbers at the bottom of the page (allowing consistent numbering throughout the thesis). This publication is the author’s original work, has been included with the co-authors’ authorisation (appropriate co-author authorisation forms have been included in this submission) and the co-authors’ contributions have been acknowledged in the *Preface & Publications* section.

Type of paper: full length article (Computers and Geotechnics - Elsevier Journal)
Date text written: November 2017
Number of words in main text and tables = 8726
Number of figures = 11
Number of tables = 4
Number of appendices = 1 (including 1 table)

A machine learning approach to energy pile design

Author 1
Nikolas Makasis, MSc (CompSc), MEng (CivEng)
Department of Infrastructure Engineering, The University of Melbourne, Parkville, Australia

Author 2
Guillermo A. Narsilio✉, PhD, MSc (Math), MSc (CE), CEng
Department of Infrastructure Engineering, The University of Melbourne, Parkville, Australia

Author 3
Asal Bidarmaghz, PhD, MSc (Eng), BSc (Eng)
Department of Engineering, University of Cambridge, Cambridge CB2 1PZ, United Kingdom
Department of Infrastructure Engineering, The University of Melbourne, Parkville, Australia

Full contact details of corresponding author
Guillermo A. Narsilio, ARC Future Fellow
Engineering Block B 208, Department of Infrastructure Engineering, The University of Melbourne, Parkville, VIC 3010, Australia
Email: narsilio@unimelb.edu.au, Phone: +61 (3) 8344 4659, Fax: +61 (3) 8344 4616

Abstract:
Incorporating ground heat exchangers (GHEs) into building foundations allows them to also provide thermal energy for space heating and cooling. However, this introduces certain constraints to ground-source heat pump (GSHP) design, such as on the geometry, and thus a different design approach is required. One such approach, introduced in this article, uses machine learning techniques to very quickly and accurately determine the maximum amount of thermal energy that can reasonably be provided. A comprehensive validation of this methodology for energy piles is presented, using different geometries and thermal load distributions, drawing conclusions about how the approach can best be utilised.

Keywords:
Energy piles, finite elements, optimisation, machine learning, regression, geothermal energy

List of Notations:

CDM	"Cooling Dominant Monthly" type of thermal load distribution, -
CON	"Constant" type of thermal load distribution, -
COP	coefficient of performance, -
$C_{p\ material}$	specific heat capacity of material, J/(kgK)
MAE	mean absolute difference between predicted and expected/ "actual" T_{fluid}, °C
R^2	coefficient of determination, -
RMSE	root mean square difference between predicted and expected// "actual" T_{fluid}, °C
t	time, sec
$T_{farfield}$	average annual ground temperature, °C
T_{fluid}	average fluid temperature within pipe loop, °C
TL	thermal load, W
TRD	"Typical Residential Daily" type of thermal load distribution, -
TS	thermal storage, W
$x_{1..n}$	input data to a prediction model or relationship, unit depends on data
$y_{1..m}$	output data to a prediction model or relationship, unit depends on data
ΔT_{max}	difference in maximum average fluid temperatures between predicted and expected/ "actual" T_{fluid}, °C
ΔT_{min}	difference in minimum average fluid temperatures difference between predicted and expected/ "actual" T_{fluid}, °C
$\lambda_{material}$	thermal conductivity of material, W/(mK)
$\rho_{material}$	density of material, kg/m^3

1 Shallow geothermal systems and energy piles

Ground-source heat pump (GSHP) systems can be used to efficiently provide geothermal energy for heating and cooling purposes. These shallow geothermal energy systems extract and reject heat from and to the ground within a few tens of metres below the surface. The heat pump upgrades this thermal energy and is connected to an acclimatisation distribution circuit within the building, which transfers the heat to and from the building, as well as to a series of ground heat exchangers (GHEs), which transfer the heat from and to the ground [1]. A GHE, which traditionally can take many forms such as vertical boreholes or horizontal trenches, contains loops (usually high-density polyethylene (HDPE) pipes) with a circulating fluid (usually water) that acts as the heat conductor in the process. These systems are known to typically be able to run at a coefficient of performance (COP) of about 4, meaning producing 4 kW of heating/cooling energy for every 1 kW of electricity consumed [2–4]. Moreover, GSHP systems are the most used amongst the different applications of direct geothermal energy [5] and have attracted much attention over the past decade for the purpose of better understanding how they can be most suitably and efficiently utilised and designed. [6–10]

A promising application of GSHP systems that can minimise their capital cost is the use of energy piles, where the GHE loops are incorporated within pile foundations as shown in Figure 1 [11–18]. Since the most significant associated cost of these installations is drilling, by adding the loops into the piles (already needed for structural purposes) that cost is considerably minimised as drilling is already accounted for; a detailed breakdown and analysis of these costs can be found in the literature [19]. However, due to the high variability of potential pile configurations and geometries and the fact that this technology is relatively new to the industry, there is a notable absence of available reliable and *fast* design tools for energy piles and limited information on not only how the design can be undertaken but also how efficient the technology can be [20].

<Figure 1 around here>

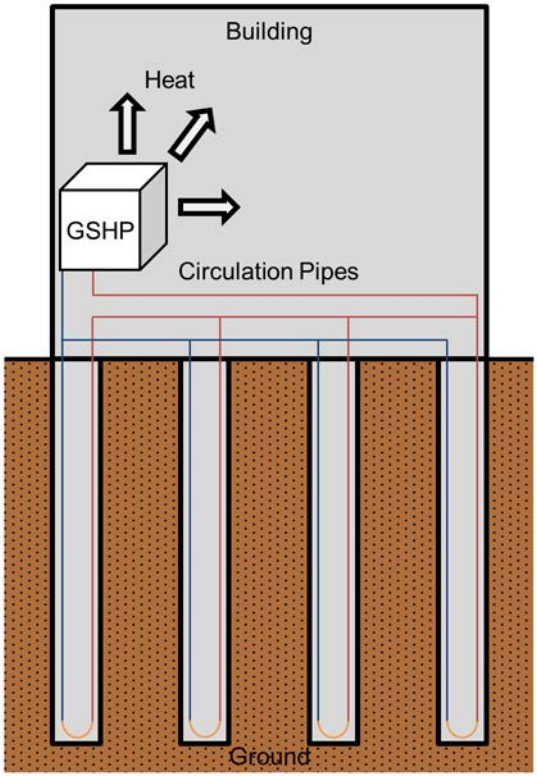


Figure 1. Energy piles schematics in heating mode (Not to scale)

A key difference between energy piles and typical vertical borehole GHEs is that for the former, the pile number, configuration and length are not primarily designed to fulfil the (thermal) energy needs of the building, but rather for its geo-mechanical stability. This leaves little room for

optimisation of the geothermal ground loop design, as the main design parameters, such as the (energy) pile length and separation, are pre-determined. Therefore, the provision of 100% of the heating and cooling energy required (thermal load) cannot be guaranteed and instead a hybrid system must often be used, to complement the produced geothermal energy using auxiliary means [21,22].

An important challenge is to accurately determine the maximum thermal energy that the geothermal system can provide using the already structurally designed energy piles, which can be either very difficult and time consuming or not as reliable as required using the limited existing design approaches (detailed numerical simulations or analytical commercial software respectively) [20]. While there exist 'geothermal' parameters that are not necessarily fixed in energy pile design projects, such as the pipe loop diameter, flow rate and geometrical configuration of the pipes, identifying the amount of thermal energy the energy piles can provide in the first place is extremely important. A further optimisation of the above-mentioned parameters can further increase heat exchange rates with the ground and thus potentially increase the amount of provided energy. However, this paper focuses on novel ways of *quickly* and *accurately* estimating how much energy can be provided first and foremost (for fixed/typical geothermal parameters), while future research is expected to expand this methodology into also accounting for pipe geometry (diameter, configuration, etc.) and fluid flow rate. The research herein expands on a study presented in [23] and incorporates machine learning techniques to overcome the challenge of estimating the amount of thermal energy that can be provided fast and accurately. The new approach is the first step in expediting and facilitating the optimisation of the design of a hybrid GSHP system. A statistical prediction model, which can be used alongside complex finite element (FE) computational models to calculate the optimal amount of energy that can be extracted from a geothermal system implemented in an underground structure (e.g., energy piles), is presented and validated against the alternative and considerably more computationally expensive FE models.

2 Proposed methodology

In this section, a summary of the limited current approaches to energy pile GSHP systems is briefly presented, followed by a detailed description of the proposed approach, including an overview of machine learning principles as well as the technical details of the proposed prediction model.

2.1 Current approaches

A common energy pile design approach, specifically for complex geometries, is to use a numerical simulation/model, to analyse a GSHP design, although semi-analytical approaches are also being developed [24]. Finite element numerical simulations are typically more flexible than analytical approaches, since they adopt significantly fewer assumptions and have fewer constraints regarding the parameters of the problem, such as its geometry, but they can be computationally expensive. Typical numerical simulation input requirements include the geometry, the material properties and operational conditions (including the fluid flow rate), the thermal load distribution and the use of appropriate (coupled) physics (i.e. governing equations and boundary conditions to model coupled heat transfer and fluid flow). The simulation computes many values relevant to design, such as the temperature of the fluid at the outlet pipe (exiting the ground loop) over time, by adopting a varying input temperature of the fluid at the inlet pipe (entering the ground loop) over time. This inlet fluid temperature arises from the thermal load distribution that needs to be satisfied, in order to provide the required thermal energy to the building (the temperature difference between the inlet and outlet should be maintained in such a way that it fulfils the thermal demand), as explained in detail in [8,25–28]. During the calculation process, the geometric and material design values remain of course constant with time (to fulfil the structural requirements). It is also very important to note that inlet fluid temperature (coming from the heat pump) can usually be controlled and programmed by a mechanical engineer. From the results of the simulation, of most interest is the fluid temperature distribution within the GHE loops. The temperature of the fluid needs to be within a specified operating range,

based on the heat pump used, as well as to avoid extremes that could cause undesirable effects, such as freezing of the ground and heave (overcooling or overheating the ground).

However, as mentioned in section 1, when designing a system with energy piles the geometry and properties of the materials available are all pre-determined. Therefore, the design needs to focus on optimising the fulfilled thermal load distribution instead (given fixed geothermal parameters, such as the pipe diameter), in order to provide the maximum possible geothermal energy for heating and cooling, while still keeping the fluid temperatures within an acceptable range. This essentially means that the task being undertaken is no longer "How can the system be designed to provide the energy requirements of the building?", but instead "How much energy can this system (with its specified/fixed geometry-materials) provide?"

2.2 Proposed approach overview

The proposed methodology involves having access to one fully solved numerical simulation, based on which to create and train a suitable prediction model. This model is designed using machine learning (ML) techniques, used in the field of data science and analytics to gain insights from data as well as understand and discover important relationships between them. These techniques have been used throughout many fields to optimise existing methodologies or introduce new ones, including in geotechnical engineering (e.g., soil classification, liquefaction and seismic slope stability) [29–32].

It is firstly worth introducing a simplified overview of the relevant machine learning techniques. As shown in Figure 2, when using ML techniques to create a prediction model, there are commonly two main phases: the training phase and the prediction phase. In each, there are four main components to the procedure. Firstly, two of these components are the input and output data ($x_{1..n}, y_{1..m}$), of which finding the relationship is the main aim of the process. Secondly, the chosen prediction algorithm (g), which defines the nature of the relationship (what function is used to connect input and output). Lastly, the model parameters ($\beta_{1..k}$), which are the values/constants fine-tuning the modelled relationship (for example how sensitive each output is to each input) and their values are unique for each trained model. The overall relationship between these is: $\boldsymbol{y_{1..m} = g(x_{1..n}, \beta_{1..k})}$, where $\beta_{1..k}$ can be either directly provided to the algorithm or may be implicitly included. During the training phase, both input and output data are known, and the algorithm is used to calculate the model parameters. Following the training, the prediction model can then predict the output for any number of different input data (since β values are known) and thus make predictions.

<Figure 2 around here>

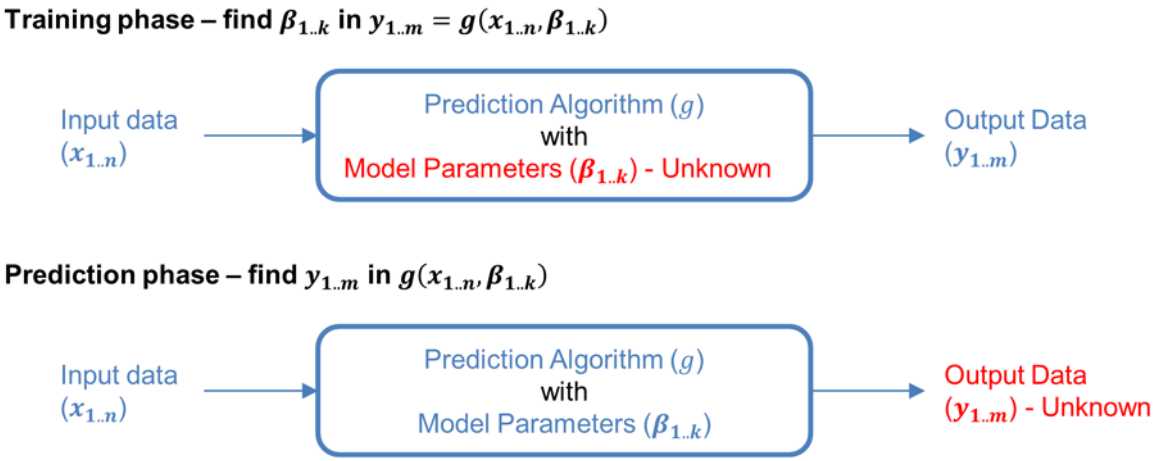


Figure 2. Generalised machine learning principles (blue = known, red = unknown)

When considering the design process of energy piles using detailed FE models, the first step a designer would naturally take is to run a numerical simulation with 100% of the required thermal load to obtain the GHE fluid temperature variations over the design life of the system and check that they

are within a tolerable range and render acceptable COPs. This is because the most desirable outcome would be the one where the provided geometry, material properties and other conditions are suitable to satisfy 100% of the energy requirements of the building. If this is the case, then no optimisation is required. However, if the system cannot provide 100% of the energy requirements efficiently, it is important to find the maximum acceptable (optimal) amount that can be provided by the proposed geothermal system. This involves more numerical simulations with long computational running times, between hours and days, depending on the complexity of the problem and the refinement of the model. The proposed prediction model (obtained from machine learning techniques) can be used to reduce this iterative optimisation time and to give a good indication of the optimal energy requirements the system can fulfil, within seconds, as shown in the diagram of Figure 3.

<Figure 3 around here>

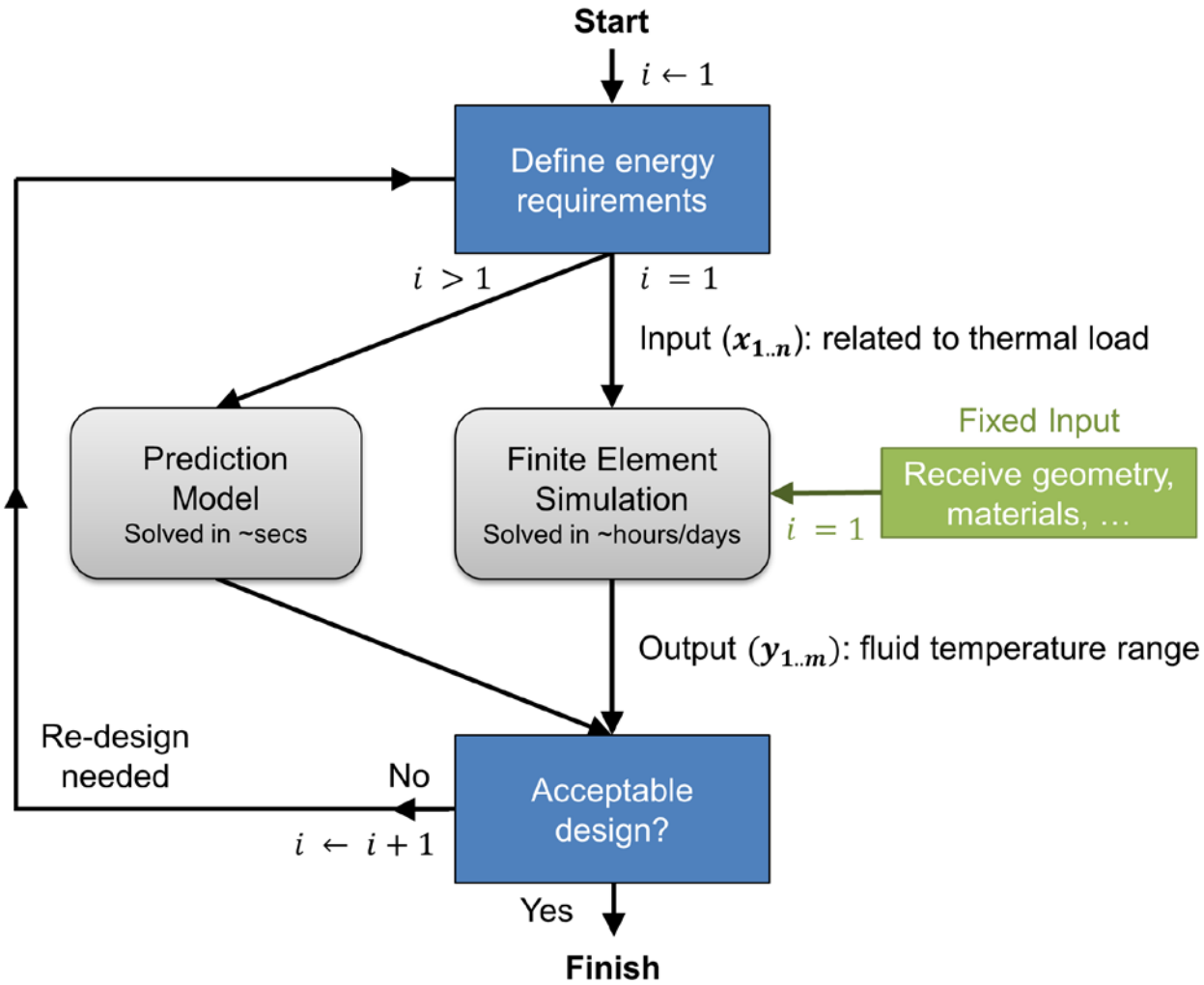


Figure 3. Flow diagram of proposed design process for energy piles

Considering the fundamental equations that take place during the design and operation of a GSHP system, the relationship between the thermal load distribution (used as input) and the resulting fluid temperatures (output) is a complex one, but simplistically indicated in Equation 1, with a number of other parameters and variables involved. However, in the scope of the prediction model, many of the parameters of that general relationship become irrelevant (pre-determined) for the specific problem and therefore there is no need to include them in the architecture of the prediction model (e.g., pile geometry). This is because the prediction model considers the variation of the thermal load, but the other parameters are constant between numerical simulations (e.g., same values for the length of the pile for two numerical simulations in which the system provides 50% and 100% of the thermal requirements respectively). This means that in the context of computing a solution, the impact of these

constant parameters (e.g., geometry, materials, …) is already taken into consideration by the FE numerical simulation of which the results are used to train the prediction model.

$$T_{fluid} = f(Thermal\ Load, Geometry, Material\ Parameters, \dots) \quad \textbf{(1)}$$

Since this methodology assumes that at least one numerical simulation has been solved (for example using 100% of the energy requirements), the data from that simulation are then used to train the prediction model, and learn the required relationship f (where f is the true or best relationship out of all possible g). This is important to note, as without a fully solved and accurate numerical simulation, the prediction model cannot be trained to learn the desired relationship between input and output and then make predictions based on that relationship. Moreover, the accuracy of the prediction model will naturally depend on the quality of the data it uses to be trained, which in this case relates to the accuracy of the numerical simulation.

The prediction model presented herein focuses on the influence of the thermal load (and thus storage as explained below) on the resulting average temperatures of the circulating fluid ($T_{fluid} = (T_{in} + T_{out})/2$)[1] and uses a time-stepping approach, as seen in Equation 2 (in this study daily time-stepping adopted, but others can also be considered). Therefore, the predictions are performed iteratively, starting from an initial condition, $T_{fluid}(initial)$, representing the time before the system firstly runs, and then using each predicted value of T_{fluid} as an input to make the prediction for the next time-step (day) together with the thermal load ($TL(t)$) and the accumulated ground thermal storage ($TS(t)$), defined below. In order for the model to learn this relationship (i.e. be trained) adequately, it uses a training set of size equal to or longer than the length/duration of the desired prediction. For example, this study adopts a simulation duration of 5 years; this time scale allows annual cumulative thermal effects to manifest, while still keeping the computational expense to a reasonable level for a large-scale analysis such as the one presented herein; a real life design would consider the lifespan of the project (20+ years). Given this simulation duration, the prediction model requires at least 1825 days of training data (distribution in which t varies from 1 to 1825), from the solved numerical simulation.

$$\underbrace{T_{fluid}(t)}_{y} \approx f(\underbrace{TL(t), TS(t), T_{fluid}(t-1)}_{x_{1..n}}) \quad \textbf{(2)}$$

To better understand the ideology behind the prediction model, it is important to define the *input parameters* used, especially what is meant by thermal storage in this context. Each variable can be thought of as representing a particular fundamental influencing parameter for the problem to solve. As this study considers a time-step of 1 day between each prediction, it is more convenient to think of time in the context of days. Firstly, the *thermal load (TL)* for a particular day can be seen as the effort that the system needs to make; if its magnitude is too high then the system will need to work harder on that day and vice versa. Secondly, the *average fluid temperature of the previous day* ($T_{fluid}(t-1)$) represents the state of the fluid before the work has begun; acting as an initial condition for that day. Finally, the *thermal storage* (TS_d) represents the thermal history of the system and can give an understanding of to what extent the ground has been cooled down or heated up in the past, leading up to the considered day. Several investigations have shown the need to account for thermal storage or thermal history of the ground while the GSHP system is in operation, in order to suitably capture the effects of heat transfer and accurately predict the system's behaviour, as well as investigated the importance of the duration parameter set d [33–37]. The thermal storage terms consist of a collection of parameters, where each represents cumulative thermal loads of different durations (d in days), as indicated by Equation 3. For example, the parameter TS_2 (i.e. d=2) for any t would be equal to the

[1] where T_{in} and T_{out} represent the fluid temperature at the inlet and outlet end of the ground loop pipes, also known as leaving water temperature (LWT) and entering water temperature (ETW) respectively when referring to the GSHP.

cumulative thermal load of the past 2 days up to t, such that $TS_2(t) = TL(t) + TL(t-1) + TL(t-2)$. It should be noted here that the d set will vary for different simulation durations and the results of the investigation of choosing these parameters (for this study adopting a 5-year duration) are presented in Equation 3. It is very important to note that the input parameters for the prediction model, introduced herein and described above, were chosen not simply for their significance and meaning, but also significantly for their availability, since no complex computations are needed to obtain them.

$$d \in \begin{Bmatrix} 2,3,4,5,6 \\ 7 * i \\ 1825 \end{Bmatrix} for \ \ i = 1,2,..,260 \quad \textbf{(3)}$$

Following the training of the model, predictions can very quickly be made for any other thermal load input, assessing the system's ability to provide different amounts of thermal energy. This process can be performed for a number of different potential thermal load distributions to find the one most suitable for the problem, meaning the one that provides the most amount of thermal energy without causing any problems for the heat pump or the ground. Therefore, using the proposed approach, the temperatures resulting from providing different amounts of thermal energy can very quickly be predicted. By reviewing the temperatures and determining the acceptability of the design iteratively for each different amount of energy provided, the maximum acceptable amount of thermal energy can be chosen for the design (while the remaining of the energy requirements is fulfilled by auxiliary means). It should be noted here that it is assumed, as it has been shown in the literature [12,38,39], that no significant geo-mechanical issues arise from the operation of energy piles (unless when embedded in normally consolidated clays). Lastly, it should also be noted that this methodology can be modified to predict the temperatures of the ground, instead of the carrier fluid (ensuring the ground is not adversely affected by the operation of the system); however, this potential will not be explored in this paper.

2.3 Multiple linear regression prediction model

Following a detailed investigation of machine learning (ML) algorithms as well as conducting experimentation with them, it was concluded that the proposed relationship in Equation 2 is best represented simply using Multiple Linear Regression, its general form shown in Equation 4. The true relationship between the energy requirements and response of a system is very complex and cannot be easily computed without either significant assumptions made or powerful and time-consuming numerical simulations. However, when looking at this particular aspect of the problem, where many variables are constant and therefore not relevant, the resulting relationship is very well fitted by linearity, as further discussed in section 4.1. In the process of coming to this conclusion, various ML techniques and models were used, including feature selection, Artificial Neural Networks and Support Vector Machines. After thorough investigation, most of the more advanced machine learning algorithms were found to be more complex than required for this problem and therefore less suitable solutions, since simplicity is a welcomed attribute for a solution.

$$y = \beta_0 + \beta_1 x_1 + \beta_2 x_2 + \beta_3 x_3 + \ldots + \beta_n x_n \quad \textbf{(4)}$$

As explained in section 2.2, the training set used consists of input and output data of one fully solved finite element numerical simulation. The parameters $x_{1..n}$ in Equation 4 represent the known input, as shown in Equation 2, while the predicted parameter y represents the average temperature of the fluid within the pipes (output), based on which the suitability of the design can be evaluated. All the $\beta_{1..n}$ factors shown in Equation 4 can therefore be calculated and then used by the trained model to make the required predictions (obtain y) for any other set of $x_{1..n}$ (thermal load distribution and thus thermal storage). Finding the $\beta_{1..n}$ factors constitutes the training of the prediction model

and these factors represent the physics, materials, geometry and all other constant parameters modelled by the FE numerical simulation. Equation 5 is utilised by the prediction model, combining Equations 2, 3 and 4.

$$T_{fluid}(t) \approx \beta_0 + \beta_1 TL(t) + \sum_{i=2}^{265} \left(\beta_i TS_{d\{i-2\}}(t)\right) + \beta_{266} T_{fluid}(t-1)) \quad \textbf{(5)}$$

3 Evaluation of the prediction model

In order to evaluate the proposed prediction model's performance and accuracy, FE numerical simulations are used to produce the required data. This paper presents three different case studies, to show the wide applicability of the methodology. These case studies model different pile and ground geometries, which are based on different geographic locations, and consider either single energy piles or a field of multiple energy piles, to account for the thermal interference between the piles.

For each case study, a number of different FE numerical simulations are computed, each modelling a different thermal load distribution. The results of one of the simulations are used to train the prediction model and the rest to evaluate its predictions. The predictions, obtained through the proposed methodology and the proposed machine learning predictive model, are compared to the respective values from the results obtained from the FE numerical simulations, which are considered as the "actual" values for the purpose of this research, since they are the values the prediction model is aiming to predict.

3.1 Finite element model and the three case studies

To perform numerical simulations, this research uses an experimentally validated state of the art 3D numerical model, developed at The University of Melbourne [8,26,27]. The model is built and solved using the finite element software package COMSOL and is based on the coupling of the governing equations of heat transfer (energy balance) and fluid flow (momentum and continuity). Heat conduction occurs primarily in the soil, concrete, HDPE pipe wall and partially in the carrier fluid while heat convection is dominant in the carrier fluid. The fluid flow equations are associated with the carrier fluid within the pipes, no groundwater movement is considered.

Three different case studies have been adopted for this research, in order to show the flexibility and wide applicability of the proposed prediction model. The first two studies model a single energy pile, a simplified version of typical multi-pile fields under buildings, to reduce the computational time and space (memory) requirements. Thus, single energy piles of different diameters and lengths are modelled, with input parameters based on the geographic locations of Melbourne, Australia, for the first case study (high ground thermal conductivity) and Cordoba, Argentina, for the second one (low ground thermal conductivity). The last case study expands on the second one and uses a field of 16 energy piles, instead of just one, to show the ability of the prediction model to fully incorporate the effects of thermal interference between the piles.

The numerical modelling in this research is based on typical weather and soil conditions for each geographic location, with the material properties presented in Table 1 [40]. In general, the geometry and dimensions used for the modelled GHEs, as can be seen in Figure 4, are of typical practice in the respective regions and all use 25 mm outer diameter pipes with 2.3 mm wall thickness. The first case study models a single 35 metre long energy pile, containing three pipe loops connected in series. The concrete pile has a diameter of 600 mm and the pipe loop horizontal connections are 20 mm at the top of the pile and 30 mm at the bottom of each of the three loops. The flow rate for the carrier fluid is set at 11 L/min. The second and third case studies use geometry and material properties from a real building study on the potential of energy piles, presented in [25,26]. These studies model 10 metre long energy piles, containing two pipe loops connected in series, having a diameter of 400 mm and pipe separations of 20 mm at both top and bottom loop connections. The flow rate for the carrier fluid is set at 6 L/min, to account for the shorter pipe depth compared to case study 1, thus allowing longer

residence time within the pipes which more suitably facilitates the heat transfer process and renders higher temperature differential between inlets and outlets. In the last case study, the piles are placed 3 metres apart in both the x and y directions. The pile for which results are shown in section 4 is the one closer to the centre of the GHE field (seen in Figure 4 – highlighted in red), where the thermal interference from the pile group will be the highest.

Table 1. Material Properties

Parameter	Value		Unit	Description
	Case 1	Cases 2, 3		
λ_{ground}	2.7	0.7	W/(mK)	Thermal conductivity of ground
ρ_{ground}	2353	1600	kg/m^3	Density of ground
$C_{p\ ground}$	850	1200	J/(kgK)	Specific heat capacity of ground
$T_{farfield}$	18	18	°C	Average annual ground temperature
$\lambda_{concrete}$	2.5	2.1	W/(mK)	Thermal conductivity of concrete
$\rho_{concrete}$	2100	2350	kg/m^3	Density of concrete
$C_{p\ concrete}$	950	850	J/(kgK)	Specific heat capacity of concrete
λ_{fluid}	0.58	0.58	W/(mK)	Thermal conductivity of carrier fluid
ρ_{fluid}	1000	1000	kg/m^3	Density of carrier fluid
$C_{p\ fluid}$	4180	4180	J/(kgK)	Specific heat capacity of carrier fluid

<Figure 4 around here>

For all cases, the ground is modelled as a cylinder around the energy piles. The diameter of this cylinder is 20 m for the first and second case studies and 30 for the third one. This is considered sufficient to avoid any ground boundary effects. In the outer boundary of the ground domain a constant *farfield* temperature is set as a boundary condition, for all cases, equal to the average annual ground temperature, $T_{farfield.}$ It should be noted that for the third case, due to the existence of the planes of symmetry only one quadrant of the entire geometry needs to be modelled, as indicated in Figure 4(c). Moreover, no thermal flux is allowed at the base (bedrock) or the surface (building floor) of any model, which regarding the latter is a conservative measure as air fluctuations bolster the performance of the system [28]. Lastly, the initial temperature of all materials is also set as $T_{farfield}$, which for all cases is around 18°C [41]. The *boundary and initial conditions* discussed are typical for local GHE design and are depicted in Figure 4 along with other geometrical details of the model, as explained above.

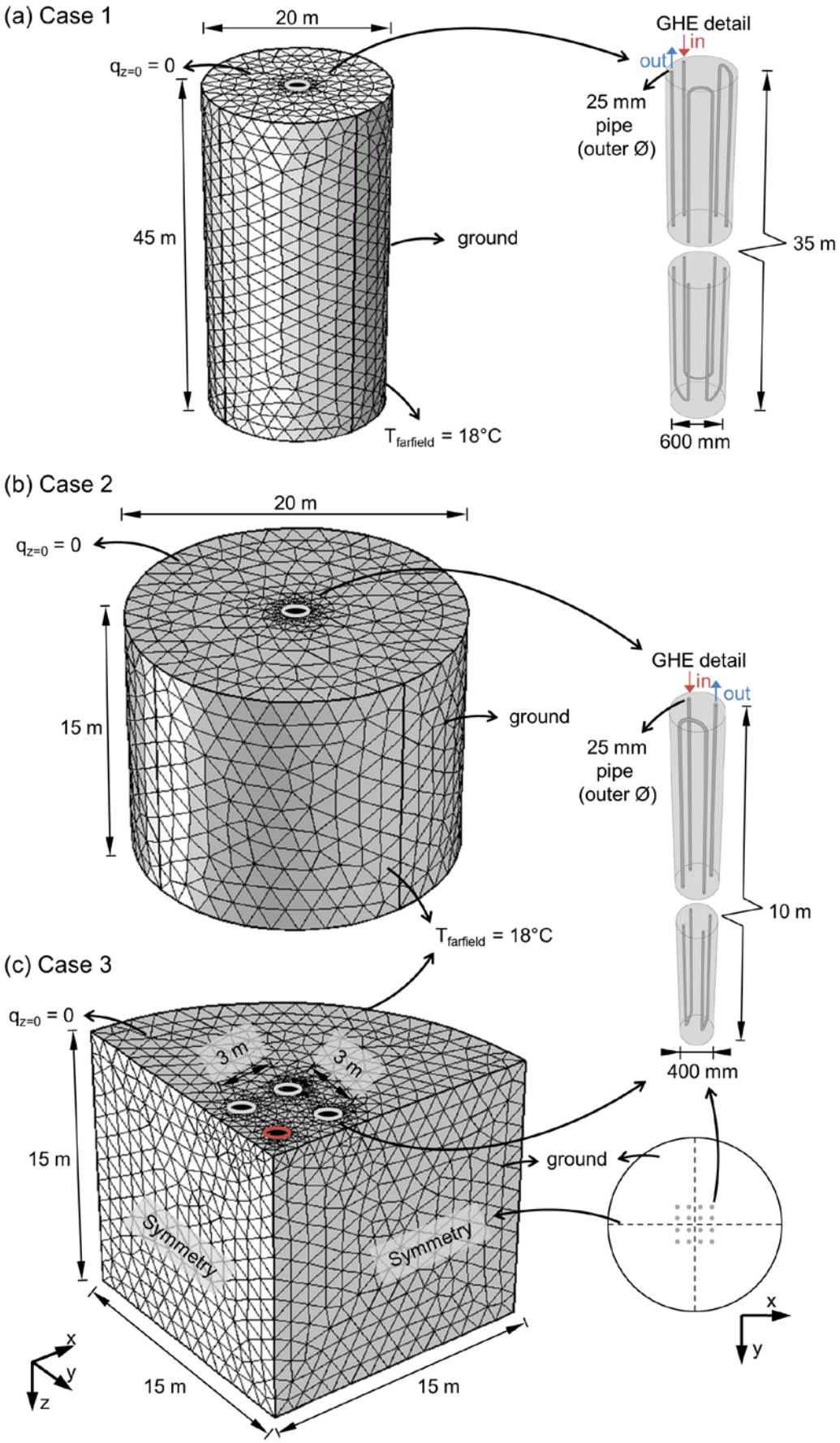


Figure 4. Geometry and model parameters for the three case studies (ground domain to the left and detail of energy pile to the right, not to scale)

3.2 Thermal load distributions

In order to evaluate the proposed methodology, for each case study, a prediction model is created and trained using one thermal load distribution (expressed as averaged daily power demand for the considered time period), based on which it will learn the relationship between input and output, as explained in section 2.2. Following, each of the three trained prediction models (one for each case study) is used to make predictions for a variety of other thermal load distributions, i.e. to predict how the specific system will respond if the daily energy requirements over the 5-year period are different to the one the model was trained with. At the same time, for each prediction, a numerical simulation using the finite element model described in section 3.1 is also undertaken, in order to compare the results of the prediction model to those from the finite element simulation (the latter being treated as correct or "actual" for this study). This section emphasises on the thermal load distributions used in this evaluation. It shows how the original thermal load distribution can be modified to be able to only satisfy a portion of the required thermal demand (and be combined with an auxiliary system to provide the rest), when 100% of that demand cannot be feasibly provided, and also presents different types of thermal load distributions used for evaluation purposes.

3.2.1 Modifying the thermal load distribution – Scaled and Limits

As explained in section 2, due to the restrictions on the design, often energy piles/the GSHP system alone will not be able to fulfil the entire energy demands of the building and therefore will need to be paired with an auxiliary system (each providing a percentage of the total demand), forming a hybrid heating and cooling system. Figure 5 shows two different approaches that can be adopted when determining how much energy the GSHP system can provide, this example case focusing on reducing the *cooling* demand of the original unbalanced distribution. The first approach is to simply scale the original distribution by a certain percentage, as seen by the distribution named *"Scaled_50%"*, in which for this example each value in cooling of the original has been scaled down by 50%. The second approach is to set limits and simply not provide energy above/below those limits, as shown by distribution *"Limits_50%"*. In this example, a limit of 50% of the cooling peak (507 W/GHE) has been set. Therefore, all thermal load values that are below that limit are identical to the original distribution, but all values above the set limit, are now constant to the value of that limit. For both variations, the remaining load is provided by auxiliary means. It can also clearly be seen that using the limiting approach is more preferable to use in reality (as the auxiliary system is only needed on specific days, instead of every day compared to the scaling approach); however, both of these approaches have been included for validation purposes.

<Figure 5 around here>

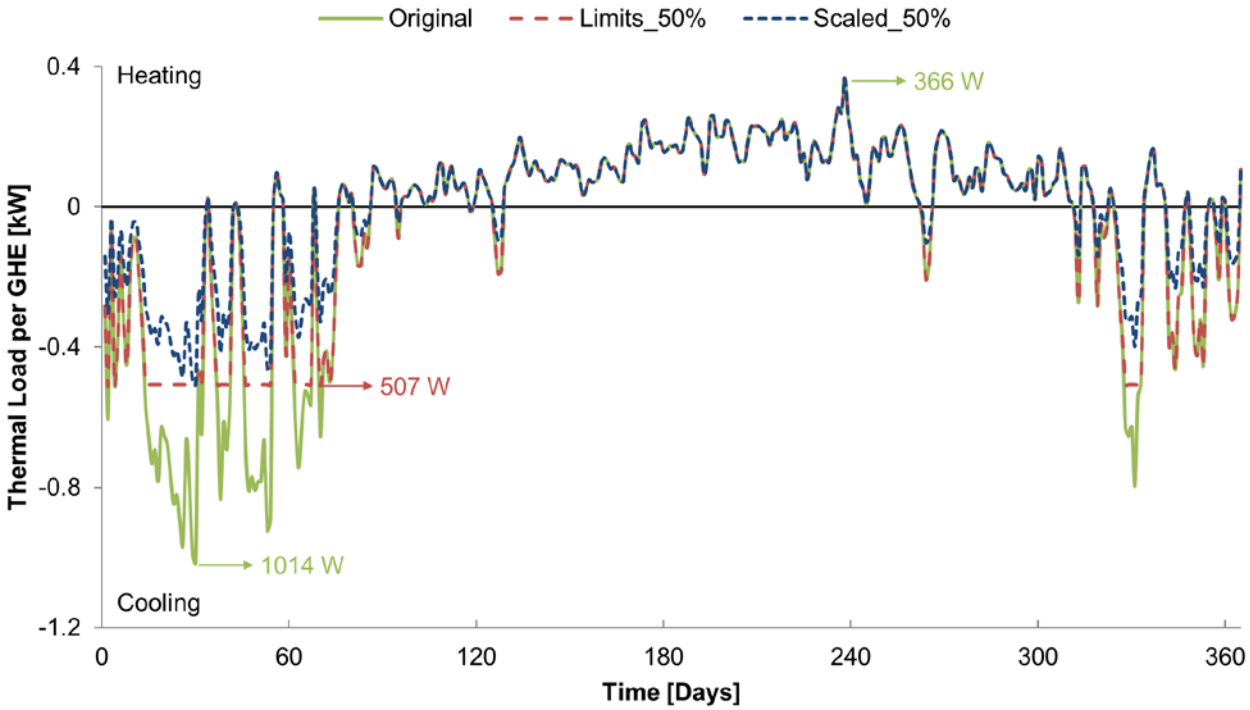


Figure 5. Creating variations of presented thermal load distributions

3.2.2 Different types of thermal load distributions

In order to evaluate the prediction model's performance more thoroughly, in addition to using variations of the original thermal load distribution as described in section 3.2.1, different types of original thermal load distributions are also used; three for each case study (case study geometries as shown in Figure 4). Firstly, a representative daily distribution for a typical residential building in each region, labelled *"TRD"* (Typical Residential Daily), is considered. This distribution is dependent on the weather of the region and varies daily. Secondly a cooling dominant monthly distribution is used, labelled *"CDM"* (Cooling Dominant Monthly). This distribution uses averaged monthly values and would be representative of energy piles installed mainly for cooling purposes, for example in office buildings or underground train stations. Lastly, two constant distributions are applied, labelled *"CON" (Constant)* where the demand is constant throughout the year, mostly for testing and validation purposes. The types of thermal load distributions can be seen in Figure 6, where (a) shows the distributions for case study 1 and (b) for both case studies 2 and 3. The reason for not using the same distributions for all three cases is that the geometry and climate (and thus the thermal demands) are different between them. The presented distributions are shown for a duration of 1 year and each subsequent year of simulation is assumed to have identical thermal load demands. It is also worth noting here that while for (b) the TRD and CDM distributions follow the same pattern (cooling and heating in same periods), (a) shows that this is not true for case study 1. This was done on purpose (by shifting the TRD distribution), in order to further test the prediction model's ability to make predictions when there is no apparent pattern between distributions.

<Figure 6 around here>

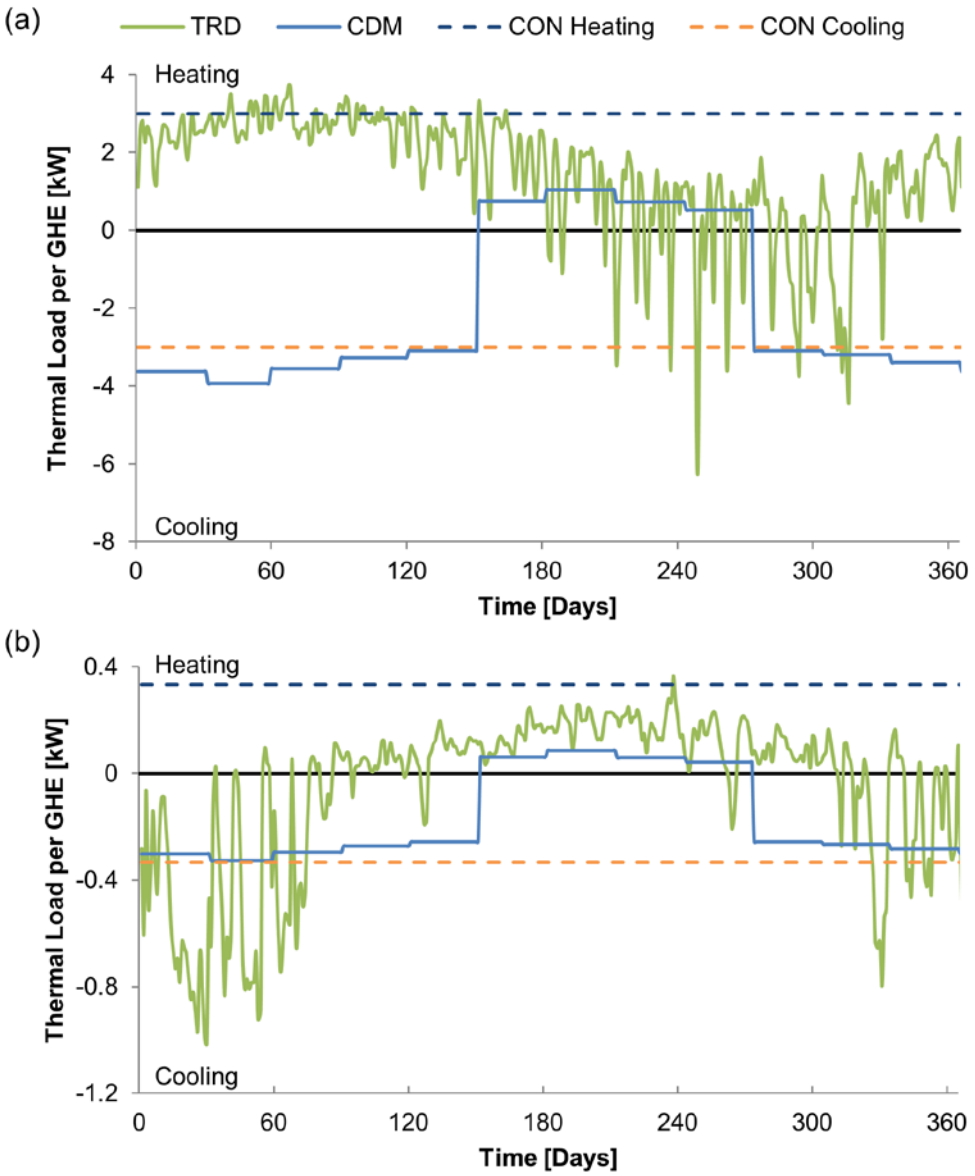


Figure 6. Thermal load distributions for (a) Case study 1 and (b) Case studies 2 and 3 (Please note –ve load: cooling, +ve load: heating)

3.2.3 The testing distributions and labelling conventions

To perform the model evaluation, the two variations shown in Figure 5 (i.e., limit and scale) will be used on the thermal load distributions shown in Figure 6. Thus, a large number of unique thermal load distributions will be generated and used to test the trained prediction model for each case study. The *"scaling"* variation will be used for all types of distributions shown in Figure 6, while the *"limit"* variation will be used only on the TRD distribution, as its use is more appropriate with a continuously varying distribution. The exact details of the different distributions used for testing can be seen in Table 2 found in section 4.2. It should be noted, that these follow the labelling convention "TYPE_VAR_H_C", where TYPE represents the original distribution (presented in Figure 6 – TRD, CDM, or CON), VAR represents the variation used (shown in Figure 5 – S (scaled) or L (limits)), H represents the percentage of scaling/limiting for heating and C the percentage for cooling. For example, a distribution with the name TRD_S_50_75 shows a distribution that was produced by scaling the TRD distribution (for that particular case study) by 50% in heating and 75% in cooling.

3.3 Evaluation metrics

In order to perform the evaluation and comparison between predicted and "actual" values, four important metrics are used. Firstly, the Root Mean Square Error (RMSE) and the Mean Absolute Error (MAE), as shown in equations 5 and 6. These are logical metrics to use and both indicate the overall performance of the model. They can be interpreted as the average difference between predicted and "actual" fluid temperature values over the entirety of the simulation:

$$RMSE = \sqrt{\frac{1}{N}\sum_{i=0}^{N}\left(T_{fluid\,(i)}^{predicted} - T_{fluid\,(i)}^{actual}\right)^2} \quad \textbf{(5)}$$

$$MAE = \frac{1}{N}\sum_{i=0}^{N}\left(\left|T_{fluid\,(i)}^{predicted} - T_{fluid\,(i)}^{actual}\right|\right) \quad \textbf{(6)}$$

However, the objective of running these simulations during the design phase is to obtain the average fluid temperatures and to check if they are within the heat pump acceptable operating range, so that it can operate efficiently. Therefore, the maximum and minimum temperatures are key outcomes for determining the suitability of the design. Considering this, two more metrics are introduced, the absolute difference of the maximum and of the minimum average fluid temperatures between the "actual" and predicted results, ΔT_{max} and ΔT_{min}.

$$\Delta T_{max} = \left|\max\left(T_{fluid}^{predicted}\right) - \max\left(T_{fluid}^{actual}\right)\right| \quad \textbf{(7)}$$

$$\Delta T_{min} = \left|min\left(T_{fluid}^{predicted}\right) - min\left(T_{fluid}^{actual}\right)\right| \quad \textbf{(8)}$$

4 Results and discussion

This section presents the results of the prediction model for different case studies (labelled as "predictions") and investigates how well they matched those from the respective numerical simulations (labelled as "actual"). A total of 72 finite element numerical simulations were computed (24 for each case study), each accounting for a 5-year operation of the system. The 24 different thermal load distributions used for the validation are presented in Table 2 where each is given an *id* to make the presentation of the results easier to follow. It should be noted again here that usual design lives for these systems are much higher than 5 years. However, this duration is adequate for long term thermal effects to start manifesting (especially for case study 3 which has very strong thermal interference between the piles) and therefore these effects are taken into account by the predictions.

Table 2. Thermal load distributions

Distribution	1	2	3	4	5	6	7	8	9	10	11	12
Type	TRD	TRD	TRD	TRD	TRD	TRD	TRD	TRD	TRD	TRD	TRD	TRD
Variation	S	S	L	S	L	S	L	S	L	S	L	S
Heating (%)	100	35	35	40	40	50	50	50	50	100	100	125
Cooling (%)	100	35	35	80	80	50	50	100	100	50	50	125
Distribution	13	14	15	16	17	18	19	20	21	22	23	24
Type	TRD	TRD	CDM	CDM	CDM	CDM	CDM	CDM	CON	CON	CON	CON
Variation	S	L	S	S	S	S	S	S	S	S	S	S
Heating (%)	65	65	40	50	50	75	75	100	0	0	33	100
Cooling (%)	45	45	80	100	200	100	200	100	33	100	0	0

Notes: TRD = Typical Residential Daily; S = Scale down; L = Limit; CDM = Cooling Dominant Monthly; CON = Constant.

4.1 Prediction model for Case Study 1

Before looking at all three case studies and different combinations of training distributions, it is worth isolating one specific example and examining the trained prediction model. Case study 1 is adopted and the prediction model is trained using the thermal load distribution 22 (100% constant cooling - CON_S_0_100). To do that, a numerical finite element simulation is run using that thermal load distribution as its input and the resulting average fluid temperatures are recorded. Using both the input thermal load distribution and the output of the simulation (fluid temperatures), the data are prepared to train the prediction model as shown earlier in Figure 2. A sample of these data can be seen in Table 3 showing the input and output parameters. After training, the β values are then calculated such that other input data can be used to produce different output data. A sample of those model parameters can be seen in Table 4 and are produced using the procedure and equations outlined in sections 2.2 and 2.3.

Table 3 Sample data for training a prediction model (Case study 1, thermal distribution 22)

Time, t [days]	$TL(t)$ [W]	$TS_d(t)$ [W]				$T_{fluid}(t-1)$ [°C]	$T_{fluid}(t)$ [°C]
		$d=2$	$d=3$	...	$d=1825$		
0	0	0	0	…	0	18	18
1	-3000	-3000	-3000	…	-3000	18	24.01
2	-3000	-6000	-6000	…	-6000	24.01	26.14
3	-3000	-6000	-9000	…	-9000	26.14	27.20
…	…	…	…	…	…	…	…
1825	-3000	-6000	-9000	…	-5475000	39.09	39.09

Table 4 Sample of prediction model parameters after training (Case study 1, thermal distribution 22)

β_0	β_1	β_2	β_3	...	β_{266}
2.9880	−0.0030	0.0008	0.0002	...	0.8340

After the prediction model parameters have been obtained they are used with other thermal load distribution inputs to predict the T_{fluid} values without the need for an additional finite element numerical simulation. The input data look similar to Table 3 with the main difference that since T_{fluid} is not known, the prediction process is done iteratively, taking the predicted value for $T_{fluid}(t)$ at each time-step and using it as the value for $T_{fluid}(t-1)$ in the next time-step, starting at $t=0$ with the initial condition $T_{fluid}(t=0) = T_{farfield} = 18°C$.

Figure 7 shows the input and output data of the model both during its training (a), using distribution 22, as well as one prediction example (b), using distribution 12, which produced amongst the largest errors. In each plot, the thermal load distribution (red y axis) comprises the input data, while the fluid temperatures the output data. As it can be seen, the prediction model very accurately predicts the expected fluid temperatures for the input related to thermal load distribution 12. What is very important to note is that when the model is trained, and therefore the β parameters are computed, the prediction model has only seen the data in Figure 7(a). However, when the trained model is provided with the input information shown in Figure 7(b), it predicts an entirely different fluid temperature distribution, both in shape and magnitude. This provides confidence to the model, showing that it accurately captures the relationship between the fluid temperature within the pipes and the thermal load (when all other parameters such as soil/material properties and geometry remain constant).

<Figure 7 around here>

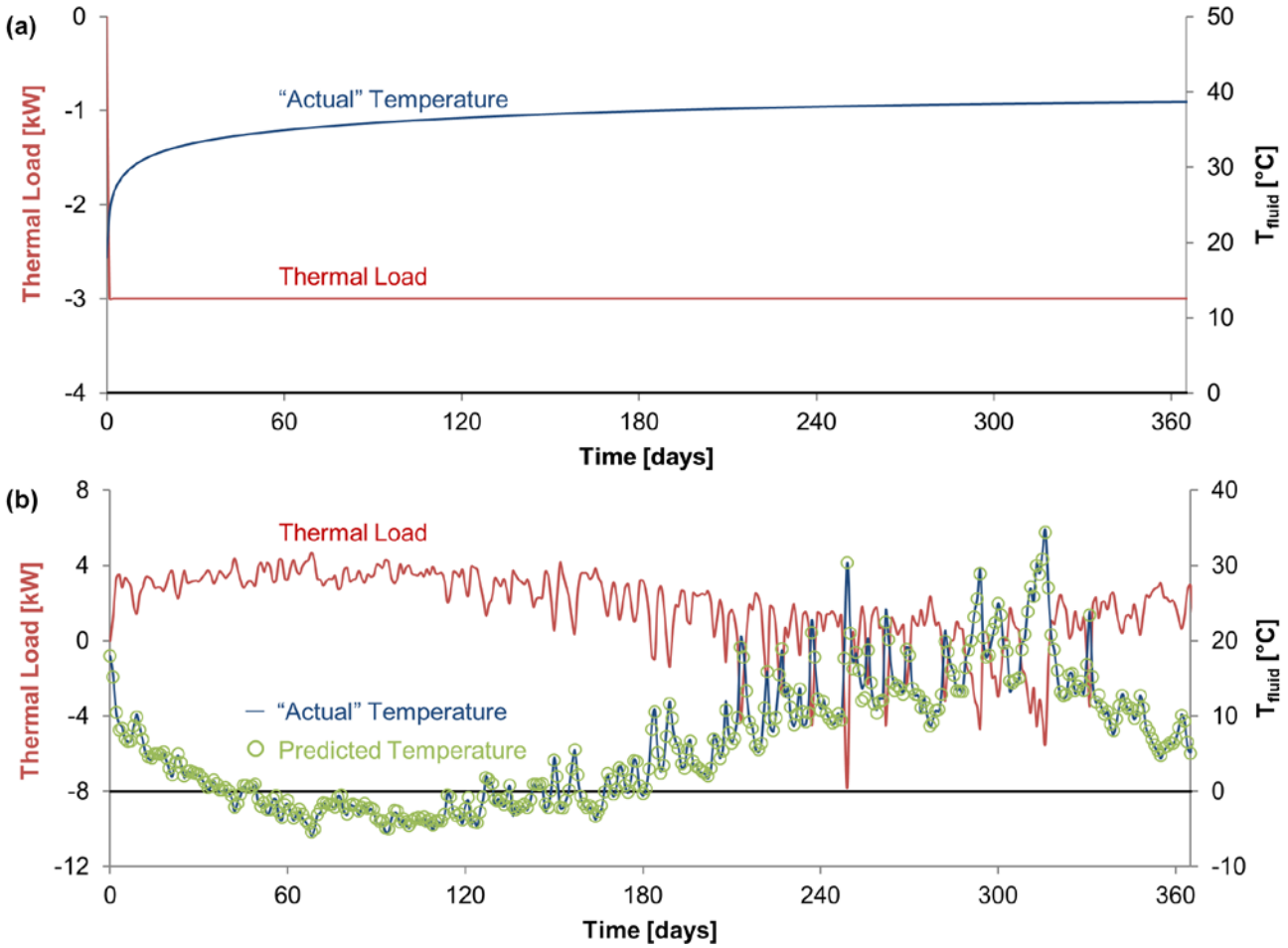


Figure 7. Thermal load and fluid temperature distributions for Case Study 1 used in (a) training of the model – Distribution 22 (b) testing the model – Distribution 12

Moreover, the presented model and results indicate a high degree of linearity within this relationship. It is very important however to note that the linearity is not simply between the thermal load ($TL(t)$) and fluid temperature values ($T_{fluid}(t)$), as shown earlier in Equation 5. Even though only the thermal load distribution changes from the training to the testing of the model, feature engineering[2] is applied such that the thermal load distribution is used to create more than one input parameter, as explained in sections 2.2 and 2.3. Moreover, since the predictions are made sequentially through the simulation time-steps, the fluid temperature of the previous time-step ($T_{fluid}(t-1)$) is another input parameter to the regression equation. Only when all the input parameters are combined, does multiple linear regression become a good model for this particular application.

The linearity of the relationship and the reason why multiple linear regression is a good fit comes from the physics that are involved. As it can be seen, there is a general correlation between the thermal load distribution and the resulting temperature distribution in Figure 7, with the shape of the two distributions being similar, but not quite identical, after the magnitudes of each have been scaled appropriately. The thermal load (input parameter) indicates the heat that needs to be transferred in each time step, while adding the temperature of the fluid on the previous day provides an initial condition for each time step prediction. These terms are more strongly connected to the heat convection occurring within the pipe by the movement of the fluid, one key relationship of which shown in Equation 10. The other important collection of terms is the thermal storage which provides information on how has the ground been heated/cooled up to the point of prediction. These variables are related to the thermal conduction that occurs in the pipe wall, the GHE backfill (concrete) and the

[2] Processing the data, transforming them to the desired input format for the model, e.g., $TS_2(t) = TL(t) + TL(t-1) + TL(t-2)$

soil. Since these materials (most importantly the ground) can accumulate heat, the history of the ground temperature variations and how it has been cooled/heated in the past affects the heat transfer processes taking place in the present. Therefore, the thermal storage parameters are important to account for these accumulative thermal effects, especially over the duration of many years, as discussed in Section 2.2.

$$Q = \dot{m} C_p (T_{out} - T_{in}) \quad \textbf{(10)}$$

where Q is the heat transferred by convection $[W]$, $\dot{m}$ is the mass flow rate $[kg/s]$, C_p represents the fluid heat capacity $[J/(kgK)]$ and $T_{out} - T_{in}$ represents the fluid temperature at the outlet and inlet of the pipe loop and therefore the temperature difference between them $[°C]$.

4.2 Prediction model performance evaluation

Following the procedure described in section 2.2, for the three case studies, three different prediction models were created. The results of the evaluation of these prediction models, in terms of the metrics discussed in section 3.3, are presented in Figure 8. All three prediction models were trained using distribution 22, using a constant cooling demand (CON_S_0_100). As it can be seen, the prediction model very accurately estimates the response of the system, for different thermal load distributions. All evaluation metrics, measuring the error in the predictions against the values obtained using finite element numerical simulations ("actual"), result in errors well below 0.6 °C, which are considered acceptable for the purpose of GSHP design. For most cases, the errors were less than or close to 0.2 °C. Moreover, considering the percentage of energy provided, a minor trend is noted, which suggests a scaling of the errors with the magnitude of the thermal load (and thus the temperature of the fluid). This can be seen as distribution 2, providing 35% of heating and cooling, had the least errors amongst TRD distribution models (i.e., less than 0.2 °C) for all 3 case studies and distribution 12, providing 125% of heating and cooling, had the highest (i.e., up to 0.6 °C). This trend is less apparent when the percentage of cooling and heating is not equal, as in those cases the impact of overheating/overcooling needs to be considered, as well as in the CDM and CON distributions, possibly due to the lower magnitudes of errors in the prediction results of those distributions.

<Figure 8 around here>

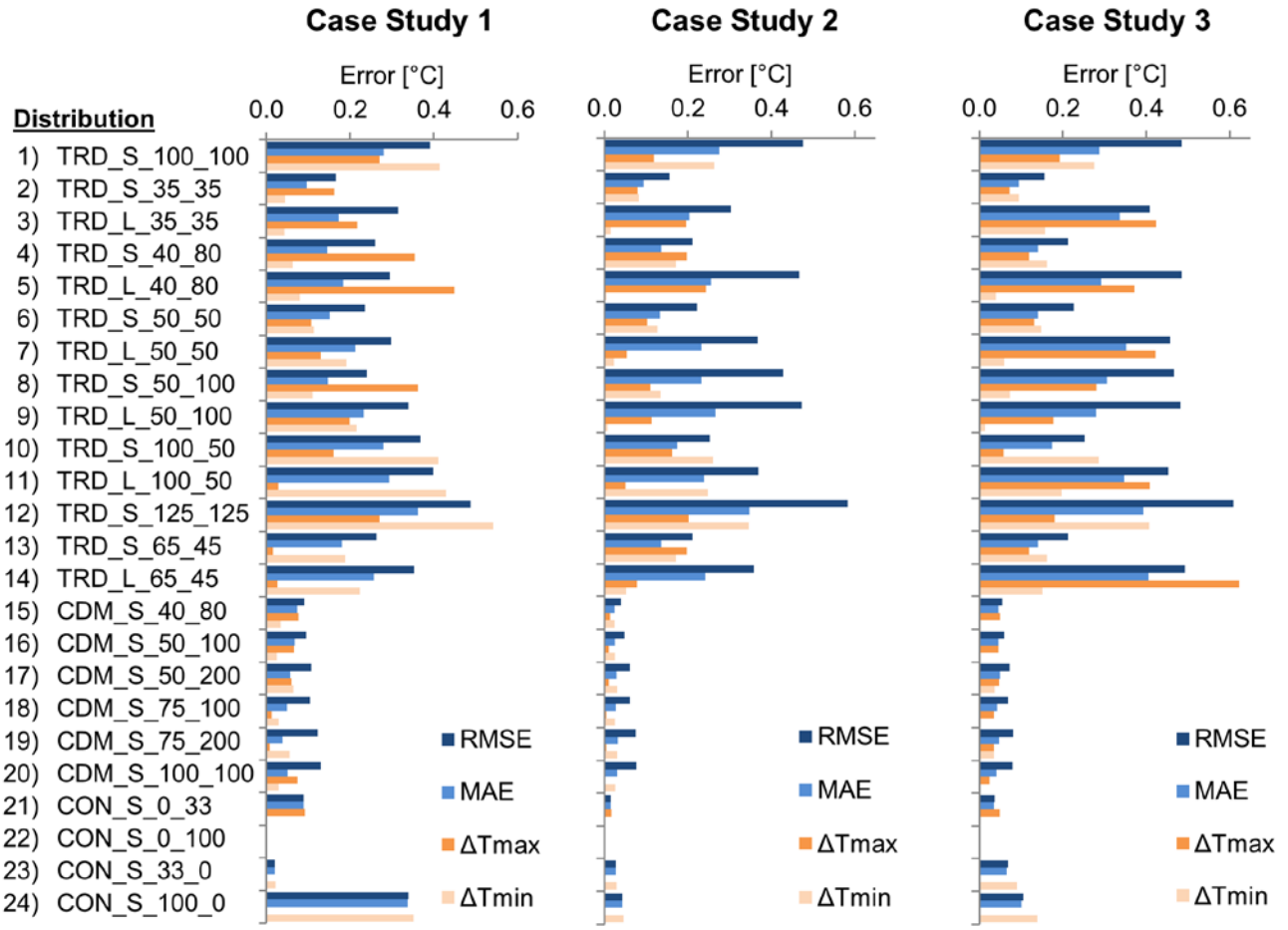


Figure 8. Validation results – evaluation metrics and errors

Considering the different types of distributions, higher errors (still relatively insignificant) were observed in the prediction of TRD distributions, which was expected, since TRD varies daily compared to CDM which varies monthly and CON which does not vary at all. The daily thermal load variations introduce more complexity in the modelling of the heat transfer physics, which could more easily lead to computational or round-off errors. For the provided distributions, this particularly affects ΔT_{max} (the absolute difference between the maximum of the predicted and "actual" results), due to the highly variable cooling loads which are responsible for the maximum temperature peaks. These variable cooling peaks, along with a visual indication of the accuracy of the prediction model, can also be seen in Figure 7(b), where the predicted/"actual" temperatures are plotted over time for the first year of simulation, as shown in section 4.1, noting that distribution 12 produced the largest errors; therefore, all other distributions have an even better match between the predicted and "actual" results.

Figure 9 shows the average temperatures of the fluid, for each day of the 5-year operating period, as calculated by the prediction model ($T_{fluid}^{predicted}$) plotted against those calculated by the FE numerical simulation, labelled "actual" (T_{fluid}^{actual}). Each column of figures represents a different case study, and each row represents testing with different types of thermal load distributions. Even though the scale of each subplot is different (due to the different responses), the data generally lie on $x = y$ (dotted line), verifying the suitability of the prediction model, since its results are almost identical to those of the numerical simulations. The goodness of fit is also shown on each plot by the computation of the coefficient of determination, R^2, which confirms almost perfect correlation between the predicted and "actual" results. It should be noted that for the last plot in Figure 9 some results are outside the plotted range and not shown (but still considered in the analysis and presented R^2 values) in order to keep the plot axes consistent throughout.

<Figure 9 around here>

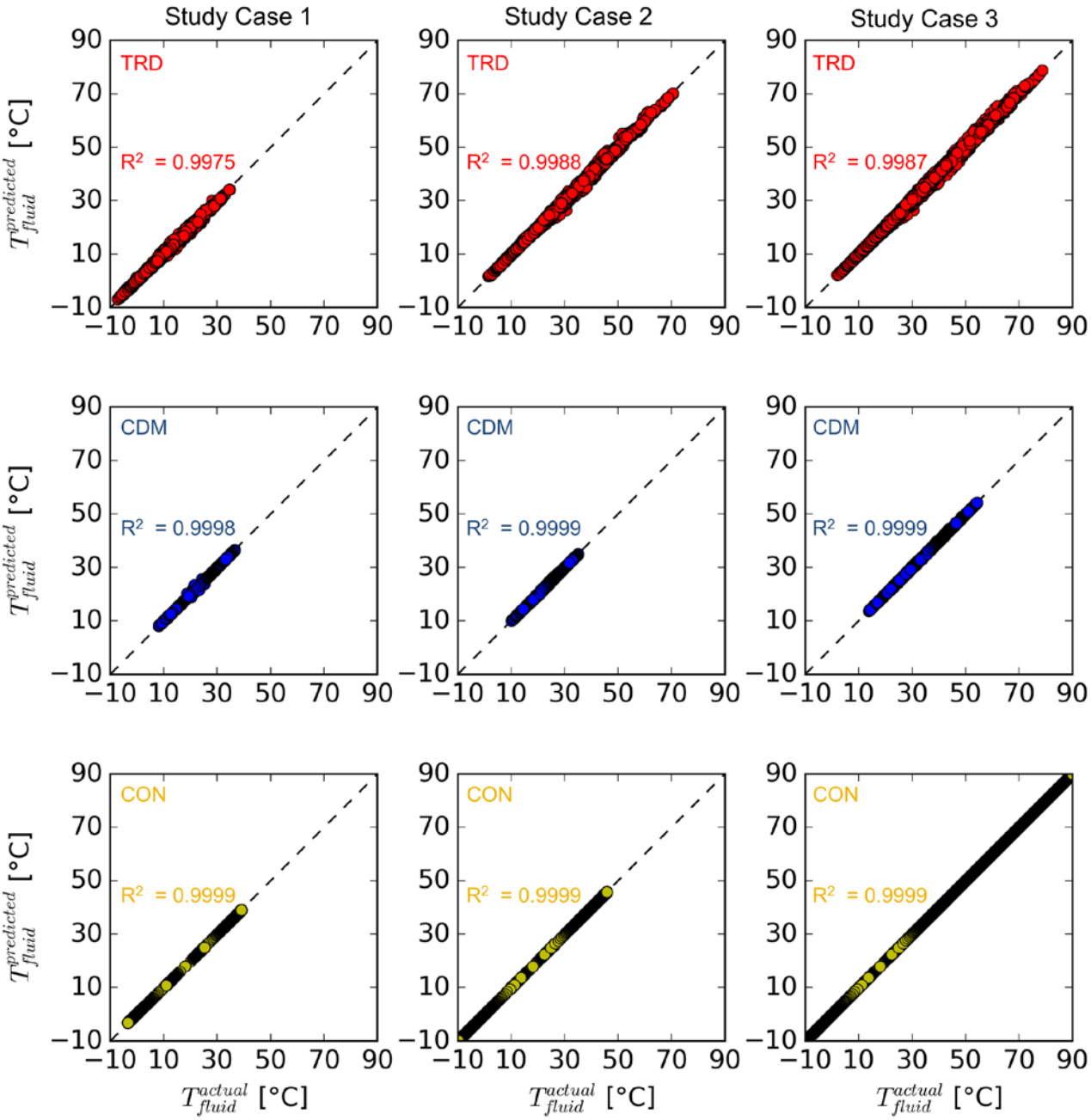


Figure 9. "Actual" temperature against predicted temperatures for all distributions of each case study. Separated into distribution types (rows) and case studies (columns)

It is also interesting to observe the performance of the prediction model in relation to the thermal effects due to accumulation of heat over time (when the thermal load is not balanced between heating and cooling), as well as the thermal interference within the piles, when they are placed close together (as in Case Study 3). Figure 10 shows the "actual" and predicted temperature results using thermal load distribution 20 for both case study 2 (Figure 10(a)), which includes a single energy pile, as well as case study 3 (Figure 10(b)), which includes a field of 16 such energy piles (of same geometry, configuration and thermal load per pile as case study 2) placed close together. The two figures show that the prediction model can very well account for these effects, as the annually increasing temperatures due to both thermal accumulation (given the imbalanced load), seen in Figure 10(a), as well as due to the thermal interference between energy piles, seen in Figure 10(b), are predicted with a high accuracy.

<Figure 10 around here>

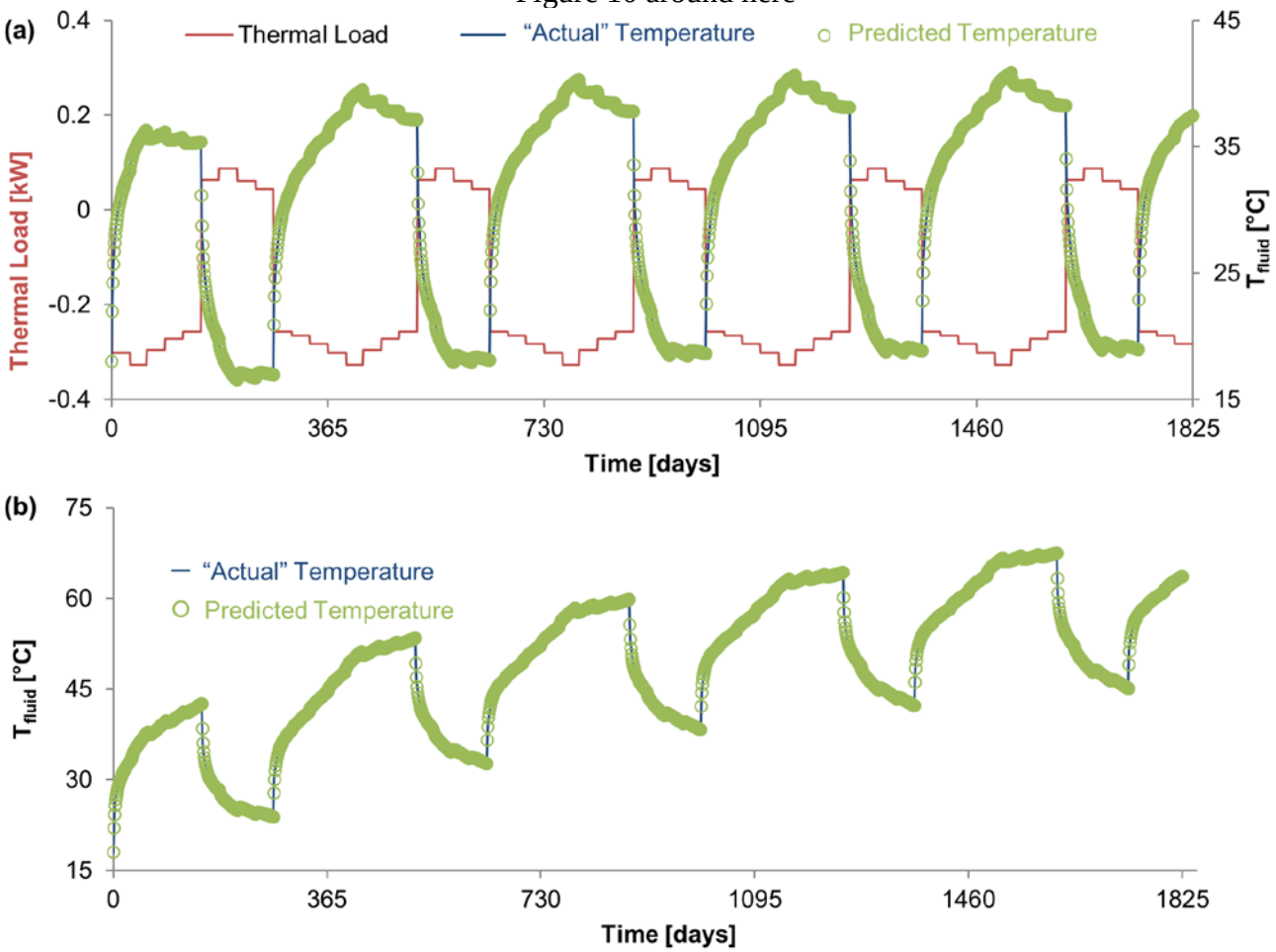


Figure 10 "Actual" and Predicted values for Distribution 20, using (a) Case Study 2 (b) Case Study 3

4.3 The significance of the training thermal load distribution

The analysis presented in section 4.2 is completed by training each prediction model with the FE numerical simulation results from distribution 22, which uses a constant cooling load. The predictive model trained with a constant thermal load distribution provides more accurate results than when trained with other load distributions, which can be justified by considering the nature of the data used for training. FE numerical simulations can present results that are fairly accurate, provided that the right governing equations, boundary conditions and mesh refinement, among others, are appropriate, but render small errors within set tolerances. These errors are usually insignificant to the accuracy of a simulation, but when fitting/learning a relationship between input and output, their impact can be less trivial. Using a constant thermal load distribution (input) for the FE numerical simulation produces a smoother fluid temperature distribution (output) and therefore these numerical errors are minimised, compared to other input thermal load distributions where there are sudden changes in the energy requirements and thus the resulting fluid temperatures. Figure 11 shows a comparison of the prediction model results for case study 1, when the prediction model is trained using each of the different types of thermal load distributions (TRD, CDM, CON). As it can be seen, using the constant thermal load distribution for training the model produces the overall best performance. Using the TRD or CDM distribution produces excellent performance when predicting other TRD or CDM distributions respectively; however, the errors increase when predicting the other two distributions. This suggests that the shape/nature of the training distribution still impacts the learnt relationship,

though at a relatively small degree, as all three prediction models produced errors that can be considered acceptable for GSHP design purposes, even when predicting different types of distributions than the one each model was trained with.

<Figure 11 around here>

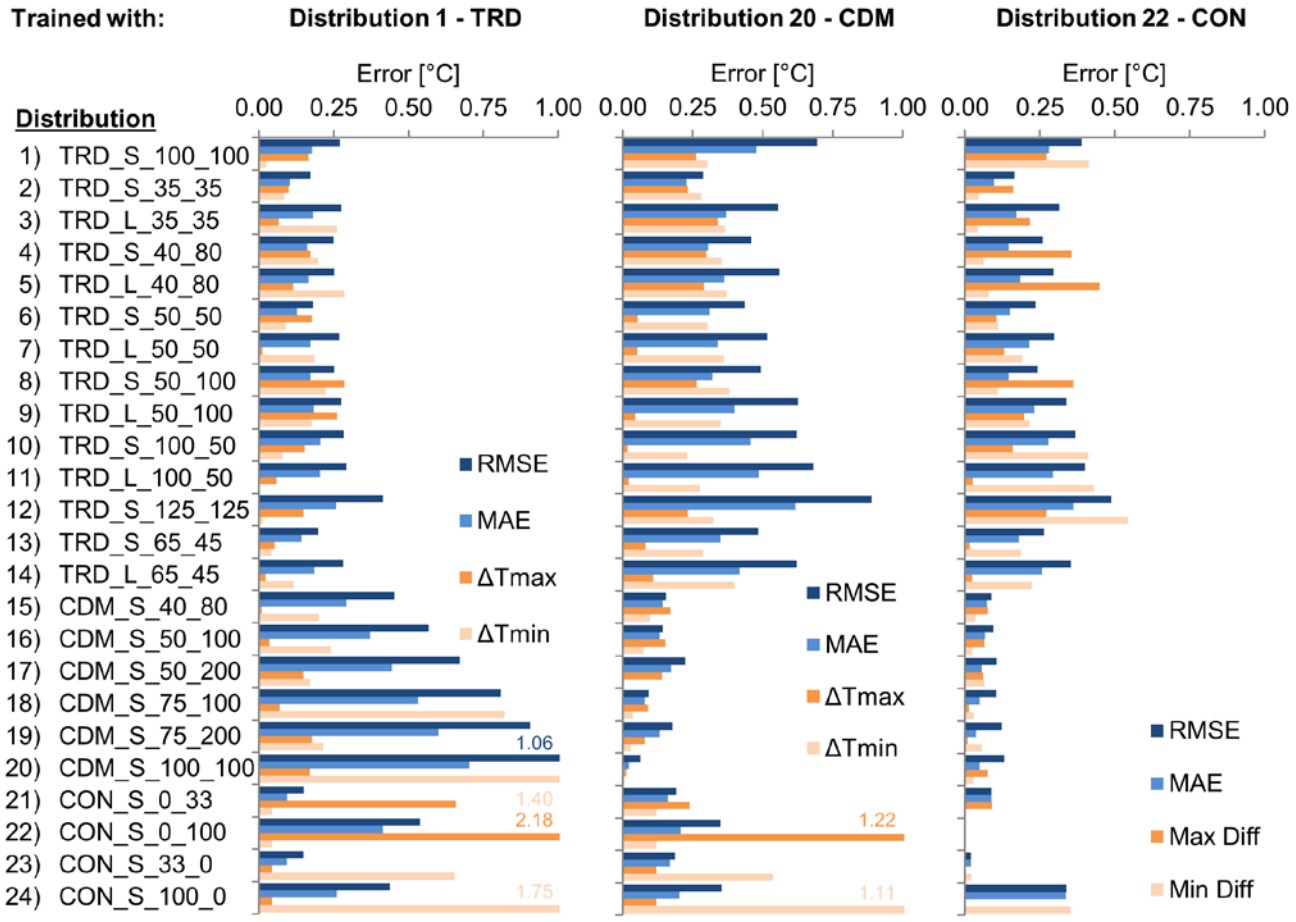


Figure 11. Validation results of case study 1, when trained with different types of thermal load distributions

From Figure 11, and taking into account the approach outlined in section 2.2, it can be inferred that the prediction model can confidently be used in energy pile design. A prediction model produces excellent results when it predicts the fluid temperatures for a distribution of a specific type (TRD, CDM, CON) with which it has also been trained. In practise, this is anticipated to be the case, as the type of the thermal load distribution is expected to be known at the start of this process. Therefore, there will rarely be a need to use more than one type of thermal load distributions for a specific case and the prediction model will be making predictions for the same type of distributions with which it has been trained. If the need for using more than one type of thermal distributions arises, the above results indicate that the model should be trained with the one that has fewer variations, for the reasons explained earlier in the section.

4.4 Computation time comparison

It should be stressed that the key benefit of this approach is the tremendous reductions in computational time and resources that are required. To run the FE numerical models used in this analysis, using high performance parallel cloud computing (which are much more powerful than typical personal computers) the required computational times varied between 1.5 and 7 hours per model, depending on the size of the geometry for each case. On the other hand, a single prediction required about 4 seconds, regardless of the case study, since the statistical prediction model is

independent of the size and complexities of the finite element models, but instead its time complexity relies on the duration of the simulation. The computational times for the FE simulations and the predictions are included in Appendix A. It is also worth noting here that the simulation duration of 5 years, adopted in this study, would not be sufficient for design purposes and a longer simulation period would be more reasonably expected. This would significantly increase the computational times for the numerical simulations but only marginally increase those of the prediction model. Considering the results from a previous study by the authors [23], an increase of simulation time from 1 to 5 years, for conditions similar to case study 1, yielded an increase in computational time required for the FE numerical simulation from about 2 hours to about 7 hours and for the prediction model from 3 seconds to 4. Overall, since the prediction model only takes seconds to run, the total time required for the design will most heavily depend on the time required to run the initial numerical simulation (based on which the prediction model will be trained).

It is also worth noting that the computational resources required are much less demanding and the prediction model can very efficiently run on any standard personal computer, minimising the need to have or to rent a high-performance computer capable of running multiple numerical simulations. This fact combined with the incredibly short amount of time the prediction model requires, allow for proper thermal load optimisation, as the designer can try many different combinations of thermal load distributions and can therefore efficiently find the heating distribution that provides the maximum acceptable amount of energy for the chosen geothermal system.

5 Summary and conclusion

This study presents a machine learning prediction model that can be used alongside numerical (in this case finite element) simulations in order to significantly reduce the time and resources that are required in energy pile design. This makes optimisation more viable during the design process, maximising the amount of energy that can be provided by the GSHP system as well as the operational efficiency of the system. With the presented methodology, the question of "how much energy can the system provide?" is addressed, by using the machine learning prediction model to repeatedly assess the suitability of a specific thermal load (i.e. thermal energy demand) distribution (by reviewing how it affects the system) and then choose the most appropriate one for the given fixed conditions.

An evaluation of the model is presented, using three different case studies, each with different geometries and materials, as well as different types and variations of thermal load distributions (24 for each case study), which represent the amount of energy the system will be providing. The results of the evaluation show that the prediction model can confidently be used, as the errors produced were well within acceptable levels for GSHP design. It was noted that the prediction model performed the best when it was predicting thermal load distributions of the same type as the one that it was trained with, which would largely be the case in real project applications. Lastly, a comparison of the computational time and resources between the finite element software and the prediction model is made. This highlights how optimisation of energy pile design becomes viable using this approach, minimising the time and resources required to find the optimal amount of energy that can be provided by the GSHP system.

Overall, this study shows and validates a statistical approach that can enhance GSHP design for energy structures. Many different types of thermal load distributions were used in the validation to make predictions (including non-ideal conditions, such as excessive cooling demand), showing the flexibility and predictive capabilities of this approach. The presented methodology adopted energy piles as the structures of choice, given their recent popularity and potential, however it is believed that this approach is valid for any type of energy structure. The suitability of other types of structures, such as energy tunnels and retaining walls, is currently being explored with very promising preliminary results and will be presented in future work. It is in general expected that this methodology will be proven suitable for any type of energy structure and combination of thermal load distributions, provided, always, that a well-defined and accurate numerical simulation procedure is available to the designer.

6 Acknowledgements

Funding from the Australian Research Council (ARC) FT140100227, The University of Melbourne and the Victorian Government is much appreciated.

7 References

[1] Florides G, Kalogirou S. Ground heat exchangers-A review of systems, models and applications. Renew Energy 2007;32:2461–78. doi:10.1016/j.renene.2006.12.014.

[2] Preene M, Powrie W. Ground energy systems: from analysis to geotechnical design. Géotechnique 2009;59:261–71. doi:10.1680/geot.2009.59.3.261.

[3] Johnston IW, Narsilio GA, Colls S. Emerging geothermal energy technologies. KSCE J Civ Eng 2011;15:643–53. doi:10.1007/s12205-011-0005-7.

[4] Narsilio GA, Johnston IW, Bidarmaghz A, Colls S, Mikhaylova O, Kivi A, et al. Geothermal energy: Introducing an emerging technology. In: Horpibulsuk S, Chinkulkijniwat A, Suksiripattanapong C, editors. Proc. Int. Conf. Adv. Civ. Eng. Sustain. Dev. (ACESD 2014). Volume 1 o, Nakhon Ratchasima, Thailand: Suranaree University of Technology,; 2014, p. 141–54.

[5] Lund J, Boyd T. Direct Utilization of Geothermal Energy 2015 Worldwide Review. Proc World Geotherm Congr 2015:25–9. doi:10.1016/j.geothermics.2011.07.004.

[6] Bayer P, de Paly M, Beck M. Strategic optimization of borehole heat exchanger field for seasonal geothermal heating and cooling. Appl Energy 2014;136:445–53. doi:10.1016/j.apenergy.2014.09.029.

[7] Retkowski W, Thöming J. Thermoeconomic optimization of vertical ground-source heat pump systems through nonlinear integer programming. Appl Energy 2014;114:492–503. doi:10.1016/j.apenergy.2013.09.012.

[8] Bidarmaghz A. 3D Numerical Modelling of Vertical Ground Heat Exchangers. The University of Melbourne, 2014.

[9] Huang S, Ma Z, Wang F. A multi-objective design optimization strategy for vertical ground heat exchangers. Energy Build 2015;87:233–42. doi:10.1016/j.enbuild.2014.11.024.

[10] Pandey N, Murugesan K, Thomas HR. Optimization of operating parameters of ground source heat pump system for space heating and cooling by Taguchi method and utility concept. Appl Energy 2017;190:421–38. doi:10.1016/j.apenergy.2013.10.065.

[11] Laloui L, Moreni M, Vulliet L. Behavior of a dual-purpose pile as foundation and heat exchangers. Can Geotech J 2003;40:388–402. doi:10.1139/t02-117.

[12] Brandl H. Energy foundations and other thermo-active ground structures. Géotechnique 2006;56:81–122. doi:10.1680/geot.2006.56.2.81.

[13] Laloui L, Nuth M, Vulliet L. Experimental and numerical investigations of the behaviour of a heat exchanger pile. Int J Numer Anal Methods Geomech 2006;30:763–81. doi:10.1002/nag.499.

[14] Hamada Y, Saitoh H, Nakamura M, Kubota H, Ochifuji K. Field performance of an energy pile system for space heating. Energy Build 2007;39:517–24. doi:10.1016/j.enbuild.2006.09.006.

[15] Gao J, Zhang X, Liu J, Li K, Yang J. Numerical and experimental assessment of thermal performance of vertical energy piles: An application. Appl Energy 2008;85:901–10. doi:10.1016/j.apenergy.2008.02.010.

[16] Amatya BL, Soga K, Bourne-Webb PJ, Amis T, Laloui L. Thermo-mechanical behaviour of energy piles. Géotechnique 2012;62:503–19. doi:10.1680/geot.10.P.116.

[17] Loveridge F, Powrie W. Pile heat exchangers: thermal behaviour and interactions. Proc ICE - Geotech Eng 2013;166:178–96. doi:10.1680/geng.11.00042.

[18] Akrouch GA, Sánchez M, Briaud JL. Thermo-mechanical behavior of energy piles in high plasticity clays. Acta Geotech 2014;9:399–412. doi:10.1007/s11440-014-0312-5.

[19] Lu Q, Narsilio GA. Economic analysis of utilising energy piles for residential buildings. Energy 2017;submitted.

[20] Fadejev J, Simson R, Kurnitski J, Haghighat F. A review on energy piles design, sizing and modelling. Energy 2017;122:390–407. doi:10.1016/j.energy.2017.01.097.
[21] Alavy M, Nguyen H V., Leong WH, Dworkin SB. A methodology and computerized approach for optimizing hybrid ground source heat pump system design. Renew Energy 2013;57:404–12. doi:10.1016/j.renene.2013.02.003.
[22] Mikhaylova O, Choudhary R, Soga K, Johnston IW. Benefits and optimisation of district hybrid ground source heat pump systems. In: Wuttke F, Bauer S, Sanchez M, editors. Energy Geotech. - Proc. 1st Int. Conf. Energy Geotech. ICEGT 2016, Kiel: CRC Press; 2016, p. 535–42.
[23] Makasis N, Narsilio GA, Bidarmaghz A. Optimising the design of energy piles using machine learning Optimisation de la conception des pieux énergétiques par apprentissage automatique. 19th Int. Conf. Soil Mech. Geotech. Energy, Seoul: 2017.
[24] Loveridge F, Powrie W. G-Functions for multiple interacting pile heat exchangers. Energy 2014;64:747–57. doi:10.1016/j.energy.2013.11.014.
[25] Narsilio GA, Franco F, Ferrero H, Bidarmaghz A, Serrano C, Perez MEC, et al. Geothermal Energy in Loess: A Detailed Numerical Case Study for Cordoba. Proc. XV Pan-American Conf. Soil Mech. Geotech. Eng., Buenos Aires: IOS Press; 2015.
[26] Bidarmaghz A, Makasis N, Narsilio GA, Franco F, Perez MEC. Geothermal Energy in Loess. Environ Geotech 2016;4:225–36.
[27] Narsilio GA, Bidarmaghz A, Johnston IW, Colls S. Geothermal Energy: detailed modelling of ground heat exchangers. Comput Geotech 2016.
[28] Bidarmaghz A, Narsilio GA, Johnston IW, Colls S. The importance of surface air temperature fluctuations on long-term performance of vertical ground heat exchangers. Geomech Energy Environ 2016;6:35–44. doi:10.1016/j.gete.2016.02.003.
[29] Bhattacharya B, Solomatine DP. Machine learning in soil classification. Neural Networks 2006;19:186–95. doi:10.1016/j.neunet.2006.01.005.
[30] Goh ATC, Goh SH. Support vector machines: Their use in geotechnical engineering as illustrated using seismic liquefaction data. Comput Geotech 2007;34:410–21. doi:10.1016/j.compgeo.2007.06.001.
[31] Gang W, Wang J, Wang S. Performance analysis of hybrid ground source heat pump systems based on ANN predictive control. Appl Energy 2014;136:1138–44. doi:10.1016/j.apenergy.2014.04.005.
[32] Gordan B, Jahed Armaghani D, Hajihassani M, Monjezi M. Prediction of seismic slope stability through combination of particle swarm optimization and neural network. Eng Comput 2015. doi:10.1007/s00366-015-0400-7.
[33] Yavuzturk C. A Transient Two-Dimensional Finite Volume Model for the Simulation of Vertical U- Tube Ground Heat Exchangers. ASHRAE Trans 1999;M:465–74.
[34] Bernier MA, Pinel P, Labib R, Paillot R. A multiple load aggregation algorithm for annual hourly simulations of GCHP systems. HVAC R Res 2004;10:471–87. doi:10.1080/10789669.2004.10391115.
[35] Philippe M, Bernier M, Eng P, Marchio D. Vertical Geothermal Borefields. Ashrae J 2010:10.
[36] Fossa M, Minchio F. The effect of borefield geometry and ground thermal load profile on hourly thermal response of geothermal heat pump systems. Energy 2013;51:323–9. doi:10.1016/j.energy.2012.12.043.
[37] Mikhaylova O. Towards Improvement of the Design of Borehole Ground Heat Exchangers. The University Of Melbourne, 2017.
[38] Stewart MA, Mccartney JS. Centrifuge Modeling of Soil-Structure Interaction in Energy Foundations. J Geotech Geoenvironmental Eng ASCE 2014;140:1–11. doi:10.1061/(ASCE)GT.1943-5606.0001061.
[39] Mccartney JS, Murphy KD. Strain Distributions in Full-Scale Energy Foundations. J Deep Found Inst 2012;6:26–38. doi:10.1179/dfi.2012.008.
[40] Colls S. Ground Heat Exchanger Design For Direct Goethermal Energy Systems. The University of Melbourne, 2013.

816 [41] Bidarmaghz A, Narsilio G, Johnston I. Numerical modelling of ground loop configurations for
817 Direct geothermal applications. Aust Geomech J 2012;47:21–6.
818

8 Appendix A

Table A1. Computational time comparison

Numerical Simulations			
Case study:	1	2	3
Average time per simulation:	0 days 7 hrs 0 mins 14 secs	0 days 1 hrs 31 mins 25 secs	0 days 6 hrs 43 mins 52 secs
Total time:	7 days 0 hrs 5 mins 30 secs	1 days 12 hrs 34 mins 7 secs	6 days 17 hrs 32 mins 54 secs
Prediction Model			
Case study:	1	2	3
Average time per prediction:	0 days 0 hrs 0 mins 4.24 secs	0 days 0 hrs 0 mins 4.21 secs	0 days 0 hrs 0 mins 4.14 secs
Total time for predictions (including model training):	0 days 0 hrs 1 mins 42 secs	0 days 0 hrs 1 mins 41 secs	0 days 0 hrs 1 mins 39 secs
Total time (including 1 numerical simulation):	0 days 7 hrs 1 mins 56 secs	0 days 1 hrs 33 mins 6 secs	0 days 6 hrs 45 mins 31 secs

5.3 Journal paper: A robust prediction model approach to energy geo-structure design

This section consists of a journal paper titled: “A robust prediction model approach to energy geo-structure design”, published in the journal *Computers and Geotechnics.* The paper has been inserted in the following pages, in its Author’s Accepted Manuscript [AAM] version, with the only modification being the addition of the thesis page numbers at the bottom of the page (allowing consistent numbering throughout the thesis). This publication is the author’s original work, has been included with the co-authors’ authorisation (appropriate co-author authorisation forms have been included in this submission) and the co-authors’ contributions have been acknowledged in the *Preface & Publications* section.

Type of paper: full length article (Computers and Geotechnics - Elsevier Journal)
Date text written: June 2018
Number of words in main text and tables = 6652
Number of figures = 13
Number of tables = 8

A robust prediction model approach to energy geo-structure design

Author 1
Nikolas Makasis, MSc (Computer Science), MEng (CE)
Department of Infrastructure Engineering, The University of Melbourne, Parkville, Australia

Author 2
Guillermo A. Narsilio✉, PhD, MSc (Math), MSc (CE), CEng
Department of Infrastructure Engineering, The University of Melbourne, Parkville, Australia

Author 3
Asal Bidarmaghz, PhD, MSc (Eng), BSc (Eng)
Department of Engineering, University of Cambridge, Cambridge CB2 1PZ, United Kingdom

Full contact details of corresponding author
Guillermo A. Narsilio, ARC Future Fellow and Associate Professor
Engineering Block B 208, Department of Infrastructure Engineering, The University of Melbourne, Parkville, VIC 3010, Australia
Email: narsilio@unimelb.edu.au, Phone: +61 (3) 8344 4659, Fax: +61 (3) 8344 4616

Abstract:
Energy geo-structures, such as piles or retaining walls, provide geothermal space heating and cooling, in addition to their structural purposes. The thermal design of these structures is undertaken on a case by case basis, commonly using costly finite element simulations, especially for complex geometries. This work introduces a simple but robust prediction methodology that can be used alongside such simulations to significantly reduce computational time and resources for the analysis of any energy geo-structure. An evaluation is presented and exemplified with energy diaphragm walls, for a range of geometrical and material conditions, showing insignificant prediction errors and vast computational savings.

Keywords
Geothermal; Prediction modelling; Numerical modelling; Sensitivity analysis; Ground heat exchangers (GHE); Energy geo-structures

List of Notations

A	Prediction factor for cooling (Equation (1)), °C
B	Prediction factor for heating (Equation (1)), °C
$C_{p\ material}$	Specific heat capacity of material, J/(kg·K)
L_{wall}	Depth of the wall excl. toe, m
s	vertical spacing between pipe legs, m
t	time, sec
T_{fluid}	average fluid temperature of a pipe loop (average of inlet and outlet), °C
$T_{farfield}$	average annual ground temperature, °C
$T_{initial}$	initial temperature of fluid in a pipe loop, °C
$\lambda_{material}$	thermal conductivity of material, W/(m·K)
$\rho_{material}$	density of material, kg/m^3

1 Ground source heat pump systems and energy geo-structures

Transitioning towards cleaner and more renewable sources of energy and finding ways to reduce energy consumption are considered as essential means to ensure a sustainable future. A technology that can contribute towards these goals is shallow geothermal, which uses the ground as a heat source or sink to efficiently heat and cool buildings, by utilising the fact that the ground temperature a few tens of metres below the surface is relatively constant throughout the year [1]. Shallow geothermal, or ground source heat pump (GSHP), systems incorporate High Density Polyethylene (HDPE) or cross-linked polyethylene (PEX) pipes with a circulating carrier fluid into underground trenches or structures such as boreholes, piles or retaining walls, creating ground heat exchangers (GHEs) that transfer the heat to and from the ground [2–6].

Energy geo-structures are underground GHEs for which energy provision is a secondary function, after structural stability, such as energy piles or retaining walls [7–13]. The main advantage of these structures is that the capital costs are potentially significantly reduced, mainly because drilling (which is amongst the highest associated capital costs) is not accounted as part of the geothermal design [14,15]. On the other hand, the main limitation of energy geo-structures is that a significant number of design parameters (such as their geometry) is governed by the structural design. Therefore, since the location of GHEs and internal piping geometry are some of the key parameters (aside from the thermal properties of the ground) that determine how much energy they can provide, energy geo-structures cannot be designed to provide a specified/target amount of thermal energy. Instead, the amount of energy they can provide needs to be determined and, if required, complemented using auxiliary means, forming a hybrid system [16–20].

Moreover, because of the wide range of variability in structures, configurations and conditions, establishing a standardised, analytical, fast approach to energy geo-structure design is non-trivial. Instead, the use of complex and computationally expensive numerical simulations is usually required, especially for complex geometries, which is time demanding. This study presents a prediction model approach, that can be used alongside those complex numerical simulations to significantly reduce the amount of time required to undertake energy geo-structure analysis and/or design and very quickly and accurately answer the question of how much energy can the geothermal system provide for any geometry and conditions.

2 The proposed prediction model approach

2.1 Energy geo-structures and current approaches

As explained in section 1, an important question needed to be answered in geothermal design as well as in research of energy geo-structures is *how much energy can the system provide* [21,22], instead of *how does the system need to be designed to provide the target energy demand*, as in traditional GSHP design. Knowing how much energy the system can reliably provide is important, as it enables an evaluation of its applicability for a given project to be performed, including a cost-benefit analysis. It is also beneficial for this information to be known relatively early in the design process, to better inform the prospective clients and investors and aid in their decision-making process about incorporating a geothermal solution to the project or not [8].

However, there exists a lack of a standardised approach to energy geo-structure design [23]. Instead, in answering this question either analytical or numerical approaches can be adopted [7,13]. The widely used commercial software for GSHP design implement analytical design approaches, which were mostly originally developed for traditional borehole systems. Such software can be used for energy pile design (which is considered similar to boreholes), even though research advises against this approach [24]. In regards to energy pile design, design guidelines have been made available [25] and some semi-analytical approaches, adopting g-functions have been proposed [26,27]. For energy retaining walls,

however, general analytical approaches may be less suitable due to the vastly different geometries and conditions compared to traditional systems, although some semi-analytical approaches have been developed [28]. Moreover, due to the large number of assumptions adopted in analytical approaches, they are unable to capture the problem in its entirety. The second and more flexible approach is using numerical models to create and run a computational simulation of the system (in this research finite elements are utilised). Numerical simulations adopt significantly fewer assumptions and constraints and can therefore be utilised for any structure, geometry and conditions. For these reasons, numerical simulations are commonly reported as used in the research of further understanding these systems as well as their thermal design with several recent examples [21,29–34]. However, the complexity behind the simulations results in them requiring significant computational resources and, very importantly, time to provide results. The proposed methodology aims to address this drawback.

2.2 The prediction model principles

In utilising a finite element numerical simulation to analyse an energy geo-structure design, the thermal demand is firstly specified and the viability of the system to provide that demand is determined by examining the resulting temperature of the fluid within the HDPE pipes. The fluid temperature range, throughout the operation of the system, determines the efficiency and viability of the design. Each numerical simulation, which can require from hours to days or weeks to compute, can be used to evaluate if the temperature of the fluid is within the operational range of the GSHP. If not, then another simulation needs to be computed, specifying a new thermal demand to be satisfied by the energy geo-structures. This iterative process can be extremely computationally expensive and time consuming. This work introduces a prediction model that can aid in speeding this iterative process by removing the need for multiple costly numerical simulations, but instead uses the results of two such simulations to more quickly and inexpensively predict the system behaviour (the fluid temperatures) for any other combination of thermal loading. The overall process can be seen in Figure 1, noting that the two finite element simulations can be run simultaneously instead of sequentially in order to further save time.

<Figure 1 around here>

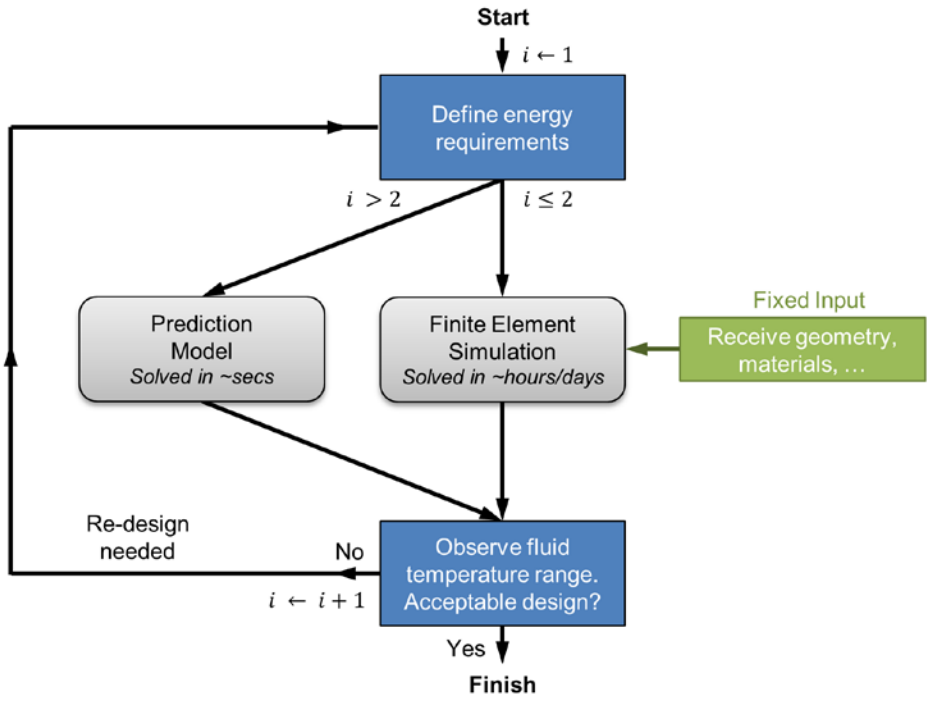


Figure 1 Energy geo-structure design methodology with prediction model

The proposed methodology involves predicting how the fluid temperature (T_{fluid}) within the system pipes at a specific time-step (t) will change, when the system provides different amounts of thermal energy for cooling and heating (to determine how much thermal energy the geothermal system can provide and how much is required to be provided by auxiliary means). This relationship turns out to be expressed in Equation (1) and can be used alongside numerical modelling techniques to substantially reduce the required time to undertake the design.

$$T_{fluid}(t) = A(t) * Cooling + B(t) * Heating + T_{initial} \quad (1)$$

In the equation, $Cooling$ [%] and $Heating$ [%] represent the percentages of thermal energy to be provided (for example, 50% of the specified cooling that the system is trying to fulfil), as explained in detail in section 3.2. The coefficients A [°C] and B [°C] represent the impact of cooling and heating (for that time-step/day t) respectively and contain the contributions of all other parameters for a specific designed system, for example the geometry, configuration and material properties (other than the thermal energy being provided). This means that when the model design parameters, such as the configuration of the pipes or the location of the project (i.e., thermal conductivity of the ground), change, the numerical values of the coefficients A and B will also change and each unique combination of design parameters for the numerical simulation will produce unique values for these coefficients. Equation (1) can be simply understood as estimating the temperature change from the initial stage of the fluid temperature ($T_{initial}$), caused by the provision of thermal energy for heating and cooling.

The above relationship has been derived based on a multitude of FEM numerical simulations and inspired by analytical solutions. Indeed, several analytical and semi-analytical approaches for traditional borehole GHEs exist (for example, the Infinite Line Source model) [35–37] that follow an approach of calculating the increase in temperature from its initial value, based on the effect of the thermal load, similar to Equation (1). Equation (2) shows a generic representation of this relationship, where T is the temperature being calculated/predicted, TL is a function of the thermal load/demand and f represents a general function that accounts for factors such as the geometry, material parameters, etc.

$$T(location, t) = TL * f(geometry, material \dots) + T_{initial} \quad (2)$$

These analytical or semi-analytical approaches, however, utilise superposition principles to account for the different thermal demand types (heating and cooling), use fixed geometry types and are aimed towards traditional borehole GSHP system design. On the other hand, the approach proposed herein can explicitly and simply account for heating/cooling demand ratios (rather than superposition) and most importantly can be used with any energy geo-structure, whose geometry can vary greatly from case to case and structure to structure.

Figure 2 illustrates an example prediction model resulting from the proposed methodology, which simply (but robustly as shown later) uses a plane that is defined by the provided percentage of cooling and heating energy as the x and y axes respectively and the resulting fluid temperatures as the z axis. In order to create the plane depicted in Figure 2, three points are required. One of these points can be computed using $(0,0,T_{initial})$, since, based on Equation (1), if no cooling or heating is provided, then this equates to the fluid temperature being the value it was initially, which is known ($T_{initial}$) and equal to the farfield ground temperature. In this study, $T_{initial} = 18.3\ °C$ is adopted (a typical mean farfield

ground temperature for Melbourne, Australia). The two remaining points required can be obtained using numerical simulations, such as finite element methods (as adopted in this study), by running a simulation of the GSHP system twice, using different thermal load distribution inputs, while keeping all other parameters, such as geometry, material etc. (and therefore the numerical values of coefficients A and B) constant.

<Figure 2 around here>

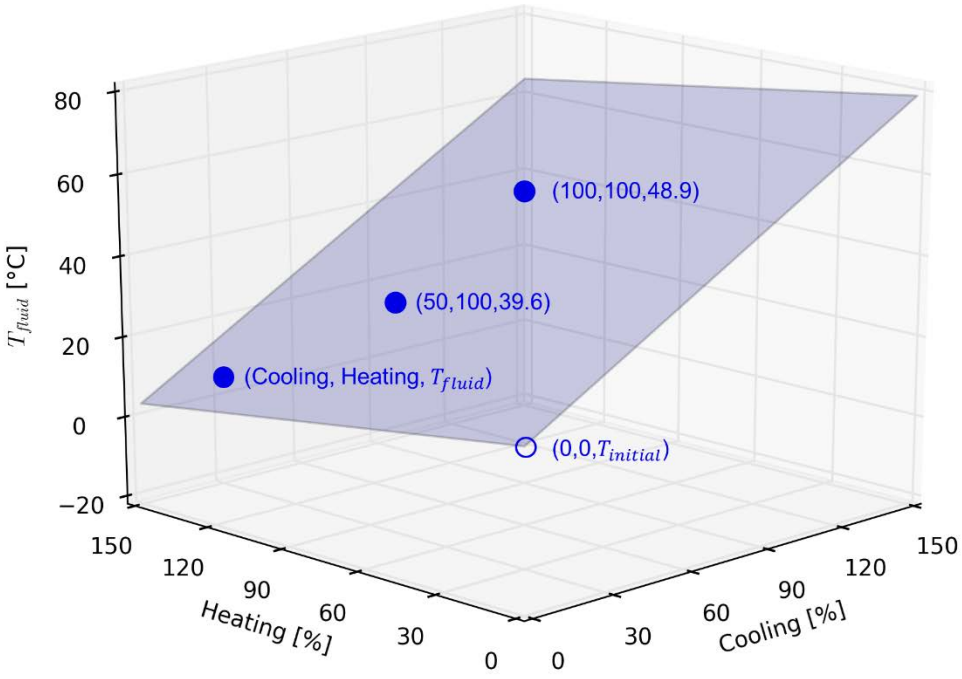


Figure 2 Example prediction plane with three points

The creation process for the prediction plane is illustrated in Figure 3, adopting an example case and dataset for this purpose. Firstly, Figure 3(a) shows an example of cooling and heating distributions used as input to the numerical simulations, where the percentages refer to the amount of energy related to a target thermal load distribution (i.e., 100% of Cooling and Heating), as it is common practice during the design phase for a target thermal demand that the geothermal system must provide to be set. It is also important to note that the percentages used for these two points cannot both be equal in cooling and heating, to provide enough information for a plane (and not a line) to be drawn. One of the outputs of the numerical simulation will be the fluid temperature distribution in the pipes over the simulation duration. The average fluid temperature T_{fluid} is used in this work, shown in Figure 3(b), which is computed based on the temperatures of the inlet and outlet pipes (T_{fluid} = (T_{in}+T_{out})/2). The output temperature distributions from the two numerical simulations can then be used to extract the fluid temperature at a specific time and thus create the plane. The figure shows two such planes, one for $t = 1514\ days$ (Figure 3(c)) and one for $t = 1718\ days$ (Figure 3(d)), which represent the days of the highest and lowest temperatures within the last year of the simulation, considered the most critical. In actuality, these critical points are usually picked at the end of the design life or as soon as steady state is reached; however, throughout this work a 5-year operational duration is adopted, which is considered enough to account for annually accumulating thermal effects in the same manner it would in longer operational periods. Similarly, with the required information obtained, the plane can be created for any/each time-step in the simulation, and the temperature of the fluid can be predicted for *any other thermal demand combination* of heating and cooling (for example, 80% of cooling, 60% of heating),

avoiding the need for running more numerical simulations, which require long running times and expensive computational resources to find a more beneficial amount of heating and cooling the geothermal system can provide.

<Figure 3 around here>

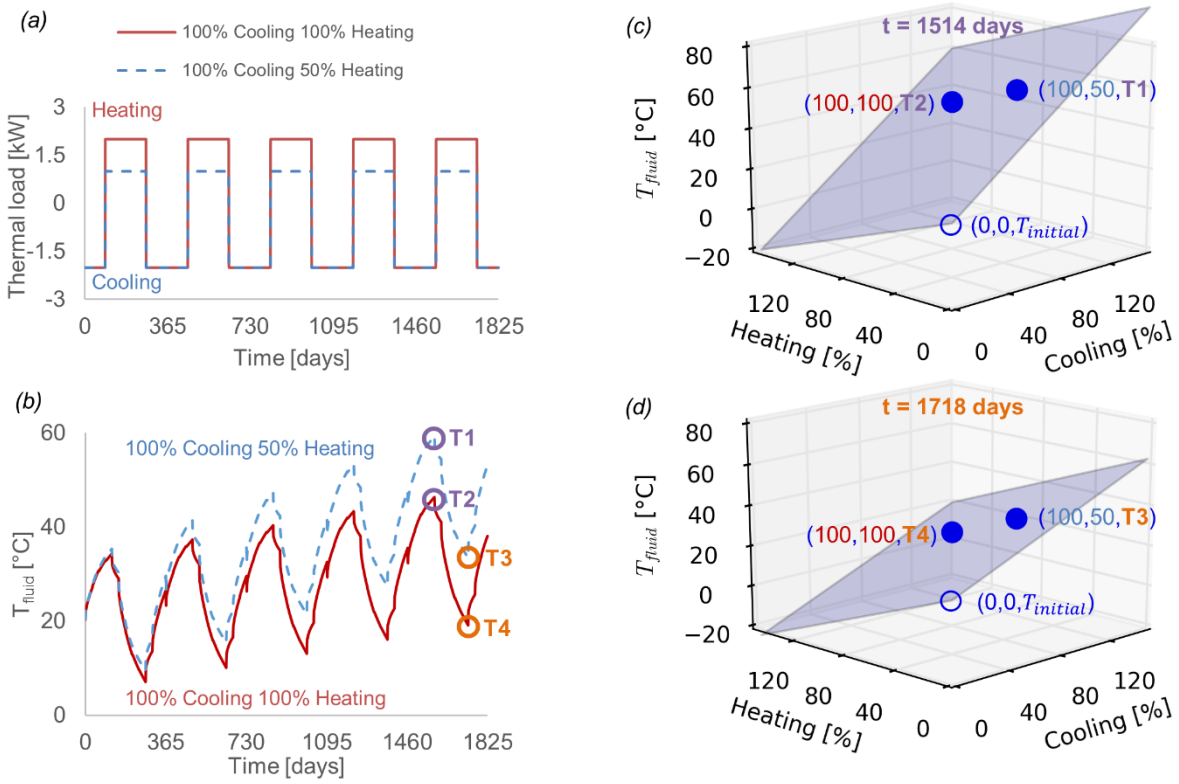


Figure 3 Example of creating the prediction model plane(s)

3 Prediction model evaluation methodology

This section presents the tools used to evaluate the accuracy of the prediction methodology presented. Firstly, an overview of the finite element modelling used to generate the numerical simulations is given, including the details of the case study adopted, such as the geometry and material parameters used. An explanation of the thermal loads adopted in the testing is also presented, showing how the percentages of cooling and heating are calculated. Lastly, a more comprehensive expanded evaluation procedure is presented, which varies 4 important design parameters to show the applicability of the prediction model for different site conditions, such as retaining wall geometries and soils around the world.

3.1 Finite element modelling of the energy diaphragm wall

In this study, finite element methods are used alongside the proposed prediction model as outlined in section 2. The numerically produced data are used to create the planes used for the predictions as well as to evaluate the methodology's accuracy. The experimentally validated 3D finite element numerical approach used, developed at the University of Melbourne, uses the software package COMSOL and couples the governing equations of heat transfer (energy balance) and fluid flow (momentum and continuity). In the application of geothermal systems, heat conduction occurs primarily in the soil, concrete, HDPE pipe wall and partially in the carrier fluid, while heat convection is dominant in the carrier fluid. The fluid flow equations relate to the carrier fluid within the pipes, as no groundwater movement is considered in this study. More detailed descriptions of this finite element methodology, including validation, can be found in the literature [38–41]

The presented prediction methodology can be used with any energy geo-structure system, such as energy piles, tunnels or walls. However, for the purposes of demonstrating this approach, as well as evaluating it, energy diaphragm retaining walls are adopted as a case study. The numerical finite element model utilised in this work can be seen in Figure 4, highlighting the model size and boundary conditions. As it can be seen, the symmetry condition is used along the *zx* and *zy* planes, to minimise the model size and computational time required. Symmetry along the *zx* plane represents the other half of the underground building with another activated retaining wall section opposite to the modelled one, while symmetry along the *zy* planes represents a continuously activated retaining wall along the *x* direction, which is a conservative approach taking into account thermal effects from nearby HDPE circuits. Moreover, thermal insulation is used at the top (assuming city centre buildings and roads, as well as being a conservative approach [42]) and bottom surfaces of the model (note that a farfield temperature would render similar results), as well as at the retaining wall and slab surfaces inside the underground building, to ensure no thermal leaking into/out of the building [43]. The latter ensures that the ground and the interior of the building are thermally separated such that, for example, as the temperature of the ground and concrete elements rises due to a cooling load, heat is not leaked into the building directly through the wall elements but instead is transferred towards the ground as intended. Lastly, a farfield temperature of 18.3 °C has been applied on the *zx* surface furthest from the energy wall, expecting that no thermal effects will reach at a distance over 100 m away.

<Figure 4 around here>

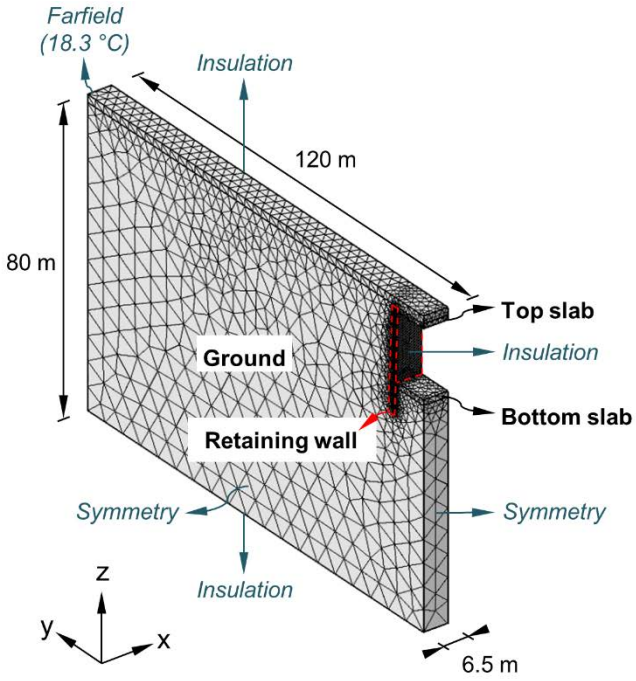


Figure 4 Finite element model

Geothermal HDPE pipes are embedded in the diaphragm retaining walls and connected to a GSHP to provide part of the thermal energy requirements of the building. A 6.5-metre-wide section of the retaining walls is modelled, containing one of the pipe circuits. The geometry utilised for the energy diaphragm wall models can be seen in Figure 5 and a summary of the material properties is presented in Table 1, noting that certain dimensions (L_{wall}, s) and properties (λ_{ground}, $\lambda_{concrete}$) are varied in later parts of the presented work. For clarity, a specific case having these parameters fixed is presented first,

while a more comprehensive analysis that varies the parameters is outlined in section 3.3. In the first case, the parameters used are λ_{ground} = 1 W/(mK), $\lambda_{concrete}$ =1.5 W/(mK), L_{wall} = 10 m and s = 0.45 m. Regarding the pipe configuration, seen in Figure 5, the pipes are placed such that the carrier fluid follows a meandering path into/down the wall, and after the meandering pipe has reached the bottom end of the wall, it returns through a straight vertical path upwards, via the return pipe, connected to the most bottom horizontal pipe leg. Lastly, it should be noted that the flow rate of the carrier fluid used throughout the analysis is 5.5 L/min, to allow time for the thermal transfer to take effect, and each simulation duration is five years, to incorporate thermal accumulation over the years and evaluate the prediction model's accuracy in accounting for these effects.

<Figure 5 around here>

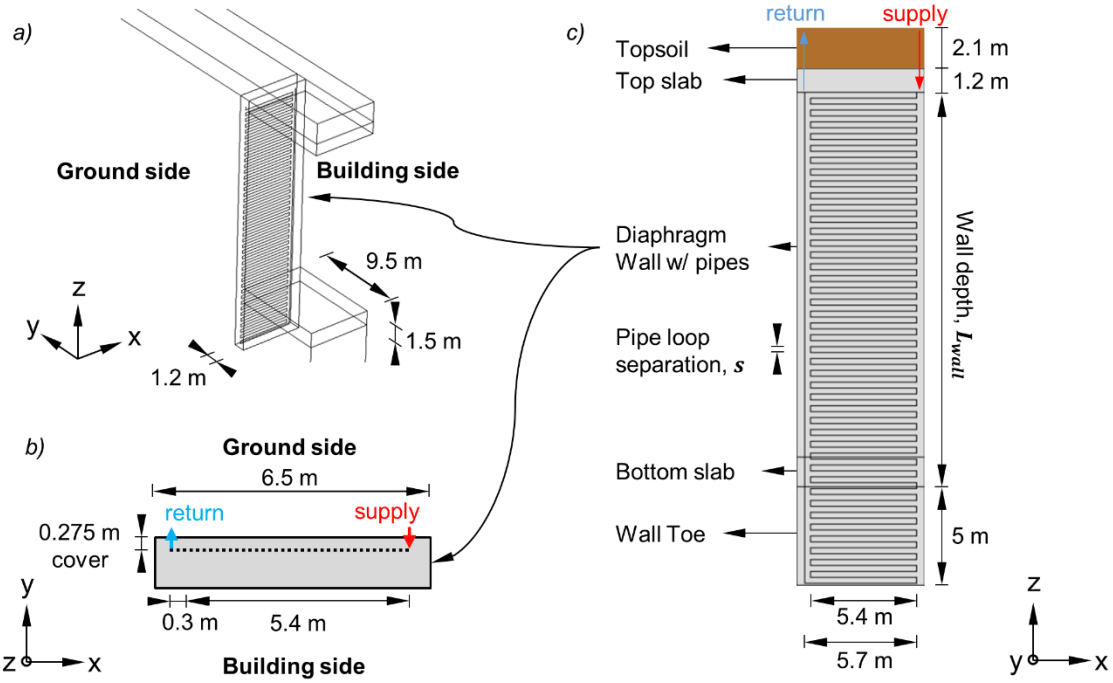


Figure 5 Model geometry

Table 1 Material properties

Parameter	Value(s)	Unit	Description
λ_{ground}	1*	W/(mK)	Thermal conductivity of ground
ρ_{ground}	2400	kg/m^3	Density of ground
$C_{p\ ground}$	830	J/(kgK)	Specific heat capacity of ground
$\lambda_{concrete}$	1.50*	W/(mK)	Thermal conductivity of concrete
$\rho_{concrete}$	2250	kg/m^3	Density of concrete
$C_{p\ concrete}$	890	J/(kgK)	Specific heat capacity of concrete
$T_{farfield}$	18.3	°C	Average annual ground temperature
λ_{fluid}	0.58	W/(mK)	Thermal conductivity of carrier fluid
ρ_{fluid}	998	kg/m^3	Density of carrier fluid
$C_{p\ fluid}$	4185	J/(kgK)	Specific heat capacity of carrier fluid

**In expanded analysis these parameters are varied as presented in section 3.3 and Table 3.*

3.2 Thermal loading

The proposed prediction approach involves estimating the geothermal system's thermal performance, for different combinations of thermal load, meaning different combinations of cooling and heating energy provided. Figure 6 shows two such combinations: distribution 1C1H represents 100% of the cooling and heating energy demand and distribution 0.5C1H represents 50% of the cooling and 100% of the heating energy demand (compared to distribution 1C1H). As it can be seen, by lowering (or increasing) the percentage of cooling or heating the system can provide, the respective thermal demand for each day decreases (or increases) by that percentage (i.e. scaling the entire distribution by the respective percentage in heating or cooling – in this case cooling is demonstrated). In the case of adopting a constant heating or cooling load with this approach, the reduction (or increase) will be uniform for all days.

<Figure 6 around here>

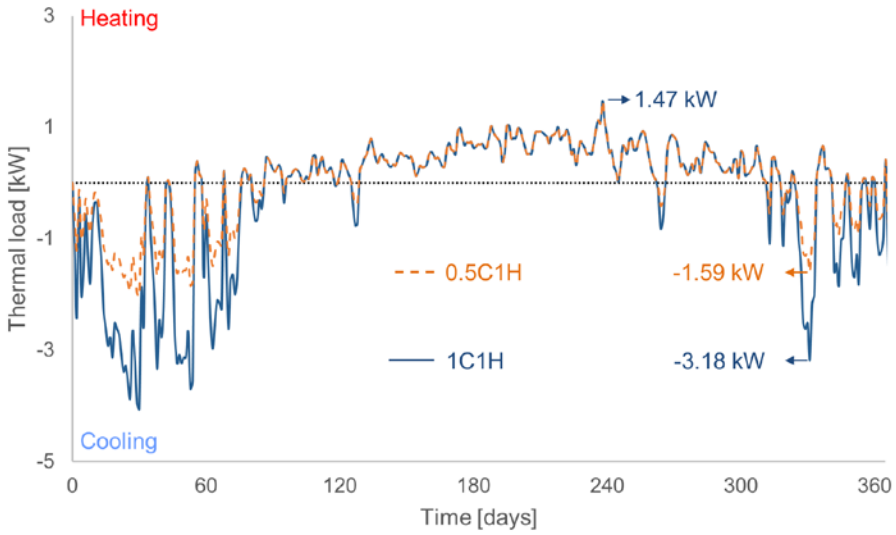


Figure 6 Thermal Load distribution per energy wall section – one pipe circuit

For the analysis presented in this work, seven different combinations of the daily varying thermal load distribution are utilised. These combinations can be seen in Table 2, noting that distributions 1C1H and 0.5C1H are shown in Figure 6. These two distributions are used for creating the prediction plane (as explained in section 2.2), while the other five are used to test the accuracy of the model, i.e., to compare the results of the expensive FEM simulations to those of the inexpensive predictive model.

Table 2 Thermal load distribution combinations

Label Purpose	1C1H Train	0.5C1H Train	1C0.5H Test	0.5C0.5H Test	0.8C0.4H Test	0.45C0.65H Test	1.25C1.25H Test
Cooling (%)	100	50	100	50	80	45	125
Heating (%)	100	100	50	50	40	65	125

3.3 Evaluation under different site conditions

In order to undertake a more complete evaluation, the potential effect of key design parameters on the prediction model's accuracy is examined, by selecting a range of values representing a gamut of commonly encountered site conditions and wall geometries as shown in Table 3. Firstly, amongst the most influencing parameters on the thermal performance of GSHP systems, the parameters that are selected to vary are the thermal conductivity values for both the ground and the concrete in the wall, varying from 0.5 to 4.0 W/(mK) and from 1.5 to 2.5 W/(mK) respectively. These values represent typical ranges for common soil/rock and concrete types, making the validation applicable for most parts of the world [44–47]. The other two parameters used for the expanded analysis are the depth of the wall and the vertical separation between the pipe legs/loops. These two relate more to the geometry of the system (instead of the materials) and represent the amount of soil volume around the wall (L_{wall}), the effect of thermal interference between the pipe legs (s) and the total length of pipe that can be incorporated into the structure (L_{wall} *and* s). Since both parameters affect the total HDPE pipe length per circuit, this value for each combination of the two can be found in Table 4. Overall, 360 total combinations of the presented parameters are studied, utilising the values in Table 3. For each combination, a total of seven numerical simulations are computed, one for each thermal load distribution as outlined in section 3.2. Therefore, a total of 2,520 numerical models are created and solved, providing the data utilised in this evaluation and showing the applicability of the prediction model for a variety of different conditions.

Table 3 Design parameter values for different site and wall conditions analysis

Parameter	Value(s)	Unit	Description
λ_{ground}	0.5, 1.0, 2.1, 3.0, 3.5, 4.0	W/(mK)	Thermal conductivity of ground
$\lambda_{concrete}$	1.5, 1.75, 2.0, 2.25, 2.5	W/(mK)	Thermal conductivity of concrete
L_{wall}	5, 10, 20, 30	m	Depth of the wall, excl. toe embedment
s	0.10, 0. 30, 0.45	m	Vertical separation between pipe legs

Table 4 Total pipe circuit length per wall section modelled for different values of L_{wall} and s

s [m]	0.10	0.30	0.45
L_{wall} [m]	Total pipe length [m]		
5	555	198	133
10	835	294	208
20	1395	498	347
30	1955	690	485

4 Results and Discussion

This section utilises the outputs of 2,520 solved numerical simulations (each requiring a running time between 1-3 hours utilising high performance computing) to present a thorough evaluation of the prediction methodology, starting from a specific set of design parameters and continuing to an expanded overall evaluation for all 360 possible parameter combinations (i.e., all possible combinations of λ_{ground}, $\lambda_{concrete}$, L_{wall}, s for the values in Table 3). The effect of the fluid temperature magnitude on the accuracy

of the model is also investigated, as well as the choice of which thermal load distributions to be used for training/creation of the prediction model. Finally, the relationships between these design parameters and the *A* and *B* cooling and heating factors of the prediction equation are investigated, showing that, with sufficient data, these factors could be predicted numerically/semi-analytically, eliminating the need for any costly numerical simulations.

4.1 Evaluation for a specific case

As explained in section 3.1, the first analysis involves fixed values for the four design parameters: λ_{ground} = 1 W/(mK), $\lambda_{concrete}$ =1.5 W/(mK), L_{wall} = 10 m and s = 0.45 m. Using these parameters and the methodology explained in sections 3.1 and 3.2, the FEM simulations are run for 1C1H and 0.5C1H and used to create the prediction models (planes) for any time-step of the simulations. Figure 7 shows example planes for days 1514 and 1718 (a prediction model or plane can be generated for any other time-step), where the blue circles are the points used to create the plane and the red stars are the points used to test its accuracy (both circles and stars being values obtained by the FEM simulations). It is also worth noting that the created planes cover any range of heating and cooling percentages, not all of which would be realistically considered in the final geothermal design, for instance those combinations of heating and cooling demands rendering average fluid temperatures above 35-40 °C. Using these two prediction planes, the error between the value obtained by the plane $T^{t,load}_{fluid,predicted}$ (when the cooling and heating percentages are entered in Equation (1)) and the value obtained by finite element simulations $T^{t,load}_{fluid,FEM}$ can be calculated for each different testing thermal load distribution. The error is measured as the absolute difference between the two resulting temperatures, which is the vertical distance from the test points (red stars) to the surface of the plane:

$$Error(t, load) = \left| T^{t,load}_{fluid,predicted} - T^{t,load}_{fluid,FEM} \right| \quad (3)$$

<Figure 7 around here>

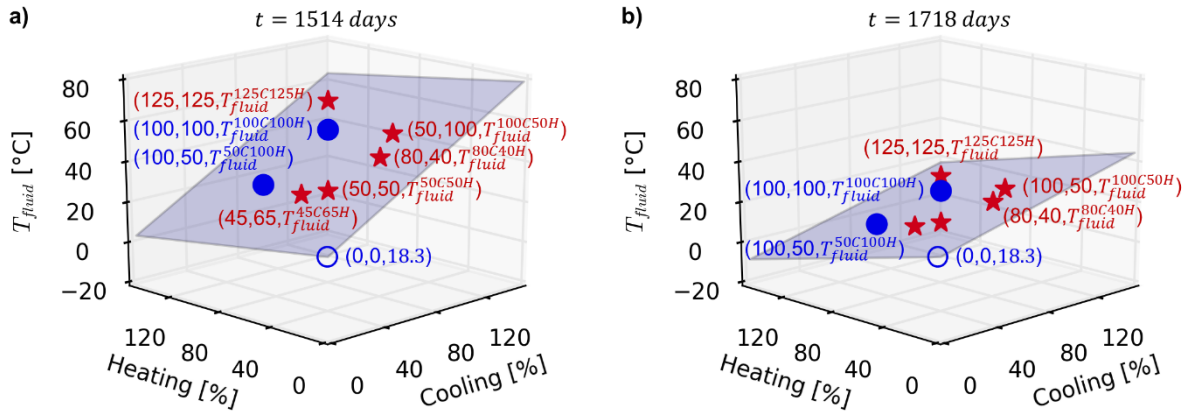


Figure 7 Creation/training and testing points for the prediction plane at time-steps t=1514 days and t=1718 days

The results for this set of parameters, summarised in Table 5, show insignificant errors between the predicted and simulated values of less than 0.05 °C. This shows that, in this case, using the very fast (~secs) prediction model to calculate the fluid temperatures through the plane equations would result in extremely similar values compared to those obtained through running expensive numerical simulations (~hours/days) and therefore the latter could be avoided to save time and computational resources.

Table 5 Absolute error (°C) in predictions for the specific case study

Label	1C1H	0.8C0.4H	0.45C0.65H	1.25C1.25H	0.5C0.5H
Absolute Error (t=1514 days):	0.02	0.03	0.02	0.00	0.03
Absolute Error (t=1718 days):	0.01	0.01	0.02	0.00	0.03

4.2 Evaluation for different site conditions

Following the demonstration of the predictive model's capability for a specific case, a total of 360 combinations of the design parameters (λ_{ground}, $\lambda_{concrete}$, L_{wall}, s) are utilised in a more comprehensive evaluation (as explained in section 3.3 and shown in Table 3). The results presented in section 4.1 represent only one such combination. An overview of the results for all combinations is shown in Table 6, highlighting the average, minimum and maximum errors among the 360 parameter combinations, for each testing thermal load distribution. For example, when the 1C0.5H thermal load distribution is adopted, the average error between the predicted and computed temperature over 360 cases with different ground and concrete thermal conductivities and wall and pipe geometries is just 0.11 °C. Figure 8 shows a comparison of all temperature values obtained through the prediction model against those obtained through numerical simulations with finite elements, illustrating a close to perfect correlation between the two approaches. Figure 9 shows the entirety of the calculated absolute errors for each parameter combination. Each subplot represents a specific time in the simulation and shows 5 histograms, one for each testing thermal load distribution, indicating the magnitude of the absolute errors. As it can be seen, in general the error distributions are skewed to the right, meaning that most of the errors are very close to the value of zero. The distributions least skewed are 1C0.5H and 0.8C0.4H, which produced the largest errors, as also shown in Table 6, with most of the errors being between 0.05 and 0.1 °C. Overall, the absolute errors throughout the investigation for all possible combination of the chosen design parameters are in general very low, with the mean values for all testing distributions being less than 0.15 °C. The highest error encountered throughout the entire analysis is 0.66 °C, when the 1C0.5H distribution is used to predict the fluid temperature at *t=1514 days*, with parameters λ_{ground}=0.5 W/(mK), $\lambda_{concrete}$=1.75 W/(mK), L_{wall}=5 m, s=300 mm. For GSHP system design using energy geo-structures, the presented errors are very acceptable and the model can (very quickly) provide the user with a very good estimate on the performance of the system, which can then be verified with a final numerical simulation.

Table 6 Prediction errors (°C) for each thermal load distribution at two particular times

Label	1C0.5H	0.8C0.4H	0.45C0.65H	1.25C1.25H	0.5C0.5H
Time:	$t = 1514\ days$				
Average:	0.11	0.11	0.04	0.03	0.05
Min:	0.00	0.00	0.00	0.00	0.00
Max:	0.66	0.55	0.15	0.21	0.21
Time:	$t = 1718\ days$				
Average:	0.08	0.08	0.04	0.03	0.05
Min:	0.00	0.00	0.00	0.00	0.01
Max:	0.35	0.32	0.14	0.17	0.22

<Figure 8 around here>

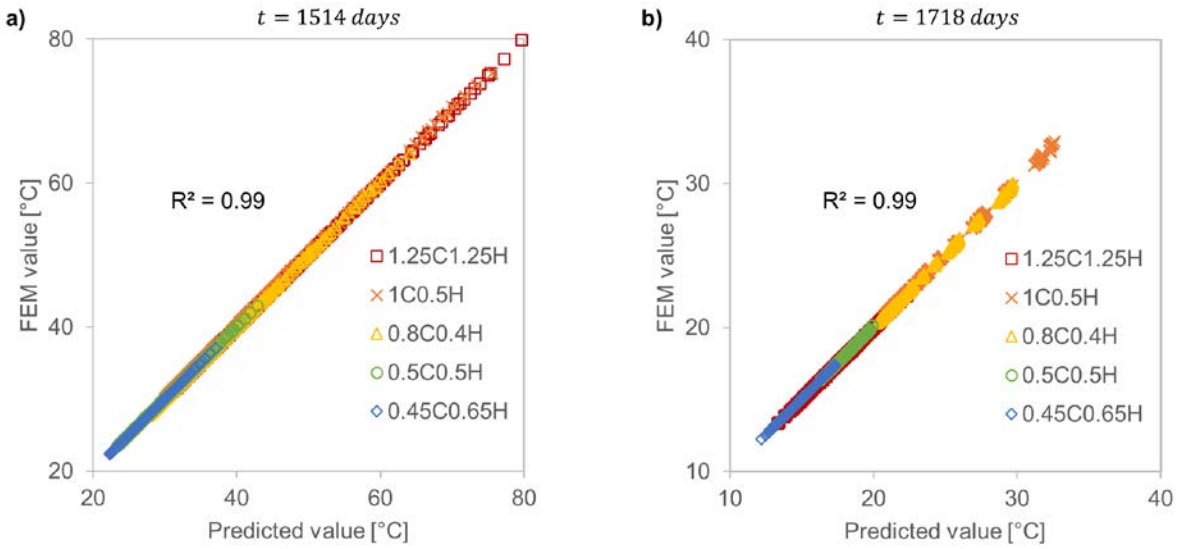


Figure 8 Predicted temperature values plotted against values obtained via full FEM simulations, for each thermal load distribution and each combination of design parameters

<Figure 9 around here>

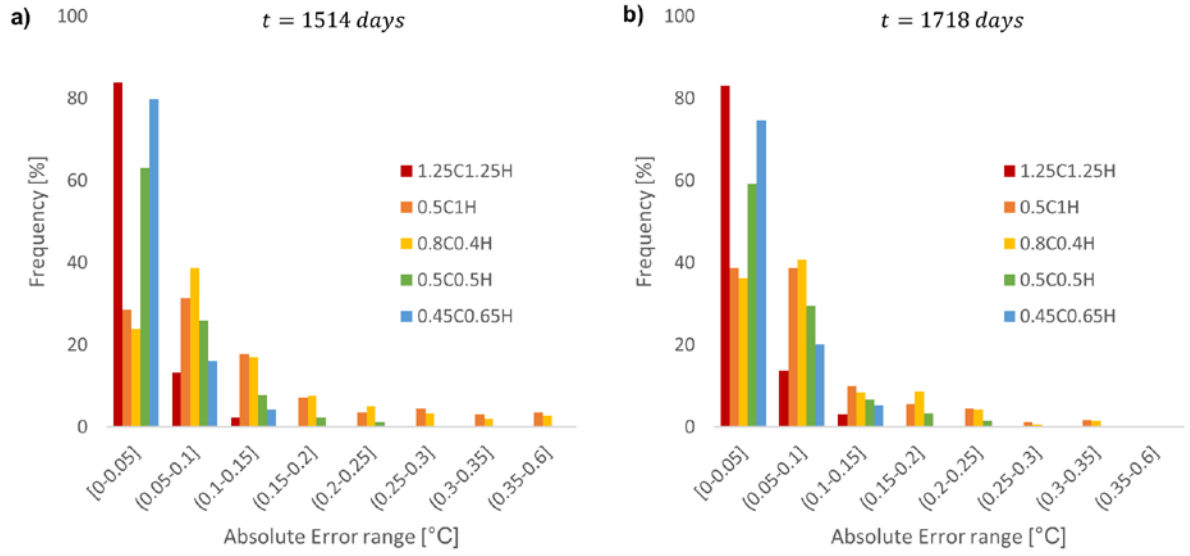


Figure 9 Absolute error for each thermal load distribution and each combination of design parameters at two particular times

It is also useful to investigate how the magnitude of the fluid temperature affects the prediction model's accuracy and whether there is a significant correlation between the two. Figure 10 shows the relationship between the absolute error and the average fluid temperature values, for distributions 1C0.5H and 0.8C0.4H at *t=1514 days* (highest temperature reached over 5-year simulation). These two distributions are chosen to illustrate the effect since they are the cases that produced the overall highest errors; however, similar trends are present in the other distributions as well. As it can be seen, there are indications of a correlation between the two parameters, as higher values of the fluid temperature tend to produce higher errors. What is important to note is that the highest values for the absolute error occur only for very high temperatures, over 40 °C (upper right corner of each plot – red shaded areas). This range of temperatures would be unacceptable for design and it is only included for completeness, due

to the nature of this investigation and the large scale of examined possibilities and values for the design parameters. Moreover, for these reasons, ineffective values for design parameters that result in high fluid temperatures (for example for λ_{ground} = 0.5 W/(mK) and L_{wall} = 5 m) show higher errors, compared to more reasonable/beneficial values. Therefore, if only a realistic range of fluid temperatures is considered the expected errors are further lowered.

<Figure 10 around here>

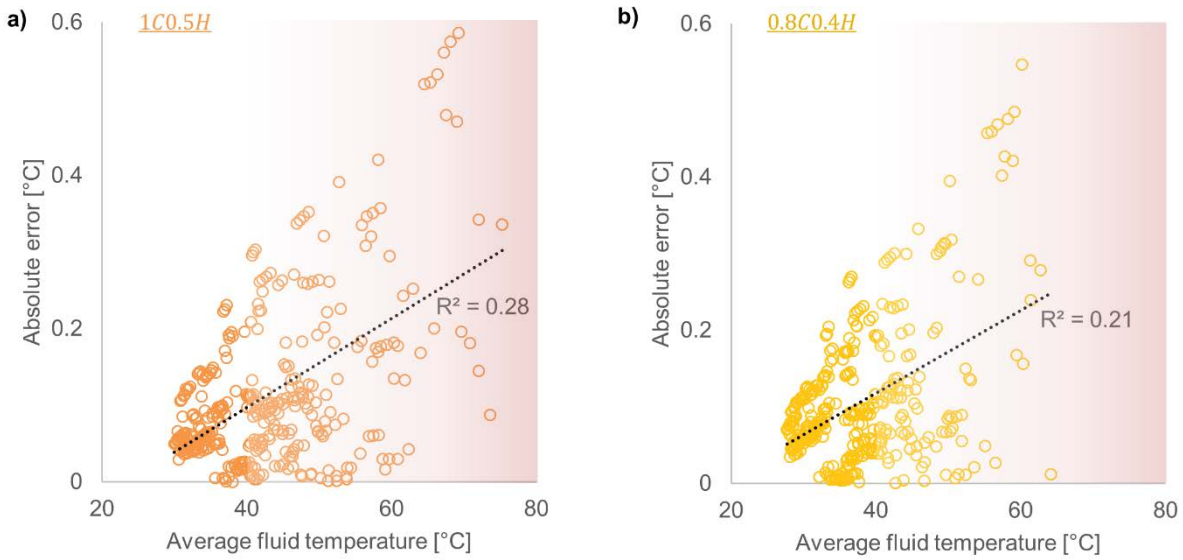


Figure 10 Average fluid temperature against the absolute error for distributions (a) 1C0.5H and (b) 0.8C0.4H at t=1514, for all parameter combinations (red areas – unrealistic situations included for completeness)

4.3 Using different training thermal load distributions

The evaluations presented throughout section 4 use the same two thermal load distributions (1C1H and 0.5C1H) to train the model, i.e. obtain data to create the prediction plane. Therefore, it is worth investigating how different the results are if other distributions are used to create the prediction plane, instead. This section uses distributions 0.5C0.5H and 0.45C0.65H to train the model and the remaining five distributions to test the model. These distributions are chosen due to the fact that the 3 points that are used to create the plane, are much closer together than the three points used to create the plane throughout the rest of the paper, which is expected to result in higher errors. The different distributions/points used are illustrated in Figure 11, where the plane shown in section 4.1 is presented with the training distributions used throughout the rest of the paper, which are reasonably far apart, (a) and the ones adopted in this section, which are closer together (b).

<Figure 11 around here>

Table 7 shows the overall prediction error results using this approach, for the same two time-steps used in previous analyses. As it can be seen, the resulting errors are slightly higher than those in Table 6, as expected, since the model now has to predict points that are much further away than those used to create it. However, despite this fact, the magnitude of these errors is very low suggesting that the model's accuracy is relatively insensitive to the choice of thermal load distributions used to create the prediction plane. This is encouraging since, even though the further away the training points are the more accurate the predictions, the difference is of little significance, which therefore leaves the choice of the training

thermal load distributions to the user and their availability, It should be noted again here, that the 2 chosen training thermal load distributions, cannot lie on the same line (for example 50% Cooling 50% Heating and 100% Cooling 100% Heating), as this would not hold enough information about the change in the *x* and *y* directions for the prediction plane to be successfully created.

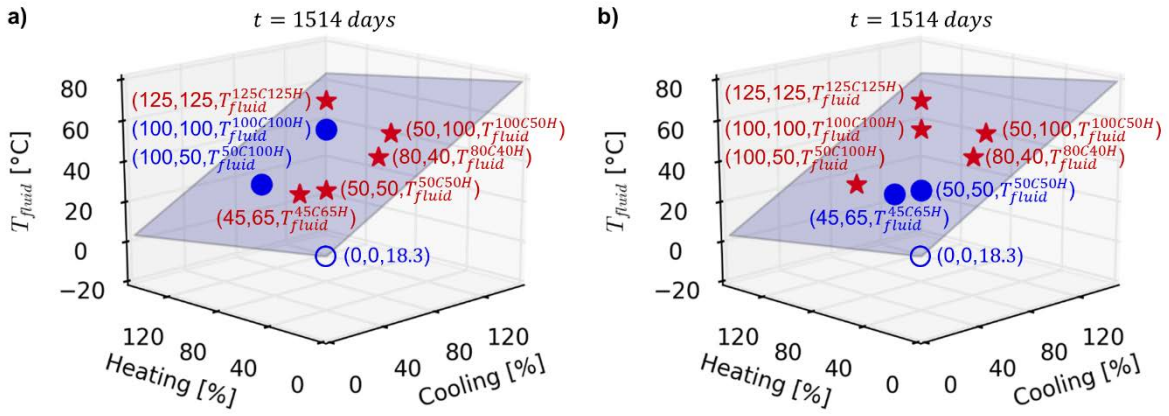


Figure 11 Using different thermal load distribution to create the prediction plane (blue circles – training/creating points, red stars – testing points): (a) using 3 points reasonably far away (b) using 3 points closer together

Table 7 Prediction errors (°C) for each thermal load distribution, when training the prediction plane with 0.45C0.65H and 0.5C0.5H.

Label	1C1H	1C0.5H	0.5C1H	0.8C0.4H	1.25C1.25H
Time:	$t = 1514\ days$				
Average:	0.10	0.13	0.04	0.10	0.15
Min:	0.01	0.00	0.00	0.00	0.03
Max:	0.41	0.70	0.22	0.58	0.62
Time:	$t = 1718\ days$				
Average:	0.11	0.11	0.03	0.07	0.17
Min:	0.02	0.00	0.00	0.00	0.04
Max:	0.44	0.48	0.16	0.29	0.66

4.4 The effect of design parameters on the cooling and heating factors A and B

The numerical values of A and B in Equation (1) are dependent on all the design parameters for the GSHP system, including the geometry of the GHEs, the configuration of the pipes and the values of the material properties. In this study, four key design parameters were varied to perform a comprehensive evaluation of the prediction methodology introduced here. Using all the different combinations of these parameters, their effect on A and B can be investigated, for example, seeing how different the GSHP system response would be at different locations (with materials of different thermal conductivities) or using different geometries (recall section - table). The time $t = 1514\ days$ is adopted in the analysis (as it is expected to yield the highest fluid temperatures and thus considered critical), however, any other time could also be used. The results are shown in Figure 12 for the cooling factor A . In each plot the red circles represent the values obtained by fitting the plane and each set of points linked by a line represents one unique combination of the other three design parameters (for example, when λ_{ground} =1.0 W/(mK), L_{wall} = 10 m and s = 0.45 m the points for each value of $\lambda_{concrete}$ from one line in Figure 12 (a)). Moreover, in each plot an equation is given that can be sufficiently fit to any of the lines, by varying the coefficients x_i, x_j, x_k where applicable.

<Figure 12 around here>

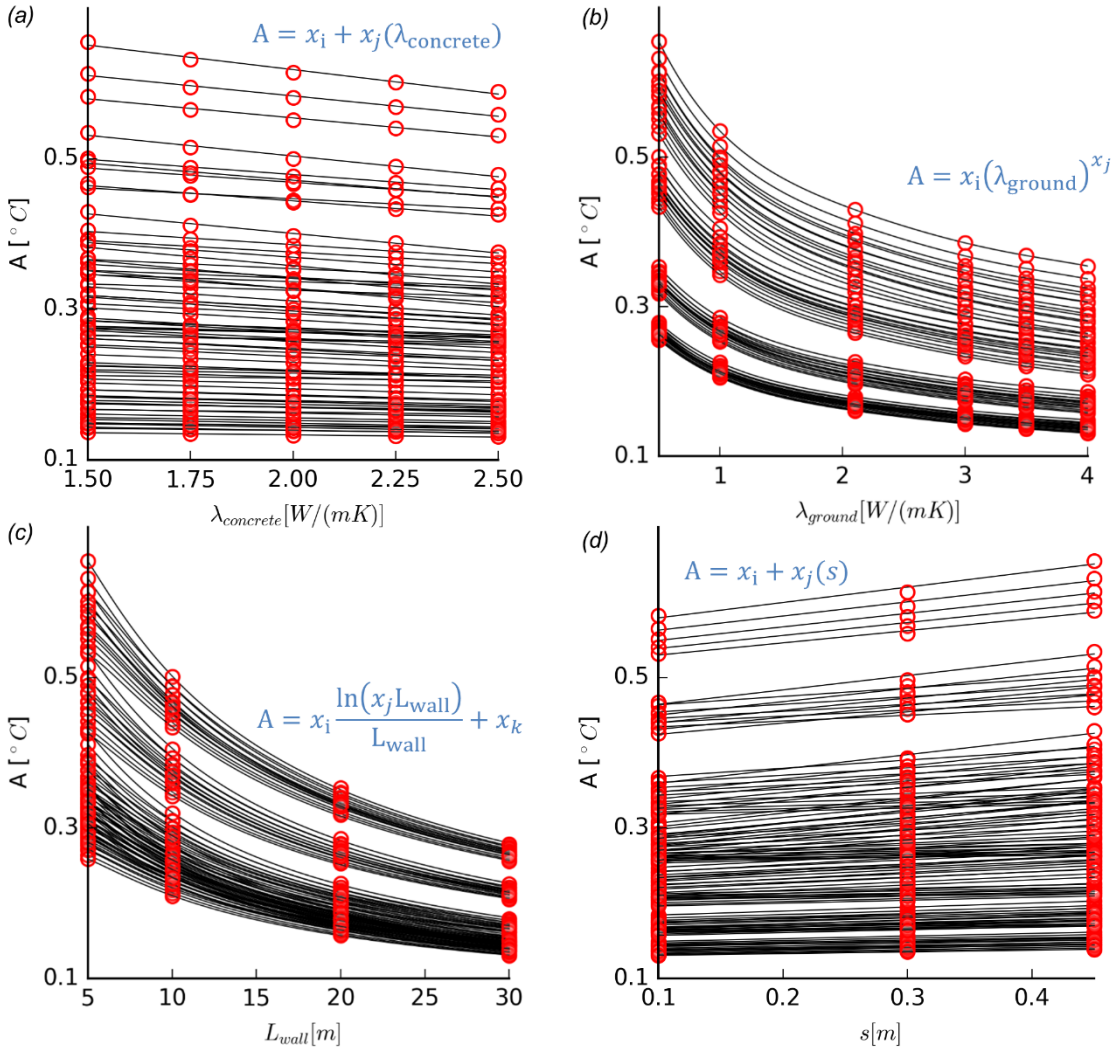


Figure 12 The effect of each studied design parameter on the value of cooling coefficient A

It is clear that there exist significant relationships within the design parameters and the resulting factors. This figure suggests that with sufficient information, the coefficients *A* and *B* could be calculated from the values of the appropriate design parameters, removing the need to run numerical simulations every time. For example, using the four design parameters investigated in this work and combining their respective relationships with *A*, for any of the 360 combinations utilised, *A* could be very well estimated, using Equation (4). It should be noted that even though *A* is adopted to illustrate these relationships, similar patterns exist for the heating coefficient *B* as well, whose predictive relationship is shown in Equation (5). Figure 13 shows how well Equations (4) and (5) can predict *A* and *B* respectively, displaying the mean absolute error (MAE) value as well as the regression coefficient (R^2).

$$A = (x_1 + x_2 s) * \lambda_{ground}^{x_3 + x_4 \lambda_{concrete}} * [(1 + x_5 s) * (1 + x_6 \lambda_{concrete}) * \frac{ln(x_7 L_{wall})}{L_{wall}} + x_8] \quad (4)$$

where $x_1 = 1.62$, $x_2 = -4.63 \cdot 10^{-1}$, $x_3 = -2.99 \cdot 10^{-1}$, $x_4 = -1.23 \cdot 10^{-2}$, $x_5 = 8.98 \cdot 10^{-1}$, $x_6 = -8.58 \cdot 10^{-2}$, $x_7 = 7.70 \cdot 10^{-1}$, $x_8 = 3.66 \cdot 10^{-2}$

$$B = (x_1 + x_2 s) * \lambda_{ground}^{x_3 + x_4 \lambda_{concrete}} * [(1 + x_5 s) * (1 + x_6 \lambda_{concrete}) * \frac{ln(x_7 L_{wall})}{L_{wall}} + x_8] \quad (5)$$

where $x_1 = -4.94 \cdot 10^{-1}$, $x_2 = -2.01 \cdot 10^{-1}$, $x_3 = -5.63 \cdot 10^{-1}$, $x_4 = -1.67 \cdot 10^{-2}$, $x_5 = -3.25 \cdot 10^{-1}$, $x_6 = -4.52 \cdot 10^{-2}$, $x_7 = 5.27 \cdot 10^{-1}$, $x_8 = 3.62 \cdot 10^{-2}$

<Figure 13 around here>

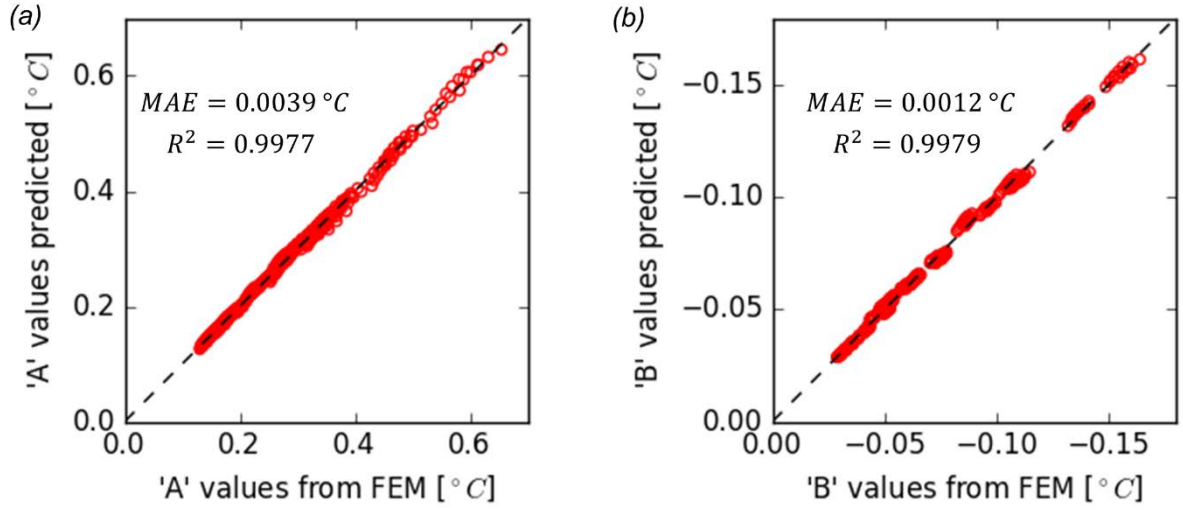


Figure 13 Accuracy of equations (4) and (5) on predicting the cooling coefficient A and B respectively

Furthermore, a useful toolset that can alternatively be adopted for obtaining A and B as function of the four key design parameters is machine learning prediction algorithms, such as "Random Forests" [48] or "Gradient Boosting" [49]. These algorithms can be used to create prediction models, which, after being trained with sufficient data, can predict the numerical values of A and B for a given thermal load distribution from the chosen design parameters for the system. Even though only four of these parameters are investigated in this work, many more could be incorporated to create a more complete model. In this case, the generated data were used to train a prediction model with each of these two algorithms. The 10-fold cross-validation technique was utilised to evaluate their predictions (which separates the dataset to 10 equal parts, excludes 1 of those in the training and uses it to test the algorithm, doing it iteratively 10 times once for each part), resulting in the averaged values shown in Table 8. As it can be seen, the mean absolute error (MAE) is very low and the regression coefficient (R^2) is close to 1 for both algorithms, which suggests very good fits. Moreover, the "feature importance" information is shown, which signifies how important each design parameter was considered by the algorithm in obtaining the value for A. The order of importance is identified with the less significant "importance score" given by the algorithm shown is brackets. In this case, even though the order of importance is not identical, both algorithms agree that λ_{ground} and L_{wall} are the two most important parameters, as it is also suggested by Figure 12.

Table 8 Using machine learning algorithms to predict the cooling coefficient A

Algorithm	$\boldsymbol{MAE}$ $[°\boldsymbol{C}]$	$\boldsymbol{R^2}[-]$	**Feature importance**			
			$\lambda_{concrete}$	λ_{ground}	L_{wall}	s
Random Forests	0.0065	0.9915	4th (0.0070)	2nd (0.4340)	1st (0.5455)	3rd (0.0130)
Gradient Boosting	0.0005	0.9983	4th (0.1290)	1st (0.4331)	2nd (0.2640)	3rd (0.1739)

Overall, this section shows that A and B are both functions of the design parameters and that the underlying relationships could be estimated with enough data and models. This could lead to the creation of guidelines, such as charts or machine learning models/programs, to be used and eliminate the need for numerical modelling entirely. This would mean that for a specific energy geo-structure and based on the parameters of the site such as the ones presented above or including others, fast estimations of A and B and therefore T_{fluid}, for any combination of a specified thermal load distribution would be achieved instantly. More detailed investigations in this topic are expected to be undertaken in future work. This paper however, presented the first steps towards this goal with a simpler yet robust methodology that uses only two detailed FEM simulations to still considerably speed up the design of energy geo-structures.

5 Summary and Conclusions

This work presented a prediction methodology that can be used alongside numerical simulations to greatly hasten and ease the design process for energy geo-structures. The methodology uses a simple but robust prediction model created using results from two numerical simulations and can aid in calculating how much thermal energy the GSHP system can reliably provide. This work selected energy retaining walls as a case study to perform the evaluation of the prediction model; however, it is expected that this approach can be used with any type of energy geo-structure.

An evaluation of the prediction methodology has been presented, utilising over 2,500 different scenarios, to compare the results of the prediction model to those obtained through the FEM simulations, which currently is the popular alternative approach. The results show excellent performance for the prediction model, with absolute error values of mostly less than 0.2 °C and in the most extreme cases less than 0.6 °C, showing that the proposed methodology can confidently be used to complement numerical simulations and greatly reduce the computational resources and time. The choice of the thermal load distributions used to create the prediction plane has also been investigated, showing an insignificant effect and therefore allowing flexibility in the selection of the training data.

Lastly, the equation cooling and heating factors A and B have been investigated, showing their underlying relationships with the design parameters and therefore their dependency on them. The analysis suggests that, given sufficient numerical simulation data and for specific thermal load distributions and structure types, it would be possible to estimate/calculate these factors based on the design parameters of each site, as demonstrated in this work using equation fitting or machine learning algorithms. This would then eliminate the need for any numerical simulations and even greater decrease the required time and resources. With a fully developed suite of semi-analytical predictive models based on the methodology presented here (using results from hundreds of FE simulations that account for many possible combinations), the amount of thermal energy an energy geo-structure system can provide could be identified in seconds, requiring as input the relevant information such as the geometry of the geo-structure and the thermal parameters of the materials (ground, concrete). This aspect of the presented study is expected to more thoroughly be investigated in future work.

6 Acknowledgements

Funding from the Australian Research Council (ARC) FT140100227, The University of Melbourne, the Cambridge Centre for Smart Infrastructure and Construction (via the Global University Alliance), and the Victorian Government is much appreciated.

7 References

[1] I.W. Johnston, G.A. Narsilio, S. Colls, Emerging geothermal energy technologies, KSCE J. Civ. Eng. 15 (2011) 643–653. doi:10.1007/s12205-011-0005-7.

[2] D. Banks, An Introduction to Thermogeology: Ground Source Heating and Cooling, Wiley - Blackwell, 2008.

[3] G. Florides, S. Kalogirou, Ground heat exchangers-A review of systems, models and applications, Renew. Energy. 32 (2007) 2461–2478. doi:10.1016/j.renene.2006.12.014.

[4] M. Preene, W. Powrie, Ground energy systems: from analysis to geotechnical design, Géotechnique. 59 (2009) 261–271. doi:10.1680/geot.2009.59.3.261.

[5] S. Lazzari, A. Priarone, E. Zanchini, Long-term performance of BHE (borehole heat exchanger) fields with negligible groundwater movement, Energy. 35 (2010) 4966–4974. doi:10.1016/j.energy.2010.08.028.

[6] S. Colls, Ground Heat Exchanger Design For Direct Goethermal Energy Systems, The University of Melbourne, 2013.

[7] H. Brandl, Energy foundations and other thermo-active ground structures, Géotechnique. 56 (2006) 81–122. doi:10.1680/geot.2006.56.2.81.

[8] H. Brandl, Geothermal Geotechnics for Urban Undergrounds, Procedia Eng. 165 (2016) 747–764. doi:10.1016/j.proeng.2016.11.773.

[9] B.L. Amatya, K. Soga, P.J. Bourne-Webb, T. Amis, L. Laloui, Thermo-mechanical behaviour of energy piles, Géotechnique. 62 (2012) 503–519. doi:10.1680/geot.10.P.116.

[10] P.J. Bourne-Webb, T.M. Bodas Freitas, R.A. Da Costa Gonçalves, Thermal and mechanical aspects of the response of embedded retaining walls used as shallow geothermal heat exchangers, Energy Build. 125 (2016) 130–141. doi:10.1016/j.enbuild.2016.04.075.

[11] A. Di Donna, F. Cecinato, F. Loveridge, M. Barla, Energy performance of diaphragm walls used as heat exchangers, Proc. Inst. Civ. Eng. - Geotech. Eng. 170 (2016) 1–14. doi:10.1680/jgeen.

[12] A. Di Donna, M. Barla, The role of ground conditions on energy tunnels' heat exchange, Environ. Geotech. 3 (2016) 214–224. doi:10.1680/jenge.15.00030.

[13] F. Loveridge, J.S. Mccartney, G.A. Narsilio, M. Sánchez, Energy geostructures: a review of analysis approaches, in situ testing and model scale experiments., Geomech. Energy Environ. (2018) under review.

[14] Q. Lu, G.A. Narsilio, Economic analysis of utilising energy piles for residential buildings, Energy. under review (2018).

[15] S. Park, C. Sung, K. Jung, B. Sohn, A. Chauchois, H. Choi, Constructability and heat exchange efficiency of large diameter cast-in-place energy piles with various configurations of heat exchange pipe, Appl. Therm. Eng. 90 (2015) 1061–1071. doi:10.1016/j.applthermaleng.2015.05.044.

[16] O. Mikhaylova, R. Choudhary, K. Soga, I.W. Johnston, Benefits and optimisation of district

hybrid ground source heat pump systems, in: F. Wuttke, S. Bauer, M. Sanchez (Eds.), Energy Geotech. - Proc. 1st Int. Conf. Energy Geotech. ICEGT 2016, CRC Press, Kiel, 2016: pp. 535–542.

[17] W. Gang, J. Wang, S. Wang, Performance analysis of hybrid ground source heat pump systems based on ANN predictive control, Appl. Energy. 136 (2014) 1138–1144. doi:10.1016/j.apenergy.2014.04.005.

[18] M. Alavy, H. V. Nguyen, W.H. Leong, S.B. Dworkin, A methodology and computerized approach for optimizing hybrid ground source heat pump system design, Renew. Energy. 57 (2013) 404–412. doi:10.1016/j.renene.2013.02.003.

[19] G.R. Aditya, O. Mikhaylova, G.A. Narsilio, J.I. W., Financial assessment of ground source heat pump systems against other selected heating and cooling systems for Australian conditions, in: IGSHPA Res. Track Conf., submitted, Stocholm, 2018.

[20] G.R. Aditya, O. Mikhaylova, G.A. Narsilio, I.W. Johnston, Financial assessment of ground source heat pump systems against other selected forms of heating and cooling, Renew. Energy. under review (2018).

[21] M. Barla, A. Perino, Energy from geo-structures: a topic of growing interest, Environ. Geotech. 2 (2015) 3–7. doi:10.1680/envgeo.13.00106.

[22] M. Barla, A. Di Donna, Energy tunnels: Concept and design aspects, Undergr. Sp. (2018). doi:10.1016/j.undsp.2018.03.003.

[23] L. Laloui, A. Di Donna, Understanding the behaviour of energy geo-structures, Proc. Inst. Civ. Eng. - Civ. Eng. 164 (2011) 184–191. doi:10.1680/cien.2011.164.4.184.

[24] J. Fadejev, R. Simson, J. Kurnitski, F. Haghighat, A review on energy piles design, sizing and modelling, Energy. 122 (2017) 390–407. doi:10.1016/j.energy.2017.01.097.

[25] GSHP Association, Thermal pile design, installation and materials standards, Milton Keynes, 2012.

[26] F. Loveridge, W. Powrie, Pile heat exchangers: thermal behaviour and interactions, Proc. ICE - Geotech. Eng. 166 (2013) 178–196. doi:10.1680/geng.11.00042.

[27] F. Loveridge, W. Powrie, G-Functions for multiple interacting pile heat exchangers, Energy. 64 (2014) 747–757. doi:10.1016/j.energy.2013.11.014.

[28] S. Kürten, D. Mottaghy, M. Ziegler, Design of plane energy geostructures based on laboratory tests and numerical modelling, Energy Build. 107 (2015) 434–444. doi:10.1016/j.enbuild.2015.08.039.

[29] D.P. Nicholson, Q. Chen, M. de Silva, A. Winter, R. Winterling, The design of thermal tunnel energy segments for Crossrail, UK., Eng. Sustain. 167 (2014) 118–134. doi:10.1680/ensu.13.00014.

[30] C. Lee, S. Park, H.-J. Choi, I.-M. Lee, H. Choi, Development of energy textile to use geothermal energy in tunnels, Tunn. Undergr. Sp. Technol. 59 (2016) 105–113. doi:10.1016/j.tust.2016.06.014.

[31] R. Katzenbach, F. Clauss, S. Lappla, T. Rupert, Potentials of environmental protection by geotechnical engineering, in: A. Anagnostopoulos (Ed.), 15th ECSMGE—Geotechnics Hard Soils, IOS Press, Athens, Greece, 2013: pp. 247–252.

[32] G.A. Narsilio, A. Bidarmaghz, M. Disfani, I.W. Johnston, N. Makasis, Shallow geothermal ('Geoexchange') feasibility study - Stage 1, Melbourne, 2016.

[33] A. Bidarmaghz, G.A. Narsilio, Heat exchange mechanisms in energy tunnel systems, Geomech.

642 Energy Environ. (2018) avail online 25 July), https://doi.org/10.1016/j.gete.2018.07.004.

643 [34] A. Bidarmaghz, G.A. Narsilio, P. Buhmann, C. Moormann, B. Westrich, Thermal interaction
644 between tunnel ground heat exchangers and borehole heat exchangers, Geomech. Energy
645 Environ. 10 (2017) 29–41. doi:10.1016/j.gete.2017.05.001.

646 [35] L.R. Ingersoll, O.J. Zobel, A.C. Ingersoll, Heat Conduction with Engineering, Geological and
647 Other Applications, University of Wisconsin Press, 1954.

648 [36] P. Eskilson, Thermal Analysis of Heat Extraction Boreholes, University of Lund, Sweden, 1987.

649 [37] L. Jun, Z. Xu, G. Jun, Y. Jie, Evaluation of heat exchange rate of GHE in geothermal heat pump
650 systems, Renew. Energy. 34 (2009) 2898–2904. doi:10.1016/j.renene.2009.04.009.

651 [38] A. Bidarmaghz, 3D Numerical Modelling of Vertical Ground Heat Exchangers, PhD Thesis,The
652 University of Melbourne, 2014.

653 [39] A. Bidarmaghz, N. Makasis, G.A. Narsilio, F. Franco, M.E.C. Perez, Geothermal Energy in
654 Loess, Environ. Geotech. 4 (2016) 225–236.

655 [40] N. Makasis, G.A. Narsilio, A. Bidarmaghz, I.W. Johnston, Carrier fluid temperature data in
656 vertical ground heat exchangers with a varying pipe separation, Data Br 18 (June), 2018, 1466-
657 1470, https://doi.org/10.1016/j.dib.2018.04.005.

658 [41] N. Makasis, G.A. Narsilio, A. Bidarmaghz, I.W. Johnston, The application of retaining walls
659 and slabs as energy structures in underground train stations, in: Int. Symp. Energy Geotech.
660 SEG-2018, Lausanne, 2018.

661 [42] A. Bidarmaghz, G.A. Narsilio, I.W. Johnston, S. Colls, The importance of surface air
662 temperature fluctuations on long-term performance of vertical ground heat exchangers,
663 Geomech. Energy Environ. 6 (2016) 35–44. doi:10.1016/j.gete.2016.02.003.

664 [43] N. Makasis, Further understanding ground source heat pump design using finite element
665 methods and machine learning techniques. PhD Thesis, The University of Melbourne; 2018.

666 [44] D. Barry-Macaulay, a. Bouazza, R.M. Singh, B. Wang, P.G. Ranjith, Thermal conductivity of
667 soils and rocks from the Melbourne (Australia) region, Eng. Geol. 164 (2013) 131–138.
668 doi:10.1016/j.enggeo.2013.06.014.

669 [45] I.N. Hamdhan, B.G. Clarke, Determination of Thermal Conductivity of Coarse and Fine Sand
670 Soils, in: World Geotherm. Congr., International Geothermal Association, Bali, Indon, 2010.

671 [46] K.Y. Shin, S.B. Kim, J.H. Kim, M. Chung, P.S. Jung, Thermo-physical properties and transient
672 heat transfer of concrete at elevated temperatures, Nucl. Eng. Des. 212 (2002) 233–241.
673 doi:10.1016/S0029-5493(01)00487-3.

674 [47] V.K.R. Kodur, W. Khaliq, Effect of Temperature on Thermal Properties of Different Types of
675 High-Strength Concrete, J. Mater. Civ. Eng. 23 (2011) 793–801. doi:10.1061/(ASCE)MT.1943-
676 5533.0000225.

677 [48] L. Breiman, Random forests, Mach. Learn. 45 (2001) 5–32. doi:10.1023/A:1010933404324.

678 [49] J.H. Friedman, Greedy Function Approximation: A Gradient Boosting Machine, Ann. Stat. 29
679 (2001) 1189–1232. doi:10.1214/aos/1013203451.

680

681

5.4 Comparing the two developed prediction models

The chapter presented two prediction models that can be used in a similar manner to complement numerical modelling approaches for GSHP system design. However, the two prediction approaches also have distinct differences which are worth discussing. The *time-series approach* presented in section 5.2 focuses on capturing the effect that the thermal load has on the fluid temperatures (and by relation to the surrounding ground) over the entire simulation duration. This allows for a more complete prediction as the model iteratively predicts the change the thermal load is causing over time. On the other hand, the *time-point approach*, presented in section 5.3, isolates a point in time and aims to predict how varying the cooling and heating components of the thermal load affects the fluid temperatures at the specific time point, without directly considering how the temperatures change at any other time outside this time point. The above lead to the first important difference between the two approaches, which is the ability to incorporate any type/shape of thermal load distribution. Since the *time-series* approach models the operation of the system iteratively, it can more completely capture how the ground is affected (in both short and long term) by the thermal load distribution, without restrictions and therefore can correctly function for any type of thermal load distribution. The *time-point* model on the other hand, which isolates results to a point in time, is only able to capture the change in temperature for a particular shape of distribution, by "scaling" (i.e. the thermal load distribution for heating, cooling or both is reduced/increased as a whole).

The second important difference between the two approaches is the dependency of the *time-series* model on the simulation procedure. Because of its iterative nature, the model currently needs to be trained using data from a numerical simulation that adopts a consistent time-step, such as a simulation calculated at daily time-steps over 10 years (even though future research is expected to overcome this limitation). However, in numerical modelling it is often easier to change the time-step between different parts of the simulation (such as having hourly time-steps in the first day, which is more sensitive to errors, and 5-day increments in the last year of the simulation). This is not an issue for the *time-point* model, which does not consider the entirety of the simulation but only a single point in time. Moreover, for the same reasoning, even though both models only need seconds to run, the *time-series* model's time complexity does depend on the length of the simulation and therefore the time required to make predictions will increase the longer the simulations, while the *time-point* model's running time is always constant at a few seconds, regardless the length of the simulation. Finally, another difference

between the models is related to how the training of each model is performed, where the *time-series* model only requires data from one solved FEM numerical simulation, while the *time-point* model requires data from two solved FEM numerical simulations in order to have sufficient information and form a prediction surface. Even though for large or complex simulations this might mean twice the time to gather the required training data, it should be noted that these two simulations could be run in parallel, to minimise that time at the expense of additional computational resources.

5.5 Summary and conclusions

This chapter presented two methodologies that can be used alongside numerical modelling simulations in GSHP system design to significantly reduce the required computational time and resources by using data from solved detailed FEM numerical simulations to make predictions. Both models focus on predicting the carrier fluid temperatures inside the geothermal pipes for different values of provided energy, therefore contributing towards answering the question: *"How much energy can the system provide?"*. Overall, both models can be useful in different circumstances and jointly can provide a powerful set of tools that can be used in GSHP system design. This is especially true for energy geo-structure design which currently mostly relies on expensive numerical simulations. Moreover, the presented methodologies provide insights on the governing equations and underlying relationships between the ground and the design parameters (such as the thermal load) and constitute foundations that can support future research to further refine the associated algorithms and/or provide additional insights on how to better undertake GSHP system design.

The key findings of this chapter can be summarised as below:

- Prediction models, based on machine learning and statistical techniques, can be used alongside numerical modelling to significantly reduce the associated computational time and resources and make GSHP system design more accessible to engineers.
- Two prediction models have been developed and introduced in this chapter as published in scientific journals. These models focus on predicting the carrier fluid temperature values, which is an essential design parameter for GSHP systems.
- These models can be specifically useful for modelling energy geo-structures and complex geometries, which currently can be hard or not feasible to analyse using analytical means at an acceptable level of accuracy/detail.

- Extensive evaluation for both prediction models has been carried out with insignificant errors, in the magnitude of less than 0.5 °C, using energy geo-structures. For the time series model (section 5.2), three different energy pile case studies were adopted for its evaluation, each having different geometry and/or design parameters. For the time-point model (section 5.3) energy diaphragm walls were adopted, with geometry and parameter variations resulting in over 2500 scenarios. The evaluations considered both effects of thermal interference (such as from other nearby GHEs) as well as thermal accumulation over time.
- Regarding the time series model (section 5.2), it was found that when the training and predicting thermal load distributions were of the same type, as expected to largely be the case in real project applications, the accuracy was significantly higher and the errors further minimised.
- Regarding the time point model (section 5.3), it was found that the choice of training distributions is relatively insignificant, allowing flexibility on this choice to the designer.
- Using a prediction methodology can result in significant computational time reductions, depending on the associated conditions. For example, for one of the cases investigated in section 5.2 the time reduced from about a week to about 7 hours.
- Investigating the effect of design parameters (such as the thermal conductivity) in section 5.3, confirmed the existence of potentially predictable underlying relationships, as showed for a specific case. This suggests that with sufficient data, a general semi-analytical model for a range of energy geo-structures can be created that can make instantaneous predictions without the need for training with a numerical simulation for each scenario/project, resulting in an even more accessible way to undertake energy geo-structure design.

Page intentionally left blank

Chapter 6 Conclusions and future work

One of the most concerning issues that our future is facing is the depletion of non-renewable "dirty" energy sources, such as fossil fuels, that account for the vast majority of the world's energy, as well as the accumulating consequences they have for the planet. This doctoral research has focused around shallow geothermal energy, a technology that can contribute to the global drive to overcome these issues, by being able to efficiently provide clean and renewable thermal energy for space heating and cooling purposes.

Shallow geothermal energy, or GSHP systems, have been utilised for many years as a form of renewable energy, with advantages such as operating very efficiently, always being available and not impacting building aesthetics. These systems utilise the ground as a heat source or sink to reject heat in hot weather and draw heat in cold weather. They are commonly designed/analysed using either fast but approximate analytical approaches or more flexible/accurate but time and resource demanding numerical approaches. A significant issue that hinders GSHP systems' wider utilisation is the relatively high capital costs that can accrue due to issues such as poor design, expensive activities such as drilling and a lack of well-defined, standardised construction practices.

A relatively recent approach to this technology is to utilise underground structures, such as piles or retaining walls, which are primarily constructed for structural stability, to also adopt the secondary purpose of thermal energy provision and thus create *energy geo-structures*. This approach can potentially reduce the capital costs associated with GSHP systems, as well as allow the technology's incorporation to new projects (unfit for traditional systems). Moreover, the literature shows that the incorporation of the geothermal technology induces none to minimal bearing capacity effects, except when dealing with normally consolidated clays, further encouraging energy geo-structure utilisation. However, the constraints from the structural design of the geo-structures, the wide range of possible associated geometries and configurations and the relative recentness of this concept introduce challenges on energy geo-structure design and currently there exist gaps in our knowledge of how to efficiently and effectively design and construct these systems.

This research has had as a main aim to further understand GSHP system design and therefore contribute towards more efficient and accessible design approaches, more accurate expectations on system performance, a better understanding of the heat transfer processes and

the parameters influencing it and an overall better and wider global utilisation of this technology. The contributions have focused around three main topics: the effects of realistic geothermal pipe installations, expanding the currently limited knowledge on energy geo-structure design – particularly energy retaining walls – and making numerical modelling, which is often needed in design, more accessible to engineers by tackling the large associated computational times and resources.

6.1 Key findings and practical applications

The first topic introduced in this research is the effect of variable pipe separation within the GHEs, which can unexpectedly stem from the nature of GSHP installations. This effect has been shown to potentially result in an under-designed, under-performing or non-functioning GSHP system. Moreover, it was shown that trying to account for this effect by increasing the depth of the boreholes can be costly (up to 24% capital cost increase was found in this case). To mitigate the consequences of variable pipe separation the material and design parameter values chosen for the design could be significant; for example, it was found that using a high value thermal conductivity grout reduced the magnitude of this effect. Furthermore, a simple methodology able to account for variable pipe separation during the early design stages was developed and presented, utilising the expected average pipe separation. This approach can easily be implemented in the real world, reduce the uncertainty that the installation process can have on the performance of the system and provide more confidence to shallow geothermal designers. Finally, the large dataset generated for the analysis, over a period of months using high performance computing, was published and made available to the scientific community to further aid towards understanding GSHP systems or other fields related to heat transfer.

The second topic presented in this research regards the detailed numerical modelling and design of energy geo-structures. Following an initial case study on energy piles, that served as a stepping stone to the field of energy geo-structures, the chapter focused on the less well-researched energy retaining walls. The unique opportunity to work on a real large-scale engineering project was utilised, undertaking a technical feasibility study on incorporating energy retaining walls within new metro stations in the Melbourne Metro project. The numerical modelling of energy retaining walls was presented for both diaphragm and soldier pile walls and important relevant parameters such as the thermal load distribution used were discussed. From the investigations it was firstly concluded that the balance of the thermal load distribution is extremely important to the performance of the system and a close to balanced distribution should be targeted, which is likely to require the cooperation of different

entities/buildings to help balance the thermal loads. Moreover, it was shown that thermally activating both the retaining walls as well as the bottom slab is likely not worth the additional costs, for the typical geometries and conditions investigated.

Following the conclusion of the technical feasibility study with the Melbourne Metro project, further investigations were undertaken, driven from academic curiosity, to examine the effect of several design parameters on the performance of energy retaining walls. Regarding energy diaphragm walls, the loop spacing was found to have an interesting influence on the performance, where even though in general a shorter spacing resulted in a better system thermal performance, within an intermediate range the effects of the longer pipe circuit length (beneficial) and the thermal interference between the pipe legs (detrimental) counteracted. Therefore, for intermediate spacings a larger spacing would be preferred as it would result in a similar thermal performance as a shorter one but with less associated costs. The analyses on soldier pile retaining walls investigated the pipe spacing, showing that incorporating over 3 pipe U-loops had only marginal gains, as well as the pile spacing, which was found significant, with longer spaced soldier piles (about 3 metres) being more ideal for energy geo-structures. The pile spacing was also investigated in the context of activating less soldier pile GHEs overall (every 2nd or every 3rd pile is an energy pile – remaining only structural piles) resulting in a decrease in the thermal performance but acknowledging the substantial reduction in installation costs when applicable. For both types of retaining walls the effect of the depth of embedment was investigated, showing that extending this depth can significantly improve the thermal performance of the system, even though it can accrue higher costs. Following the investigations, both under real project/industry and academic conditions, the need for standardised design approaches and more available information was noted, with examples on how these could have aided in this project. Lastly, the importance of correctly identifying the new boundary conditions that energy retaining walls introduce was discussed, emphasising that different projects and scenarios can require different boundary conditions to be realistically modelled.

The third topic presented in this research regards the development of two prediction model approaches that can be used to complement numerical design approaches, significantly reducing the computational time and resources and making these approaches more accessible to engineers. The models can be specifically useful in the modelling of energy geo-structures and complex geometries, which currently can be hard or not feasible to analyse using analytical means at an acceptable level of accuracy/detail. Extensive evaluations of both models have

been conducted and presented, adopting a range of geometries and conditions, both energy piles and diaphragm walls and resulting in high accuracies and insignificant errors. The vast computational savings were noted, with case study examples reporting computational time reductions of several magnitudes (for example days to seconds in certain cases). Lastly, it was acknowledged (and shown for a specific example) that the underlying relationships between several design parameters and the resulting thermal performance of energy geo-structures can be potentially predicted, which could result (with sufficient data) to a more powerful and flexible semi-analytical model.

6.2 Recommendations for future work

Considering firstly Chapter 3 and the effect of variable pipe separation, it is acknowledged that this work focused entirely on vertical borehole GHEs. Therefore, it is believed worth investigating the applicability of this effect on energy geo-structures as well, such as energy piles or walls. Since installing the HDPE pipes in these structures is still a relatively new approach, specifically in certain parts of the world, and even though attaching the pipes on the reinforcement of the structures is a more secure approach compared to traditional GHE pipe separators, there can still be several uncertainties on the exact positioning of the pipes due to a variety of reasons such as inexperience or construction implications and it is worth quantifying the potential implications of this effect. Moreover, it is acknowledged that the presented research only considered a 1-year simulation period which could potentially ignore annually accumulating thermal effects (which could result in an even more significant effect of variable pipe separation). It is therefore recommended that future studies, both on borehole and energy geo-structure GHEs adopt a longer simulation duration to incorporate these thermal effects.

Considering Chapter 4, a potentially useful improvement to the analyses presented, regarding the numerical modelling and design of energy geo-structures, would be quantifying the thermal performance in different terms than the presented fluid temperature, such as the amount of energy provided. This could be more informative for the reader but is a non-trivial task for the large scope of the analyses. It should also be acknowledged that limited information has been presented regarding the costs of these systems, capital and running, as well as a quantification of the potential savings from the various concluded recommendations, which would be valuable. The work presented herein investigates several design parameters, however more parameters could be incorporated such as different pipe configurations (placement, connections, diameter amongst others) or the effect of material properties. Moreover, full scale experimental verification of these results on energy piles and energy walls under Australian

conditions is also highly desirable and expected to be completed in the future. Furthermore, extending the analysis presented in section 4.3.5.4, regarding the new boundary conditions associated with energy retaining walls, would be beneficial, incorporating different types of walls, thermal load distributions and scenarios, to gain a better understanding and confidence on their applicability. Overall, the need for more thorough information on this topic has been expressed throughout and examples of the value and impact this can have on a real project (potential savings/improvement in design) have been highlighted in section 4.3.4.4. Other structures or applications, for example pad foundations, could also be investigated in detail. In this relatively not well researched area, the more aspects are investigated the more likely the establishment of standardised design approaches becomes, which can result to a wider utilisation of these systems around the world.

Finally, considering the work presented in Chapter 5 and the developed prediction models, there are different ways in which these models can be further improved and made more helpful to geothermal designers and engineers, all of which would require a significant amount of additional simulations and generated data. Section 5.4 discussed some potential improvements, such as removing the time-step restriction of the time-series model and the “scaled” thermal load dependency of the time-point model. In addition, it could be beneficial to further expand these models by incorporating more design parameters, such as the thermal conductivity of the ground/structure or the pipe spacing. Incorporation of geo-mechanical behaviour to the thermal behaviour is also desirable, in appropriate conditions as pointed out by the literature. Lastly, as discussed in the journal paper presented in section 5.3, a future aim stemming from this work can be the development of a general semi-analytical model that can instantaneously provide results and potentially be easily implemented in a design software for engineers to use.

References

[1] REN21. Renewables 2018 global status report. 2018.

[2] Energy Information Administration (EIA). International Energy Outlook Executive Summary. 2017.

[3] Glassley WE. Geothermal Energy: Renewable Energy and the Environment. CRC Press; 2010.

[4] Matek B. 2016 Annual U . S . & Global Geothermal Power Production Report. 2016.

[5] Banks D. An Introduction to Thermogeology: Ground Source Heating and Cooling. Wiley - Blackwell; 2008.

[6] Colls S. Ground Heat Exchanger Design For Direct Goethermal Energy Systems. The University of Melbourne, 2013.

[7] Mikhaylova O, Johnston IW, Narsilio GA, Kivi A V, Aditya R, Noonan G. Performance of borehole ground heat exchangers under thermal loads from a school building: Full-scale experiment in Melbourne, Australia. Proc. World Geotherm. Congr., Melbourne: 2015, p. 19–25.

[8] Mikhaylova O. Towards Improvement of the Design of Borehole Ground Heat Exchangers. The University Of Melbourne, 2017.

[9] Brandl H. Energy foundations and other thermo-active ground structures. Géotechnique 2006;56:81–122. doi:10.1680/geot.2006.56.2.81.

[10] Johnston IW, Narsilio GA, Colls S. Emerging geothermal energy technologies. KSCE J Civ Eng 2011;15:643–53. doi:10.1007/s12205-011-0005-7.

[11] Preene M, Powrie W. Ground energy systems: from analysis to geotechnical design. Géotechnique 2009;59:261–71. doi:10.1680/geot.2009.59.3.261.

[12] Florides G, Kalogirou S. Ground heat exchangers-A review of systems, models and applications. Renew Energy 2007;32:2461–78. doi:10.1016/j.renene.2006.12.014.

[13] Florides G, Kalogirou S. Gound Heat Exchangers-A review. Proc. 3rd Int. Conf. Heat Powered Cycles, HPC 2004-Cooling, Heat. Power Gener. Syst., Larnaca, Cyprus: Cyprus University of Technology; 2004, p. 8.

[14] Laloui L, Moreni M, Vulliet L. Behavior of a dual-purpose pile as foundation and heat exchangers. Can Geotech J 2003;40:388–402. doi:10.1139/t02-117.

[15] Laloui L, Nuth M, Vulliet L. Experimental and numerical investigations of the behaviour of a heat exchanger pile. Int J Numer Anal Methods Geomech 2006;30:763–81. doi:10.1002/nag.499.

[16] Brandl H. Energy foundations and other thermo-active ground structures. Géotechnique 2006;56:81–122. doi:10.1680/geot.2006.56.2.81.

[17] Amatya BL, Soga K, Bourne-Webb PJ, Amis T, Laloui L. Thermo-mechanical behaviour of energy piles. Géotechnique 2012;62:503–19. doi:10.1680/geot.10.P.116.

[18] Lu Q, Narsilio GA. Economic analysis of utilising energy piles for residential buildings. Energy 2018;under revi.

[19] Hamada Y, Saitoh H, Nakamura M, Kubota H, Ochifuji K. Field performance of an energy pile system for space heating. Energy Build 2007;39:517–24. doi:10.1016/j.enbuild.2006.09.006.

[20] Gao J, Zhang X, Liu J, Li K, Yang J. Numerical and experimental assessment of thermal performance of vertical energy piles: An application. Appl Energy 2008;85:901–10. doi:10.1016/j.apenergy.2008.02.010.

[21] Cecinato F, Loveridge F. Influences on the thermal efficiency of energy piles. Energy 2015;82:1021–33. doi:10.1016/j.energy.2015.02.001.

[22] Akrouch GA, Sánchez M, Briaud JL. Thermo-mechanical behavior of energy piles in high plasticity clays. Acta Geotech 2014;9:399–412. doi:10.1007/s11440-014-0312-5.

[23] Amis T, Robinson CAW, Wong S. Integrating Geothermal Loops into the Diaphragm Walls of the Knightsbridge Palace Hotel Project. Proceeding 11th DFI / EFFC Int Conf London 2010.

[24] ICConsulten. Wirtschaftliche Optimierung von Tunnelthermie Absorberanlagen, Grundlagenuntersuchung und Planungsleitfaden. Vienna, Austria (in German): 2005.

[25] Katzenbach R, Clauss F, Lappla S, Rupert T. Potentials of environmental protection by geotechnical engineering. In: Anagnostopoulos A, editor. 15th ECSMGE—Geotechnics Hard Soils, Athens, Greece: IOS Press; 2013, p. 247–52.

[26] Lee C, Park S, Choi H-J, Lee I-M, Choi H. Development of energy textile to use geothermal energy in tunnels. Tunn Undergr Sp Technol 2016;59:105–13. doi:10.1016/j.tust.2016.06.014.

[27] Barla M, Donna A Di. Energy tunnels: Concept and design aspects. Undergr Sp 2018. doi:10.1016/j.undsp.2018.03.003.

[28] Barla M, Perino A. Energy from geo-structures: a topic of growing interest. Environ Geotech 2015;2:3–7. doi:10.1680/envgeo.13.00106.

[29] Nicholson DP, Chen Q, de Silva M, Winter A, Winterling R. The design of thermal tunnel energy segments for Crossrail, UK. Eng Sustain 2014;167:118–34. doi:10.1680/ensu.13.00014.

[30] Narsilio GA, Bidarmaghz A, Disfani M, Johnston IW, Makasis N. Shallow geothermal ('Geoexchange') feasibility study - Stage 1. Melbourne: 2016.

[31] Narsilio GA, Makasis N, Lu Q, Jensen-Page L, Bidarmaghz A, Disfani M. Shallow geothermal ('Geoexchange') feasibility study - Study 2: Parkville. Melbourne: 2016.

[32] Bidarmaghz A, Makasis N, Narsilio GA, Franco F, Perez MEC. Geothermal Energy in Loess. Environ Geotech 2016;4:225–36.

[33] Bidarmaghz A, Narsilio GA, Johnston IW, Colls S. The importance of surface air temperature fluctuations on long-term performance of vertical ground heat exchangers. Geomech Energy Environ 2016;6:35–44. doi:10.1016/j.gete.2016.02.003.

[34] Mimouni T, Laloui L. Towards a secure basis for the design of geothermal piles. Acta Geotech 2014;9:355–66. doi:10.1007/s11440-013-0245-4.

[35] Rotta Loria AF, Laloui L. The interaction factor method for energy pile groups. Comput Geotech 2016;80:121–37. doi:10.1016/j.compgeo.2016.07.002.

[36] Stewart MA, Mccartney JS. Centrifuge Modeling of Soil-Structure Interaction in Energy Foundations. J Geotech Geoenvironmental Eng ASCE 2014;140:1–11. doi:10.1061/(ASCE)GT.1943-5606.0001061.

[37] Bourne-Webb PJ, Amatya B, Soga K, Amis T, Davidson C, Payne P. Energy pile test at Lambeth College, London: geotechnical and thermodynamic aspects of pile response to heat cycles. Géotechnique 2009;59:237–48. doi:10.1680/geot.2009.59.3.237.

[38] Mccartney JS, Murphy KD. Strain Distributions in Full-Scale Energy Foundations. J Deep Found Inst 2012;6:26–38. doi:10.1179/dfi.2012.008.

[39] Coletto A, Sterpi D. Structural and Geotechnical Effects of Thermal Loads in Energy Walls. Procedia Eng 2016;158:224–9. doi:10.1016/j.proeng.2016.08.433.

[40] Sterpi D, Coletto A, Mauri L. Investigation on the behaviour of a thermo-active diaphragm wall by thermo-mechanical analyses. Geomech Energy Environ 2017;9:1–20. doi:10.1016/j.gete.2016.10.001.

[41] Rui Y, Yin M. Thermo-hydro-mechanical coupling analysis of a thermo-active diaphragm wall. Can Geotech J 2017. doi:10.1139/cgj-2017-0158.

[42] Narsilio GA, Johnston IW, Bidarmaghz A, Colls S, Mikhaylova O, Kivi A, et al. Geothermal energy: Introducing an emerging technology. In: Horpibulsuk S, Chinkulkijniwat A, Suksiripattanapong C, editors. Proc. Int. Conf. Adv. Civ. Eng. Sustain. Dev. (ACESD 2014). Volume 1 o, Nakhon Ratchasima, Thailand: Suranaree University of Technology,; 2014, p. 141–54.

[43] Department of the Environment and Energy. Australian energy update 2017. Canberra: 2017.

[44] Energy Consult. Residential Energy Baseline Study: Australia. Jindivick, Victoria: 2015.

[45] United States Environmental Protection Agenc. Greenhouse Gas Equivalencies Calculator 2017. https://www.epa.gov/energy/greenhouse-gas-equivalencies-calculator (accessed June 12, 2018).

[46] Brandl H. Geothermal Geotechnics for Urban Undergrounds. Procedia Eng 2016;165:747–64. doi:10.1016/j.proeng.2016.11.773.

[47] Carlslaw KS, Jaeger JC. Conduction of Heat in Solids. Oxford: Clarendon Press; 1959.

[48] Ingersoll LR, Zobel OJ, Ingersoll AC. Heat Conduction with Engineering, Geological and Other Applications. University of Wisconsin Press; 1954.

[49] Kakac S, Yener Y. Heat Conduction. Washington DC: Hemisphere Publishing Corp; 1985.

[50] Eskilson P. Thermal Analysis of Heat Extraction Boreholes. University of Lund, Sweden, 1987.

[51] Philippe M, Bernier M, Marchio D. Validity ranges of three analytical solutions to heat transfer in the vicinity of single boreholes. Geothermics 2009;38:407–13. doi:10.1016/j.geothermics.2009.07.002.

[52] Al-Khoury R. Computational Modelling of Shallow Geothermal Systems. Delft: CRC Press; 2012.

[53] Yavuzturk C. Modeling of vertical ground loop heat exchangers for ground source heat pump systems. Oklahoma State University, 1999.

[54] Yavuzturk C. A Short Time Step Response Factor Model for Vertical Ground Loop Heat Exchangers. ASHRAE Trans 1999;105:475–85.

[55] Bernier MA, Pinel P, Labib R, Paillot R. A multiple load aggregation algorithm for annual hourly simulations of GCHP systems. HVAC R Res 2004;10:471–87. doi:10.1080/10789669.2004.10391115.

[56] Yang H, Cui P, Fang Z. Vertical-borehole ground-coupled heat pumps: A review of models and systems. Appl Energy 2010;87:16–27. doi:10.1016/j.apenergy.2009.04.038.

[57] Loveridge F, Powrie W. Temperature response functions (G-functions) for single pile heat exchangers. Energy 2013;57:554–64. doi:10.1016/j.energy.2013.04.060.

[58] Loveridge F, Powrie W. G-Functions for multiple interacting pile heat exchangers. Energy 2014;64:747–57. doi:10.1016/j.energy.2013.11.014.

[59] Narsilio GA, Aye L. Shallow Geothermal Energy: An Emerging Technology. In: Sharma A, Shukla A, Aye L, editors. Low Carbon Energy Supply. Green Energy Technol., Singapore: Springer; 2018, p. 387–411.

[60] Jensen-Page L, Loveridge FA, Narsilio GA. Thermal response testing in large diameter energy piles. Appl Energy 2018:under review.

[61] Marcotte D, Pasquier P, Sheriff F, Bernier M. The importance of axial effects for borehole design of geothermal heat-pump systems. Renew Energy 2010;35:763–70. doi:10.1016/j.renene.2009.09.015.

[62] Sharqawy MH, Mokheimer EM, Badr HM. Effective pipe-to-borehole thermal resistance for vertical ground heat exchangers. Geothermics 2009;38:271–7. doi:10.1016/j.geothermics.2009.02.001.

[63] Michopoulos A, Kyriakis N. Predicting the fluid temperature at the exit of the vertical ground heat exchangers. Appl Energy 2009;86:2065–70. doi:10.1016/j.apenergy.2009.02.002.

[64] Lazzari S, Priarone A, Zanchini E. Long-term performance of BHE (borehole heat exchanger) fields with negligible groundwater movement. Energy 2010;35:4966–74. doi:10.1016/j.energy.2010.08.028.

[65] Al-Khoury R, Kölbel T, Schramedei R. Efficient numerical modeling of borehole heat exchangers. Comput Geosci 2010;36:1301–15. doi:10.1016/j.cageo.2009.12.010.

[66] Bauer D, Heidemann W, Diersch HJG. Transient 3D analysis of borehole heat exchanger modeling. Geothermics 2011;40:250–60. doi:10.1016/j.geothermics.2011.08.001.

[67] He M. Numerical modelling of geothermal borehole heat exchanger systems. De Montfort University, 2012.

[68] Rees SJ, He M. A three-dimensional numerical model of borehole heat exchanger heat transfer and fluid flow. Geothermics 2013;46:1–13. doi:10.1016/j.geothermics.2012.10.004.

[69] Ozudogru TY, Olgun CG, Senol A. 3D numerical modeling of vertical geothermal heat exchangers. Geothermics 2014;51:312–24. doi:10.1016/j.geothermics.2014.02.005.

[70] Ozudogru TY, Ghasemi-Fare O, Olgun CG, Basu P. Numerical Modeling of Vertical Geothermal Heat Exchangers Using Finite Difference and Finite Element Techniques. Geotech Geol Eng 2015;33:291–306. doi:10.1007/s10706-014-9822-z.

[71] Yavuzturk C. A Transient Two-Dimensional Finite Volume Model for the Simulation of Vertical U- Tube Ground Heat Exchangers. ASHRAE Trans 1999;M:465–74.

[72] Narsilio GA, Bidarmaghz A, Johnston IW, Colls S. Detailed numerical modelling of ground heat exchangers based on first principles. Comput Geotech 2018:accepted.

[73] Rottmayer SP, Beckman WA, Mitchell JW. Simulation of a single vertical U-tube ground heat exchanger in an infinite medium. Atlanta: 1997.

[74] Thornton JW, McDowell TP, Shonder JA, Hughes PJ, Pahud D, Hellström GAJ. Residential Vertical GEothermal Heat Pump System Models: Calibration to Data. ASHRAE Trans 1997;8:660–74.

[75] Austin WAI, Yavuzturk C, Spitler JD. Development of an in-situ system and analysis procedure for measuring ground thermal properties. ASHRAE Trans 2000;106:365–79.

[76] Gehlin SEA, Hellström G. Influence on thermal response test by groundwater flow in vertical fractures in hard rock. Renew Energy 2003;28:2221–38. doi:10.1016/S0960-1481(03)00128-9.

[77] Signorelli S, Bassetti S, Pahud D, Kohl T. Numerical evaluation of thermal response tests. Geothermics 2007;36:141–66. doi:10.1016/j.geothermics.2006.10.006.

[78] Nam Y, Ooka R, Hwang S. Development of a numerical model to predict heat exchange rates for a ground-source heat pump system. Energy Build 2008;40:2133–40. doi:10.1016/j.enbuild.2008.06.004.

[79] Marcotte D, Pasquier P. On the estimation of thermal resistance in borehole thermal conductivity test. Renew Energy 2008;33:2407–15. doi:10.1016/j.renene.2008.01.021.

[80] Hellström G. Duct ground heat storage model, manual for computer code. 1989.

[81] Hellström G, Sanner B. Software for dimensioning of deep boreholes for heat extraction. CALORSTOCK 94, Espoo/Helsinki: 1994, p. 195–202.

[82] Fisher DE, Rees SJ, Padhmanabhan SK, Murugappan A. Implementation and Validation of Ground-Source Heat Pump System Models in an Integrated Building and System Simulation Environment. HVAC&R Res 2006;12:693–710.

[83] Spitler JD. GLHEPRO-A design tool for commercial building ground loop heat exchangers. Proceeedings fourth Int. heat pumps cold Clim. Conf., 2000, p. 1–15.

doi:10.1007/s13398-014-0173-7.2.

[84] Zeng HY, Diao NR, Fang ZH. A finite line-source model for boreholes in geothermal heat exchangers. Heat Transf - Asian Res 2002;31:558–67. doi:10.1002/htj.10057.

[85] Lamarche L, Beauchamp B. A new contribution to the finite line-source model for geothermal boreholes. Energy Build 2007;39:188–98. doi:10.1016/j.enbuild.2006.06.003.

[86] Alavy M, Nguyen H V., Leong WH, Dworkin SB. A methodology and computerized approach for optimizing hybrid ground source heat pump system design. Renew Energy 2013;57:404–12. doi:10.1016/j.renene.2013.02.003.

[87] Mikhaylova O, Choudhary R, Soga K, Johnston IW. Benefits and optimisation of district hybrid ground source heat pump systems. In: Wuttke F, Bauer S, Sanchez M, editors. Energy Geotech. - Proc. 1st Int. Conf. Energy Geotech. ICEGT 2016, Kiel: CRC Press; 2016, p. 535–42.

[88] Aditya GR, Mikhaylova O, Narsilio GA, W. JI. Financial assessment of ground source heat pump systems against other selected heating and cooling systems for Australian conditions. IGSHPA Res. track Conf., Stocholm: submitted; 2018.

[89] Loveridge F, Powrie W. Pile heat exchangers: thermal behaviour and interactions. Proc ICE - Geotech Eng 2013;166:178–96. doi:10.1680/geng.11.00042.

[90] Fadejev J, Simson R, Kurnitski J, Haghighat F. A review on energy piles design, sizing and modelling. Energy 2017;122:390–407. doi:10.1016/j.energy.2017.01.097.

[91] Mimouni T, Laloui L. Thermo-Pile: A Numerical Tool for the Design of Energy Piles. In: Laloui L, Di Donna A, editors. Energy Geostructures Innov. Undergr. Eng., ISTE Ltd. and John Wiley and Sons; 2013, p. 265–78.

[92] Pahud D. PILESIM2: Simulation Tool for Heating/Cooling Systems with Energy Piles or multiple Borehole Heat Exchangers. User Manual 2007:50.

[93] Loveridge F, Mccartney JS, Narsilio GA, Sánchez M. Energy geostructures: a review of analysis approaches, in situ testing and model scale experiments. Geomech Energy Environ 2018:under review.

[94] Sun M, Xia C, Zhang G. Heat transfer model and design method for geothermal heat exchange tubes in diaphragm walls. Energy Build 2013;61:250–9. doi:10.1016/j.enbuild.2013.02.017.

[95] Kürten S, Mottaghy D, Ziegler M. Design of plane energy geostructures based on laboratory tests and numerical modelling. Energy Build 2015;107:434–44. doi:10.1016/j.enbuild.2015.08.039.

[96] Di Donna A, Barla M. The role of ground conditions on energy tunnels' heat exchange. Environ Geotech 2016;3:214–24. doi:10.1680/jenge.15.00030.

[97] Nicholson DP, Chen Q, de Silva M, Winter A, Winterling R. The design of thermal tunnel energy segments for Crossrail, UK. Eng Sustain 2014;167:118–34. doi:10.1680/ensu.13.00014.

[98] Bourne-Webb P, Burlon S, Javed S, Kürten S, Loveridge F. Analysis and design methods

for energy geostructures. Renew Sustain Energy Rev 2016;65:402–19. doi:10.1016/j.rser.2016.06.046.

[99] Soga K, Qi H, Rui Y, Nicholson DP. Some considerations for designing GSHP coupled geotechnical structures based on a case study. 7th Int. Congr. Environ. Geotech., Melbourne: 2014.

[100] Zhang G, Xia C, Sun M, Zou Y, Xiao S. A new model and analytical solution for the heat conduction of tunnel lining ground heat exchangers. Cold Reg Sci Technol 2013;88:59–66. doi:10.1016/j.coldregions.2013.01.003.

[101] Bidarmaghz A, Narsilio GA. Heat exchange mechanisms in energy tunnel systems. Geomech Energy Environ 2018:conditionally accepted.

[102] Bourne-Webb PJ, Bodas Freitas TM, Da Costa Gonçalves RA. Thermal and mechanical aspects of the response of embedded retaining walls used as shallow geothermal heat exchangers. Energy Build 2016;125:130–41. doi:10.1016/j.enbuild.2016.04.075.

[103] Zhang G, Xia C, Yang Y, Sun M, Zou Y. Experimental study on the thermal performance of tunnel lining ground heat exchangers. Energy Build 2014;77:149–57. doi:10.1016/j.enbuild.2014.03.043.

[104] International Ground Source Heat Pump Association. GLHEPRO 2018. https://igshpa.org/software (accessed June 13, 2018).

[105] Ground Loop Design. GLD Software 2017. http://www.groundloopdesign.com/ (accessed June 13, 2018).

[106] Geokiss. GshpCalc 2018. http://www.geokiss.com/gsoftware.htm (accessed June 13, 2018).

[107] U.S. Department of Energy. EnergyPlus 2018. https://energyplus.net/ (accessed June 13, 2018).

[108] Fadejev J, Kurnitski J. Geothermal energy piles and boreholes design with heat pump in a whole building simulation software. Energy Build 2015;106:23–34. doi:10.1016/j.enbuild.2015.06.014.

[109] Shonder JA, Baxter V, Thornton J, Hughes P. A New Comparison of Vertical Ground Heat Exchanger. 1999.

[110] Spitler JD, Cullin JR, Lee E, Fisher DE, Bernier M, Kummert M, et al. Preliminary Intermodel Comparison of Ground Heat Exchanger Simulation Models. Proc. Effstock 2009 11th Int. Conf. Therm. energy storages, 14-17 Jun, 2009, p. 155.1--155.8.

[111] Lu Q. Shallow geothermal system: Feasibility and design practices in Melbourne, Australia. The University of Melbourne, 2018.

[112] Bidarmaghz A. 3D Numerical Modelling of Vertical Ground Heat Exchangers. The University of Melbourne, 2014.

[113] Barnard ACL, Hunt WA, Timlake WP, Varley E. A Theory of Fluid Flow in Compliant Tubes. Biophys J 1966;6:717–24. doi:10.1016/S0006-3495(66)86690-0.

[114] Lurie M V. Modeling and Calculation of Stationary Operating Regimes of Oil and Gas

Pipelines. Model. Oil Prod. Gas Pipeline Transp., Weinheim: Wiley Online Library; 2009, p. 73–108.

[115] Bidarmaghz A, Narsilio GA, Buhmann P, Moormann C, Westrich B. Thermal interaction between tunnel ground heat exchangers and borehole heat exchangers. Geomech Energy Environ 2017;10:29–41. doi:10.1016/j.gete.2017.05.001.

[116] Mitchell TM. The Discipline of Machine Learning. Mach Learn 2006;17:1–7. doi:10.1080/026404199365326.

[117] Bishop C. Pattern Recognition and Machine Learning. New York: Springer; 2006.

[118] Hastie T, Tibshirani R, Friedman J. The Elements of Statistical Learning: Data Mining, Inference and Prediction. Stanford: Springer; 2001. doi:10.1007/b94608.

[119] Dutton DM, Conroy G V. A review of machine learning. Knowl Eng Rev 1996;12:341–67.

[120] Mosteller F, Tukey J. Data analysis, including statistics. Handb. Soc. Psychol., Reading: Addison-Wesley; 1968.

[121] Li X, Claramunt C. Research Article A Spatial Entropy-Based Decision Tree for Classification of Geographical Information. Trans GIS 2006;10:451–67. doi:10.1111/j.1467-9671.2006.01006.x.

[122] Erdem RT, Seker S, Ozturk AU, Gucuyen E. Numerical analysis on corrosion resistance of mild steel structures. Eng Comput 2012:529–33. doi:10.1007/s00366-012-0279-5.

[123] Zhao H. Slope reliability analysis using a support vector machine. Comput Geotech 2008;35:459–67. doi:10.1016/j.compgeo.2007.08.002.

[124] Goh ATC, Goh SH. Support vector machines: Their use in geotechnical engineering as illustrated using seismic liquefaction data. Comput Geotech 2007;34:410–21. doi:10.1016/j.compgeo.2007.06.001.

[125] Esen H, Inalli M. Modelling of a vertical ground coupled heat pump system by using artificial neural networks. Expert Syst Appl 2009;36:10229–38. doi:10.1016/j.eswa.2009.01.055.

[126] Casteleiro-Roca JL, Quintián H, Calvo-Rolle JL, Corchado E, del Carmen Meizoso-López M, Piñón-Pazos A. An intelligent fault detection system for a heat pump installation based on a geothermal heat exchanger. J Appl Log 2016;17:36–47. doi:10.1016/j.jal.2015.09.007.

[127] Park SK, Moon HJ, Min KC, Hwang C, Kim S. Application of a multiple linear regression and an artificial neural network model for the heating performance analysis and hourly prediction of a large-scale ground source heat pump system. Energy Build 2018;165:206–15. doi:10.1016/j.enbuild.2018.01.029.

[128] Zhang Y, Zhou L, Hu Z, Yu Z, Hao S, Lei Z, et al. Prediction of Layered Thermal Conductivity Using Artificial Neural Network in Order to Have Better Design of Ground Source Heat Pump System. Energies 2018;11:1896. doi:10.3390/en11071896.

[129] Gordan B, Jahed Armaghani D, Hajihassani M, Monjezi M. Prediction of seismic slope stability through combination of particle swarm optimization and neural network. Eng

Comput 2015. doi:10.1007/s00366-015-0400-7.

[130] Bateni SM, Jeng D-S, Mortazavi Naeini SM. Estimating soil thermal properties from sequences of land surface temperature using hybrid Genetic Algorithm–Finite Difference method. Eng Appl Artif Intell 2012;25:1425–36. doi:10.1016/j.engappai.2012.02.017.

[131] Gang W, Wang J. Predictive ANN models of ground heat exchanger for the control of hybrid ground source heat pump systems. Appl Energy 2013;112:1146–53. doi:10.1016/j.apenergy.2012.12.031.

[132] Gang W, Wang J, Wang S. Performance analysis of hybrid ground source heat pump systems based on ANN predictive control. Appl Energy 2014;136:1138–44. doi:10.1016/j.apenergy.2014.04.005.

[133] Esen H, Ozgen F, Esen M, Sengur A. Artificial neural network and wavelet neural network approaches for modelling of a solar air heater. Expert Syst Appl 2009;36:11240–8. doi:10.1016/j.eswa.2009.02.073.

[134] Mohanraj M, Jayaraj S, Muraleedharan C. Applications of artificial neural networks for refrigeration, air-conditioning and heat pump systems - A review. Renew Sustain Energy Rev 2012;16:1340–58. doi:10.1016/j.rser.2011.10.015.

[135] Shahin M a, Jaksa MB. State of the Art of Artificial Neural Networks in Geotechnical Engineering. Electron J Geotech Eng 2008;8:1–26.

[136] Samui P, Sitharam TG. Least-square support vector machine applied to settlement of shallow foundations on cohesionless soils. Int J Numer Anal Methods Geomech 2008;32:2033–43. doi:10.1002/nag.731.

[137] Wilcox DC. Turbulence Modeling for CFD. 3rd ed. D C W Industries; 2006.

[138] Xia C, Sun M, Zhang G, Xiao S, Zou Y. Experimental study on geothermal heat exchangers buried in diaphragm walls. Energy Build 2012;52:50–5. doi:10.1016/j.enbuild.2012.03.054.

[139] Di Donna A, Cecinato F, Loveridge F, Barla M. Energy performance of diaphragm walls used as heat exchangers. Proc Inst Civ Eng - Geotech Eng 2016;170:1–14. doi:10.1680/jgeen.

[140] Narsilio GA, Disfani M, Bidarmaghz A, Jensen-Page L, Aditya R, Lu Q. Geothermal testing -Estimation of thermal conductivity of soil and rock using a borehole heat exchanger and laboratory testing. 2016.

[141] Remund C, Carda R. Ground Source Heat Pump Residential and Light Commercial Design and Installation Guide (Geothermal Installer Manuals). International Ground Source Heat Pump Association; 2009.

[142] M.J. G, Duffy S, Thompson J. The Potential for Heat Recovery from London Underground Stations and Tunnels. CIBSE Tech. Symp., Leicester, U.K.: 2011.

Appendix A – Geothermal energy in loess

This section consists of a journal paper titled: “Geothermal energy in loess”, published in the journal *Environmental Geotechnics.* The paper has been inserted in the following pages, in its Author’s Accepted Manuscript [AAM] version, with the only modification being the addition of the thesis page numbers at the bottom of the page (allowing consistent numbering throughout the thesis).

- Article type: paper (max 5000 words with one illustration per 500 words)
- Date text written: April 2015, text revised: September 2015
- Number of words in your main text and tables: ~4,800 (excluding references)
- Number of figures: 10

Geothermal Energy in Loess

Author 1

- Asal Bidarmaghz, PhD, MSc (Eng), BSc (Eng)
  Department of Infrastructure Engineering, The University of Melbourne, Parkville, Australia

Author 2

- Nikolas Makasis, MSc (Computer Science), MEng (Civil)
  Department of Infrastructure Engineering, The University of Melbourne, Parkville, Australia

Author 3

- Guillermo A. Narsilio✉, PhD, MSc (Math), MSc (CE), CEng
  Department of Infrastructure Engineering, The University of Melbourne, Parkville, Australia

Author 4

- Franco M. Francisca, PhD, CEng
  Institute for Advanced Studies in Engineering and Technology (IDIT), Universidad Nacional de Cordoba, and CONICET, Cordoba, Argentina

Author 5

- Magalí E. Carro Pérez, PhD, MSc (CE), CEng
  Institute for Advanced Studies in Engineering and Technology (IDIT), Universidad Nacional de Cordoba, and CONICET, Cordoba, Argentina

Full contact details of corresponding author.

- Guillermo A. Narsilio, ARC Future Fellow and Senior Lecturer, Department of Infrastructure Engineering, The University of Melbourne, Parkville, VIC 3010, Australia;
  E-mail: narsilio@unimelb.edu.au Phone: +61 3 8344 4659, Fax: +61 3 8344 4616.

Abstract

Ground-source heat pump (GSHP) systems efficiently heat and cool buildings using sustainable geothermal energy accessed via ground heat exchangers (GHEs). Loess covers vast parts of the world, about 10% of the landmass; therefore, the use of piles or 'micro-piles' is extensive in these areas, particularly where the thickness of loessic soils is significant. These deep foundations have the potential to be used as 'energy piles' in GSHP systems, with a minimal additional cost. This paper presents a case study of a representative real building in Cordoba, Argentina where foundations are also used as GHEs. The thermal properties of local soils were experimentally measured and used in detailed state-of-the-art finite element models recently developed. Results from the realistic simulations show that the partial substitution of electrical heating and cooling systems with geothermal systems could significantly reduce energy consumption and the size of associated infrastructure, despite the relatively low thermal conductivity of local loess. Moreover, the effects of surface air temperature fluctuations, which are routinely ignored in GHE design, are accounted for in these simulations. This case study shows the potential of GSHP technology in loessic environments and gives incentives to engineers to start considering the technology in their designs and practices.

Keywords (chosen from ICE Publishing list)
Numerical modelling; Temperature effects; Piles; Geothermal

Keywords (preferred by the authors for this paper)
Energy pile; Geothermal; Thermal conductivity; Loess; Numerical Modelling

List of notation

A	inner cross sectional area of a pipe, m^2
As	earth surface temperature annual swing above and below the average ground
$C_{p,m}$	specific heat capacity of solid material, J/(kgK)
$C_{p,w}$	specific heat capacity of carrier fluid, J/(kgK)
d_h	hydraulic diameter of pipe, m
f_D	Darcy friction factor
k_v	vegetation coefficient
p	pressure, Pa
Q_{wall}	external heat exchange rate though pipe walls, W/m
SDR	standard dimension ratio
t	time, sec (Eqs. 1 to 4), day (Eq. 5)
t_0	number of days after January 1st to the minimum earth surface temperature,
T	fluid temperature, C
$T(z,t)$	depth and time varying temperature, C

$T_{farfield}$	undisturbed ground temperature, C
T_g	annual average ground temperature, C
T_{inlet}	average inlet pipe temperature, C
T_m	temperature of solid material, C
$T_{m,pipe\ wall}$	temperature of solid material at the pipe outer wall, C
T_{outlet}	average outlet pipe temperature, C
$\mathbf{v}$	fluid velocity field, m/s
x,y,z	cartesian coordinates, with z denoting depth, m
z	depth below the ground surface, m
α	soil thermal diffusivity, x 10^{-2} cm^2/sec
λ_m	thermal conductivity of solid material, W/(mK)
λ_w	thermal conductivity of the carrier fluid, W/(mK)
ρ_m	density of solid material, kg/m^3
ρ_w	density of carrier fluid, kg/m^3

1. Introduction: Ground source heat pump systems and loess deposits

Ground-source heat pump (GSHP) systems efficiently heat and cool buildings using sustainable geothermal energy accessed via ground heat exchangers (GHEs). In closed loop systems, GHEs comprise high density polyethylene (HDPE) pipes embedded in specifically drilled boreholes or trenches or even built into foundations, all within a few tens of meters from the surface (Figure 1). GSHP systems operate at a coefficient of performance of about four throughout the year, basically delivering four kilowatts of heating or cooling for every kilowatt input into running the heat pumps (Amatya et al., 2012, Brandl, 2006, Johnston et al., 2011, Preene, 2009).

<<Figure 1 about here>>

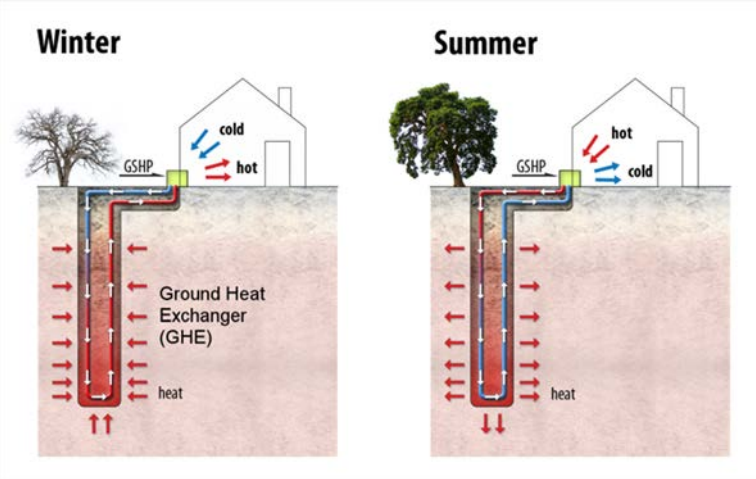


Figure 1 Schematic of a GSHP system in heating (winter) and cooling (summer) modes. (Note: not to scale).

Loess is an unstable soil that develops collapse due to water content and/or load increases. Loessial soils are loosely cemented Aeolian sediments composed mainly by fine sand, silt and clay particles that accumulate when deposited by wind (*primary loess*) and sometimes particles are re-transported by either water or snow (*secondary loess*). In both cases, particles are frequently cemented by either precipitated calcium carbonate or silicates (Francisca, 2007, Moll and Rocca, 1991, Rocca et al., 2006). Loess covers vast parts of the world, about 10% of the landmass, and is encountered across New Zealand, from Western Europe to China (including Russia), across North America and in regions across South America (Quintana Crespo, 2005, Rocca et al., 2006, Zárate, 2003). In particular, loess deposits cover large areas of Cordoba, Argentina and are tens of metres in thickness.

To support the structures constructed on this type of soil, the use of piles (> 300 mm diameter) for multi-storey buildings or 'micro-piles' (< 300 mm diameter) for lighter residential buildings is quite extensive. These foundations, which are already required for construction purposes, can serve a dual purpose both as foundations and as GHEs (i.e., energy piles). No extra costs (except the minor pipe costs) for drilling and installation are added as the already built structural

piles are used as GHEs. However, there are virtually no studies conducted on the feasibility and design of geothermal systems in loessial soils and there is a missed opportunity in current practice to use deep foundations as structural elements and as GHEs when dealing with loessial sites. The GSHP alternative becomes even more attractive in the areas where natural gas infrastructure is not available and only expensive LPG gas or wood is used for heating. GSHP systems can significantly reduce the use of these fuels in these (predominantly rural) areas and at the same time can provide an alternative clean energy for conditioning of buildings.

To exemplify the benefits of GSHP systems in loess deposits and highlight potential issues, this paper presents a numerical case study of a representative real building in Cordoba, where foundations are also used as GHEs. While this study focuses on the thermal performance of energy piles, the effect of cyclical heating and cooling on the structural and geotechnical strength of piles is a necessary aspect to also consider in geothermal projects; however, this later aspect is kept out of the scope of this work. Nevertheless, it is important to note that in the case of loess, structural concerns may arise from rupture or leakage of HDPE pipes and water filtration into this collapsible soil. It is therefore crucial to ensure a high standard in quality assurance and quality control of the thermo-fused pipe joints. This is routinely achieved via visual inspections and subsequent pressure tests of the U-loops before and after casting and during commissioning of the GSHP systems, as outlined in various IGSHPA guidelines (Oklahoma State University, 2009).

2. Main characteristics of Loess

Loess is a quaternary sediment composed mainly of fine particles that form an open micro-structure. Therefore, this soil is characterised by an internal structure that controls the thermo-hydro-mechanical behaviour of these formations. Loess is an unstable soil that develops collapse due to water or internal pressure increases. This produces significant settlements that affect civil infrastructure and structures that suffer significant distortions (Rocca et al., 2006). Loessial soils cover approximately 10% of the continents including North America, Europe, Asia and South America (Rinaldi et al., 2007). The most significant loess formations are found in Argentina (Iriondo 1997, Zárate 2003), Czech Republic (Marschalko et al., 2013), China (Kukla and An, 1989), Russia (Little et al., 2002), Spain (Günster et al., 2001) and the United States (Leighton and Willman, 1950). All these formations are characterised by a macro-porous structure with very high void ratio (typically from 0.9 to 1.25), predominantly fine granulometry mainly composed of silt- and clay-size particles and poorly accommodated structure. As consequence, loess collapses when water and pressure increases. This phenomenon produces significant damage to buildings founded by shallows foundations (Rocca, 1985). Different loessial soils can be found depending whether they suffered changes in the original structure. *Primary loess* are those that preserve their original structure generated when they were

deposited, while *secondary loess* arises when particles of primary loess are transported by any other action such as gravity, water or snow.

Loess formations cover approximately 35% of Argentina (Terzariol, 2009) with a thickness that varies from 10 m to more than 60 m, thus making these formations a good candidate to investigate GSHP system applicability in loess. In general, the mineralogy of Argentinean loess is characterised by abundance of plagioclase (20–60%), relatively little quartz (20–30%) and a significant percentage of volcanic glass (15 to 30%), and calcium carbonate (2-10%) (Teruggi, 1957). The Argentinean loess has also significant fraction of volcanic glass as a major component of the silt and sand fractions in comparison with other loess formations around the world (Kröhling and Iriondo, 1999, Kostić and Protić, 2000).

The open structure, large void ratio and mineralogy of loess control the heat flow in these formations. In addition, tillage systems and compaction influence soil thermal properties as well as volumetric water content (Guan et al., 2009, Usowicz et al., 1996). There is limited literature about the thermal characteristics of loess. Nevertheless, Table 1 summarises the most significant thermal properties of different loessial soils around the world. The most frequent thermal conductivity of Argentinean loess is close to 0.65 W/(mK) and tends to increase with the water content and bulk density of the soil (Gogół et al., 1973, Guan et al., 2009, Johnson and Lorenz, 2000, Kangning et al., 2000, Kodešová et al., 2013, Narsilio et al., 2015, Usowicz et al., 1996, Wang et al., 2007, Zuo et al., 2011, Dec et al., 2009).

<<Table 1 about here>>

3. Site description and thermal characterisation

The case study, a residential building, is located 2 km west of Cordoba city (Argentina) and consists of a typical residential 2-storey building with a footprint of approximately 85 m^2 in a 475 m^2 block of land (17.6 x 27 m) (Figure 2-a). The geological formation corresponds to a wind plain aggradation mid-Pleistocene early Holocene. This domain is characterised in the field of Cordoba city and its periphery, on both sides of the valley of the Suquía river, by a gently undulating plane of sedimentary cover-loessial silt with a regional tilt to the east of the order of 0.5%.

<<Figure 2 about here>>

The formation consists of four distinguishable layers (Figure 2-b): non-plastic silt with some organic matter (z=0 to z=0.3 m below ground surface); collapsible non-plastic silt with some clay and sand (z=0.3 m to z=9.5 m) (primary loess); low plasticity silt with sand (z=9.5 m to 13 m); and a sand with silt and gravel layer (z>13 m).

Table 1. Loess thermal conductivity ranges in different places around the world.

Site/Location	Thermal Conductivity W/(mK)	Volumetric Heat Capacity MJ/(m^{3}K)	Specific Heat Capacity* J/(kgK)	Bulk Density kg/m^3	Volumetric Moisture Content %	Source
Poland	0.5 – 1.75			1230 – 1820	0.0 – 20.0	Gogól et al. (1973)
Felin, Poland	0.47 – 1.98	1.39 – 2.42		1320 – 1410	10.5 – 24.8	Usowicz et al. (1996)
Fangshan County, China.	0.352, 0.344, 0.311	1.44, 1.39, 1.27		-	-	Kangning et al. (2000)
Alaska, USA: CRREL Permafrost Tunnel Birch Hill field sample Chena Spur Road sample	0.07 – 0.18 0.15 0.73 and 0.8	-		700 – 1000 1160 1350 and 1360	5.7 – 8.0 1.9 3.8 and 6.5	Johnson and Lorenz (2000)
China	0.29 – 1.65	1.497 – 2.95		1050 – 1650	0.5 – 43.5	Wang et al. (2007)
Loess Plateau, China	0.4 – 1.5	0.01 – 2.5		-	5.5 – 16.0	Guan et al. (2009)
Northern Germany	0.91 – 1.08	2.00 – 2.90		1470 – 1530	18.0 – 42.5	Dec et al. (2009)
Gansu, China	1.0	-		1200 – 1240	-	Zuo et al. (2011)
Suchdol, Czech Republic	0.25 – 1.5	1.1 – 3.1		1310	-	Kodešová et al. (2013)
Cordoba, Argentina	0.36 – 0.88	-		1200 – 1400	13.5 – 33.0	Narsilio et al. (2015)

*estimated based on the reported data

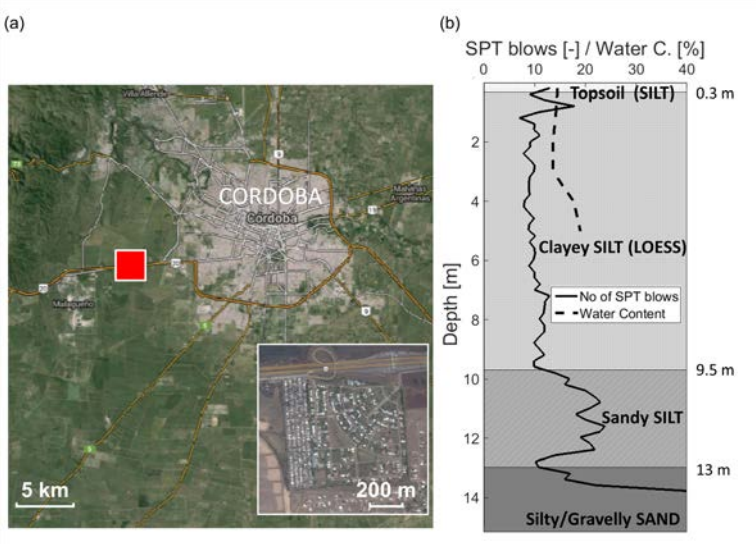


Figure 2 Site location (a). Representative soil profile, water content and profile within the site (b). Data courtesy of GEoS and Profundar.

The water table was not found within 14 m below the ground surface at the time of the geotechnical site investigation which was conducted during the dry season (winter). However, the groundwater table in this region is known to be located deeper than 20 m. In the loess layer, the natural water content was found to be about 17% and the dry density was about 1,400 kg/m^3 (thus, a total density of the order of 1,600 kg/m^3). The water content profile

measured up to 5 m in depth is shown in Figure 2-b and for modelling purposes (Section 4), it is assumed constant throughout the year, with the above value taken as representative.
The foundations of this case study involves a total of thirteen bored piles, 9.5 m deep, with nine piles of 0.4 m diameter and four (central) piles of 0.6 m diameter. Due to the relatively short length of the piles, the groundwater table is expected to be deeper than the depth of the piles throughout the year.

The thermal needle probe method was used for the determination of thermal conductivity of 'typical' loessial silts from Cordoba following ASTM recommendations (ASTM-D5334, 2008). Figure 3 summarises the measured thermal conductivities for a range of dry densities and water contents, resulting between 0.36 and 0.88 W/(mK).

<<Figure 3 about here>>

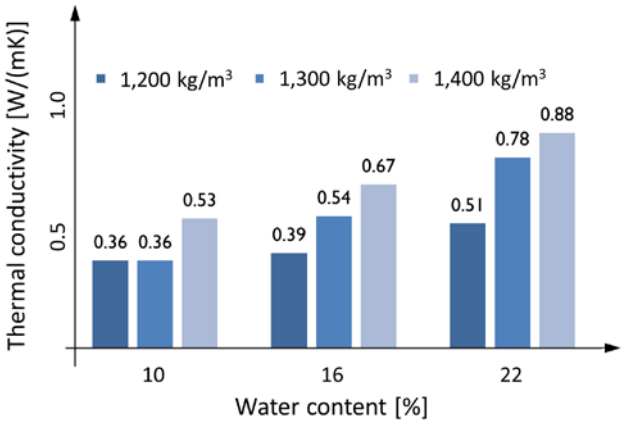


Figure 3 Measured Cordoba loess thermal conductivity for a range of water contents and dry densities.

4. Numerical modelling

The aforementioned information is used in detailed finite element simulations of the GHE-field corresponding to the building foundations using a state-of-the-art model recently developed, details of which can be found in Bidarmaghz (2014) and Bidarmaghz et al (2016). The model can account for the local geology, surface thermal recharge and the local weather for a more realistic representation of GHEs' thermal behaviour. An overview of the model, the geometry and initial and boundary conditions of the case study follows.

4.1 Governing equations

A 3D numerical model based on fundamental principles has been developed and implemented using finite element methods. The governing equations for fluid flow and heat transfer are coupled numerically within the finite element package COMSOL Multiphysics to evaluate the thermal performance of GHEs. Although important, the mechanical behaviour of the energy

piles are outside the scope of this work and this study focuses on only the thermal responses of energy piles under realistic heating and cooling cycles.

Heat transfer around and in the GHEs is modelled primarily by conduction and convection. Heat conduction occurs in the soil, GHE backfilling material (concrete) and HDPE pipe wall, and partially in the carrier fluid (water). Heat convection dominates in the carrier fluid circulating in the pipes since there is no groundwater flow in the ground (the groundwater table was not found at the site). In this modelling, the fluid flow and heat transfer in the carrier fluid are coupled to the heat transfer in the pipes, the GHEs and the surrounding soil.

The fluid flow regime in the long pipes is considered as fully developed (e.g., the entrance length of a typical 25 mm round pipe is only about 0.5 m), thus, the fluid flow and heat transfer in the fluid are simulated using 1D elements and are coupled to the 3D heat transfer in the GHEs and the surrounding soil.

To model the 1D fluid flow inside the pipes, the continuity and momentum equations for incompressible fluid are used as follow (Barnard et al., 1966):

$$\boldsymbol{\nabla}.(\boldsymbol{A}\boldsymbol{\rho_w}\boldsymbol{v}) = \mathbf{0} \tag{1}$$

$$\boldsymbol{\rho_w}\left(\frac{\boldsymbol{\partial v}}{\boldsymbol{\partial t}}\right) = -\boldsymbol{\nabla p} - \boldsymbol{f_D}\frac{\boldsymbol{\rho_w}}{\mathbf{2}\boldsymbol{d_h}}|\boldsymbol{v}|\boldsymbol{v} \tag{2}$$

where A is the inner cross-section of the HDPE pipe, ρ_w is the carrier fluid density, **v** represents the fluid velocity field, t shows the time, p is the pressure, f_D represents the Darcy friction factor and d_h is the hydraulic diameter of the pipe. The energy equation for the fluid flow to describe the convective-conductive heat transfer for an incompressible fluid is (Lurie, 2008):

$$\boldsymbol{\rho_w}\boldsymbol{AC_{p,w}}\frac{\boldsymbol{\partial T}}{\boldsymbol{\partial t}} + \boldsymbol{\rho_w}\boldsymbol{AC_{p,w}}\boldsymbol{v}\,\boldsymbol{\nabla T} = \boldsymbol{\nabla}(\boldsymbol{A}\boldsymbol{\lambda_w}\boldsymbol{\nabla T}) + \boldsymbol{f_D}\frac{\boldsymbol{\rho_w}\boldsymbol{A}}{\mathbf{2}\boldsymbol{d_h}}|\boldsymbol{v}|\boldsymbol{v}^{\mathbf{2}} + \boldsymbol{Q_{wall}} \tag{3}$$

where $C_{p,w}$ is the specific heat capacity of the fluid, λ_w represents the thermal conductivity of the fluid and Q_{wall} is the external heat exchange rate through the pipe wall. The above equations are solved for pressure p, velocity field **v** and temperature field T in the carrier fluid and are coupled to the temperature field T_m obtained from the conductive heat transfer equations solved for the soil, the GHEs and the pipes (Eq. 4). The coupling arises from the Q_{wall} term in Eq. 3, as Q_{wall} is directly proportional to the temperature inside the HDPE pipe T and the temperature on the outer wall of the HDPE pipe $T_{m,pipe\ wall}$. It should be noted that heat transfer in the soil, the GHEs and the pipe wall is purely conductive due to the absence of ground water flow:

$$\rho_m C_{p,m} \frac{\partial T_m}{\partial t} = \nabla . (\lambda_m \nabla T_m) \quad (4)$$

where ρ_m represents the solid material density, $C_{p,m}$ and λ_m are the specific heat capacity and thermal conductivity of the given solid material (soil, concrete, HDPE) respectively. This model, completed with appropriate initial and boundary conditions, has been recently validated against available analytical solutions, and full-scale experimental data (Bidarmaghz, 2014; Bidarmaghz et al., 2016;). The model is capable of accurately predicting heat transfer between the ground and the GHEs in both laminar and turbulent regimes, homogeneous and heterogeneous soil profiles, and flexible to explore a number of different pipe placement configurations in steady state and transient conditions.

4.2 Case study: geometry, initial and boundary conditions

The finite element model and the key initial and boundary conditions, together with the GHEs (piles) configuration are shown in Figure 4. The thirteen GHEs are spaced between ~2 m to 4.4 m. Only the four piles in the middle row are 0.6 m in diameter, allowing the insertion of three HDPE U-loops, whose spacing between inlet and outlet pipes is 0.16 m (a detail is shown in the figure as well). The remaining nine piles can accommodate only two of these U-loops, given their reduced diameter of 0.4 m. It should be noted that these GHEs are bored piles; therefore, a full contact between the concrete and the soil is expected and considered in these simulations. However, isolated air pockets (incomplete concreting or imperfections in the pile) may reduce GHE (structural and thermal) efficiency. The size of the ground domain in the numerical model(s) is based on a sensitivity analysis conducted on the distance between the outer GHEs and the 'external' boundaries of the ground, such that the farfield boundaries are far enough from the GHEs in all models to avoid artificial edge effects (minimum distance 8 m).

The parameters used in all numerical models are shown in Table 2. The initial and farfield ground temperature $T_{farfield}$ varies with depth z and time t of the year; these variations derive from the surface air fluctuations throughout the year, particularly in the upper few metres of the soil (i.e., about 4 m in Cordoba, Argentina). However, the average soil temperature deeper than about 4 m tends to be very close to the mean ambient temperature throughout the year at this location (i.e., 18˚C).

<<Figure 4 about here>>

<<Table 2 about here>>

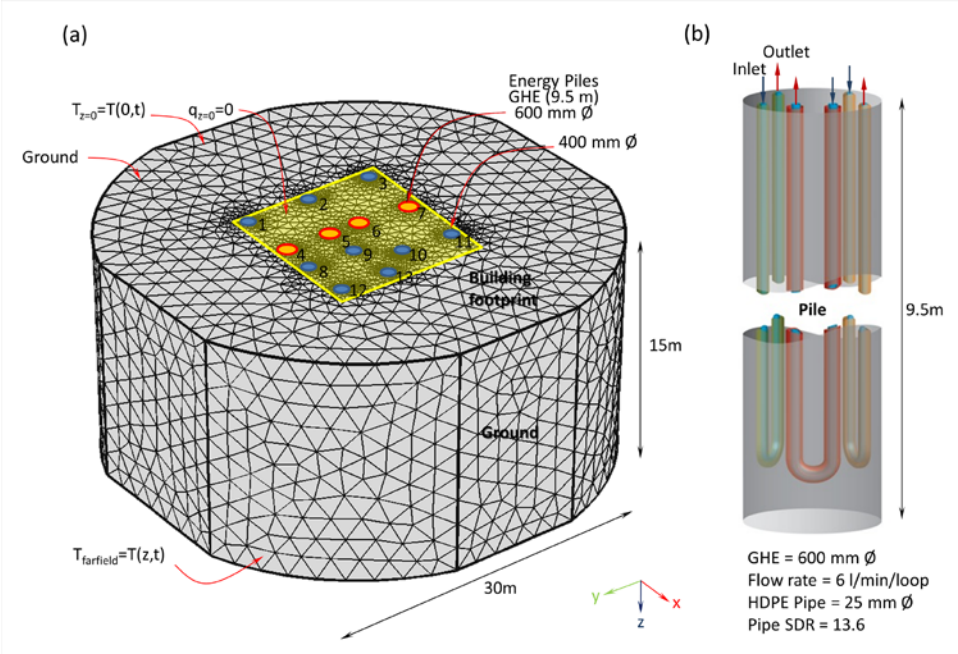


Figure 4 Finite-element model used in the simulations, with soil limits far enough to minimise artificial boundary effects (a). The building footprint (a) and a detail of a 0.6 m energy pile (b) are also shown.

Table 2. Summary of the key input parameters used in the numerical models.

Material	Thermal Conductivity W/(mK)	Specific Heat capacity J/(kgK)	Density kg/m³	$T_{farfield}$ ˚C	Diameter m	Spacing m
Loess (soil)	0.700	1,200	1,600	*T(z,t)*	-	-
Concrete (piles)	2.100	850	2,350	-	0.4, 0.6	2 - 4.4
HDPE (pipe)	0.400			-	0.025	0.16
Water (fluid)	0.582	4,180	1,000	-	-	-

Thus, some heat is exchanged between the air and the ground (surface thermal recharge/discharge) and it is accounted for in additional simulations following Baggs' adjusted empirical formulations (Baggs et al., 1991).

$$T(z,t) = T_g + 1.07 k_v A_s Exp\left[-0.0031552 z \left(\frac{1}{\alpha}\right)^{0.5}\right] * cos\left[\frac{2\pi}{365}\left((t - t_0 - 0.18335z)\left(\frac{1}{\alpha}\right)^{0.5}\right)\right] \quad 5$$

where *T(z,t)* is the ground temperature at depth of *z* metres, after *t* days from January 1st taken as $T_{farfield}$ and as initial condition, T_g, is the average annual ground temperature (18˚C in Cordoba, Argentina), k_v is the vegetation coefficient taken equal to 0.50 in this study (according to Baggs et al. (1991), for ground in full sun, k_v = 1 and for a long grass covered area k_v = 0.25), A_s is the earth surface temperature annual swing above and below the average ground temperature (14°C), t_0 represents the number of days after January 1st to the minimum earth surface temperature (238 days in Cordoba), and α stands for the soil thermal diffusivity (0.3645 x 10^{-2} cm^2/sec).

For simplicity, the annual peak building thermal load was estimated based on rules of thumb for typical gated community residencies in Cordoba (heating = 0.035 kW/m^3 or 30 kcal/(hm^3); cooling = 0.058 kW/m^3 or 50 kcal/(hm^3)) rather than detailed energy balance calculations. Our case study comprises a total of 160 m^2 covered area, of which 20 m^2 is for a double garage that does not need conditioning. Thus, for 2.6 m height ceilings, the peak heating and cooling demands result in approximately 12.7 kW and 21.1 kW respectively.

5. Results and discussions

There are a number of design strategies that could be implemented when deciding on a residential GSHP system, including aiming to provide 100% of the heating and cooling required or to combine geothermal with auxiliary systems (i.e., designing a hybrid system) in all cases avoiding ground freezing that could lead to ground heave or damage to concrete in the pile (Loveridge and Powrie, 2014). Perhaps the first question to be answered is what the geothermal installed capacity of this residential building would be if all thirteen of its piles were used as GHEs. Figure 5-a shows the total building heating and cooling demand distribution throughout a year, based on the peak demands (12.7 kW and 21.1 kW, Section 4.2) and the air temperature recorded in 2014.

The newly developed numerical model revealed that the thirteen piles are unable to satisfy 100% of both heating and cooling thermal demands of the building. Thus, one alternative is to consider hybrid systems: the GSHP system covers part of the demand and the auxiliary systems (e.g., smaller gas heater(s), smaller air conditioner unit(s), thermal solar panels and busters, etc.) are either used to top up the supply of heating or cooling (Case 1) or just turned on when this base demand exceeds the geothermal capacity (Case 2). Case 1 implies that the auxiliary system is running all the time concurrently with the GSHP, while Case 2, only a number of days each year.

As presented in Figure 5-a, Case 1 indicates that the GSHP system is designed to provide half and one third of total heating and cooling demand of the house respectively, with an auxiliary system being used 246 days in heating mode and 118 days in cooling mode. The geothermal system satisfies up to 7 kW of the peak heating and cooling demand of the house. In the other case (Case 2), the GSHP system also has the same 7 kW peak capacity; however, due to the different thermal load distribution, the geothermal system is aimed at satisfying almost all heating and more than half the cooling demand of the house with significantly less days of auxiliary systems being used.

To highlight how the GHE-field will perform and react to the defined thermal loads, the modelled average fluid temperature variations (i.e., $(T_{inlet}+T_{outlet})/2$)) in the most demanded GHE (pile #5-Figure 4) obtained from 20-year numerical simulations are presented in Figure 5-b. It is observed that satisfying Case 1's thermal load distribution results in a reasonable temperature

range (3.1˚C to 44.3˚C) compatible with most commercially available heat pumps. On the other hand, Case 2 results in a fluid temperature drop to a minimum of -2.2˚C in cold seasons (which is acceptable with an antifreeze solution used as carrier fluid instead of plain water) and rise to the maximum of 56.5˚C in warm seasons. This maximum fluid temperature for Case 2 is higher than typical GSHP recommended EWT (entering water temperature to the heat pump). It follows that this GHE-field, using the structural piles, is not capable of delivering the more desirable thermal load defined for Case 2. Thus, this article focuses on Case 1 from now on.

<<Figure 5 about here>>

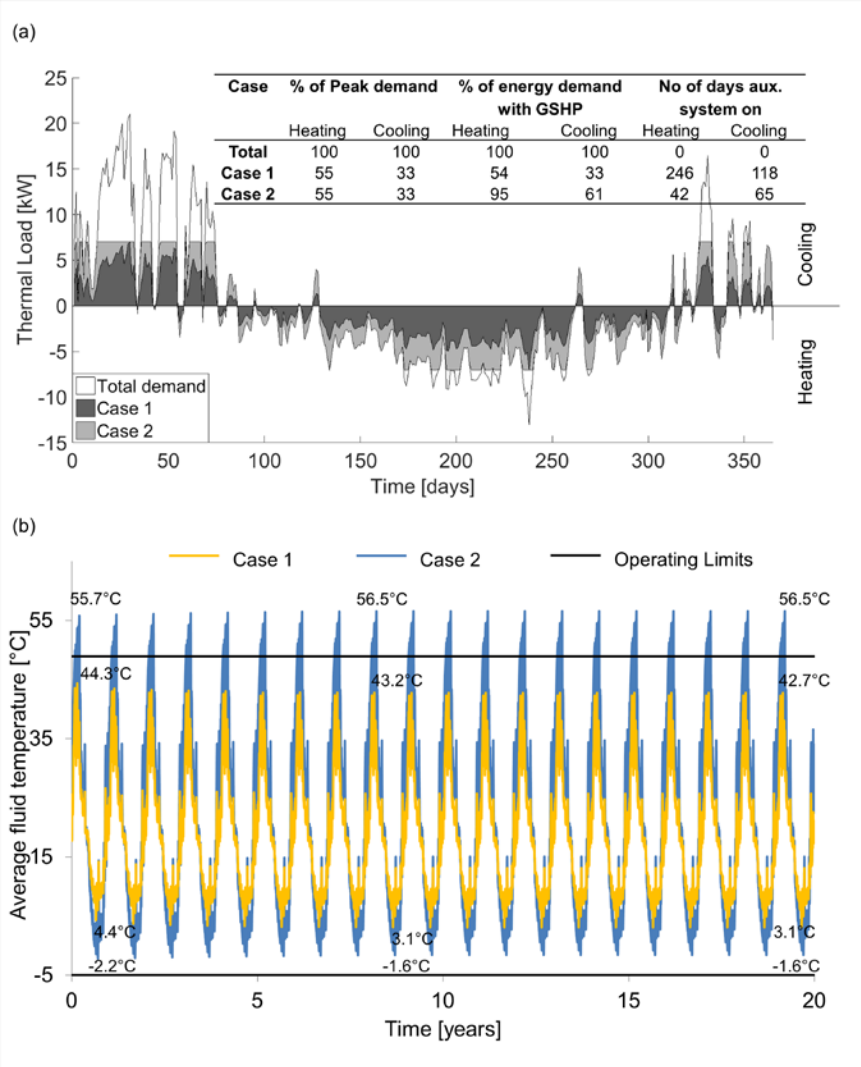


Figure 5 Thermal load distributions throughout a year (a) and GHE response along 20 years (including typical GSHP operating EWT range) (b).

Figure 6 shows the temperature field at mid-depth of the energy piles (about 5 m below ground surface) (year 10). The figure shows that freezing is avoided in the GHE-field for Case 1, with no point within the soil or the energy piles reaching less than 4.8˚C, even during the coolest seasons when the GHEs extract more of the thermal heat from the ground. Therefore, potential structural problems due to concrete freezing and/or soil heaving are circumvented.

<<Figure 6 about here>>

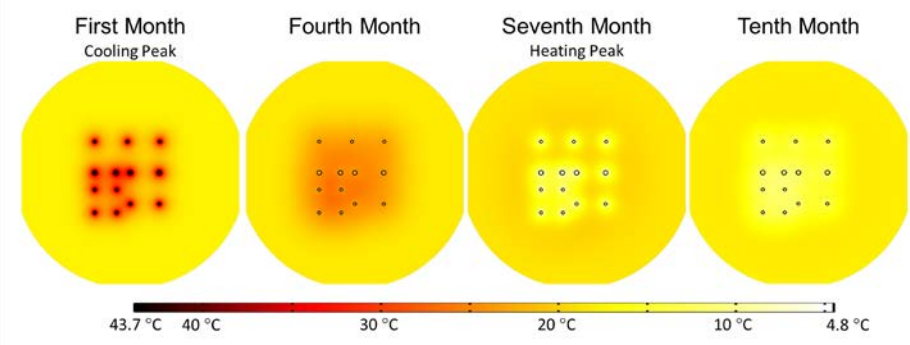


Figure 6 Temperature field in the thirteen piles and surrounding soil at 5 m below surface (year 10).

From these results, it follows that even though the low thermal conductivity of loess (0.7 W/(mK)) and relatively shallow GHEs (~10 m) affect thermal efficiency of the GSHP systems, the incorporation of a GSHP system into the inexorably needed thirteen structural piles (described in Section 3) leads to about 30% savings in the conventional energy usage (e.g., electricity or fossil fuels) and in the energy bills, with the GSHP satisfying at least 54% of the heating needs and 33% of the cooling needs. Although this GHE-field cannot provide 100% of the required heating and cooling demand, it can be used to provide part of the building thermal demand with little additional capital cost.

To increase the capacity of the GSHP system conditioning the case study building, another alternative would be drilling additional GHEs outside the footprint of the house in the available block of land. Increasing the number of GHEs may lead to some extra drilling costs; however, may also have significant influence on further reducing running energy costs. Therefore, twelve 9.5 m long GHEs are added to the original GHE-field, bringing the total number to twenty five. These additional GHEs do not serve any structural purpose. Surface thermal recharge is also accounted for. Figure 7 shows a schematic of the GHEs and their locations within the available block of land with twelve GHEs being added to the original GHE-field. The extra GHEs are of 0.6 m diameter, contain three U-loops, and are of the same depth as the rest of the GHE-field (9.5 m long GHEs).

<<Figure 7 about here>>

The building thermal load applied as one of the boundary conditions on the model is shown in Figure 8 with 12.7 kW of peak heating and cooling demand now aimed to be satisfied (instead of 7 kW).

<<Figure 8 about here>>

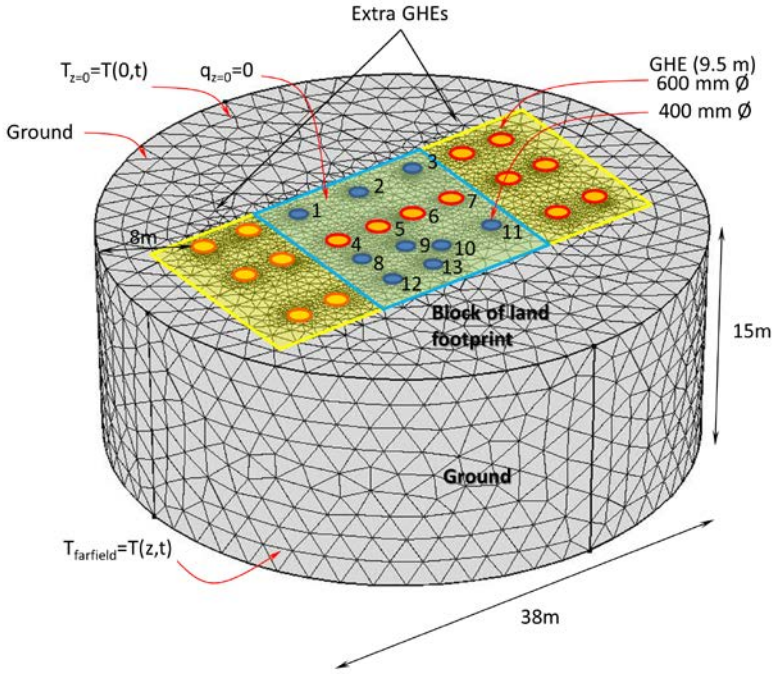


Figure 7 Schematic of the expanded GHE-field and location of the GHEs within the block of land.

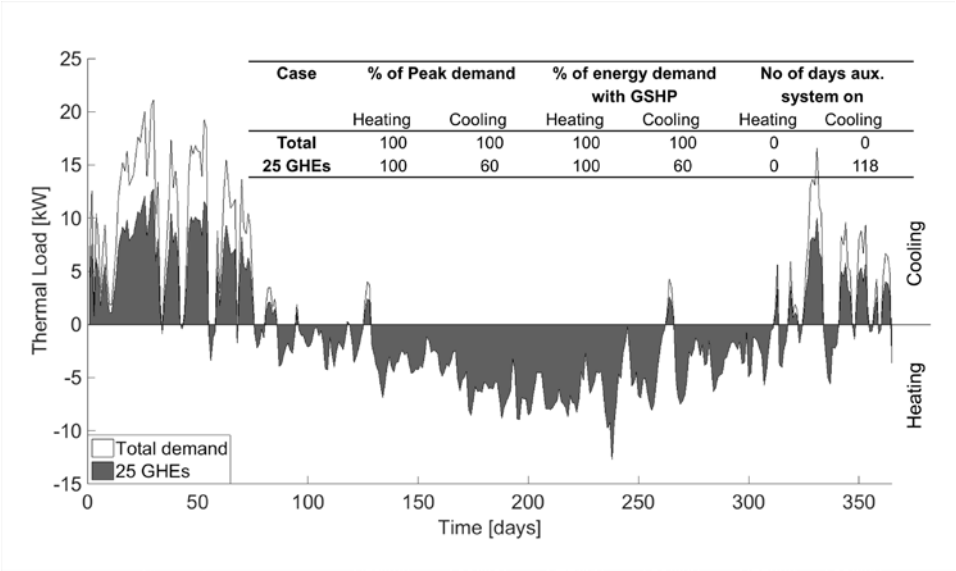


Figure 8 Building thermal load applied on the model with extended number of GHEs (25 GHEs).

The average fluid temperature obtained from one of the most thermally influenced GHEs (pile #5) is shown in Figure 9. Satisfying a peak load of 12.7 kW heating and cooling, leads to the fluid temperature varying within a reasonable range (i.e., maximum of 37.2°C and minimum of 6.8°C). The extra twelve GHEs in the GHE-field results in 100% of the heating demand and 60.2% of the cooling demand being provided by the GSHP system. A significant improvement in heating and cooling capability of the system is obtained in comparison to the cases investigated in Section 4.2 (Cases 1 and 2). Moreover, the even smaller (and cheaper) auxiliary conditioning system is required for 118 days per year, and only in cooling mode. The savings in the

installation of auxiliary systems and on running costs would determine the economic feasibility of the additional drilling costs.

<<Figure 9 about here>>

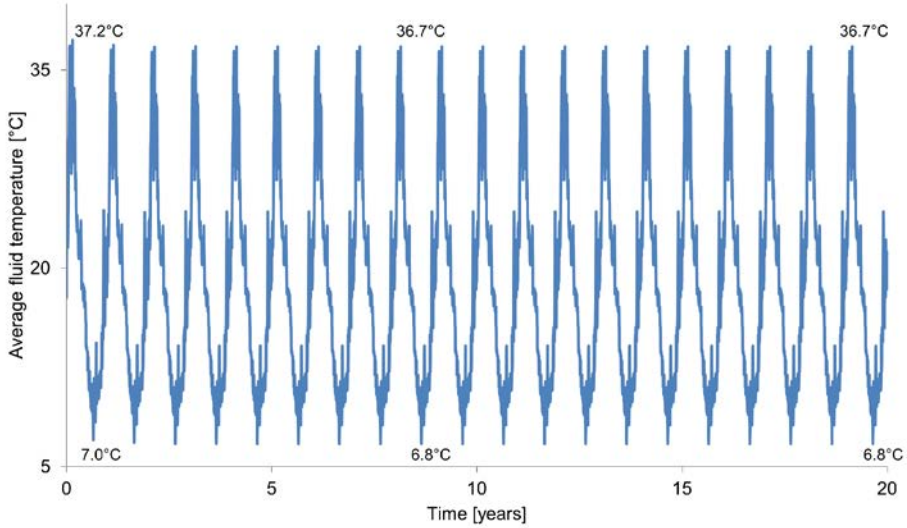


Figure 9 Average GHE fluid temperature in the expanded GHE-field during 20 years of operation.

GSHP system designers and potential users of these systems should be aware that inadequate designs (or drastic changes in the thermal load patterns) may lead to more pronounced overheating or overcooling of the soil in the medium term until reaching a periodic thermal equilibrium. This change or drift in the overall ground temperature from year to year inevitably influence the efficiency of the system over time, thus affecting the running costs and saving levels of the GSHP systems during their lifespan.

Loessial soils in Cordoba, Argentina are of relatively low thermal conductivities. However, loess covers extensive areas in Asia, Europe and America, for which higher thermal conductivities have been reported (see Table 1). To investigate the effect of higher soil thermal conductivities on thermal exchange capacity of GHEs in loess, numerical models with thermal conductivities of 1.1 and 1.6 W/(mK) are built and solved and results for 20 years of system operation are shown in Figure 10. The building thermal load distribution applied on this model follows the pattern shown in Figure 5-a indicated as Case 1, which is applied on thirteen 9.5 m long GHEs. It is observed that loessial soil with higher thermal conductivity will significantly improve thermal performance of GHEs. The maximum fluid temperature in the most thermally affected GHE is about 5.4°C lower than Case 1 when the soil thermal conductivity is equal to 1.1 W/(mK) (38.9°C vs 44.3°C). Increasing the thermal conductivity to 1.6 W/(mK), which can be considered as an average value of highly conductive loessial soils based on Table 1, further decreases the maximum fluid temperature to about 33.6°C, which is 10.7°C lower than the maximum fluid temperature observed in Case 1. These results suggest that with higher thermal conductivity

loess, the GHE-field is not working at its full capacity and either the thermal load aimed to be satisfied by the GSHP system can be increased or alternatively the number of additional GHEs can be reduced.

<<Figure 10 about here>>

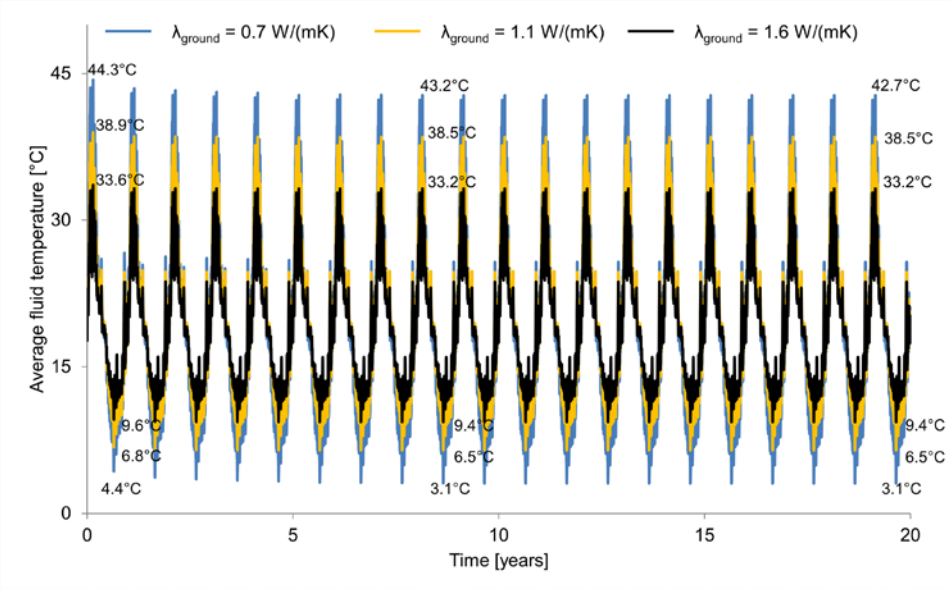


Figure 10 Average GHE fluid temperature during 20 years of operation for higher thermally conductive loessial soils (based on Case 1).

6. Conclusions

Pile and micro-piles in loessial areas can be easily converted into GHEs while being built. Results from the realistic detailed modelling show that the partial substitution of electrical heating and cooling systems with geothermal systems consisting of thirteen energy piles could significantly reduce energy consumption and the size of associated infrastructure (electricity grid). The temperate climate dominating in Cordoba presents ideal conditions for GSHP systems allowing thermal recharge of the ground between seasons and thus maximizing the heating and cooling capacity that energy piles can achieve; similar conditions apply to other parts of the world. Results shows that the thirteen energy piles embedded under the residential case study building are capable of delivering approximately 54% and 33% of the heating and cooling demand of the building respectively. The addition of twelve extra GHEs to the GHE-field allows satisfying 100% of the heating demand and 60% of the cooling. Consequently additional savings are achieved on the energy bills (running costs) and on the (smaller) auxiliary systems still needed to cover the remaining 40% cooling demand (capital costs). This case study shows the potential of GSHP technology in a local environment dominated by loess and gives some bases to geotechnical engineers to start considering the technology in their designs and practices.

A parametric analysis of thermal conductivity of loessial soil confirms that higher thermal conductivity of the soil significantly helps to reduce the number of GHEs in the system. As the loessial soils around the world show thermal conductivities varying between 0.1 W/(mK) and

about 2 W/(mK), numerical results suggest that GSHP systems in loessial soils of higher thermal conductivity (e.g., Europe, Asia) show a great potential to economically satisfy conditioning of buildings and encourages further application of this technology in loessial soils.

Acknowledgments

Funding from ARC FT140100227 and The University of Melbourne is much appreciated. The authors would like to also acknowledge the contributions of H Ferrero (Profundar), C Serrano (GEoS and UCC) and E. Delacoste (UNC) in terms of information about the residential case study and loess thermal properties.

References

Amatya B, Soga K, Bourne-Webb P & Laloui L (2012) Thermo-mechanical performance of energy piles. *Geotechnique* **62 (6)**: 503-519.

Astm-D5334 (2008) Standard Test Method for Determination of Thermal Conductivity of Soil and Soft Rock by Thermal Needle Probe Procedure. *ASTM International.* West Conshohocken, PA, USA.

Baggs S, Baggs D & Baggs JC (1991) *Australian Earth-Covered Buildings,* New South Wales University Press. NSW, Australia.

Barnard A, Hunt W, Timlake W & Varley E (1966) A theory of fluid flow in compliant tubes. *Biophysical Journal,* **6 (6)**: 717-724.

Bidarmaghz A. (2014) *3D numerical modelling of vertical ground heat exchangers.* PhD thesis, The University of Melbourne, Asutralia.

Bidarmaghz A, Narsilio G, Johnston I & Colls S (2016) The importance of surface air temperature fluctuations on long-term performance of vertical ground heat exchangers. *Geomechanics for Energy and the Environment*: (in press).

Brandl H (2006) Energy foundations and other thermo-active ground structures. *Geotechnique,* **56 (2)**: 81-122.

Dec D, Dörner J & Horn R (2009) Effect of soil management on their thermal properties. *Revista de la Ciencia del Suelo y Nutrición Vegetal,* **9 (1)**: 26-39.

Francisca FM (2007) Evaluating the constrained modulus and collapsibility of loess from standard penetration test. *International Journal of Geomechanics,* **7 (4)**: 307-310.

Gogół W, Gogół E & Artecka E (1973) Thermal Conductivity Investigations of Moist Soils. *Journal of Power Technologies,* **40**: 49-69.

Guan X, Huang J, Guo N, Bi J & Wang G (2009) Variability of soil moisture and its relationship with surface albedo and soil thermal parameters over the Loess Plateau. *Advances in Atmospheric Sciences,* **26**: 692-700.

Günster N, Eck P, Skowronek A & Zöller L (2001) Late Pleistocene loess and their paleosols in the Granada Basin, Southern Spain. *Quaternary International,* **76**: 241-245.

Johnson JB & Lorenz RD (2000) Thermophysical properties of Alaskan loess: An analog material for the Martian polar layered terrain. *Geophysical Research Letters,* **27 (17)**: 2769-2772.

Johnston I, Narsilio G & Colls S (2011) Emerging geothermal energy technologies. *KSCE Journal of Civil Engineering,* **15 (4)**: 643-653.

Kangning H, Binri W & Guangcan Z (2000) Study on soil thermal properties in forest land of catchment in loess. *Journal of Beijing Forestry University,* **22 (3)**: 27-32.

Kodešová R, Vlasakova M, Fer M, Tepla D, Jakšík O, Neuberger P & Adamovský R (2013) Thermal properties of representative soils of the Czech Republic. *Soil Water Res,* **8 (4)**: 141-150.

Kostić N & Protić N (2000) Pedology and mineralogy of loess profiles at Kapela-Batajnica and Stalać, Serbia. *Catena,* **41 (1)**: 217-227.

Kröhling DM & Iriondo MN (1999) Upper Quaternary palaeoclimates of the Mar Chiquita area, North Pampa, Argentina. *Quaternary International,* **57**: 149-163.

Kukla G & An Z (1989) Loess stratigraphy in central China. *Palaeogeography, Palaeoclimatology, Palaeoecology,* **72**: 203-225.

Leighton MM & Willman HB (1950) Loess formations of the Mississippi Valley. *The Journal of Geology,* **58 (6)**: 599-623.

Little EC, Lian OB, Velichko A, Morozova T, Nechaev V, Dlussky K & Rutter N (2002) Quaternary stratigraphy and optical dating of loess from the east european plain (Russia). *Quaternary Science Reviews,* **21 (14)**: 1745-1762.

Loveridge F & Powrie W (2014) 2D thermal resistance of pile heat exchangers. *Geothermics,* **50**: 122-135.

Lurie MV (2008) *Modeling and Calculation of Stationary Operating Regimes of Oil and Gas Pipelines,* Wiley-VCH Verlag GmbH & Co. KGaA. Weinheim, Germany.

Marschalko M, Yilmaz I, Fojtova L, Lamich D & Bednarik M (2013) Properties of the loess sediments in Ostrava region (Czech Republic) and comparison with some other loess sediments. *The Scientific World Journal,* **2013**: 7 pages.

Moll L & Rocca R (1991) Properties of loess in the center of Argentina. In *XI Pan American Conference on Soil Mechanics and Foundation Engineering*, Viña del Mar, Chile. 1-14.

Narsilio G, Francisca F, Ferrero H, Bidarmaghz A, Serrano C, Perez M, Makasis N & Delacoste E (2015) Geothermal Energy in Loess: A Detailed Numerical Case Study for Cordoba. *XV Panamerican Conference on Soil Mechanics and Geotechnical Engineering.* Buenos Aires, Argentina.

Oklahoma State University (2009) *Ground Source Heat Pump Residential and Light Commercial Design and Installation Guide (IGSHPA)*. Oklahoma, USA.

Preene M, Powrie, W. (2009) Ground energy systems: from analysis to geotechnical design. *Geotechnique,* **59 (3)**: 261-271.

Quintana Crespo E. (2005) *Relación entre las propiedades geotécnicas y los componentes puzolánicos de los sedimentos pampeanos.* PhD, Universidad Nacional de Córdoba. Argentina,

Rinaldi V, Rocca R & Zeballos M (2007) *Geotechnical characterization and behavior of Argentinean collapsible loess,* Taylor & Francis, Boca Raton, Fla, USA.

Rocca R. (1985) *Review of engineering properties of loess.* M.Sc. thesis, University of California, Berkeley, CA, United States.

Rocca RJ, Redolfi ER & Terzariol RE (2006) Características geotécnicas de los loess de Argentina. *Revista Internacional de Desastres Naturales, Accidentes e Infraestructura Civil,* **6 (2)**: 149-166.

Teruggi ME (1957) The nature and origin of Argentine loess. *Journal of Sedimentary Research,* **27 (3)**: 322-332.

Terzariol RE (2009) años de estudio de los suelos loessicos en Córdoba, Argentina. *Desafíos y avances de la geotecnia joven en Sudamérica,* **1**: 323-337 (in Spanish).

Usowicz B, Kossowski J & Baranowski P (1996) Spatial variability of soil thermal properties in cultivated fields. *Soil and Tillage Research,* **39 (1)**: 85-100.

Wang T-H, Liu Z-C & Lu J (2007) Experimental study on coefficient of thermal conductivity and specific volume heat of loess. *Yantu Lixue(Rock and Soil Mechanics),* **28 (4)**: 655-658.

Zárate MA (2003) Loess of southern South America. *Quaternary Science Reviews,* **22 (18)**: 1987-2006.

Zuo J, Wang J, Huang J, Li W, Wang G & Ren H (2011) Estimation of ground heat flux and its impact on the surface energy budget for a semi-arid grassland. *Sci Cold Arid Region,* **3 (1)**: 41-50.

Appendix B – The application of retaining walls and slabs as energy structures in underground train stations

This section consists of a journal paper titled: “The application of retaining walls and slabs as energy structures in underground train stations”, published in the conference proceedings titled *Energy Geotechnics*, of the conference SEG 2018 in Lausanne, Switzerland. The paper has been inserted in the following pages.

The Application of Retaining Walls and Slabs as Energy Structures in Underground Train Stations

Nikolas Makasis[1(✉)], Guillermo A. Narsilio[1], Asal Bidarmaghz[2], and Ian W. Johnston[1]

[1] The University of Melbourne, Parkville, Australia
nikolas.makasis@unimelb.edu.au
[2] University of Cambridge, Cambridge CB2 1PZ, UK

Abstract. Shallow geothermal technologies have proven to efficiently provide renewable energy for heating and cooling. Recently much attention has been given to utilising sub-surface structures, primarily designed for stability, to also transfer heat to and from the ground, converting them into energy geo-structures. This work investigates the potential of applying this technology to the geo-structures of underground train stations in the city of Melbourne (Australia) to fulfil some of their heating and cooling demands. The diaphragm retaining walls and slabs that form part of a case study station are designed to also incorporate geothermal pipe loops. A finite element numerical model comprising the station walls and slabs is presented and used to investigate the thermal performance of these systems, for the temperate climate and geological conditions of Melbourne, adopting an expected lifespan of at least 25 years. The technical applicability of this technology is discussed for different thermal load scenarios, showing the importance of thermal storage and the balanced distribution of the thermal load.

1 Introduction

With energy demand rising and the necessary movement towards cleaner sources of energy, significant attention has been given to shallow geothermal technologies, which can very efficiently provide thermal energy for heating and cooling buildings (Johnston *et al.* 2011). Traditionally, these technologies use boreholes or trenches, incorporating piping with a circulating carrier fluid, to form ground heat exchangers (GHEs) that use the ground as a heat sink/source (Florides and Kalogirou 2004). However, traditional GHEs come with high capital costs either due to drilling or the land space requirements. To overcome this drawback, a relatively recent alternative approach incorporates the piping loops in underground structures that are primarily designed for stability, such as tunnel linings, pile foundations or retaining walls (Brandl 2006, 2016). This makes energy provision a secondary function for these (energy) structures, but also introduces limitations to the geothermal designer, making the provision of the entire energy demands not guaranteed and instead encourages the use of a hybrid

© Springer Nature Switzerland AG 2019
A. Ferrari and L. Laloui (Eds.): SEG 2018, SSGG, pp. 43–50, 2019.
https://doi.org/10.1007/978-3-319-99670-7_6

nikolas.makasis@unimelb.edu.au

system (Mikhaylova *et al.* 2016; Aditya *et al.* 2018), that incorporates energy structures with other auxiliary (conventional) heating and cooling systems.

The most well researched energy structure has been energy piles (Loveridge and Powrie 2013; Cecinato and Loveridge 2015), most likely due to the similarities with the traditional borehole. However, little research exists on the applicability and use of energy retaining walls (Bourne-Webb *et al.* 2016; Di Donna *et al.* 2016), which compared to energy piles, introduce an important difference, since walls are not all surrounded by soil, but instead one side of the wall faces the interior of the underground building (such as an underground train station's platform), as depicted in Fig. 1. There is currently limited information regarding how energy retaining walls can be best utilised, especially regarding long-term thermal performance. This study examines the suitability of energy diaphragm retaining walls for an underground train station based in the city of Melbourne, Australia, and presents a novel analysis focusing on thermal performance for two different geometrical configurations over an operating period of 25 years.

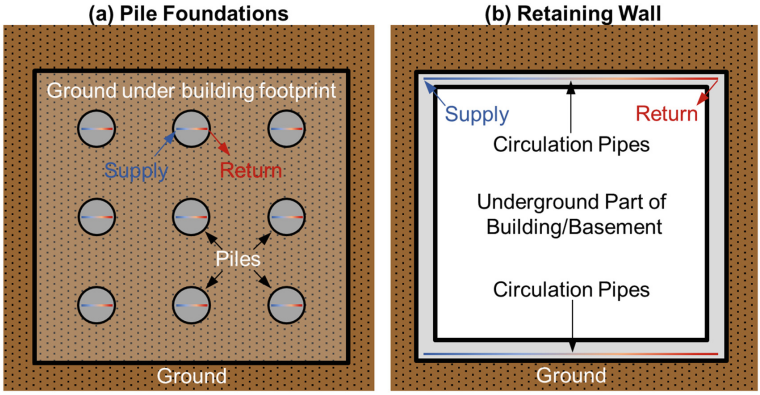


Fig. 1. Schematic top view of energy piles and energy retaining walls (not to scale)

2 Methodology

This study focuses on the *thermal* performance of energy diaphragm retaining walls. The main research questions relate to the importance of the thermal load distribution on the more thermally constrained energy retaining walls, as well as the benefits of adding piping in the bottom slab as well as the retaining walls. To perform this research 3D finite element modelling has been developed and used, adopting an experimentally validated methodology developed at the University of Melbourne (Bidarmaghz 2014). This approach is implemented using the software package COMSOL and couples the governing equations of heat transfer (energy balance) and fluid flow (momentum and continuity), modelling the heat transfer primarily by *conduction* (ground, concrete, pipe walls, partially in circ. fluid) and *convection* (circ. fluid). This methodology has been

nikolas.makasis@unimelb.edu.au

experimentally validated with both traditional systems, as well as energy structures (Bidarmaghz *et al.* 2017; Bidarmaghz and Narsilio 2018).

The modelling, geometry and parameters used can be seen in Fig. 2 and Table 1. As can be noticed, the symmetry boundary condition has been used in both XZ and YZ planes to reduce the computational costs (the latter conservatively assuming an infinite wall length along the x axis). Moreover, a constant undisturbed temperature of 18.5 °C is used at the far boundary, assuming that the heat transfer will not influence the ground at this distance. The bottom surface is modelled as a no heat flux boundary (i.e., thermal insulation), assuming negligible bedrock heat flux. Finally, the surfaces of the wall and slabs inside the station have also been modelled as thermally insulated, to avoid thermal leaking in/out of the station, even though this technique may result in additional capital costs. A detailed investigation on the boundary conditions for these surfaces can be found in (Makasis *et al.* 2018). Regarding the geometry, it is worth noting that the pipes in the wall have 275 mm cover on the ground side while the ones in the slab have 156 mm cover on the bottom and 100 mm cover on each end along the y axis.

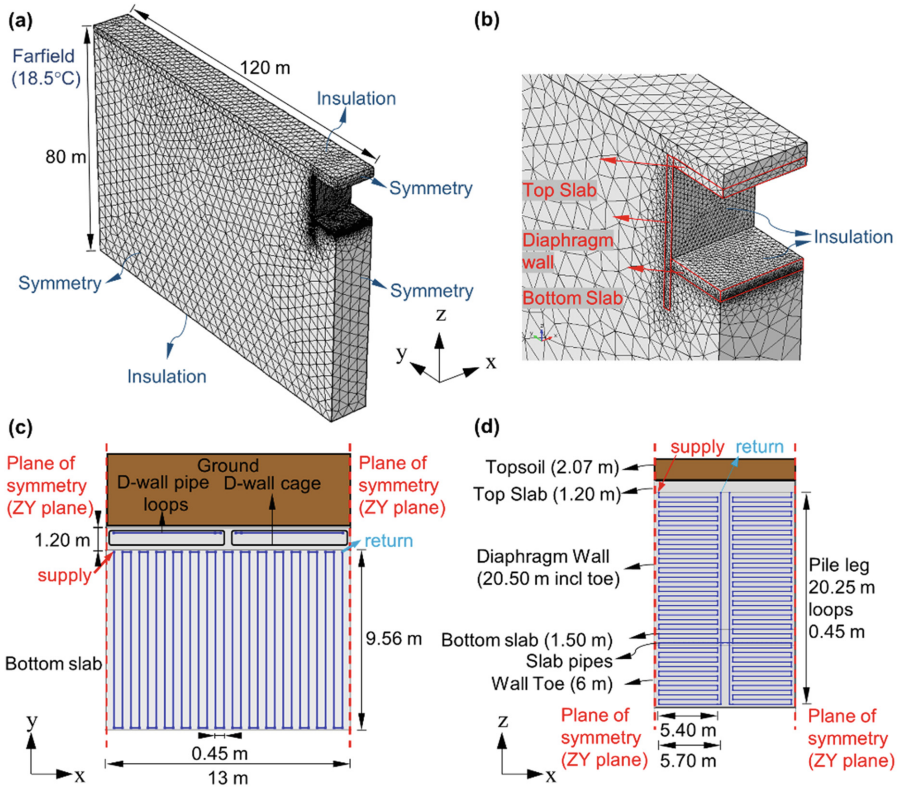


Fig. 2. Finite element modelling: overview (a), detail (b), model geometry in the XY (c) and ZX (d) planes

nikolas.makasis@unimelb.edu.au

Table 1. Modelling parameters

Parameter	Value	Unit	Description
λ_{ground}	3.4	W/(mK)	Effective thermal conductivity of ground (from TRT)
ρ_{ground}	2400	kg/m^3	Density of ground
$C_{p\ ground}$	830	J/(kgK)	Specific heat capacity of ground
$T_{farfield}$	18.5	°C	Average annual ground temperature
$\lambda_{concrete}$	2.1	W/(mK)	Thermal conductivity of concrete
$\rho_{concrete}$	2250	kg/m^3	Density of concrete
$C_{p\ concrete}$	890	J/(kgK)	Specific heat capacity of concrete
λ_{fluid}	0.58	W/(mK)	Thermal conductivity of carrier fluid
ρ_{fluid}	1000	kg/m^3	Density of carrier fluid
$C_{p\ fluid}$	4180	J/(kgK)	Specific heat capacity of carrier fluid

A crucial parameter for the modelling is the thermal load distribution, representing the amount of thermal energy the system needs to provide. Figure 3 shows two thermal load distributions adopted for this work. The first one (*original)* represents typical requirements for an underground train station in Melbourne, Australia, those being heavily cooling dominant due to the large amounts of heat generated by the trains, plants and commuters. It should be noted that this distribution represents 100% of the heating demand for the entire station and 20% of the cooling demand, with the rest being supplemented using auxiliary means (such as chillers and cooling towers). The second one is a modified balanced version of the first (equal amounts of cooling and heating) where additional heating is supplied. Since the station has no need for more heating, this additional heating is assumed to be supplied to nearby buildings, such as schools, hospitals or apartment blocks amongst others. In all cases, the thermal load is equally distributed over 67 diaphragm wall pipe loops and (if applicable) 33 slab loops of the entire (about 200 m long) train station.

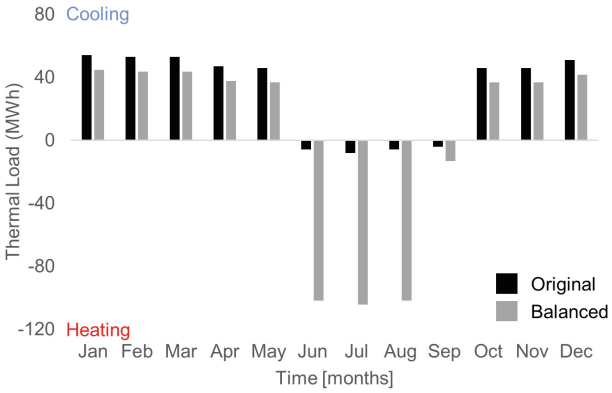


Fig. 3. Annual thermal load distributions

nikolas.makasis@unimelb.edu.au

3 Results and Discussion

The results of the numerical simulations are presented Fig. 4, showing the average fluid temperature within the pipes (average of inlet and outlet of header pipe) over an operating period of 25 years. In the geothermal design of these systems, it is crucial that this temperature range is within the acceptable operating limits of the heat pump, as well as that they are not extreme such that can cause, for example, freezing in the ground. Therefore, in this work, the fluid temperatures are to be restrained between 0 °C and 40 °C, the latter of which is indicated on the figures for reference. Furthermore, the first figure shows the results when geothermal piping is implemented only in the diaphragm walls while the second when geothermal piping is implemented in both the diaphragm walls as well as the bottom slab. This shows the relative improvement on the system performance, by the addition of the slab, with an average lowering of about 1 °C in the maximum mean fluid temperature. Finally, each figure presents the results for both thermal load distributions presented in Fig. 3, as well as variations of the *original*, where the cooling load provided is reduced to make the design technically feasible (since providing 100% of the *original* thermal load results in temperatures over 40 °C).

Looking at Fig. 4(a), it can be seen that only about 80% of the *original* thermal demand can be satisfied, assuming that the system will stop running after 25 years to restore the thermal balance. This is because of the cooling dominant nature of the thermal load, with heat being continuously extracted from the station towards the ground, where it keeps accumulating, increasing the ground temperatures. This heat accumulation will make the operation of the geothermal system less efficient over the years as the temperatures become higher. Using the *balanced* load, on the other hand, results in a greatly improved system performance with the fluid temperatures kept stable, approximately between 7 °C and 25 °C. Since equal amounts of heat get injected to and extracted from the ground, thermal equilibrium is preserved each year and there are no thermal accumulation effects in the long term. Due to these reasons, a system adopting the *balanced* thermal load would also comfortably run for much longer periods of time.

Figure 4(b) shows similar results, with only about 85% of cooling being comfortably provided when the *original* thermal load is considered, while using the *balanced* thermal load results in a stable performance with the fluid temperatures fluctuating approximately between 10 °C and 24 °C. Therefore, the addition of the slab piping improves the performance of the system, by shifting the fluid temperatures away from the upper and lower limits (reducing the max and increases the min). In this particular case, it would allow the system to provide about 5% more cooling energy for the *original* load case. However, in the case where the extra heating could be supplied to balance the load, adding geothermal pipping in the slab would not result in significant improvements. Even though the fluid temperature extremes are reduced/increased by 1 to 3 °C, the temperature range without the slab piping is already acceptable and therefore the improvement would only be in terms of the coefficient of performance (COP), meaning that less electricity would be required to run the system, and therefore resulting in a small reduction in the operational costs. To properly quantify the benefits of adding the piping in the slab, a thorough analysis of the relevant cost is required,

nikolas.makasis@unimelb.edu.au

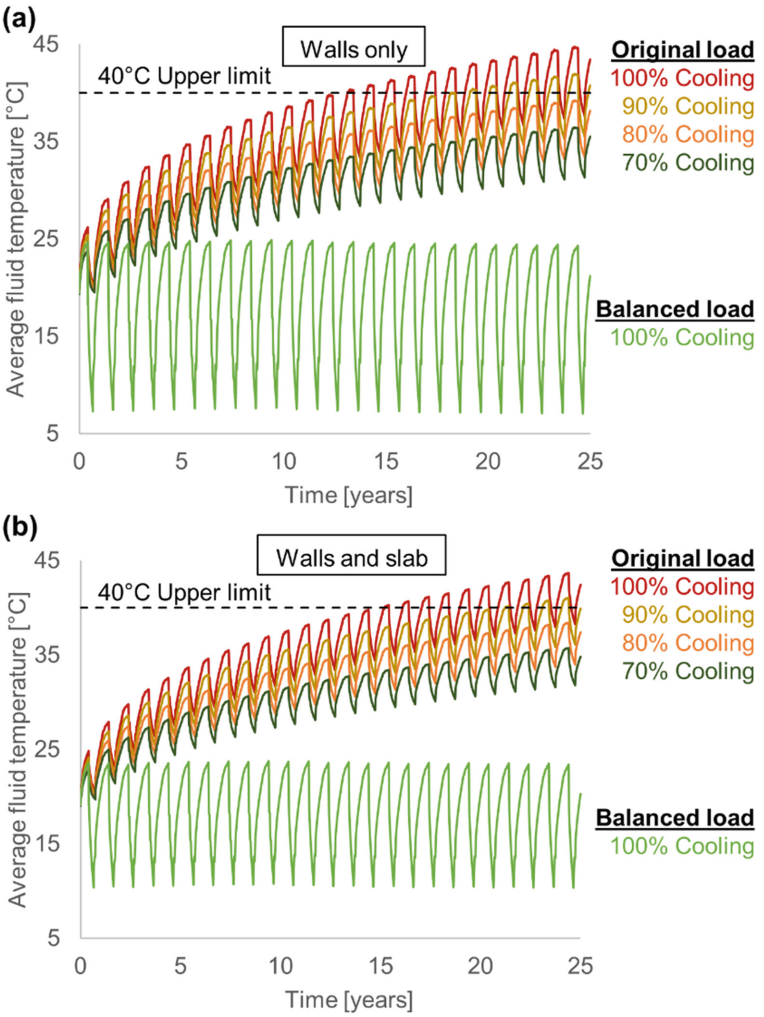


Fig. 4. Results for geothermal piping implemented in diaphragm walls only (a) and in diaphragm walls *and* bottom slab (b)

taking into account the relative novelty of this concept and therefore the associated risks, as well as the benefits, both monetary and environmental (such as providing more renewable energy).

The investigation shows that a large portion (80–85%) of its target cooling demand (or 16–17% of total station demand) can be provided by the energy walls (and slabs). However, the fluid temperatures keep rising, indicating that the system can only run for a finite amount of time, before requiring shutting down for some time, to restore the thermal state of the ground. On the other hand, balancing the thermal load not only results in a much better running system, but also would be less costly to operate and

nikolas.makasis@unimelb.edu.au

would be able to run for much longer time. Moreover, the resulting fluid temperature ranges suggest that if even more heating demand existed for the surrounding structures, the system could be able to provide even more amounts of cooling, reducing the energy dependencies on auxiliary systems (for example 200% of the target cooling, or 40% of the total station cooling demand).

4 Conclusion

This work briefly presented an investigation on the use of diaphragm retaining walls as energy structures to provide geothermal energy for space heating and cooling purposes. An underground station in Melbourne, Australia, was adopted as a case study and the investigation focused on the importance of the thermal load distribution as well as two potential designs, one incorporating the technology only in the diaphragm walls and the second also adding it to the bottom slab of the station.

The thermal load investigation showed that this is a crucial parameter to energy retaining walls, likely more significant than for traditional boreholes or energy piles, due to the more limited available ground. An evaluation of the maximum feasible amount of thermal energy that can be provided for a typical underground station in Melbourne, showed that the system could only provide 80–85% of its initial target cooling demand (16–17% of the total cooling of the station) eventually overheating the ground, due to the cooling dominant load. On the other hand, *balancing* the thermal load by providing equal amounts of heating, transferred to nearby buildings, resulted in a much better running system that would be less costly to operate, be able to run for much longer time and could almost certainly exceed the initial target demands, given that sufficient heating demand is also present. Thermally activating the bottom slab marginally improves the system performance. However, these benefits may not outweigh the additional capital costs associated and a cost-benefit analysis should be undertaken for a definite position.

Overall, even though the thermal energy availability for energy retaining walls is lower than other structures, this investigation shows that there is potential in their application. The thermal load distribution will be a key factor on the viability of these structures and ideally the possibility of providing equal amounts of heating and cooling should be seriously considered, perhaps by providing heating to nearby buildings on the surface, since it very significantly affects the performance of the system, potentially solely determining its viability.

Acknowledgements. The Australian Research Council (ARC) FT140100227 and The University of Melbourne are acknowledged for their contributions to this work.

nikolas.makasis@unimelb.edu.au

References

Aditya, G.R., et al.: Financial assessment of ground source heat pump systems against other selected heating and cooling systems for Australian conditions. In: IGSHPA Research Track Conference. Stockholm (2018) (Submitted)

Bidarmaghz, A.: 3D numerical modelling of vertical ground heat exchangers. The University of Melbourne (2014)

Bidarmaghz, A., et al.: Thermal interaction between tunnel ground heat exchangers and borehole heat exchangers. Geomech. Energy Environ. **10**, 29–41 (2017). https://doi.org/10.1016/j.gete.2017.05.001

Bidarmaghz, A., Narsilio, G.A.: Heat exchange mechanisms in energy tunnel systems. Geomech. Energy Environ (2018, in press). https://doi.org/10.1016/j.gete.2018.07.004

Bourne-Webb, P., et al.: Analysis and design methods for energy geostructures. Renew. Sustain. Energy Rev. **65**, 402–419 (2016). https://doi.org/10.1016/j.rser.2016.06.046

Brandl, H.: Energy foundations and other thermo-active ground structures. Géotechnique **56**(2), 81–122 (2006). https://doi.org/10.1680/geot.2006.56.2.81

Brandl, H.: Geothermal geotechnics for urban undergrounds. Procedia Eng. **165**, 747–764 (2016). https://doi.org/10.1016/j.proeng.2016.11.773

Cecinato, F., Loveridge, F.: Influences on the thermal efficiency of energy piles. Energy **82**, 1021–1033 (2015). https://doi.org/10.1016/j.energy.2015.02.001

Di Donna, A., et al.: Energy performance of diaphragm walls used as heat exchangers. Proc. Inst. Civil Eng. Geotech. Eng. **170**, 1–14 (2016). https://doi.org/10.1680/jgeen

Florides, G., Kalogirou, S.: Ground heat exchangers-a review. In: Proceedings of the 3rd International Conference on Heat Powered Cycles, HPC 2004-Cooling, Heating and Power Generation Systems. Cyprus University of Technology, Larnaca (2004)

Johnston, I.W., Narsilio, G.A., Colls, S.: Emerging geothermal energy technologies. KSCE J. Civ. Eng. **15**(4), 643–653 (2011). https://doi.org/10.1007/s12205-011-0005-7

Loveridge, F., Powrie, W.: Pile heat exchangers: thermal behaviour and interactions. Proc. ICE Geotech. Eng. **166**(2), 178–196 (2013). https://doi.org/10.1680/geng.11.00042

Makasis, N.: Further understanding ground source heat pump design using finite element methods and machine learning techniques. PhD Thesis, The University of Melbourne (2018)

Mikhaylova, O., et al.: Benefits and optimisation of district hybrid ground source heat pump systems. In: Wuttke, F., Bauer, S., Sanchez, M. (eds.) Energy Geotechnics—Proceedings of the 1st International Conference on Energy Geotechnics, ICEGT 2016, pp. 535–542. CRC Press, Kiel (2016)

nikolas.makasis@unimelb.edu.au